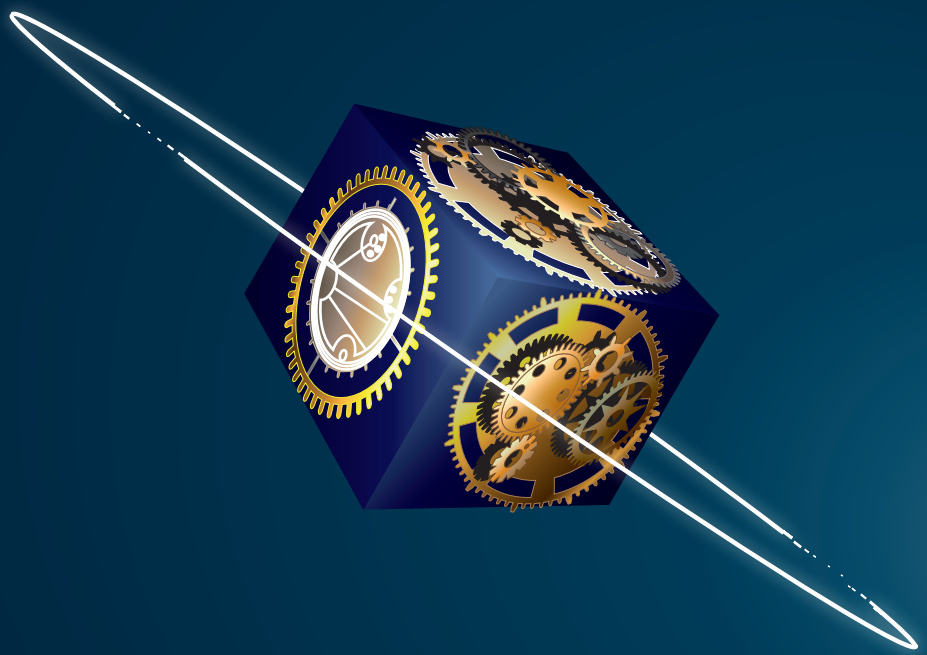
Folding of CFTR transmembrane domains in the endoplasmic reticulum



Hui Ying Yeoh

Folding of CFTR transmembrane domains in the endoplasmic reticulum

Hui Ying Yeoh

Folding of CFTR transmembrane domains in the endoplasmic reticulum
Ph.D. thesis, Utrecht University, The Netherlands

Author
Hui Ying Yeoh

ISBN
978-90-393-7277-7

Designed and Edited by
Hui Ying Yeoh

©2020 Hui Ying Yeoh
All rights reserved. No part of this thesis may be reproduced, stored in a retrieval system or transmitted in any form or by any means without permission of the author.

Folding of CFTR transmembrane domains in the endoplasmic reticulum

Vouwing van CFTR transmembraandomeinen in het endoplasmic reticulum

(met een samenvatting in het Nederlands)

Thesis/Proefschrift

ter verkrijging van de graad van doctor aan de Universiteit Utrecht op gezag van de rector magnificus, prof.dr. H.R.B.M. Kummeling, ingevolge het besluit van het college voor promoties in het openbaar te verdedigen op

woensdag 8 april 2020 des ochtends te 10.30 uur

door

Hui Ying Yeoh

geboren op 7 juli 1988
te Melaka, Maleisië

Promotor:
Prof. dr. L. J. Braakman

Copromotor:
Dr. P. van der Sluijs

This thesis was accomplished with financial support from CFF, the Dutch Research Council (NWO), the Netherlands Organization for Health Research and Development, and the Netherlands Cystic Fibrosis Foundation.

CONTENTS

Chapter 1

Introduction - Membrane-embedded chaperones for transmembrane domains folding in the endoplasmic reticulum 7

Chapter 2

Analysis of protein folding, transport, and degradation in living cells by radioactive pulse chase 37

Chapter 3

Analysis of CFTR domain assembly with antibodies against transmembrane domains 57

Chapter 4

Folding-function relationship of the most common Cystic-Fibrosis-causing CFTR conductance mutants 87

Chapter 5

R751L-CFTR: description of clinical phenotype and molecular characterisation 115

Chapter 6

The role of the EMC ER membrane complex in CFTR folding and stability 137

Chapter 7

The role of Bap31 in CFTR folding and quality control 163

Chapter 8

General discussion 193

Summary/ Samenvatting 207

Acknowledgment 213

Curriculum vitae 214

Chapter 1: Introduction

Membrane-embedded chaperones for transmembrane domains folding in the endoplasmic reticulum

AUTHORS:
Hui Ying Yeoh, Peter van der Sluijs, Ineke Braakman

Introduction: Membrane-embedded chaperones for transmembrane domains folding in the endoplasmic reticulum

In mammalian cells, 20-30% of all opening reading frames (ORFs) encode membrane proteins. (Wallin and von Heijne, 1998). These proteins are synthesized and folded in the endoplasmic reticulum (ER) and carry out a wide variety of functions, including small molecule transfer, signal transduction, cell adhesion, intracellular trafficking, as well as membrane and organelle biogenesis (von Heijne, 2007). Membrane proteins contain one or more transmembrane domains (TMDs), which are formed by stretches of hydrophobic amino acids that span the lipid bilayers as α-helices. TM helices establish their topology at the start of protein synthesis and which is maintained throughout the lifetime of the protein (Shao and Hegde, 2011). At the beginning of translation, signal recognition particle (SRP) recognizes the hydrophobic sequence of nascent chains emerging from translating ribosomes (Figure 1, i) and guides the ribosome/nascent chain complex to the translocon. The complex docks on top of the translocon by aligning the ribosome exit tunnel with the translocon center pore, forming a so called ribosomal translocon complex (RTC) (Figure 1, ii-iii). This allows nascent chains to extend into the translocon central pore without contacting the cytosol and insertion of nascent chains by the Sec61 translocon based on the hydrophobicity of the TM helix (Figure 1, iv) (Guna and Hegde, 2018; Kida et al., 2016). Three challenges exist for membrane protein topogenesis and subsequent folding and as of yet the cellular mechanisms to overcome them are incompletely understood.

The first challenge is re-arranging TM helixes in the membrane from their initial positioning, such as retrieving TM stretches back into the ER membrane from the ER lumen and/or cytosol or converting the topology of the TM helix from N_{exo} to N_{cyt} or from N_{cyt} to N_{exo}. In the N_{exo} topology, the N-terminus of the TM helix is in the extracellular space once the membrane protein is transported to the cell surface. In the N_{cyt} topology, the N-terminus faces the cytosol when the membrane protein is at the cell surface. An example of topology conversion can be seen in the water channel Aquaporin-1, which re-orients its TM helixes after translation (Lu et al., 2000). Such a conformational change may be driven by charged residues flanking the N- and C-terminii (Figure 2A, i-iv) (Goder and Spiess, 2003; Lerch-Bader et al., 2008; Seppala et al., 2010). Whether such re-orientation of TM helices within the ER membrane is purely self-driven or requires chaperone assistance is still unclear. Most membrane proteins are inserted by the Sec61 translocon (Ellgaard et al., 2016), which has difficulty recognizing TM helixes with low hydrophobicity and allows them to either extend into the ER lumen or remain in the cytosol during translation (Figure 2A, v-vi) (Feige and Hendershot, 2013). Such helixes are retrieved back to the ER membrane after translocation (Figure 2A, vii-viii), though the exact

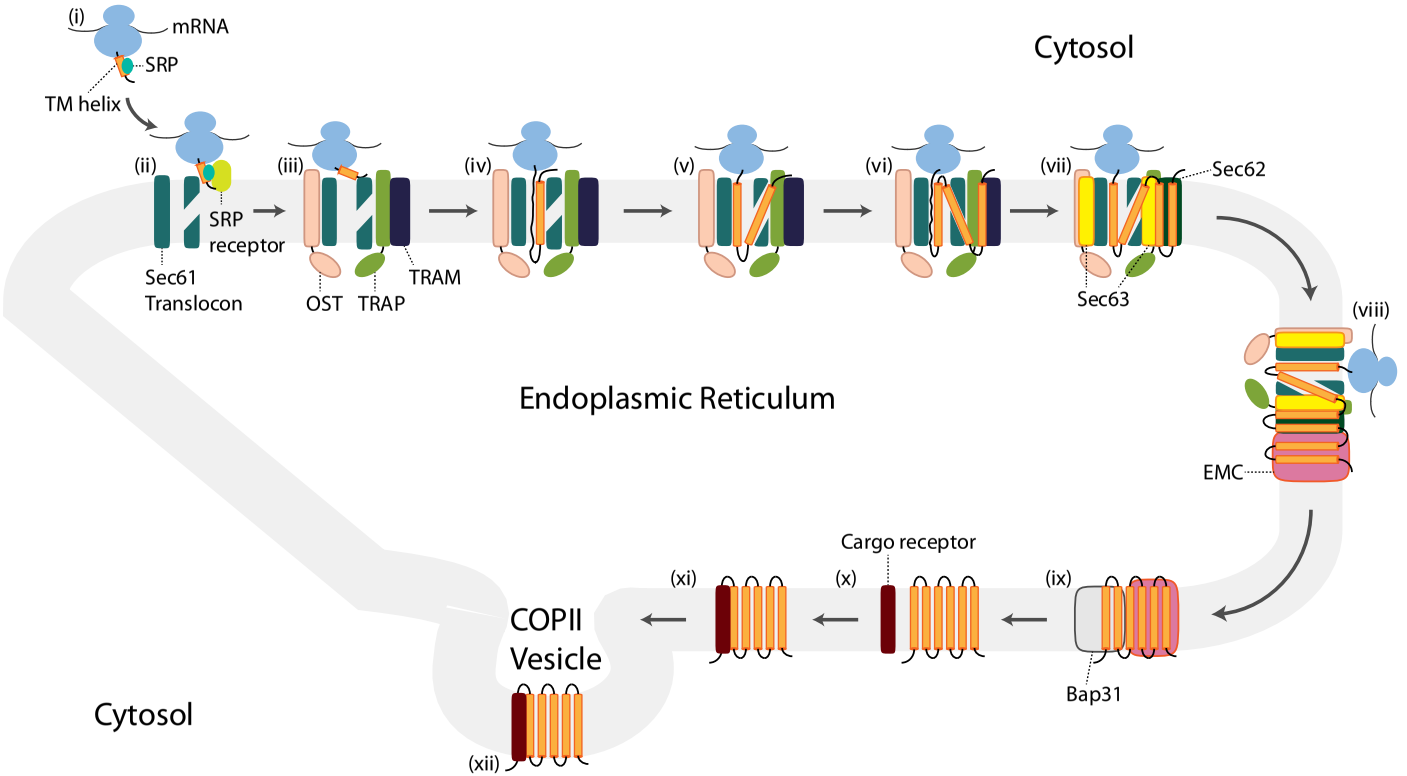


Figure 1: Membrane-bound factors that stabilize TMD during folding.
Scheme depicting possible chaperone interactions with the nascent chain of a membrane protein. Chaperones bind to the nascent chain in a client-dependent manner. (i) The hydrophobic sequence of the first TM helix will be recognized by signal recognition particle (SRP) when emerging from the translating ribosome. (ii) SRP will guide the nascent chain-ribosome complex to the ER membrane and bind to the SRP receptor, thereby aligning the ribosome with the Sec61 complex. (iii) Other translocon components, including TRAP, TRAM and OST, bind to the Sec61 complex forming a ribosome-translocon complex (RTC) and the nascent chain will start extending into the translocon center pore. (iv) After the TM helix is translated and (v) translocated, (vi) it is transferred from translocon to TRAP and TRAM for further topogenesis and assisted insertion. (vii) The translocation of TM helixes can be facilitated by Sec63 binding to the Sec61 complex, whereas Sec62 assists their topogenesis. (viii) The EMC complex binds to the nascent chain after it has reached a certain length to stabilize the TM helixes that contain folding-challenged sequences. (ix) After the TMDs are inserted properly and stabilized by helix-helix packing with assistance of EMC, they are bound by Bap31 for quality control. (x) Membrane proteins that acquired their proper folding will be released by Bap31 into the lipid bilayer, (xi) where they will encounter cargo receptors. (x) Cargo receptors bind to their substrates and (xi) transfer them into COPII vesicle for ER export.

mechanism and possible required proteins remain unknown.

The second challenge is the possible hydrophobic mismatch between TMDs and the ER membrane, which is caused by differences between the hydrophobic stretches of the TMDs and the thickness of the ER membrane. TMDs of membrane proteins are diverse in length and this determines the destination of these proteins in the secretory pathway (Quiroga et al., 2013; Sharpe et al., 2010). Golgi and plasma membranes are thicker than the ER membrane, therefore TM helixes of membrane proteins that are directed to these two locations will be longer than those destined for integration in the ER membrane. Hydrophobic mismatch occurs during residency of Golgi and plasma membrane proteins in the ER membrane, thereby exposing hydrophobic residues of TM helixes to the cytosol or ER lumen. Longer exposure of hydrophobic TM stretches to such aqueous environments will enhance non-specific binding between several nearby TMs and can lead to protein aggregation (Figure 2B, i-iv) (Basu et al., 2014; Killian and Nyholm, 2006). Two mechanisms may prevent aggregation, namely tilting and/or chaperones. Longer TM helices can be tilted by 20^{o} once inserted into the ER membrane (Figure 2B, v-vi) (Kim and Im, 2010), to avoid extending into the cytosol or ER lumen, though a higher degree of tilting could cause a rearrangement in the TMD conformation (Figure 2B, vii-viii). Longer TM helices can also bind to chaperones with TM helixes of similar length to support the structure of the protein and prevent hydrophobic mismatch (Milovanovic et al., 2015; Quiroga et al., 2013). After the TMD has completed its folding and is ready to enter the secretory pathway, it may bind to cargo receptor to avoid hydrophobic mismatch (Herzig et al., 2012; Louie et al., 2012).

The last problem is more common in membrane proteins such as ion channels, which contain charged and polar residues in the TM helixes that form the channel (Johnson and Chen, 2017; Kim and Chen, 2018; Li et al., 2017; Taylor et al., 2017). These hydrophilic residues are placed there to shield the aqueous environment in the tunnel from the hydrophobic lipid bilayer surroundings and for functional purposes (El Hiani et al., 2016). Before protein folding is completed, the charged residues in the TM area will be exposed in the ER membrane lipid bilayer and may cause random interactions between proteins, which can lead to aggregation (Figure 2C i-iv) (Dorairaj and Allen, 2007). This can be overcome by binding of chaperones to the exposed residues until the interaction partners of these residues, such as the other charged residues from the same or different TMD, are translated and available for subsequent interfacing (Kida et al., 2016). Polar and charged residues within the lipid bilayer can only interact with molecules that have similar chemical properties. Therefore, chaperones for these destabilising sequences should also contain charged residues within their TM helixes and have similar hydrophobicity.

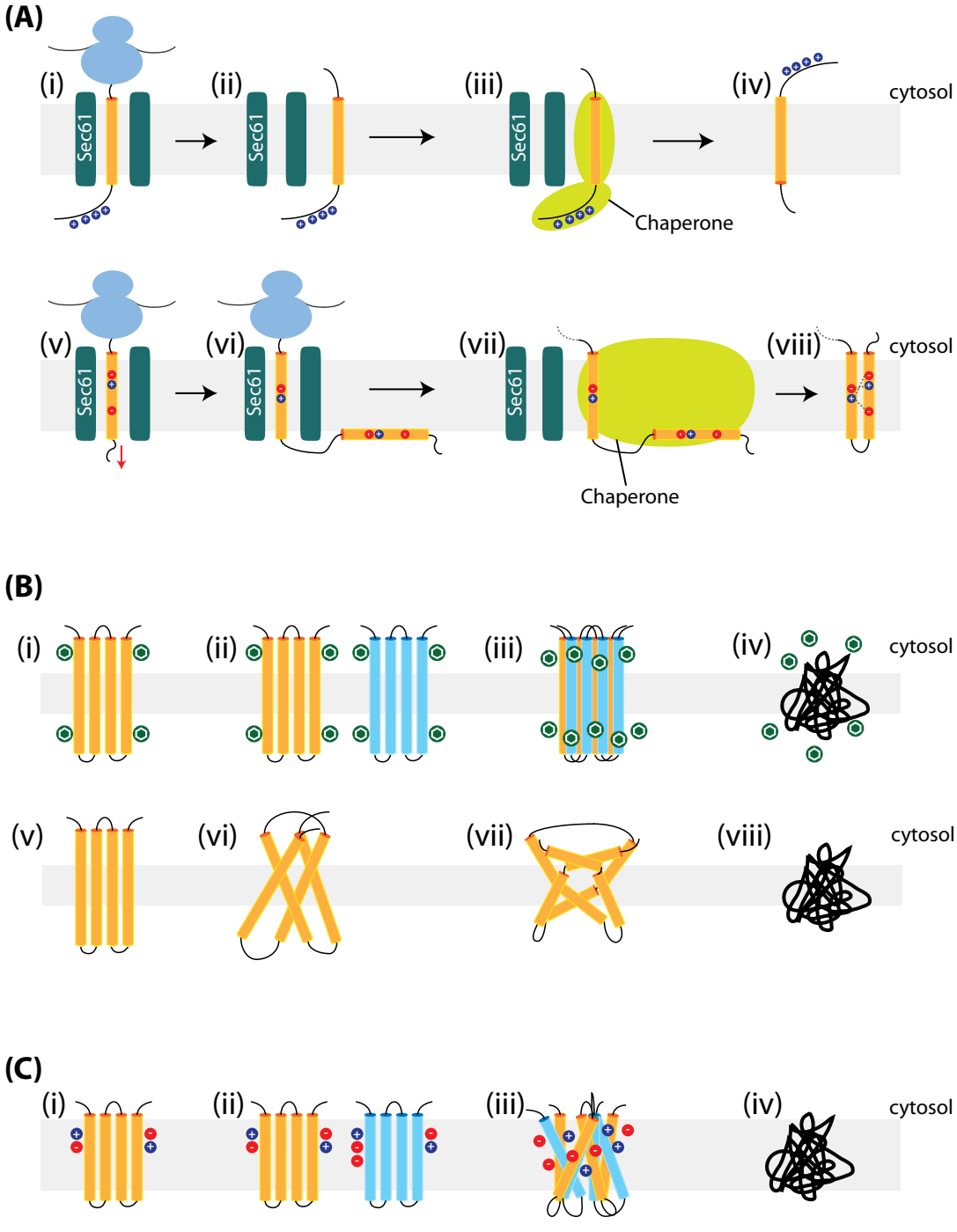

(A)
(i)
(ii)
(iii)
(iv)
Sec61
cytosol
Chaperone
(v)
(vi)
(vii)
(viii)
(B)
(C)

Figure 2: The challenges of TMD folding.
Membrane proteins encounter three challenges during their folding (A-C). (A) TM helixes can be re-positioned from their initial topology after insertion into the lipid bilayer. This re-positioning can happen in two ways: TM helixes can be re-orientated under the influence of 'positive inside rule' or retrieved back from the ER lumen or cytosol after unsuccessful insertion. The TM helix is (i) translocated and (ii) inserted into the lipid bilayer by translocon. (iii) The 'Positive inside rule' will drive the helix to flip in the other direction and this flipping may be assisted by chaperones (Seppala et al., 2010). (iv) After flipping, TM helixes will have either its N- or C-terminus, depending on which is enriched in positive charges, positioned in the cytosol. (v) In the second model, a TM helix with charged residues will have decreased recognition by the Sec61 translocon and extend into ER lumen (Feige and Hendershot, 2013). (vi) TM helixes will be held at the aqueous-lipidic boundary at the luminal side of the ER membrane and (vii) can be retrieved back to the lipid bilayer by chaperones. (viii) After the TMD has been stabilized, it is released into the lipid bilayer by the chaperone. (B) TMDs destined for late secretory pathway membranes will have longer TM helixes compared to those destined for the ER membrane (Quiroga et al., 2013). (i-iii) The exposed hydrophobic residues at the top and bottom of the TM helixes can drive random interactions with other membrane proteins at the ER membrane (Killian and Nyholm, 2006), (iv) which may cause aggregation at the ER membrane and lead to degradation by ERAD. (v), (vi) Long TM helixes can also adapt to the length of the ER membrane by slightly bending into the lipid bilayer (Kim and Im, 2010). (vii) Once the bending angle is bigger than 20°, the helixes will lose their conformation, (viii) leading to aggregation in the ER membrane. The protein aggregates may then be cleared by ERAD. (C) (i) Uncoupled charged residues in TMD can generate free charges, (ii) which can randomly interact with other charges in the lipid bilayer. (iii), (iv) Random interactions can cause aggregation in the ER membrane, followed by degradation by ERAD (Dorairaj and Allen, 2007). (Blue circle: positive charge, red circle: negative charge, green and white circle: hydrophobic forces)

These three challenges indicate that a single membrane protein, especially a multi-pass ion channel, requires assistance to maintain the stability of its TMD before it acquires its native conformation. This assistance will mainly come from membrane-embedded chaperones, which have not received much attention until recently. Membrane-embedded chaperones are not only responsible for insertion and topogenesis of translating nascent chains but also for maintaining the stability of newly synthesized TMDs during protein folding (Cross and High, 2009; Kida et al., 2016; Shurtleff et al., 2018; Sommer et al., 2013). A membrane protein can not fully assemble into its native structure before translation of its last domain is completed (Du and Lukacs, 2009; Riordan, 2005). If the membrane protein contains more than one TMD, the TMD that has already been translated will stay uncoupled in the ER membrane until its partner TMD is made. In such a case, chaperone binding will be necessary for maintaining the stability of the TMDs if they contain charged residues.

In general, the molecular chaperones providing the main assistance for protein folding include cytosolic, ER and membrane-embedded chaperones. These chaperones are often also coupled with the ubiquitination and degradation machinery and act as members of protein quality control pathways. Cytosolic chaperones, such as Hsp40/Hsp70, Hsp90, CHIP, CRYAN and Ubiquilin, target exposed hydrophobic residues of cytosolic proteins and cytosolic domains of membrane proteins (D'Agostino et al., 2013; Ellgaard et al., 2016; Itakura et al., 2016). ER chaperones, including ER Hsp70 chaperone Bip, ER Hsp90 chaperone Grp94, Calreticulin (CRT), and the PDI family, detect exposed hydrophobic residues

and mispaired disulphide bonds in soluble secretory proteins (Ellgaard et al., 2016). Membrane-bound chaperones, for example the Sec 61/62/63 translocon, TRAM, TRAP, EMC, and Bap31, help insertion and topogenesis of membrane proteins (Figure 1, v-xii) (Shurtleff et al., 2018). Two well-known membrane bound proteins involved in membrane protein production are oligosaccharyltransferase (OST) and Calnexin (CNX). Membrane bound factor OST is a translocon component but only responsible for transferring oligosaccharide to the nascent chain and is not involved in TMD folding. Membrane-bound chaperone CNX is not involved in maintaining TMDs stability but coregulates the co- and post-translational folding of its substrates together with its soluble homologue Calreticulin. These chaperones bind to their substrates at their mono-glucosylated (Glc1Man9GlcNac2) trimming intermediates of the core glycan (Tannous et al., 2015). The function of these two membrane-bound factors will not be described in this chapter. The mode-of-action of a wide variety of cytosolic and ER luminal chaperones, like the heat shock protein and PDI families, has been studied extensively, but the molecular mechanisms of chaperones that assist TMD folding are not well understood. Here, we will discuss how membrane-embedded chaperones, or intramembrane chaperones, are involved in establishing membrane protein topology and maintaining the stability of TMDs with destabilizing sequences such as charged residues or hydrophobic mismatch.

The Sec61 translocon

The core component of the Sec translocon is the Sec61 complex. This complex contains three subunits (α, β, γ) and is homologuous to SecY, E, and β in prokaryotes and archaea (Tsukazaki et al., 2008; Van den Berg et al., 2004; Voorhees et al., 2014). The Sec61 translocon is well known for modulating soluble protein translocation across the ER membrane (Rapoport, 2007). For membrane proteins, the translocon integrates targeted nascent chains into the ER membrane through its lateral gate in Sec61α (Gogala et al., 2014; Reithinger et al., 2014).

The insertion of TM helixes with low hydrophobicity into the ER membrane is more problematic than for hydrophobic TM helixes (Onishi et al., 2013). During translation, the ribosome detains the TM helix in the Sec61 tunnel by holding the nascent chain and restricting it in this resting position to facilitate the binding between hydrophobic residues and Sec61α. Hydrophobic residues bind to Sec61α and induce translocation arrest, allowing TM helixes to diffuse into the lipid bilayer through the translocon lateral gate. However, hydrophilic residues decrease the chance of stalling and may cause the TM helix to extend into the ER lumen (Feige and Hendershot, 2013). After binding to Sec61α, high hydrophobicity TM helixes will incorporate easily into the lipid bilayer (Figure 3A i-iii), but low hydrophobicity TM helixes will be harboured as an intermediate translation state at the lateral

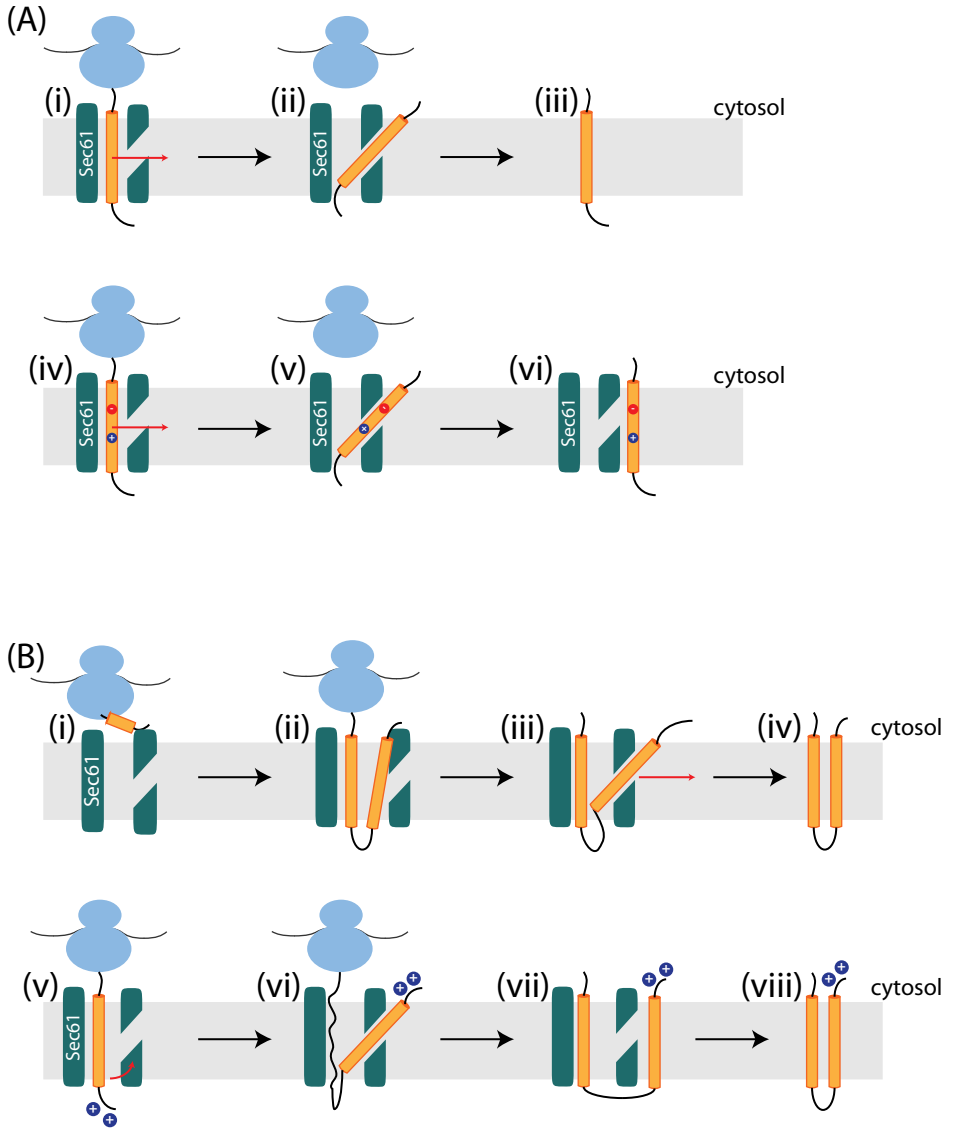


Figure 3: Insertion and topogenesis of TM helixes by Sec61 Translocon.
(A) (i), (ii) A highly hydrophobic TM helix can be easily inserted into the lipid bilayer after translocation and (iii) diffuse away from the translocon. Low hydrophobicity TM helixes can also be (iv) translocated and (v) inserted into the lipid bilayer, but (vi) they will be held at the aqueous-lipidic boundary at the lateral gate of the translocon (Kida et al., 2016). (B) The translocon can assist topogenesis either by reading the signal sequence and stop transfer sequence or allowing TM helix flipping. (i) The signal sequence in the first TM helix will be recognized and bound to the Sec61 complex and (ii) the remaining part of the nascent chain will be extended down the center pore, forming a N_{cyt} orientation (Skach, 2009). (iii) The translocation stops after the Sec61 complex recognizes a stop transfer sequence. (iv) The helices are inserted into the lipid bilayer via the lateral gate of the translocon. (v) TM helixes can also be translocated in N_{exo} orientation from the beginning. (vi) The C-terminus of the nascent chain continues to lengthen until the TM helixes are able to flip 180° into N_{cyt} orientation based on its own sequence or under the influence of 'positive inside rule' (Devaraneni et al., 2011). (vii), (viii) The nascent chain is then released into the ER membrane via the translocon lateral gate.

gate of the translocon, which has a lipidic-aqueous boundary (Figure 3A, iv-vi). Low hydrophobicity TM segments can diffuse into the lipid bilayer with the help of their hydrophobic residues, but this insertion is unstable. These TM helixes are able to re-bind the translocon in the lipid bilayer after translation is completed, suggesting that their hydrophilic residues are still exposed and active. Low hydrophobic TM helixes are only fully integrated into the lipid phase after their partnering TM segment has been translated. (Kida et al., 2016).

While the translocon has a channel that can provide an aqueous-lipidic boundary, such a boundary could potentially also be provided by other chaperones that contain charged or hydrophilic residues in their TMDs. Low hydrophobicity TMDs were found nearby to the Sec61 translocon (Kida et al., 2016), indicating that the potential chaperones such as TRAM, TRAP, Sec62 or Sec63 or the recently found insertase EMC may be associated with the translocon complex (Heinrich and Rapoport, 2003; Meyer et al., 2000; Pfeffer et al., 2017; Shurtleff et al., 2018). These proteins not only contain hydrophilic residues in their TMDs, there are also reports on their preference on binding to low hydrophobicity TMDs to maintain their folding and stability in the lipid environment (Shurtleff et al., 2018; Tamborero et al., 2011). It is therefore likely that low hydrophobicity TM helixes are passed from the translocon to translocon-associated chaperones.

TMDs establish their initial topology during integration into the ER membrane by the translocon, though the exact role of the translocon in TMD topogenesis remains unclear. Correct topology facilitates the following folding process by encouraging TM helix-helix packing within the lipid bilayer. At first, the translocon was proposed to assist TMD topogenesis by determining the orientation of the inserting TM helix. In this model, the translocation of TM helixes is controlled by the signal sequence and the stop transfer sequence (Figure 3B, i-iv). Signal sequences in polytopic membrane protein are represented by the start of their TM helixes, while the stop transfer sequence has not been clearly defined. The former triggers translocation, whereas the latter closes the translocon luminal gate and allows for peptide chain elongation in the cytosol until the next signal sequence is recognized, re-opening the translocon gate and re-initiating translocation. During translocational stalling, TM helixes are able to bind to Sec61α and incorporate into the lipid bilayer (Figure 3B, iii-iv). In membrane proteins with N_{exo} topology the signal sequence is located in the beginning of their first TM helix, with the stop transfer sequence at the end of the same TM helix. In membrane proteins with N_{cyt} topology, the signal sequence is located at the start of the first TM helix and the end of the second TM helix will function as stop transfer sequence (Figure 3B, ii) (Skach, 2009).

TM helixes may also acquire topogenesis by flipping their initial topology. For

instance, a TM helix with N_{exo} orientation can flip into N_{cyt}, or vice versa, during insertion by Sec61 translocon (Figure 3B, v-viii) (Devaraneni et al., 2011). One of the driving forces for this flipping is the "positive inside rule", which describes the phenomenon that the terminus of a TM helix that is rich in positive charges should always face the cytosol side, regardless whether it is an N- or C-terminus (Figure 3B, v-viii). However, the location and the mechanistical details of this flipping is enigmatic, as the translocon lumen is not large enough to sustain a 180° turn of a helix unless the helix undergoes full or partial unfolding during the flip. The flipping could also happen at or adjacent to the opening lateral gate of the translocon with assistance of other translocon members such as TRAP and TRAM (Skach, 2009).

Most likely, the translocon's only functions are in TMDs insertion and topogenesis and not in chaperoning the folding of TMDs. Firstly, a translocon is unable to accommodate more than 2 helixes in its lumen, and therefore cannot support the co-translational folding of a whole TMD. Secondly, the translocon does not provide binding sites for hydrophilic residues within the TM segments, but interacts with the hydrophobic residues to facilitate insertion. Therefore, other chaperones may be involved to fulfil this task.

TRAP and TRAM

Two other major constituents of the Sec translocon are translocon-associated protein (TRAP) (Pfeffer et al., 2017) and translocating chain-associating membrane protein (TRAM) (Gorlich et al., 1992). The TRAP complex includes subunits α, β, γ, and δ (Hartmann et al., 1993), which form the three main segments of TRAP: the cytosolic domain binding the ribosome, one transmembrane bundle enclosing the Sec61 channel at the C-terminal of Sec61α, and an ER luminal domain positioned beneath the translocon channel and that binds to the hinge region between N- and C-terminii of Sec61 (Pfeffer et al., 2017). TRAP is involved in initiating translocation of TM helixes that have low translocation efficiency, a function most likely mediated by its cytosolic domain. TRAP also associates with the Sec61 translocon to facilitate the topogenesis of membrane proteins (Fons et al., 2003; Sommer et al., 2013).

The positive-inside rule (Figure 2A, i-iv) is not the only factor that determines the topology of membrane protein. A study using human asialoglycoprotein receptor H1 mutant, in which the charged residues flanking its TM helixes were inverted, showed that about 40% of this mutant obeyed the positive-inside rule, whereas 60% still remained in its wildtype topology. The positive inside topology is enhanced during TRAP silencing, suggesting that TRAP assists TM helices in acquiring their native topology even when it should be in the opposite orientation as predicted by the positive-inside rule (Sommer et al., 2013). This implies that TRAP may help TM helices establish their topology by recognizing particular sequences within them

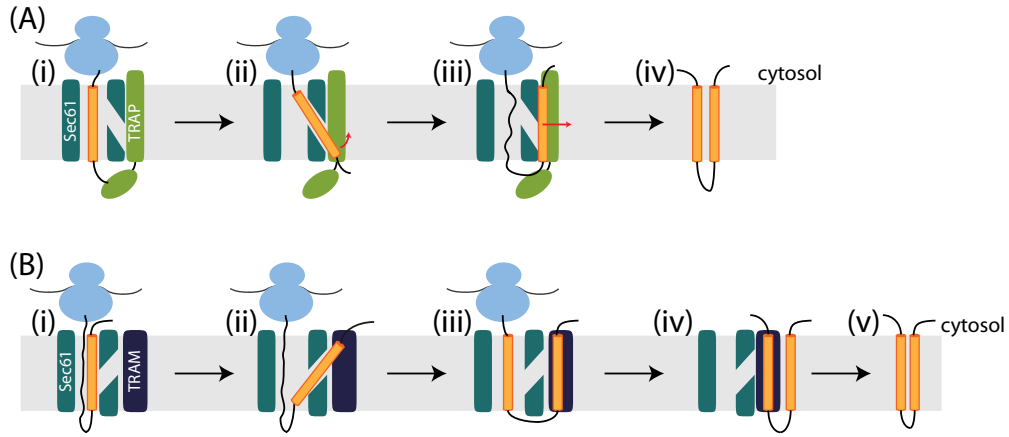


Figure 4: The roles of TRAP and TRAM during TMD folding.
(A) TRAP is required for TM helix topogenesis. (i) TRAP binds to the translocated nascent chain with its C-terminus and (ii) may also interact with the TM helixes at the lateral gate of translocon during insertion. (iii) TRAP may be involved in flipping the TM helix into its native topology before (iv) releasing the TM helixes into the ER membrane. (Sommer et al., 2013) (B) (i) After translation and translocation, (ii)-(iv) TM helixes are passed one by one from translocon to TRAM and (v) are inserted into the lipid bilayer by TRAM (Sauri et al., 2007).

(Figure 4A, i-iv) (Fons et al., 2003). Sommer et al., 2013 also suggests that TRAP tends to assist topogenesis of low hydrophobicity TM helixes. Signal sequences with high hydrophobicity do not respond to TRAP silencing while TM helixes with low hydrophobicity fail to establish their native topology during TRAP silencing (Sommer et al., 2013). TM helixes are still able to be inserted into the lipid bilayer during the elimination of TRAP, indicating that TRAP does not interfere with the translocation and insertion of TM helixes, but interacts with them after their integration into the ER membrane. TRAP may be able to access the lateral gate of the Sec61 translocon and the newly synthesized TM helixes during their integration into the ER membrane. The cryo-electron tomography (CET) structure of TRAP shows that its TM area flanks the C-terminal half of Sec61 translocon, but the study does not provide further information on this interaction. TRAP can also interact with the nascent chain with its ER luminal domain, which binds the loop of the hinge region between N- and C-terminal of Sec61α (Pfeffer et al., 2017). This interaction may be important for the coordination between Sec61 translocon and TRAP for topogenesis of TM helixes. In general, the interaction of TRAP to newly-translated TM helixes within the lipid bilayer remains unclear.

The translocating chain-associating membrane protein (TRAM) is a glycoprotein that associates with the translocon (Gorlich et al., 1992). TRAM is involved in translocation of proteins into the ER lumen and the insertion of membrane proteins into the lipid bilayer (Do et al., 1996; Gorlich et al., 1992; Krieg et al., 1989). TRAM has a high number of positively charged residues in its TM segment,

suggesting that TRAM may have a possible chaperone function for TM helixes with low hydrophobicity and negative charged TM residues (Tamborero et al., 2011). TRAM cross-links with a wide variety of TM segments (Do et al., 1996; Heinrich and Rapoport, 2003; Martinez-Gil et al., 2010; Martinez-Gil et al., 2011; McCormick et al., 2003; Sauri et al., 2007), some of them containing charged residues at their TM area (Cross and High, 2009; Heinrich et al., 2000; Meacock et al., 2002). Binding to TRAM enhances their insertion into the ER membrane. TRAM also assists the insertion of TM helixes with short hydrophobic sequences (Voigt et al., 1996). Sec61α and TRAM were demonstrated to be sequentially adjacent to viral membrane protein p9, which has hydrophilic residues in its TM segments, until translation is terminated (Sauri et al., 2007). The sequences of the TM segments that crosslinked to Sec61α were the same as those that crosslinked with TRAM, suggesting that both TRAM and Sec61α bind to the same region on the TM helixes. During nascent chain elongation, crosslinking between TM helixes of p9 and TRAM increases, whereas binding of the TM helixes to Sec61α decreases, indicating that the TM helixes are transferred from the Sec61 translocon to TRAM (Figure 4B, i-v). This process continues until translation termination and the nascent chain is fully integrated into the lipid bilayer. Surprisingly, replacing the viral TM helixes with highly hydrophobic TM helixes does not change the interaction between the substrate and TRAM, indicating that the binding between TRAM and its client does not fully depend on the hydrophilic content of the TM segments (Sauri et al., 2007).

Both TRAP and TRAM interact with low hydrophobic TM helixes: TRAP assists their topogenesis while TRAM may chaperone their insertion into the lipid bilayer. Though both TRAP and TRAM are not sufficiently big to accommodate a full TMD during its folding, they may also coordinate with other protein folding and quality control machinery for maintaining TMD stability.

Sec62 and Sec 63

Sec62 and Sec63 are ubiquitously expressed in the ER and are associated with Sec61 translocon in both yeast and mammalian cells (Meyer et al., 2000; Tyedmers et al., 2000). The complex of the Sec61 translocon, Sec62p, and Sec63p in yeast forms post-translationally, whereas in mammalian cells this interaction happens co-translationally. Sec62 binds to the ribosome-translocon complex (RTC) and Sec63 via its N- and C-terminus, respectively. Mammalian Sec62 contains two N-terminally located basic oligopeptide motifs, MAERRRHKKRIQEVG and PGTPKKKETKKKFKL (aa 1-15 and aa 156-170), which allow for attachment to the ribosome and assist co-translational translocation (Dudek et al., 2005; Muller et al., 2010; Zimmermann and Blatch, 2009). These basic motives are absent in yeast Sec62, which explains why Sec62p only binds to the translocon post-translationally in that organism. Sec62 and Sec63 bind directly to each other, with the positively charged N-terminus of Sec62

binding to the overall negatively charged C-terminus of Sec63 (Muller et al., 2010; Willer et al., 2003; Wittke et al., 2000). Concurrently, Sec63 recruits the luminal Hsp70 immunoglobulin heavy chain binding protein (Bip) to the ER membrane with its luminal J-domain (Lang et al., 2012; Matlack et al., 1999; Panzner et al., 1995). The interaction between Sec62/63 and RTC may be triggered by the translocation of nascent chains of certain substrates, such as prion protein (PrP) and ERj3 (Conti et al., 2015; Lang et al., 2012). These proteins have a remarkably late translocation initiation time, suggesting that Sec62 and Sec63 may be required for assisting the protein with problematic translocation. The engagement of Bip, which mediates effective ER import and prevents the nascent chain from sliding back to the cytosol (Matlack et al., 1999), at the RTC complex during protein translation also supports Sec62/63's function of enhancing protein translocation (Muller et al., 2010).

Sec62 and Sec63 can transiently associate with newly synthesized polypeptides during ER membrane insertion (Figure 5A, i-iv) (Abell et al., 2003). Sec62 crosslinked with nascent chains during the later stage of insertion, in which the TM helix transits from the translocon complex into the phospholipid bilayer. In yeast, Sec62 is required for post-translationally integrating moderately hydrophobic TM helixes with the N_{cyt} topology into the ER membrane (Reithinger et al., 2013). Expression of a model protein with N_{cyt} orientation insertion decreases in a yeast strain containing defective Sec62p (Figure 5A, ii). How Sec62 specifically binds to moderately hydrophobic TM helix remains unclear. TM helices with low hydrophobicity tend to be retained at the lateral gate of the Sec61 translocon until translation is complete and the entire protein is integrated into the lipid bilayer. Sec62 is proposed to come in contact with these TM helixes when they are still held at the lateral gate of the Sec61 translocon and helps position their C-terminii into the luminal side of the ER membrane to establish the N_{cyt} topology.

In contrast to Sec62, Sec63 is found to be cross-linked with membrane proteins in the early stage of their insertion (Abell et al., 2003). This is consistent with the fact that Sec63 facilitates the translocation of the nascent chain with Bip and with a recent study in yeast. This study revealed that Sec63p, blocks ribosome access to the Sec61 translocon with its large cytosolic Brl domain in order to occupy the translocon for post-translational insertion of TM helixes into the ER membrane. Concurrently, the three TM segments and N-terminus of Sec63p interact with the Sec61 translocon and act as a scaffold to hold the translocon in its open-gate conformation for TM helices to transit into the lipid bilayer (Figure 5A, i) (Wu et al., 2019). After the TM helix exits the translocon channel, it will encounter Sec62p for further topogenesis (Figure 5A, ii-iv). Sec63 is also reported to have a quality control function during co-translational translocation of membrane proteins in mammalian cells (Mades et al., 2012). Overexpressing Sec63 decreased the steady state level of

polytopic HBV.S envelope protein. However, overexpressing Sec63 with a mutated J domain, which decreases the binding of Sec63 to Hsp70 chaperone Bip, reduces the downregulating effect. This suggests that the detected quality control function of Sec63 probably stems from Bip. How Sec62 and Sec63 assist membrane protein insertion has so far have only been studied in yeast. These studies only describe the role of Sec62p and Sec63p in post- but not co-translational TM helix insertion, as post-translational insertion is more common in yeast membrane protein biogenesis. However, mammalian cells insert most of their membrane protein co-translationally. Thus the exact mechanism of how Sec62 and Sec63 insert multipass membrane protein into mammalian ER membrane is still under investigation.

The EMC complex

Chaperones like the ER membrane complex (EMC) assist the folding and insertion of low-hydrophobic TMDs. The EMC contains 6 core components (EMC1-6) and 3 non-essential members (EMC7, 8 or 9, 10) (Figure 5B) (Christianson et al., 2011; Jonikas et al., 2009). This complex was first discovered to have a post-translational insertase function for tail-anchored (TA) proteins (Guna et al., 2018). The expression of squalene synthase (SQS), a TA protein with low hydrophobic TMD, decreased in EMC knock-out (KO) cells while the expression of VAMP, a TA protein with high hydrophobic TMD, was almost unaffected. The insertase function of EMC may be regulated by EMC3, as EMC3 has weak resemblance with eukaryotic Get1 and a region of prokaryotic YidC (Anghel et al., 2017), which are both insertases for membrane proteins (Guna and Hegde, 2018). EMC3 is also reported to interact with multi-pass membrane protein, and its expression is elevated during the unfolded protein response (Bircham et al., 2011; Jonikas et al., 2009; Travers et al., 2000), suggesting that EMC3 may also be a chaperone for membrane proteins.

Previous studies indicated that one of the most reported functions of EMC is inserting TM helixes into the ER membrane (Bircham et al., 2011; Lahiri et al., 2014; Louie et al., 2012; Richard et al., 2013; Satoh et al., 2015; Shurtleff et al., 2018). EMC is required for co-translational insertion of the first TM helix of membrane proteins with N_{exo} topology. Such membrane proteins have their N-terminal translocated into the ER lumen before TM helix insertion. In the absence of EMC, the insertion efficiency of N_{exo} membrane proteins decreased, whereas the insertion of N_{cyt} membrane proteins, which is mainly dependent on Sec61 translocon, was almost unimpaired. Recent data show that EMC is required for insertion of the first TM of N_{exo} membrane proteins, while the insertion of the rest of the TM helixes of the proteins are presumable engaged with Sec61 translocon (Chitwood and Hegde, 2019; Chitwood et al., 2018). Both N_{exo} multi-pass membrane proteins and N_{cyt} TA-proteins, the substrates of EMC as an insertase, only translocate stretches of 50 aa or less into the ER lumen, with a larger part remaining at the cytosol side. This

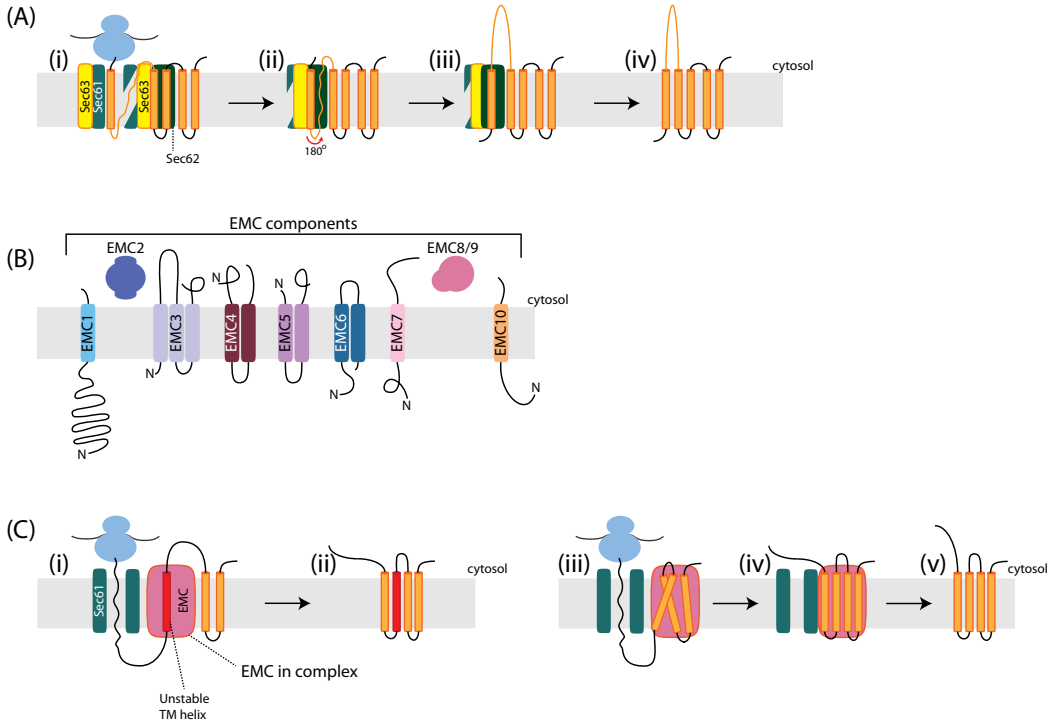


Figure 5: The roles of Sec62/63 and EMC in TMD topogenesis and insertion.
(A) (i) Sec63 binds to the Sec61 complex with its N- and C-terminus and acts as a scaffold to open the lateral gate of the translocon (Wu et al., 2019). (ii) The inserted TM helixes will bind to Sec62, which assist their re-orientation (Reithinger et al., 2013). (iii), (iv) After the TM helixes acquire their native topology, they are released into the ER membrane by Sec62. (B) Schematic representation of EMC components, including its 6 core components, EMC1-6, and three associated members, EMC7-10 (Chitwood and Hegde, 2019). EMC9 is only present in vertebrates and appears to be a recent duplication of EMC8. (C) EMC may function as a chaperone by (i) binding to TM helixes that contain folding-challenged sequences and stabilizing and correcting their folding. (ii) TM helixes that are inserted in their correct position will be released into the lipid bilayer. (iii) An alternative model suggests that EMC may act as an active chaperone involved in TMD folding. In this model, EMC binds to TM helixes that are not inserted well, (iv) corrects their folding, (v) and releases them into the ER membrane after they acquire their native conformation.

structural feature is proposed to be the selection criteria of EMC for assisting the insertion of these substrates.

Besides from functioning as an insertase, the EMC also acts as a chaperone for maintaining stability of TMDs (Shurtleff et al., 2018). Yeast and mammalian cell screenings show that EMC KO impacts a wide variety of membrane proteins, including N_{cyt} multi-pass membrane proteins, suggesting that EMC has another role other than assisting TM helix insertion. Proximity ribosome profiling discovered that EMC interacts with its clients co-translationally and most of its clients are transporters with TMDs enriched in charged residues. These clients include

mammalian membrane protein ABCA3 and yeast membrane proteins Fks1, Fks2, Mrh1, and Pma1 (Bircham et al., 2011; Lahiri et al., 2014; Louie et al., 2012; Richard et al., 2013; Satoh et al., 2015; Shurtleff et al., 2018; Tang et al., 2017). Physical association between EMC and these clients has been confirmed via co-immunoprecipitation and expression of these proteins was impacted during EMC KO. EMC is speculated to stabilize the nascent chains during co-translational binding, preventing pre-mature degradation by the ER associated degradation (ERAD) pathway, and in the meantime recruit other substrate-specific and general chaperones to assist folding of newly-synthesized membrane proteins (Figure 5C, i-ii). The second model hypothesizes that EMC actively acts as a chaperone and binds to the TMD of its substrate until it folds into its native conformation (Figure 5C, iii-v) (Zhang et al., 2017a). Both models are not mutually exclusive but remain to be tested. Although most EMC actions occur co-translationally, EMC also engages clients until post-ER targeting.

Bap31

Bap31 is an ER resident protein with 3 N-terminal transmembrane helices and an extracellular C-terminus with a coiled-coil region and a double lysine (KKEE) motif (Kim et al., 2017). It is ubiquitously expressed in the ER and mainly functions in the quality control of membrane proteins together with its homolog Bap29 and modulates apoptosis in conjunction with caspase-8 (Breckenridge et al., 2003). Bap31 may also act as a molecular chaperone for TMDs that contain charged residues at their TM area, as it contains three charged residues in its TM area allowing it to bind to TM charged residues of other membrane proteins. Clients of Bap31 for quality control include MHC class I (Abe et al., 2009; Ladasky et al., 2006), membrane bound-immunoglobulin D (Adachi et al., 1996; Schamel et al., 2003), tetraspanin (Bartee et al., 2010), cellubrevin (Annaert et al., 1997), CD11b/CD18 (Zen et al., 2004), and CFTR (Lambert et al., 2001; Wang et al., 2008). The interaction of Bap31 with these clients occurs via different principles, for instance, Bap31 binds to MHC class I in the presence of its homolog Bap29 for entering COPII vesicles (Paquet et al., 2004). Together with Bap29, Bap31 also coregulates the dislocation of SV40 from the ER to the cytoplasm (Geiger et al., 2011). Alternatively, Bap31 interacts with CD11b/CD18 through its cytosolic tail which is also important in transport of cellubrevin (Annaert et al., 1997; Zen et al., 2004). The interactions between membrane-bound immunoglobulin D and Bap31 occur via the transmembrane regions of both proteins (Adachi et al., 1996), and last but not least, Bap31 is involved in quality control of Cystic Fibrosis transmembrane conductance regulator (CFTR) and promotes CFTR degradation through Derlin-1 mediated ER-associated degradation (ERAD) (Wang et al., 2008).

Most of Bap31's clients contain at least one charged residue in their TM area,

such as membrane-bound IgD and CFTR (Schamel et al., 2003; Wang et al., 2008). This information suggests a possibility of Bap31 to function as a chaperone for membrane proteins that contain a low hydrophobicity TMD. A previous study also shows that the charged residues in Bap31's TM area are required for transporting the VP2 protein of SV40 virus out of the ER (Geiger et al., 2011). VP2 contains a negative charged glutamic acid in its TM helix and functions as bait to interact with Bap31. Mutating the three charged residues in Bap31 into alanine reduces the binding of VP2 to Bap31 and prevents VP2 transportat from the ER to the cytosol. This finding demonstrates that the charged residues in the TM area of Bap31 can be critical for its interaction with substrate. Therefore, when Bap31 interacts with membrane-bound IgD or CFTR at their TMDs, it is very likely that the interaction occurs between the TM charged residues of these proteins. As Bap31 has no reported function on assisting insertion of TM helices into the ER membrane, its interaction with its substrates may occur after insertion (Schamel et al., 2003; Wang et al., 2008). Bap31 only binds to premature CFTR at its first transmembrane domain (TMD1), which has 4-6 charged residues distributed throughout its 6 TM helixes (Wang et al., 2008). In this case, the selection criteria for Bap31 on sorting CFTR into ERAD pathway may be based on presence of the uncoupled, active TM charged residues.

Bap31 may be responsible for protecting polar or charged residues in the TMD from exposure to the lipid bilayer after TMD insertion. It is unclear how Bap31 comes into contact with its substrates after they are released from the translocon/insertion machinery, and when Bap31 releases its substrates for further maturation processes and transferral into the secretory pathway. Previous findings show that Bap31 is able to escort its clients out of the ER (Annaert et al., 1997; Zen et al., 2004), suggesting that Bap31 may be involved in post-translational folding of its clients even after they are exported out of the ER.

Cargo receptors

Membrane proteins that complete folding will be released from ER chaperones and gathered into COPII vesicles, which transfer all secretory proteins from the ER to the Golgi complex (Barlowe et al., 1994; Orci et al., 1991). COPII vesicles collect membrane proteins by binding them directly or indirectly with either coat components Sec24 or cargo receptors. Cargo receptors assist membrane proteins that failed to bind to Sec24 to enter the COPII vesicle and act as a quality control machinery for sorting their substrates to either ERAD or ER export pathway (Dancourt and Barlowe, 2010; Ljungdahl et al., 1992; Miller and Barlowe, 2010). In contrast to membrane proteins, most soluble proteins enter COPII vesicle by bulk flow and do not need to bind to Sec24, while some of them may also tether to cargo receptors to be packaged into the COPII vesicle (Barlowe and Helenius, 2016).

Different cargo receptors have different substrate specificities. In yeast, cargo receptor Erv14 binds to membrane proteins, Erv26 interacts with Golgi-localized mannosyltransferases, while substrates of Erv29 are soluble proteins and membrane proteins that are destined for the vacuole or endosome, and Gs2f, EMP47, and Shr3 bind to respectively sugar transporters, ssp120, and amino acid permease (Belden and Barlowe, 2001; Caldwell et al., 2001; Herzig et al., 2012; Inadome et al., 2005; Kota et al., 2007; Noda and Yoda, 2013; Powers and Barlowe, 1998; Sherwood and Carlson, 1999). Among these cargo receptors, Erv14 interacts specifically to membrane proteins and most of its substrates enter the late secretory pathway. Erv14 has 3 TM helixes and the second one contains the substrate binding site that includes three conserved residues, F62, L63, and N74. Mutating these residues impairs Erv14 binding to its substrate Yor1, the yeast homologue of CFTR. Erv14 may provide structural support for membrane proteins during protein trafficking (Herzig et al., 2012; Louie et al., 2012). As the membranes in the late Golgi apparatus and at the cell surface (plasma membrane) are thicker than the ER membrane (Quiroga et al., 2013; Sharpe et al., 2010), the substrates of Erv14, most of them destined for late secretary pathways, will contain long TMDs that may create hydrophobic mismatch in the ER and during trafficking to the Golgi. Possibly besides sending its substrates to their final destinations, Erv14 may also help its cargo to maintain the long hydrophobic stretches in their TMDs in their correct position during protein trafficking (Herzig et al., 2012). However, this notion has not been well studied. The eukaryotic homologues of Erv14, Cornichons (CNIHs), are also reported to be responsible for sorting many membrane proteins to ER export pathway. CNIH2 and CNIH3 are closely involved in the cell surface expression of α-amino-3-hydroxy-5-methyl-4-isoxazolepropionic acid (AMPA) receptor (Schober et al., 2011; Schwenk et al., 2012), and CNIH4 is responsible for trafficking of G-couple protein receptors (GPCR) (Sauvageau et al., 2014). Therefore, understanding the mechanism of how Erv14 or CNIHs interacts with their substrates may provide insight on how membrane proteins maintain their structural stability in the secretory pathway.

CFTR: the model protein of this thesis

Cystic Fibrosis Transmembrane Conductance Regulator (CFTR) is used as the model protein in this thesis for studying how TMDs fold assisted by membrane-bound chaperones. CFTR belongs to the ABC transporter family and contains two transmembrane domains (TMDs), two nucleotide binding domains (NBDs) and an unstructured R-region (Figure 6A) (Liu et al., 2017; Riordan et al., 1989; Zhang et al., 2017b). Its structure and domain hierarchy, which are arranged in the order TMD1, NBD1, R, TMD2, and NBD2, is highly conserved among type-I ABC transporters and therefore its folding mechanism likely is representative of this protein family.

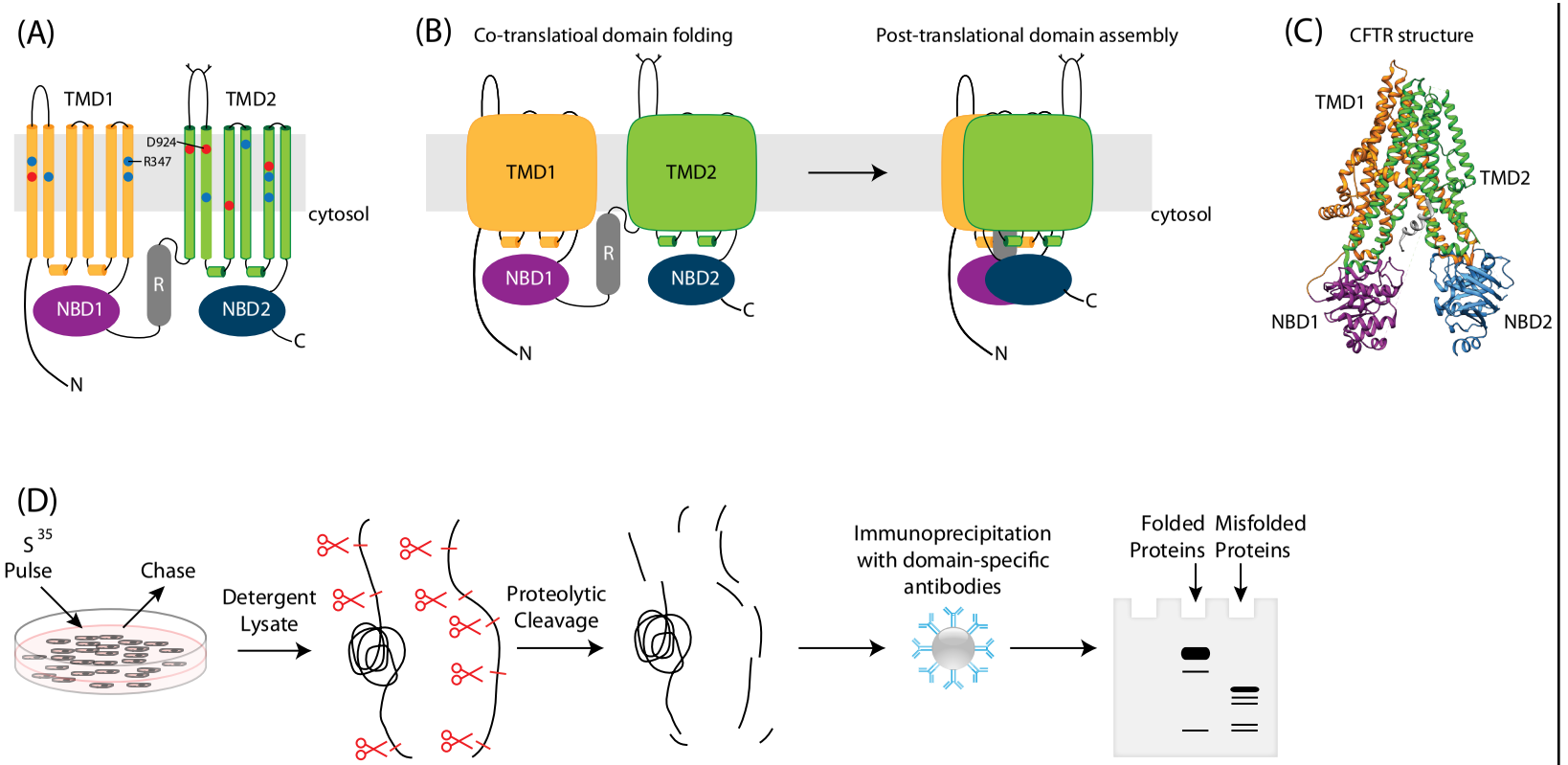


Figure 6: The folding of CFTR.
(A) Cartoon showing the domain architecture of CFTR, the positions of charged residues in the TM area, and the position of R347 and D924. (B) CFTR folding includes two steps: co-translational domain folding, where all domains acquire their correct conformation, and post-translational domain assembly, in which all domains assemble together to form a functional ion channel (Hoelen et al., 2010; Kleizen et al., 2005). (C) Structure of human CFTR from cryo electron microscopy (5UAK; Liu et al., 2017). (D) Scheme of radioactive pulse and chase and limited proteolysis assay. Cells are pulse radiolabelled with ^{35}S-methionine and -cysteine for a short period and subsequently cultured in growth medium with non-radiolabelled amino acids for a certain amount of time, i.e., chase. Subsequently, cells are lysed with detergent and protease is added to the lysates. The protease cleaves unstructured regions in the protein, and folded areas will be protected and not accessible by the protease. After limited proteolysis, fragments of the target protein are immunoprecipitated with domain specific antibodies to determine the folding of each domain. (Blue circle: Positive-charged residue, Red circle: negative-charged residue)

CFTR functions as a chloride ion channel and is opened upon ATP-binding at the NBDs and phosphorylation of the R-region (Cheng et al., 1991; Gunderson and Kopito, 1995). Disruption of the CFTR conformation causes Cystic Fibrosis (CF), which is a disease where movement of ion and water across the apical membrane is compromised, leading to accumulation of fluid in the respiratory, digestive and reproductive systems (Cheung and Deber, 2008; Cohen and Prince, 2012; Ratjen and Grasemann, 2012). The most common mutation in the *CFTR* gene that causes Cystic Fibrosis is F508del. Loss of the phenylalanine at this position impairs NBD1 folding and promotes CFTR degradation in the ER (Du et al., 2005; Riordan, 2008). Many studies have been focused on understanding the disease development of Cystic Fibrosis (Pitonzo et al., 2009; Sosnay et al., 2013; van Willigen et al., 2019). These investigations generated a large number of tools including many antibodies against CFTR NBDs and a database comprising an extensive list of CF patient mutations that can be used for studying CFTR folding.

The folding of CFTR includes two steps: co-translational domain folding and post-translational domain assembly (Figure 6B) (Hoelen et al., 2010; Kleizen et al., 2005). Each CFTR domain acquires its secondary structure during translation, and these domains interact post-translationally with each other and assemble together to form a functioning protein. As CFTR's channel is formed by interaction between its TMDs, proper folding of both TMDs is critical to maintain CFTR's structure and function (Figure 6C). Charged or polar residues are situated at the inner surface of the channel's tunnel to stabilize the contact site between the hydrophobic TMDs and the aqueous environment in the channel (El Hiani et al., 2016; Li et al., 2018; Zhang et al., 2017b). These charged residues also form salt bridges to further stabilize interactions between the TMDs (Cotten and Welsh, 1999; Pitonzo et al., 2009; Skach, 2009). A well identified salt bridge between the TMDs of CFTR is formed between R347 in TMD1 and D924 in TMD2 (Figure 6A). Mutating R347 into a proline profoundly impairs the function of CFTR, however, the effect of this mutation on CFTR folding remains unclear. Each CFTR TMD contains at least 2 charged residues in its TM region (El Hiani et al., 2016). Exposing these charges to the lipid bilayer can disrupt the thermodynamics of the hydrophobic surroundings of the TMDs, increase random interactions with other charged residues and result in protein aggregation in the ER membrane. Therefore, chaperone binding may be required to stabilize these free charges before CFTR is properly folded. Charged residues within the lipid bilayer can only interact with molecules that have similar chemical properties such as membrane proteins that also have charged residues within their TM areas. Fortunately, some of the CFTR-associated membrane-bound chaperones are reported to have charged residues in their TM regions. These chaperones include the EMC complex (Louie et al., 2012), and Bap31 (Lambert et al., 2001; Wang et al., 2008). Nevertheless, the details of how they bind to CFTR are

poorly understood.

Besides charged residues, CFTR also contains two other structural features that result in problematic folding. Firstly, the hydrophilic residues D924 in CFTR TM8, which is the second TM helix in TMD2, will prevents Sec61 recognition of this TM helix and allows it to enter the ER lumen during translocation. TM8 will be retrieved back to the ER membrane by helix-helix packing with TM7 in the later stage of domain folding but the chaperone that may be involved in this procedure has not been identified. Secondly, CFTR is also a cell surface-expressed protein. As the plasma membrane is thicker than the ER membrane, CFTR TM helices will be longer than the ER membrane creating hydrophobic mismatch during protein folding in the ER. Chaperones binding may be required to resolve this problem.

In this thesis, we will study how the TMDs in CFTR maintain their stability during protein folding. We first detect the co- and post-translational folding of CFTR TMDs, examine their domain-domain interaction, and study their interactions with membrane-bound chaperones Bap31 and the EMC. To pursue these aims we created: three antibodies against CFTR TMDs; mutants that disrupt the TMD1-TMD2 interaction; and cell lines with Bap31 or EMC deletion. Subsequently, we examined the folding mechanism of CFTR using these reagents, in coupled radioactive pulse-chase and protease-sensitivity assays (Figure 6D) (Hoelen et al., 2010; Kleizen et al., 2005; McCaul et al., 2019). CFTR biogenesis will be study by pulse radiolabeled the cells with ^{35}S-methionine and -cysteine for a short period of time and protein maturation will be followed by incubating the cells in medium with non-radioactive amino acid, i.e., chase. Subsequently, folding of CFTR domains will be detected using a protease-sensitivity assay, wherein regions with compacted structure will be protected from protease cleavage, while non-structured regions will be proteolyzed. Proteolytic fragments will be detected by domain specific antibodies, providing a fingerprint of the folding state of the protein. Our findings will contribute to the understanding of the chaperones involved in the folding of CFTR. Because CFTR structurally resembles Type-I ABC transporters and faces all of the three common problems of folding, these results also reveal the chaperones that may be involved in the folding of Type-I ABC transporters and other membrane proteins with similar folding problem. As we focus on studying the mechanism of the EMC and Bap31, our study also shows how these chaperones coordinate and what their selection criteria for their substrates are.

REFERENCES

Abe, F., Van Prooyen, N., Ladasky, J.J., and Edidin, M. (2009). Interaction of Bap31 and MHC class I molecules and their traffic out of the endoplasmic reticulum. J Immunol *182*, 4776-4783.

Abell, B.M., Jung, M., Oliver, J.D., Knight, B.C., Tyedmers, J., Zimmermann, R., and High, S. (2003). Tail-anchored and signal-anchored proteins utilize overlapping pathways during membrane insertion. J Biol Chem *278*, 5669-5678.

Adachi, T., Schamel, W.W., Kim, K.M., Watanabe, T., Becker, B., Nielsen, P.J., and Reth, M. (1996). The specificity of association of the IgD molecule with the accessory proteins BAP31/BAP29 lies in the IgD transmembrane sequence. EMBO J *15*, 1534-1541.

Anghel, S.A., McGilvray, P.T., Hegde, R.S., and Keenan, R.J. (2017). Identification of Oxa1 homologs operating in the eukaryotic endoplasmic reticulum. Cell Rep *21*, 3708-3716.

Annaert, W.G., Becker, B., Kistner, U., Reth, M., and Jahn, R. (1997). Export of cellubrevin from the endoplasmic reticulum is controlled by BAP31. J Cell Biol *139*, 1397-1410.

Barlowe, C., and Helenius, A. (2016). Cargo capture and bulk flow in the early secretory pathway. Annu Rev Cell Dev Biol *32*, 197-222.

Bartee, E., Eyster, C.A., Viswanathan, K., Mansouri, M., Donaldson, J.G., and Fruh, K. (2010). Membrane-Associated RING-CH proteins associate with Bap31 and target CD81 and CD44 to lysosomes. PLoS One *5*, e15132.

Basu, I., Chattopadhyay, A., and Mukhopadhyay, C. (2014). Ion channel stability of Gramicidin A in lipid bilayers: effect of hydrophobic mismatch. Biochim Biophys Acta *1838*, 328-338.

Belden, W.J., and Barlowe, C. (2001). Role of Erv29p in collecting soluble secretory proteins into ER-derived transport vesicles. Science *294*, 1528-1531.

Bircham, P.W., Maass, D.R., Roberts, C.A., Kiew, P.Y., Low, Y.S., Yegambaram, M., Matthews, J., Jack, C.A., and Atkinson, P.H. (2011). Secretory pathway genes assessed by high-throughput microscopy and synthetic genetic array analysis. Mol Biosyst *7*, 2589-2598.

Breckenridge, D.G., Stojanovic, M., Marcellus, R.C., and Shore, G.C. (2003). Caspase cleavage product of BAP31 induces mitochondrial fission through endoplasmic reticulum calcium signals, enhancing cytochrome c release to the cytosol. J Cell Biol *160*, 1115-1127.

Caldwell, S.R., Hill, K.J., and Cooper, A.A. (2001). Degradation of endoplasmic reticulum (ER) quality control substrates requires transport between the ER and Golgi. J Biol Chem *276*, 23296-23303.

Cheng, S.H., Rich, D.P., Marshall, J., Gregory, R.J., Welsh, M.J., and Smith, A.E. (1991). Phosphorylation of the R domain by cAMP-dependent protein kinase regulates the CFTR chloride channel. Cell *66*, 1027-1036.

Cheung, J.C., and Deber, C.M. (2008). Misfolding of the cystic fibrosis transmembrane conductance regulator and disease. Biochemistry *47*, 1465-1473.

Chitwood, P.J., and Hegde, R.S. (2019). The role of EMC during membrane protein biogenesis. Trends Cell Biol *29*, 371-384.

Chitwood, P.J., Juszkiewicz, S., Guna, A., Shao, S., and Hegde, R.S. (2018). EMC is required to Initiate accurate membrane protein topogenesis. Cell *175*, 1507-1519 e1516.

Christianson, J.C., Olzmann, J.A., Shaler, T.A., Sowa, M.E., Bennett, E.J., Richter, C.M., Tyler, R.E., Greenblatt, E.J., Harper, J.W., and Kopito, R.R. (2011). Defining human ERAD networks through an integrative mapping strategy. Nat Cell Biol *14*, 93-105.

Cohen, T.S., and Prince, A. (2012). Cystic fibrosis: a mucosal immunodeficiency syndrome. Nat Med *18*, 509-519.

Conti, B.J., Devaraneni, P.K., Yang, Z., David, L.L., and Skach, W.R. (2015). Cotranslational stabilization of Sec62/63 within the ER Sec61 translocon is controlled by distinct substrate-driven translocation events. Mol Cell *58*, 269-283.

Cotten, J.F., and Welsh, M.J. (1999). Cystic fibrosis-associated mutations at arginine 347 alter the pore architecture of CFTR. Evidence for disruption of a salt bridge. J Biol Chem *274*, 5429-5435.

Cross, B.C., and High, S. (2009). Dissecting the physiological role of selective transmembrane-segment retention at the ER translocon. J Cell Sci *122*, 1768-1777.

D'Agostino, M., Lemma, V., Chesi, G., Stornaiuolo, M., Cannata Serio, M., D'Ambrosio, C., Scaloni, A., Polishchuk, R., and Bonatti, S. (2013). The cytosolic chaperone alpha-crystallin B rescues folding and compartmentalization of misfolded multispan transmembrane proteins. J Cell Sci *126*, 4160-4172.

Dancourt, J., and Barlowe, C. (2010). Protein sorting receptors in the early secretory pathway. Annu Rev Biochem *79*, 777-802.

Devaraneni, P.K., Conti, B., Matsumura, Y., Yang, Z., Johnson, A.E., and Skach, W.R. (2011). Stepwise insertion and inversion of a type II signal anchor sequence in the ribosome-Sec61 translocon complex. Cell *146*, 134-147.

Do, H., Falcone, D., Lin, J., Andrews, D.W., and Johnson, A.E. (1996). The cotranslational integration of membrane proteins into the phospholipid bilayer is a multistep process. Cell *85*, 369-378.

Dorairaj, S., and Allen, T.W. (2007). On the thermodynamic stability of a charged arginine side chain in a transmembrane helix. Proc Natl Acad Sci U S A *104*, 4943-4948.

Du, K., and Lukacs, G.L. (2009). Cooperative assembly and misfolding of CFTR domains in vivo. Mol Biol Cell *20*, 1903-1915.

Du, K., Sharma, M., and Lukacs, G.L. (2005). The DeltaF508 cystic fibrosis mutation impairs domain-domain interactions and arrests post-translational folding of CFTR. Nat Struct Mol Biol *12*, 17-25.

Dudek, J., Greiner, M., Muller, A., Hendershot, L.M., Kopsch, K., Nastainczyk, W., and Zimmermann, R. (2005). ERj1p has a basic role in protein biogenesis at the endoplasmic reticulum. Nat Struct Mol Biol *12*, 1008-1014.

El Hiani, Y., Negoda, A., and Linsdell, P. (2016). Cytoplasmic pathway followed by chloride ions to enter the CFTR channel pore. Cell Mol Life Sci *73*, 1917-1925.

Ellgaard, L., McCaul, N., Chatsisvili, A., and Braakman, I. (2016). Co- and post-translational protein folding in the ER. Traffic *17*, 615-638.

Feige, M.J., and Hendershot, L.M. (2013). Quality control of integral membrane proteins by assembly-dependent membrane integration. Mol Cell *51*, 297-309.

Fons, R.D., Bogert, B.A., and Hegde, R.S. (2003). Substrate-specific function of the translocon-associated protein complex during translocation across the ER membrane. J Cell Biol *160*, 529-539.

Geiger, R., Andritschke, D., Friebe, S., Herzog, F., Luisoni, S., Heger, T., and Helenius, A. (2011). BAP31 and BiP are essential for dislocation of SV40 from the endoplasmic reticulum to the cytosol. Nat Cell Biol *13*, 1305-1314.

Goder, V., and Spiess, M. (2003). Molecular mechanism of signal sequence orientation in the endoplasmic reticulum. EMBO J *22*, 3645-3653.

Gogala, M., Becker, T., Beatrix, B., Armache, J.P., Barrio-Garcia, C., Berninghausen, O., and Beckmann, R. (2014). Structures of the Sec61 complex engaged in nascent peptide translocation or membrane insertion. Nature *506*, 107-110.

Gorlich, D., Hartmann, E., Prehn, S., and Rapoport, T.A. (1992). A protein of the endoplasmic reticulum involved early in polypeptide translocation. Nature *357*, 47-52.

Guna, A., and Hegde, R.S. (2018). Transmembrane domain recognition during membrane protein biogenesis and quality control. Curr Biol *28*, R498-R511.

Guna, A., Volkmar, N., Christianson, J.C., and Hegde, R.S. (2018). The ER membrane protein complex is a transmembrane domain insertase. Science *359*, 470-473.

Gunderson, K.L., and Kopito, R.R. (1995).

Conformational states of CFTR associated with channel gating: the role ATP binding and hydrolysis. Cell *82*, 231-239.

Hartmann, E., Gorlich, D., Kostka, S., Otto, A., Kraft, R., Knespel, S., Burger, E., Rapoport, T.A., and Prehn, S. (1993). A tetrameric complex of membrane proteins in the endoplasmic reticulum. Eur J Biochem *214*, 375-381.

Heinrich, S.U., Mothes, W., Brunner, J., and Rapoport, T.A. (2000). The Sec61p complex mediates the integration of a membrane protein by allowing lipid partitioning of the transmembrane domain. Cell *102*, 233-244.

Heinrich, S.U., and Rapoport, T.A. (2003). Cooperation of transmembrane segments during the integration of a double-spanning protein into the ER membrane. EMBO J *22*, 3654-3663.

Herzig, Y., Sharpe, H.J., Elbaz, Y., Munro, S., and Schuldiner, M. (2012). A systematic approach to pair secretory cargo receptors with their cargo suggests a mechanism for cargo selection by Erv14. PLoS Biol *10*, e1001329.

Hoelen, H., Kleizen, B., Schmidt, A., Richardson, J., Charitou, P., Thomas, P.J., and Braakman, I. (2010). The primary folding defect and rescue of DeltaF508 CFTR emerge during translation of the mutant domain. PLoS One *5*, e15458.

Inadome, H., Noda, Y., Adachi, H., and Yoda, K. (2005). Immunoisolaton of the yeast Golgi subcompartments and characterization of a novel membrane protein, Svp26, discovered in the Sed5-containing compartments. Mol Cell Biol *25*, 7696-7710.

Itakura, E., Zavodszky, E., Shao, S., Wohlever, M.L., Keenan, R.J., and Hegde, R.S. (2016). Ubiquilins chaperone and triage mitochondrial membrane proteins for degradation. Mol Cell *63*, 21-33.

Johnson, Z.L., and Chen, J. (2017). Structural basis of substrate recognition by the multidrug resistance protein MRP1. Cell *168*, 1075-1085 e1079.

Jonikas, M.C., Collins, S.R., Denic, V., Oh, E., Quan, E.M., Schmid, V., Weibezahn, J., Schwappach, B., Walter, P., Weissman, J.S*., et al.* (2009). Comprehensive characterization of genes required for protein folding in the endoplasmic reticulum. Science *323*, 1693-1697.

Kida, Y., Ishihara, Y., Fujita, H., Onishi, Y., and Sakaguchi, M. (2016). Stability and flexibility of marginally hydrophobic-segment stalling at the endoplasmic reticulum translocon. Mol Biol Cell *27*, 930-940.

Killian, J.A., and Nyholm, T.K. (2006). Peptides in lipid bilayers: the power of simple models. Curr Opin Struct Biol *16*, 473-479.

Kim, W.T., Choi, H.S., Hwang, H.J., Jung, H.S., and Ryu, C.J. (2017). Correction: Epitope mapping of antibodies suggests the novel membrane topology of B-cell receptor associated protein 31 on the cell surface of embryonic stem cells: The novel membrane topology of BAP31. PLoS One *12*, e0170145.

Kim, Y., and Chen, J. (2018). Molecular structure of human P-glycoprotein in the ATP-bound, outward-facing conformation. Science *359*, 915-919.

Kleizen, B., van Vlijmen, T., de Jonge, H.R., and Braakman, I. (2005). Folding of CFTR is predominantly cotranslational. Mol Cell *20*, 277-287.

Kota, J., Gilstring, C.F., and Ljungdahl, P.O. (2007). Membrane chaperone Shr3 assists in folding amino acid permeases preventing precocious ERAD. J Cell Biol *176*, 617-628.

Krieg, U.C., Johnson, A.E., and Walter, P. (1989). Protein translocation across the endoplasmic reticulum membrane: identification by photocross-linking of a 39-kD integral membrane glycoprotein as part of a putative translocation tunnel. J Cell Biol *109*, 2033-2043.

Ladasky, J.J., Boyle, S., Seth, M., Li, H., Pentcheva, T., Abe, F., Steinberg, S.J., and Edidin, M. (2006). Bap31 enhances the endoplasmic reticulum export and quality control of human class I MHC molecules. J Immunol *177*, 6172-6181.

Lahiri, S., Chao, J.T., Tavassoli, S., Wong, A.K., Choudhary, V., Young, B.P., Loewen, C.J., and Prinz, W.A. (2014). A conserved endoplasmic reticulum membrane protein complex (EMC)

facilitates phospholipid transfer from the ER to mitochondria. PLoS Biol *12*, e1001969.

Lambert, G., Becker, B., Schreiber, R., Boucherot, A., Reth, M., and Kunzelmann, K. (2001). Control of cystic fibrosis transmembrane conductance regulator expression by BAP31. J Biol Chem *276*, 20340-20345.

Lang, S., Benedix, J., Fedeles, S.V., Schorr, S., Schirra, C., Schauble, N., Jalal, C., Greiner, M., Hassdenteufel, S., Tatzelt, J.*, et al.* (2012). Different effects of Sec61alpha, Sec62 and Sec63 depletion on transport of polypeptides into the endoplasmic reticulum of mammalian cells. J Cell Sci *125*, 1958-1969.

Lerch-Bader, M., Lundin, C., Kim, H., Nilsson, I., and von Heijne, G. (2008). Contribution of positively charged flanking residues to the insertion of transmembrane helices into the endoplasmic reticulum. Proc Natl Acad Sci U S A *105*, 4127-4132.

Li, M.S., Cowley, E.A., El Hiani, Y., and Linsdell, P. (2018). Functional organization of cytoplasmic portals controlling access to the cystic fibrosis transmembrane conductance regulator (CFTR) chloride channel pore. J Biol Chem *293*, 5649-5658.

Li, N., Wu, J.X., Ding, D., Cheng, J., Gao, N., and Chen, L. (2017). Structure of a pancreatic ATP-sensitive potassium channel. Cell *168*, 101-110 e110.

Liu, F., Zhang, Z., Csanady, L., Gadsby, D.C., and Chen, J. (2017). Molecular structure of the human CFTR ion channel. Cell *169*, 85-95 e88.

Ljungdahl, P.O., Gimeno, C.J., Styles, C.A., and Fink, G.R. (1992). SHR3: a novel component of the secretory pathway specifically required for localization of amino acid permeases in yeast. Cell *71*, 463-478.

Louie, R.J., Guo, J., Rodgers, J.W., White, R., Shah, N., Pagant, S., Kim, P., Livstone, M., Dolinski, K., McKinney, B.A.*, et al.* (2012). A yeast phenomic model for the gene interaction network modulating CFTR-DeltaF508 protein biogenesis. Genome Med *4*, 103.

Lu, Y., Turnbull, I.R., Bragin, A., Carveth, K., Verkman, A.S., and Skach, W.R. (2000). Reorientation of aquaporin-1 topology during maturation in the endoplasmic reticulum. Mol Biol Cell *11*, 2973-2985.

Mades, A., Gotthardt, K., Awe, K., Stieler, J., Doring, T., Fuser, S., and Prange, R. (2012). Role of human sec63 in modulating the steady-state levels of multi-spanning membrane proteins. PLoS One *7*, e49243.

Martinez-Gil, L., Johnson, A.E., and Mingarro, I. (2010). Membrane insertion and biogenesis of the Turnip crinkle virus p9 movement protein. J Virol *84*, 5520-5527.

Martinez-Gil, L., Sauri, A., Marti-Renom, M.A., and Mingarro, I. (2011). Membrane protein integration into the endoplasmic reticulum. FEBS J *278*, 3846-3858.

Matlack, K.E., Misselwitz, B., Plath, K., and Rapoport, T.A. (1999). BiP acts as a molecular ratchet during posttranslational transport of prepro-alpha factor across the ER membrane. Cell *97*, 553-564.

McCaul, N., Yeoh, H.Y., van Zadelhoff, G., Lodder, N., Kleizen, B., and Braakman, I. (2019). Analysis of protein folding, transport, and degradation in living cells by radioactive pulse chase. J Vis Exp.

McCormick, P.J., Miao, Y., Shao, Y., Lin, J., and Johnson, A.E. (2003). Cotranslational protein integration into the ER membrane is mediated by the binding of nascent chains to translocon proteins. Mol Cell *12*, 329-341.

Meacock, S.L., Lecomte, F.J., Crawshaw, S.G., and High, S. (2002). Different transmembrane domains associate with distinct endoplasmic reticulum components during membrane integration of a polytopic protein. Mol Biol Cell *13*, 4114-4129.

Meyer, H.A., Grau, H., Kraft, R., Kostka, S., Prehn, S., Kalies, K.U., and Hartmann, E. (2000). Mammalian Sec61 is associated with Sec62 and Sec63. J Biol Chem *275*, 14550-14557.

Miller, E.A., and Barlowe, C. (2010). Regulation of coat assembly--sorting things out at the ER. Curr Opin Cell Biol *22*, 447-453.

Milovanovic, D., Honigmann, A., Koike, S., Gottfert, F., Pahler, G., Junius, M., Mullar, S., Diederichsen, U., Janshoff, A., Grubmuller, H.*, et al.* (2015). Hydrophobic mismatch sorts SNARE proteins into distinct membrane domains. Nat Commun *6*, 5984.

Muller, L., de Escauriaza, M.D., Lajoie, P., Theis, M., Jung, M., Muller, A., Burgard, C., Greiner, M., Snapp, E.L., Dudek, J.*, et al.* (2010). Evolutionary gain of function for the ER membrane protein Sec62 from yeast to humans. Mol Biol Cell *21*, 691-703.

Noda, Y., and Yoda, K. (2013). Molecular mechanisms of the localization of membrane proteins in the yeast Golgi compartments. Biosci Biotechnol Biochem *77*, 435-445.

Onishi, Y., Yamagishi, M., Imai, K., Fujita, H., Kida, Y., and Sakaguchi, M. (2013). Stop-and-move of a marginally hydrophobic segment translocating across the endoplasmic reticulum membrane. J Mol Biol *425*, 3205-3216.

Orci, L., Ravazzola, M., Meda, P., Holcomb, C., Moore, H.P., Hicke, L., and Schekman, R. (1991). Mammalian Sec23p homologue is restricted to the endoplasmic reticulum transitional cytoplasm. Proc Natl Acad Sci U S A *88*, 8611-8615.

Panzner, S., Dreier, L., Hartmann, E., Kostka, S., and Rapoport, T.A. (1995). Posttranslational protein transport in yeast reconstituted with a purified complex of Sec proteins and Kar2p. Cell *81*, 561-570.

Paquet, M.E., Cohen-Doyle, M., Shore, G.C., and Williams, D.B. (2004). Bap29/31 influences the intracellular traffic of MHC class I molecules. J Immunol *172*, 7548-7555.

Pfeffer, S., Dudek, J., Schaffer, M., Ng, B.G., Albert, S., Plitzko, J.M., Baumeister, W., Zimmermann, R., Freeze, H.H., Engel, B.D.*, et al.* (2017). Dissecting the molecular organization of the translocon-associated protein complex. Nat Commun *8*, 14516.

Pitonzo, D., Yang, Z., Matsumura, Y., Johnson, A.E., and Skach, W.R. (2009). Sequence-specific retention and regulated integration of a nascent membrane protein by the endoplasmic reticulum Sec61 translocon. Mol Biol Cell *20*, 685-698.

Powers, J., and Barlowe, C. (1998). Transport of axl2p depends on erv14p, an ER-vesicle protein related to the Drosophila cornichon gene product. J Cell Biol *142*, 1209-1222.

Quiroga, R., Trenchi, A., Gonzalez Montoro, A., Valdez Taubas, J., and Maccioni, H.J. (2013). Short transmembrane domains with high-volume exoplasmic halves determine retention of Type II membrane proteins in the Golgi complex. J Cell Sci *126*, 5344-5349.

Rapoport, T.A. (2007). Protein translocation across the eukaryotic endoplasmic reticulum and bacterial plasma membranes. Nature *450*, 663-669.

Ratjen, F., and Grasemann, H. (2012). New therapies in cystic fibrosis. Curr Pharm Des *18*, 614-627.

Reithinger, J.H., Kim, J.E., and Kim, H. (2013). Sec62 protein mediates membrane insertion and orientation of moderately hydrophobic signal anchor proteins in the endoplasmic reticulum (ER). J Biol Chem *288*, 18058-18067.

Reithinger, J.H., Yim, C., Kim, S., Lee, H., and Kim, H. (2014). Structural and functional profiling of the lateral gate of the Sec61 translocon. J Biol Chem *289*, 15845-15855.

Richard, M., Boulin, T., Robert, V.J., Richmond, J.E., and Bessereau, J.L. (2013). Biosynthesis of ionotropic acetylcholine receptors requires the evolutionarily conserved ER membrane complex. Proc Natl Acad Sci U S A *110*, E1055-1063.

Riordan, J.R. (2005). Assembly of functional CFTR chloride channels. Annu Rev Physiol *67*, 701-718.

Riordan, J.R. (2008). CFTR function and prospects for therapy. Annu Rev Biochem *77*, 701-726.

Riordan, J.R., Rommens, J.M., Kerem, B., Alon, N., Rozmahel, R., Grzelczak, Z., Zielenski, J., Lok, S., Plavsic, N., Chou, J.L.*, et al.* (1989). Identification of the cystic fibrosis gene: cloning and characterization of complementary DNA. Science *245*, 1066-1073.

Satoh, T., Ohba, A., Liu, Z., Inagaki, T., and

Satoh, A.K. (2015). dPob/EMC is essential for biosynthesis of rhodopsin and other multi-pass membrane proteins in Drosophila photoreceptors. Elife *4*.

Sauri, A., McCormick, P.J., Johnson, A.E., and Mingarro, I. (2007). Sec61alpha and TRAM are sequentially adjacent to a nascent viral membrane protein during its ER integration. J Mol Biol *366*, 366-374.

Sauvageau, E., Rochdi, M.D., Oueslati, M., Hamdan, F.F., Percherancier, Y., Simpson, J.C., Pepperkok, R., and Bouvier, M. (2014). CNIH4 interacts with newly synthesized GPCR and controls their export from the endoplasmic reticulum. Traffic *15*, 383-400.

Schamel, W.W., Kuppig, S., Becker, B., Gimborn, K., Hauri, H.P., and Reth, M. (2003). A high-molecular-weight complex of membrane proteins BAP29/BAP31 is involved in the retention of membrane-bound IgD in the endoplasmic reticulum. Proc Natl Acad Sci U S A *100*, 9861-9866.

Schober, D.A., Gill, M.B., Yu, H., Gernert, D.L., Jeffries, M.W., Ornstein, P.L., Kato, A.S., Felder, C.C., and Bredt, D.S. (2011). Transmembrane AMPA receptor regulatory proteins and cornichon-2 allosterically regulate AMPA receptor antagonists and potentiators. J Biol Chem *286*, 13134-13142.

Schwenk, J., Harmel, N., Brechet, A., Zolles, G., Berkefeld, H., Muller, C.S., Bildl, W., Baehrens, D., Huber, B., Kulik, A.*, et al.* (2012). High-resolution proteomics unravel architecture and molecular diversity of native AMPA receptor complexes. Neuron *74*, 621-633.

Seppala, S., Slusky, J.S., Lloris-Garcera, P., Rapp, M., and von Heijne, G. (2010). Control of membrane protein topology by a single C-terminal residue. Science *328*, 1698-1700.

Shao, S., and Hegde, R.S. (2011). Membrane protein insertion at the endoplasmic reticulum. Annu Rev Cell Dev Biol *27*, 25-56.

Sharpe, H.J., Stevens, T.J., and Munro, S. (2010). A comprehensive comparison of transmembrane domains reveals organelle-specific properties. Cell *142*, 158-169.

Sherwood, P.W., and Carlson, M. (1999). Efficient export of the glucose transporter Hxt1p from the endoplasmic reticulum requires Gsf2p. Proc Natl Acad Sci U S A *96*, 7415-7420.

Shurtleff, M.J., Itzhak, D.N., Hussmann, J.A., Schirle Oakdale, N.T., Costa, E.A., Jonikas, M., Weibezahn, J., Popova, K.D., Jan, C.H., Sinitcyn, P.*, et al.* (2018). The ER membrane protein complex interacts cotranslationally to enable biogenesis of multipass membrane proteins. Elife *7*, e37018.

Skach, W.R. (2009). Cellular mechanisms of membrane protein folding. Nat Struct Mol Biol *16*, 606-612.

Sommer, N., Junne, T., Kalies, K.U., Spiess, M., and Hartmann, E. (2013). TRAP assists membrane protein topogenesis at the mammalian ER membrane. Biochim Biophys Acta *1833*, 3104-3111.

Sosnay, P.R., Siklosi, K.R., Van Goor, F., Kaniecki, K., Yu, H., Sharma, N., Ramalho, A.S., Amaral, M.D., Dorfman, R., Zielenski, J.*, et al.* (2013). Defining the disease liability of variants in the cystic fibrosis transmembrane conductance regulator gene. Nat Genet *45*, 1160-1167.

Tamborero, S., Vilar, M., Martinez-Gil, L., Johnson, A.E., and Mingarro, I. (2011). Membrane insertion and topology of the translocating chain-associating membrane protein (TRAM). J Mol Biol *406*, 571-582.

Tang, X., Snowball, J.M., Xu, Y., Na, C.L., Weaver, T.E., Clair, G., Kyle, J.E., Zink, E.M., Ansong, C., Wei, W.*, et al.* (2017). EMC3 coordinates surfactant protein and lipid homeostasis required for respiration. J Clin Invest *127*, 4314-4325.

Tannous, A., Pisoni, G.B., Hebert, D.N., and Molinari, M. (2015). N-linked sugar-regulated protein folding and quality control in the ER. Semin Cell Dev Biol *41*, 79-89.

Taylor, N.M.I., Manolaridis, I., Jackson, S.M., Kowal, J., Stahlberg, H., and Locher, K.P. (2017). Structure of the human multidrug transporter ABCG2. Nature *546*, 504-509.

Travers, K.J., Patil, C.K., Wodicka, L., Lockhart, D.J., Weissman, J.S., and Walter, P. (2000). Functional and genomic analyses reveal an essential coordination between the unfolded protein response and ER-associated degradation. Cell *101*, 249-258.

Tsukazaki, T., Mori, H., Fukai, S., Ishitani, R., Mori, T., Dohmae, N., Perederina, A., Sugita, Y., Vassylyev, D.G., Ito, K.*, et al.* (2008). Conformational transition of Sec machinery inferred from bacterial SecYE structures. Nature *455*, 988-991.

Tyedmers, J., Lerner, M., Bies, C., Dudek, J., Skowronek, M.H., Haas, I.G., Heim, N., Nastainczyk, W., Volkmer, J., and Zimmermann, R. (2000). Homologs of the yeast Sec complex subunits Sec62p and Sec63p are abundant proteins in dog pancreas microsomes. Proc Natl Acad Sci U S A *97*, 7214-7219.

Van den Berg, B., Clemons, W.M., Jr., Collinson, I., Modis, Y., Hartmann, E., Harrison, S.C., and Rapoport, T.A. (2004). X-ray structure of a protein-conducting channel. Nature *427*, 36-44.

van Willigen, M., Vonk, A.M., Yeoh, H.Y., Kruisselbrink, E., Kleizen, B., van der Ent, C.K., Egmond, M.R., de Jonge, H.R., Braakman, I., Beekman, J.M.*, et al.* (2019). Folding-function relationship of the most common cystic fibrosis-causing CFTR conductance mutants. Life Sci Alliance *2*.

Voigt, S., Jungnickel, B., Hartmann, E., and Rapoport, T.A. (1996). Signal sequence-dependent function of the TRAM protein during early phases of protein transport across the endoplasmic reticulum membrane. J Cell Biol *134*, 25-35.

von Heijne, G. (2007). The membrane protein universe: what's out there and why bother? J Intern Med *261*, 543-557.

Voorhees, R.M., Fernandez, I.S., Scheres, S.H., and Hegde, R.S. (2014). Structure of the mammalian ribosome-Sec61 complex to 3.4 A resolution. Cell *157*, 1632-1643.

Wallin, E., and von Heijne, G. (1998). Genome-wide analysis of integral membrane proteins from eubacterial, archaean, and eukaryotic organisms. Protein Sci *7*, 1029-1038.

Wang, B., Heath-Engel, H., Zhang, D., Nguyen, N., Thomas, D.Y., Hanrahan, J.W., and Shore, G.C. (2008). BAP31 interacts with Sec61 translocons and promotes retrotranslocation of CFTRDeltaF508 via the derlin-1 complex. Cell *133*, 1080-1092.

Willer, M., Jermy, A.J., Young, B.P., and Stirling, C.J. (2003). Identification of novel protein-protein interactions at the cytosolic surface of the Sec63 complex in the yeast ER membrane. Yeast *20*, 133-148.

Wittke, S., Dunnwald, M., and Johnsson, N. (2000). Sec62p, a component of the endoplasmic reticulum protein translocation machinery, contains multiple binding sites for the Sec-complex. Mol Biol Cell *11*, 3859-3871.

Wu, X., Cabanos, C., and Rapoport, T.A. (2019). Structure of the post-translational protein translocation machinery of the ER membrane. Nature *566*, 136-139.

Zen, K., Utech, M., Liu, Y., Soto, I., Nusrat, A., and Parkos, C.A. (2004). Association of BAP31 with CD11b/CD18. Potential role in intracellular trafficking of CD11b/CD18 in neutrophils. J Biol Chem *279*, 44924-44930.

Zhang, S., Xu, C., Larrimore, K.E., and Ng, D.T.W. (2017a). Slp1-Emp65: A guardian factor that protects folding polypeptides from promiscuous degradation. Cell *171*, 346-357 e312.

Zhang, Z., Liu, F., and Chen, J. (2017b). Conformational changes of CFTR upon phosphorylation and ATP binding. Cell *170*, 483-491 e488.

Zimmermann, R., and Blatch, G.L. (2009). A novel twist to protein secretion in eukaryotes. Trends Parasitol *25*, 147-150.

Chapter 2

Analysis of protein folding, transport, and degradation in living cells by radioactive pulse chase

AUTHORS AND AFFILIATIONS:
Nicholas McCaul[1,2], Hui Ying Yeoh[1], Guus van Zadelhoff[1], Naomi Lodder[1], Bertrand Kleizen[1], Ineke Braakman[1]
[1]Cellular Protein Chemistry, Utrecht University, Utrecht, The Netherlands
[2]Program in Cellular and Molecular Medicine, Boston Children's Hospital, Boston, MA, USA

Article published in Journal of Visualized Experiments, 2019.
Video Website: https://www.jove.com/video/58952/analysis-protein-folding-transport-degradation-living-cells

KEYWORDS:
Protein folding; radiolabeling; SDS-PAGE; immunoprecipitation; pulse chase; conformational analysis; kinetics

SUMMARY:
Here we describe a protocol for a general pulse-chase method that allows the kinetic analysis of folding, transport, and degradation of proteins to be followed in live cells.

ABSTRACT

Radioactive pulse-chase labeling is a powerful tool for studying the conformational maturation, the transport to their functional cellular location, and the degradation of target proteins in live cells. By using short (pulse) radiolabeling times (<30 min) and tightly controlled chase times, it is possible to label only a small fraction of the total protein pool and follow its folding. When combined with nonreducing/reducing SDS-polyacrylamide gel electrophoresis (SDS-PAGE) and immunoprecipitation with (conformation-specific) antibodies, folding processes can be examined in great detail. This system has been used to analyze the folding of proteins with a huge variation in properties such as soluble proteins, single and multi-pass transmembrane proteins, heavily N- and O-glycosylated proteins, and proteins with and without extensive disulfide bonding. Pulse-chase methods are the basis of kinetic studies into a range of additional features, including co- and posttranslational modifications, oligomerization, and polymerization, essentially allowing the analysis of a protein from birth to death. Pulse-chase studies on protein folding are complementary with other biochemical and biophysical methods for studying proteins *in vitro* by providing increased temporal resolution and physiological information. The methods as described within this paper are adapted easily to study the folding of almost any protein that can be expressed in mammalian or insect-cell systems.

INTRODUCTION

The folding of even relatively simple proteins involves many different folding enzymes, molecular chaperones, and covalent modifications[1]. A complete reconstitution of these processes *in vitro* is practically impossible, given the vast number of different components involved. It is highly desirable, therefore, to study protein folding *in vivo*, in live cells. Radioactive pulse-chase techniques prove a powerful tool for studying the synthesis, folding, transport, and degradation of proteins in their natural environment.

The metabolic labeling of proteins during a short pulse with ^{35}S-labeled methionine/cysteine, followed by a chase in the absence of a radioactive label, allows specific tracking of a population of newly synthesized proteins in the wider cellular milieu. Then, target proteins can be isolated *via* immunoprecipitation and analyzed *via* SDS-PAGE or other techniques. For many proteins, their journey through the cell is marked by modifications that are visible on SDS-PAGE gel. For example, the transport of glycosylated proteins from the endoplasmic reticulum (ER) to the Golgi complex is often accompanied by modifications of N-linked glycans or the addition of O-linked glycans[2,3]. These modifications cause large increases in the apparent molecular mass, which can be seen by mobility changes in SDS-PAGE. Maturation can also be marked by proteolytic cleavages, such as signal-peptide cleavage or the removal of pro-peptides, resulting in changes in the apparent molecular mass that can be followed easily on SDS-PAGE gel[4]. Radioactivity has considerable advantages over comparable techniques such as cycloheximide chases, where novel protein synthesis is prevented, as longer treatments are toxic to cells and do not exclude the majority of older, steady-state proteins from the analysis, as some proteins have half-lives of days. The comparison of proteins under both nonreducing and reducing conditions allows the analysis of disulfide bond formation, an important step in the folding of many secretory proteins[4-7].

Here we describe a general method for the analysis of protein folding and transport in intact cells, using a radioactive pulse-chase approach. While we have aimed to provide the method as detailed as possible, the protocol has an almost limitless potential for adaptability and will allow optimization to study each reader's specific proteins.

Two alternative pulse-chase protocols, one for adherent cells (step 1.1 of the protocol presented here) and one for suspension cells (step 1.2 of the protocol presented here) are provided. The conditions provided here are sufficient to visualize a protein expressed with medium- to high-expression levels. If the reader is working with poorly expressed proteins or various posttreatment conditions, such

as multiple immunoprecipitations, it is necessary to increase the dish size or cell number appropriately.

For suspension pulse chase, the chase samples taken at each time point are all taken from a single tube of cells. The wash steps after the pulse are omitted; instead, further incorporation of ^{35}S is prevented by dilution with a high excess of unlabeled methionine and cysteine.

The presented protocols use radioactive ^{35}S-labeled cysteine and methionine to follow cellular protein-folding processes. All operations with radioactive reagents should be performed using appropriate protective measures to minimize any exposure of the operator and the environment to radioactive radiation and be performed in a designated laboratory. As the pulse-chase labeling technique is relatively inefficient at short pulse times (<15 min), less than 1% of the starting amount of radioactivity is incorporated in the newly synthesized proteins. After the enrichment of the target protein *via* immunoprecipitation, the sample for SDS-PAGE contains less than 0.05% of the starting amount of radioactivity.

Although the ^{35}S methionine and cysteine labeling mix is stabilized, some decomposition, yielding volatile radioactive compounds, will occur. To protect the researcher and the apparatus, some precautions should be taken. The researcher should always obey the local radiation safety rules and may wear a charcoal nursing mask, besides a lab coat and (double) gloves. Stock vials with ^{35}S methionine and cysteine should always be opened in a fume hood, or under a local aspiration point. Known laboratory contamination spots are centrifuges, pipettes, water baths, incubators, and shakers. The contamination of these areas is reduced by using pipette tips with a charcoal filter, positive-seal microcentrifuge tubes (see **Table of Materials**), aquarium charcoal sponges in water baths, charcoal filter papers glued in the pulse-chase dishes, charcoal guard in the aspiration system, and the placement of dishes containing charcoal grains in incubators and storage containers.

PROTOCOL

All radioactive reagents and procedures were handled in accordance with local Utrecht University radiation rules and regulations.

1. Pulse Chase

1.1 Pulse Chase for Adherent Cells

NOTE: The volumes given here are based on 35 mm cell culture dishes. For 60 mm or 100 mm dishes, multiply the volumes by 2 or 4, respectively. This protocol uses a pulse time of 10 min and chase times of 0, 15, 30, 60, 120, and 240 min. These can be varied depending on the specific proteins being studied (discussed below).

1.1.1. Seed adherent cells (*e.g.*, HEK 293, HeLa, CHO) in six 35 mm cell culture dishes so that they will be subconfluent (80% - 90%) on the day of the pulse chase. Use at least one dish per time point and/or condition.

1.1.2. If required, transfect the cells with commercially available transfection reagents according to the manufacturer's instructions; or, virally transduce[8] the cells 1 day before the pulse-chase experiment with the appropriate construct for expression.

1.1.3. Wash the dishes with 1 mL of wash buffer (Hank's balanced salt solution [HBSS]), add 1 mL of starvation medium (normal culture medium lacking methionine and cysteine and fetal bovine serum [FBS], such as minimum essential medium [MEM] without methionine and cysteine but with 10 mM HEPES, pH 7.4), and place the dishes in a 37 °C humidified incubator with 5% CO_2 for 15 min.

1.1.4. Transfer the dishes to the racks in a prewarmed 37 °C water bath so that they are in contact with water but do not float. Start a timer.

1.1.5. At 40 s, aspirate the starvation medium, draw up 300 µL of pulse solution (starvation media + 55 µCi/35 mm dish label, see the note preceding step 1.1.1) into the pipette, and add it gently to the center of the dish at exactly 1 min. Repeat this step at 1 min intervals for the remaining dishes.

NOTE: When handling radioactive material, it is essential to follow appropriate precautions and local rules and regulations to prevent accidental exposure and/or contamination.

1.1.6. At exactly 11 min and for all following dishes, except for the 0 min chase sample, add 1 mL of chase medium directly to the dish, aspirate it, and again, add 1 mL of chase medium. Repeat this step at 1 min intervals for remaining dishes. Transfer all dishes to a 37 °C incubator.

1.1.7. At exactly 16 min, add 1 mL of chase medium (normal culture medium + 10 mM HEPES [pH 7.4], 5 mM cysteine, and 5 mM methionine) directly to the dish on top of the pulse medium to stop labeling; then, aspirate immediately, transfer the dish to a cooled aluminum plate, and add 1 mL of ice-cold stop buffer (HBSS + 20 mM *N*-ethylmaleimide [NEM]).

NOTE: This is the 0 min chase sample. For this sample, proceed directly to step 1.1.9.

1.1.8. Transfer each chase dish back to the water bath 2 min before each chase time (*e.g.*, 24 min for a 15 min chase) and, at the exact chase time (*e.g.*, 26 min for a 15 min chase), aspirate the chase media (or transfer it to a microcentrifuge tube if following protein secretion) and transfer the dish to a cooled aluminum plate. Add 1 mL of ice-cold stop buffer.

1.1.9. Incubate all dishes on ice in the stop buffer for ≥5 min; then, aspirate the stop solution and wash it with 1 mL of ice-cold stop solution. Aspirate the wash and lyse dishes with 300 µL of lysis buffer (phosphate-buffered saline [PBS] + nondenaturing detergent [see **Table of Materials**] + protease inhibitors + 20 mM NEM). Use a cell scraper to ensure that the dishes are lysed quantitatively.

1.1.10. Transfer the lysate to a 1.5 mL microcentrifuge tube and centrifuge for 10 min at 15,000 - 20,000 x *g* and 4 °C to pellet the nuclei.

1.2 Pulse Chase for Suspension Cells

NOTE: To ensure efficient labeling, cells should be pulsed at a concentration of 3 x 10^6 to 5 x 10^6 cells/mL, and chase volumes should be 4x the pulse volume. In the following example, we pulsed 5 x 10^6 cells in a volume of 1 mL for 10 min, to yield five chase time points (0, 15, 30, 60, and 120 min) of 1 mL, containing 1 x 10^6 cells per time point. All solutions are the same as in section 1.1.

1.2.1. Culture the suspension cells (*e.g.*, 3T3, Jurkat) according to a previously published protocol[9] so that there is a sufficient number of cells at the time of the experiment, at least 1 x 10^6 cells per time point and/or condition.

1.2.2. If required, transfect cells with commercially available transfection reagents according to the manufacturer's instructions, or virally transduce[8] the cells 1 day before the pulse-chase experiment with the appropriate construct for expression.

1.2.3. Pellet 5 x 10^6 cells per condition in a 50 mL tube for 5 min at 250 x *g* at room temperature, wash them 1x with 5 mL of starvation media, pellet them again, and resuspend them in 1 mL of starvation media.

1.2.4. Transfer the cells to a 37 °C water bath and incubate them for 10 - 25 min. Agitate the tubes every 10 - 15 min to prevent the cells from settling at the bottom.

1.2.5. Start the timer. At exactly 1 min, add 275 µCi (55 µCi/1 x 10^6 cells) of undiluted label directly to the tube containing cells and swirl to mix.

NOTE: When handling radioactive material, it is essential to follow appropriate precautions and local rules and regulations to prevent accidental exposure and/or contamination.

1.2.6. At exactly 11 min, stop labeling by adding 4 mL of chase media. Mix the sample and immediately transfer 1 mL to a 15 mL tube on ice, containing 9 mL of ice-cold stop solution.

NOTE: This is the 0 min chase sample.

1.2.7. Repeat these steps for each successive time point. Once all time points are collected, pellet the cells for 5 min at 250 x *g* at 4 °C. Aspirate the medium (or transfer it to a new 15 mL tube if following protein secretion). Wash the cells with 5 mL of stop solution and pellet the cells for 5 min at 250 x *g* at 4 °C.

1.2.10. Aspirate the stop solution, completely lyse the cells with 300 µL of ice-cold lysis buffer and incubate them for 20 min on ice to ensure a complete lysis. Transfer the lysate to a 1.5 mL microcentrifuge tube and centrifuge for 10 min at 15,000 - 20,000 x *g* at 4 °C to pellet the nuclei.

2. Immunoprecipitation

2.1. Combine antibody (see the discussion) and 50 µL of immunoprecipitation beads (e.g., protein A-Sepharose) (10% suspension [v/v] in lysis buffer + 0.25% bovine serum albumin [BSA]) in a microcentrifuge tube and incubate them at 4 °C for ~30 min in a shaker.

2.2. Pellet the beads for 1 min at 12,000 x *g* at room temperature and aspirate the supernatant. Add 200 µL of lysate to the antibody-bead mixture and incubate at 4 °C in a shaker for 1 h or head-over-head if the immunoprecipitation requires >1 h.

2.3. Pellet the beads for 1 min at 12,000 x *g* at room temperature. Aspirate the supernatant and add 1 mL of immunoprecipitation wash buffer. Place the sample in a shaker at room temperature for 5 min.

2.4. Pellet the beads as described in step 2.3 and repeat the wash 1x. Then, aspirate the supernatant and resuspend the beads in 20 µL of TE buffer, pH 6.8 (10 mM Tris-HCl, 1 mM EDTA).

2.5. Add 20 µL of 2x sample buffer without the reducing agent, vortex it, heat it for 5 min at 95 °C, and vortex again.

NOTE: If only preparing reducing samples, 2 µL of 500 mM DTT should be added at this point. Then, proceed to step 2.7.

2.6. Pellet the beads as described in step 2.3. Transfer 19 µL of the nonreduced supernatant to a fresh microcentrifuge tube containing 1 µL of 500 mM DTT, centrifuge the sample, and vortex it before heating it for 5 min at 95 °C again.

NOTE: The supernatant is the nonreduced sample.

2.7. Spin down the sample for 1 min at 12,000 x *g*; this is the reduced sample. Cool it down to room temperature and add 1.1 µL of 1 M NEM to both the reduced and the nonreduced sample.

3. SDS-PAGE

3.1. First, determine the appropriate SDS-PAGE resolving gel percentage for the protein of interest. For example, HIV-1 gp120, when deglycosylated, runs at ~60 kDa and is analyzed in a 7.5% gel.

3.2. Prepare the resolving gel mixture without TEMED according to the manufacturer's instructions (x% acrylamide, 375 mM Tris-HCl [pH 8.8,] 0.1% SDS [w/v], and 0.05% SDS ammonium persulfate [APS] [w/v]) and degas under vacuum for >15 min. While the gel mixture is degassing, thoroughly clean the gel glass plates with 70% ethanol and lint-free tissues and place them into a casting apparatus.

3.3. Add TEMED to the resolving gel mixture (at a final concentration of 0.005%

[v/v]), mix thoroughly, and pipette between glass plates, leaving ~1.5 cm space for the stacking gel. Carefully overlay the gel with deionized H_2O or isopropanol and leave it to polymerize.

3.4. Once the resolving gel has polymerized, prepare the stacking gel mixture (4% acrylamide, 125 mM Tris-HCl [pH 6.8], 0.1% SDS [w/v], and 0.025% APS [w/v]).

3.5. Flush the top of the resolving gel with deionized H_2O and, then, remove all water.
Note: Use filter paper to remove the last drops.

3.6 Add TEMED to the stacking gel mixture (0.005% [v/v]), mix thoroughly, and overlay the resolving gel with stacking gel and insert a 15-well comb. Once the stacking gel has polymerized, transfer it to a running chamber and fill the upper and lower chambers with running buffer (25 mM Tris-HCl, 192 mM glycine [pH 8.3], and 0.1% SDS [w/v]).

3.7. Load 10 µL of sample per lane in a 15-lane minigel. Avoid loading the samples in the first and the last lane on the gel and load the nonreducing sample buffer in all empty lanes to prevent the smiling of bands. Run the gels at constant a 25 mA/gel until the dye front is at the bottom of the gel.

3.8. Remove the gels from the glass plates, stain the gels with protein-staining solution (10% acetic acid and 30% methanol in H_2O + 0.25% brilliant blue R250 [w/v]) for 5 min with agitation, and then, destain for 30 min with destaining solution (staining solution without brilliant blue R250).

3.9. Arrange the gels face-down on a plastic wrap and, then, place 0.4 mm chromatography paper on top of them. Place the gel sandwich chromatography paper-side down onto a gel dryer. Following the manufacturer's instructions, dry the gels for 2 h at 80 °C.

3.10. Transfer the dried gels to a cassette and overlay them with autoradiography film or phosphor screen. If using autoradiography film, this step must be performed in a dark room.

REPRESENTATIVE RESULTS

The folding and secretion of HIV-1 gp120 from an adherent pulse chase is shown in **Figure 2.** The nonreducing gel (Cells NR in the figure) shows the oxidative folding of gp120. Immediately after the pulse labeling of 5 min (0 min chase) gp120 appears as a diffuse band higher in the gel, and as the chase progresses, the band migrates down the gel through even more diffused folding intermediates (IT) until it accumulates in the tight band (NT) that represents natively folded gp120. This occurs as the formation of disulfide bonds increases the compactness of the protein, causing it to migrate faster than the fully reduced protein. On the reducing gel (Cells R in the figure), the disulfide bonds on all forms have been reduced such that, at all chase times, they do not affect mobility. This allows the analysis of other modifications. The shift over time from Ru to Rc represents the posttranslational signal-peptide cleavage of gp120: the mobility increases due to the loss of the signal peptide, which increases during the chase as more proteins attain the native fold and lose their signal peptide. On both the nonreducing and reducing gel, the signal begins to decrease from ~1 h onward due to the secretion of gp120. This can be monitored by analyzing the media (Medium in the figure). A comparison of the nonreducing and reducing gels uncovers disulfide bond changes and signal-peptide removal. This was only possible because another modification, N-linked glycosylation, and glycan modifications, were removed from gp120 (and the analysis) by digestion with endoglycosidase H just before SDS-PAGE.

The trafficking of the μ heavy chain of immunoglobulin M (IgM) from a suspension pulse chase is shown in **Figure 3**. A shift over time from HC_{ER} to HC_{Golgi} represents the trafficking of the μ chain from the ER to the Golgi, which precedes secretion from the cell. This change in molecular mass is caused by the modification of N-linked glycans in the Golgi.



Figure 1: Schematic diagram of the protocol for pulse chase, immunoprecipitation, and SDS-PAGE.

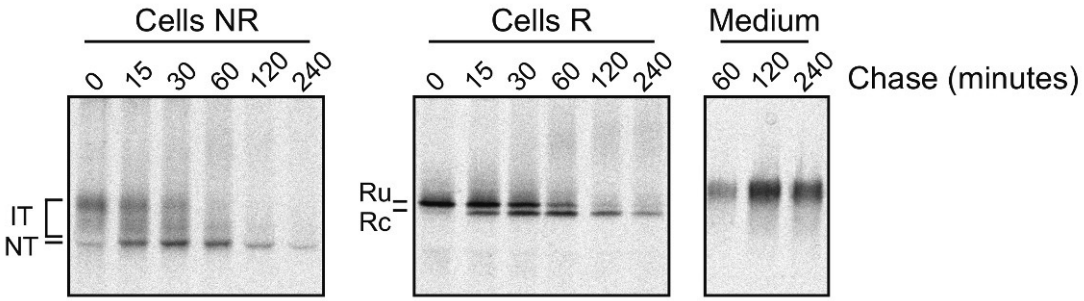


Figure 2: Folding and secretion of HIV-1 gp120, determined by adherent pulse chase.
Subconfluent 35 mm dishes of HeLa cells expressing HIV-1 gp120 were pulse labeled for 5 min and chased for the indicated times. After the immunoprecipitation of gp120, the samples were deglycosylated and analyzed using a 7.5% SDS-PAGE gel. IT = folding intermediates; NT = native gp120; Ru = reduced signal-peptide-uncleaved gp120; Rc = reduced signal-peptide-cleaved gp120; NR: = nonreducing; R = reducing.

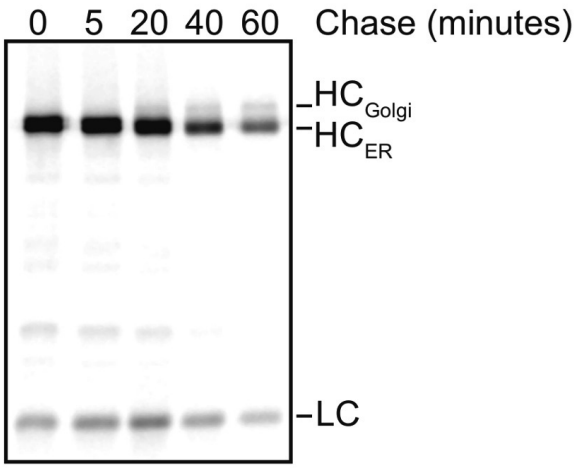


Figure 3: Trafficking of the heavy chain of IgM, determined by suspension pulse chase.
5 x 106 I.29 µ+ B cells were pulse labeled for 5 min and chased for the indicated times. After immunoprecipitation, the samples were analyzed using a 10% SDS-PAGE gel. HC = immunoglobulin µ heavy chain; LC = immunoglobulin light chain.

DISCUSSION

Pulse-chase methods have been essential for developing scientists' understanding of protein folding in intact cells. While we have attempted to provide a method that is as general as possible, this approach has the potential for almost limitless variations to study various processes that occur during the folding, the transport, and the life of proteins inside the cell.

When performing a pulse chase using adherent cells in dishes, it is essential to treat each dish the same as much as possible, as a separate dish is used for each time point and/or condition in an experiment. Especially for short pulse and chase times (<5 min), it is essential to maintain a tight control over the pulse and chase times (with a digital timer). Pulse chases with suspension cells can help to reduce this variability as all samples are taken from a single tube. As some cell types adhere less well to culture dishes than others, care should be taken to ensure that the cells are not washed away during the various medium changes. This can be overcome by either using these cells in suspension or by coating the dishes with poly-L lysine or gelatin, for example, to adhere the cells to the culture dishes. To measure the reproducibility of labeling between dishes, a sample of lysate should be examined by SDS-PAGE to check all samples for identical total labeling and protein pattern. Alternatively, liquid scintillation counting of lysates will establish the total counts-per-minute (cpm) incorporated but will not provide information on the protein population labeled.

If a target protein labels poorly, the signal is increased by increasing the number of cells (or dishes) rather than by increasing the amount of label. Lengthening the pulse time is an option when the kinetics of the studied process will allow this. The ideal pulse time will vary with each target owing to factors such as the expression level, the transcription rate, the number of methionines/cysteines, and the folding rate of the protein. As such, experimentation must be undertaken to determine the best balance between the above-mentioned factors in each experiment while keeping the experimental aim in mind. If intermediates during folding are being studied, for example, it is desirable to pulse the label for as short a time as possible to have the starting material as close to an unfolded state as possible, while balancing expression levels. Alternatively, if the transport or degradation of a protein is the target of study, pulse times may be lengthened to provide the highest levels of signal possible without compromising kinetic information. In general, pulse times can range from 2 - 15 min when using this protocol without modification. Previous experimentation[5] has demonstrated a lag time of ~10 s after the pulse before the incorporation of radioactivity into the total protein pool; this is important to keep in mind when deriving kinetic information from pulse-

chase experiments. If extended pulse times (>1 h) are being used, it is advisable to increase the pulse volume by 1.5 times and place dishes on a rocker in a 37 °C incubator during the pulse to prevent the dishes from drying out. While labeling solutions containing individual ^{35}S-methionine/cysteine or a mix are available, the mix is preferred even when proteins that only contain methionine or cysteine are being labeled as both are needed to maintain general protein synthesis in the cell. If experimental conditions require specific methionine/cysteine labeling, the levels of nonradioactive methionine/cysteine during the pulse must be adjusted accordingly.

Chase times (and the number of time points) are determined in a similar fashion. A good starting place is to set the first chase time (after the 0 min chase) as equal to the pulse time and, then, double the length of time for each successive time point (*e.g.*, 5, 10, 20, and 40 min). However, this must be optimized for each specific protein and question.

To prevent the activation of stress responses by starvation (which may affect protein synthesis and folding), ideally, some unlabeled methionine and cysteine should be added to the starvation and radiolabeling solutions. The quantity will depend on the cell line, the labeling time, the quantity of the radiolabel used, and media volumes, and will need testing. A good starting point is 1% of the amount of cysteine and methionine present in the cell culture medium, which can be increased with increasing pulse times. Starvation periods, whether with or without unlabeled amino acids, should be kept in the range of 15 - 30 min to ensure adequate label incorporation and prevent the activation of stress responses. When using an extended pulse (≥1 h), starvation is not required.

The lysis buffer described here will be suitable for most purposes, but in principle, any buffer system, such as HEPES, Tris, or MES, will work. The detergent concentration needed to lyse cells will depend on the number of cells and detergent volume. The concentration should always be above the critical micelle concentration (CMC) and the quantity of detergent sufficient to lyse cells. An empirical rule of thumb is that 200 µL of 0.5% nondenaturing detergent (see **Table of Materials**) is sufficient to lyse the cell equivalent of ~1 mg of protein (~1 x 10^6 cells). The salt concentration and detergents may also be varied according to the application, but in general, conditions that break open nuclei (high salt, >0.1% SDS) should be avoided as the presence of free DNA will interfere with immunoprecipitation. If this cannot be avoided, for instance, when complete cell lysates including nuclei or pelleted proteins need to be analyzed, DNA can be sheared by passing the cells through a small gauge needle prior to immunoprecipitation. This is preferred over sonication so as to prevent excessive foaming and the production of radioactive aerosols.

For immunoprecipitation, both the optimal quantity of antibodies and the best wash buffer for each antibody-antigen combination must be tested thoroughly to achieve a balance between the desired antigen signal and background. Antibodies should always be present in excess over antigens to ensure quantitative immunoprecipitation; a good starting point is 1 µg of antibodies per immunoprecipitation from a 35 mm dish/1 x 10^6 cells. The background can be decreased by increasing the detergent or salt concentrations. In particular, the addition of ≤0.1% SDS can help to greatly reduce the background but may also disrupt antibody-antigen interactions. To control for the specificity of antibodies during immunoprecipitation, identical cells lacking the target protein should be used when available. If this is not straightforward, such as when endogenous proteins are being analyzed, the overexpression or depletion of the antigen will work. To control for background (and specificity), either preimmune sera (where possible) or isotype controls should be used. To control for antigens binding directly to immunoprecipitation beads, beads without antibody should also be used. The conditions provided here should be considered as a starting point as each antibody-antigen pair will require an optimization of both wash buffer and wash conditions. In case of too much background, do not increase the number of washes but rather the time of washing and/or the composition of the wash buffer. If particularly sensitive interactions such as in coimmunoprecipitations have to be dealt with, it may be preferable to carry out all wash steps at 4 °C, using ice-cold buffers.

One advantage of adherent cells over suspension cells is that drug treatments can be performed at virtually any point during the pulse chase. If used with chaperone inhibitors, for example, it is possible to differentiate its effects on the co- *versus* posttranslational phases of a folding process. This can be extended by adapting the lysis and immunoprecipitation wash buffers (discussed above) to allow the coimmunoprecipitation of protein-chaperone complexes during folding[10-12].

The postlysis treatment of samples will widen the scope of questions that can be addressed. The limited protease digestion of target proteins before immunoprecipitation will provide additional conformational information and has been successfully used to monitor the folding of proteins, especially those lacking disulfide bonds[13,14]. Protein aggregation and complex formation can be monitored by sucrose density-gradient centrifugation prior to immunoprecipitation[15,16].

To take full advantage of pulse chases, the availability of high-quality reagents is required for immunoprecipitations. When examining folding intermediates, it is essential to have antibodies that are capable of pulling down all forms of the protein under analysis. If specific antibodies to the target protein are not available, this can be substituted by using affinity tags. However, this severely restricts the usefulness

of postlysis methods, such as the limited proteolysis, to directly probe the protein conformation, as only tagged fragments can be recovered.

The sensitivity of pulse chases is limited by the number of methionine and cysteine residues in the protein in question. Proteins with low numbers of methionine/cysteine residues coupled with a low expression level are undetectable in pulse-chase experiments. When performing postlysis modifications such as limited proteolysis, only methionine/cysteine-containing fragments will be detectable.

To conclude, given the kinetic detail that pulse chases provide, they are complementary to many other techniques and tools used to study molecular cell biology at the steady-state level. As such, they continue to be an invaluable component in the molecular biologist's toolbox.

ACKNOWLEDGMENTS

The authors thank all members of the Braakman lab, past and present, for their fruitful discussions and help in developing the methods presented in this article. This project has received funding from both the European Research Council under the European Union's Seventh Framework Programme (FP7/2007-2013) N° 235649 and the Netherlands Organization of Scientific Research (NWO) under the ECHO-program N° 711.012.008.

REFERENCES

1. Ellgaard, L., McCaul, N., Chatsisvili, A., Braakman, I. Co- and post-translational protein folding in the ER. *Traffic.* **17** (6), 615-638 (2016).

2. Pisoni, G. B., Molinari, M. Five questions (with their Answers) on ER-associated degradation. *Traffic.* **17** (4), 341-350 (2016).

3. Lamriben, L., Graham, J. B., Adams, B. M., Hebert, D. N. N-glycan-based ER molecular chaperone and protein quality control system: The calnexin binding cycle. *Traffic.* **17** (4), 308-326 (2016).

4. Snapp, E. L. *et al.* Structure and topology around the cleavage site regulate post-translational cleavage of the HIV-1 gp160 signal peptide. *Elife.* **6**, e26067 (2017).

5. Braakman, I., Hoover-Litty, H., Wagner, K. R., Helenius, A. Folding of influenza hemagglutinin in the endoplasmic reticulum. *Journal of Cell Biology.* **114** (3), 401-411 (1991).

6. Jansens, A., van Duijn, E., Braakman, I. Coordinated nonvectorial folding in a newly synthesized multidomain protein. *Science.* **298** (5602), 2401-2403 (2002).

7. Land, A., Braakman, I. Folding of the human immunodeficiency virus type 1 envelope glycoprotein in the endoplasmic reticulum. *Biochimie.* **83** (8), 783-790 (2001).

8. Singh, Y., Garden, O. A., Lang, F., Cobb, B. S. Retroviral transduction of helper T cells as a genetic approach to study mechanisms controlling their differentiation and function. *Journal of Visualized Experiments.* (117), e54698 (2016).

9. Das, A. T., Land, A., Braakman, I., Klaver, B., Berkhout, B. HIV-1 evolves into a nonsyncytium-inducing virus upon prolonged culture *in vitro*. *Virology.* **263** (1), 55-69 (1999).

10. Chen, W., Helenius, J., Braakman, I., Helenius, A. Cotranslational folding and calnexin binding during glycoprotein synthesis. *Proceedings of the National Academy of Sciences.* **92** (14), 6229-6233 (1995).

11. Daniels, R., Kurowski, B., Johnson, A. E., Hebert, D. N. N-linked glycans direct the cotranslational folding pathway of influenza hemagglutinin. *Molecular Cell.* **11** (1), 79-90 (2003).

12. Ferreira, L. R., Norris, K., Smith, T., Hebert, C., Sauk, J. J. Association of Hsp47, Grp78, and Grp94 with procollagen supports the successive or coupled action of molecular chaperones. *Journal of Cellular Biochemistry.* **56** (4), 518-526 (1994).

13. Hoelen, H. *et al.* The primary folding defect and rescue of DeltaF508 CFTR emerge during translation of the mutant domain. *PLoS One.* **5** (11), e15458 (2010).

14. Kleizen, B., van Vlijmen, T., de Jonge, H. R., Braakman, I. Folding of CFTR is predominantly cotranslational. *Molecular Cell.* **20** (2), 277-287 (2005).

15. Hagiwara, M., Ling, J., Koenig, P. A., Ploegh, H. L. Posttranscriptional regulation of glycoprotein quality control in the endoplasmic reticulum Is controlled by the E2 Ub-conjugating enzyme UBC6e. *Molecular Cell.* **63** (5), 753-767 (2016).

16. Copeland, C. S., Doms, R. W., Bolzau, E. M., Webster, R. G., Helenius, A. Assembly of influenza hemagglutinin trimers and its role in intracellular transport. *Journal of Cell Biology.* **103** (4), 1179-1191 (1986).

MATERIALS

Name	Company	Catalog Number	Comments
1.5 mL safeseal micro-centrifuge tubes	Sarstedt	72.706.400	
Acetic Acid	Sigma	A6283	glacial acetic acid
BAS Storage phosphor screen 20x25 cm	GE Life Sciences	28956475	
Bromophenol Blue	Sigma	B8026	Molecular biology grade
Carestream Biomax MR films	Kodak	Z350370-50EA	
Cell-culture media	Various	N/A	Normal cell culture media for specific cell-lines used
Cell-culture media, no methionine/ cysteine	Various	N/A	Same media formulation as normal culture media e.g DMEM/ MEM/ RPMI, lacking methionine and cysteine
Charcoal filter paper	Whatman	1872047	
Charcoal filtered pipette tips	Molecular bioproducts	5069B	
Charcoal vacu-guard	Whatman	67221001	
Coomassie Brilliant Blue R250	Sigma	112,553	for electrophoresis
Cysteine	Sigma	C7352	Molecular biology grade, Make 500 mM stock, store at -20
Dithiothreitol (DTT)	Sigma	10197777001	Molecular biology grade
EasyTag Express35S Protein Labeling Mix	Perkin Elmer	NEG772014MC	Other size batches of label are available depending on useage
EDTA	Sigma	E1644	Molecular biology grade
Gel-drying equipment	Various	N/A	
Glycerol	Sigma	G5516	Molecular biology grade
Grade 3 chromatography paper	GE Life Sciences	3003-917	
Hank's Balanced Salt Solution (HBSS)	Gibco	24020117	
Kimwipes delicate task wipes	VWR	21905-026	
MES	Sigma	M3671	Molecular biology grade

Methanol	Sigma	MX0490	
Methionine	Sigma	M5308	Molecular biology grade, Make 250 mM stock, store at -20
Minigel casting/running equipment	Various	N/A	
NaCl	Sigma	S7653	Molecular biology grade
N-ethylmaleimide	Sigma	E3876	Molecular biology grade, Make 1M stock in 100% ethanol, store at -20
PBS	Sigma	P5368	Molecular biology grade
Protein-A Sepharose fastflow beads	GE health-care	17-5280-04	
Sodium Dodecyl Sulfate (SDS)	Sigma	L3771	Molecular biology grade
Triton X-100	Sigma	T8787	Molecular biology grade
Trizma base (Tris)	Sigma	T6066	Molecular biology grade
Typhoon IP Biomolecular imager	Amersham	29187194	
Unwire Test Tube Rack 20 mm for waterbath	Nalgene	5970-0320PK	

Chapter 3

Analysis of CFTR domain assembly with antibodies against transmembrane domains

AUTHORS:
Hui Ying Yeoh, Marjolein Mijnders, Marcel van Willigen, Floor Peters, Bertrand Kleizen, Peter van der Sluijs, and Ineke Braakman

ABSTRACT

The Cystic Fibrosis Transmembrane Conductance Regulator (CFTR) is a multispan membrane protein that functions as ion channel. Its domains fold during biosynthesis and need to assemble to form a functional protein. Misfolded CFTR domains can impair CFTR function and thereby cause Cystic Fibrosis. It is therefore important to understand the folding of each domain. Due to the lack of reagents, the folding of CFTR transmembrane domains (TMDs) and their assembly is poorly understood. To study CFTR TMD folding, we generated antibodies against TMD1 and TMD2. By using radiolabeling, limited proteolysis, and immunoprecipitation, these antibodies revealed that the TMDs became more protease resistant, suggestive of post-translational conformational changes. To analyze these conformational changes, we identified the proteolytic fragments derived from the TMDs using different CFTR mutants and truncations. Fragment identification indicated that TMD post-translational conformational changes were the result of CFTR domain assembly. Our findings enhance the understanding of the folding dynamics of CFTR, a conserved structure among Type I ABC transporters.

INTRODUCTION

CFTR is a protein channel that regulates the flow of chloride across the apical membrane of epithelial cells by switching between open and closed states (Gadsby et al., 2006). CFTR belongs to the ABC transporter superfamily and contains 2 TMDs, 2 nucleotide binding domains (NBD) and an unstructured regulatory region R. These domains need to interact and assemble with each other to form a functional anion channel. Disrupting CFTR domain folding and assembly can cause cystic fibrosis (CF), a disease where movement of ion and water across the apical membrane is compromised, leading to accumulation of fluid in the respiratory, digestive and reproductive organs (Cohen and Prince, 2012; Ratjen and McColley, 2012). The most common mutation in the CFTR gene that causes CF is F508del. Loss of the phenylalanine at this position impairs NBD1 folding and results in protein degradation from the ER (Du et al., 2005; Riordan, 2008).

CFTR domains fold co-translationally and assemble mostly post-translationally (Du et al., 2005; Khushoo et al., 2011; Kleizen et al., 2005). An assembled CFTR will travel through the secretory pathway, become complex-glycosylated in the Golgi complex and reach the plasma membrane. The cryo-EM structure revealed that assembled and complex-glycosylated CFTR has a tight packing of TMD1-NBD2 and TMD2-NBD1 (Figure 1, Left panel) (Liu et al., 2017; Zhang et al., 2017). These interactions are established during domain assembly via the intercellular-loops (ICLs) (Kleizen et al., submitted; Marjolein Mijnders Thesis, 2019). The TMD-NBD interactions are involved in opening and closing the channel. When CFTR is in a closed dephosphorylated state, its R-region is located between the N-terminal and C-terminal halves of the molecule, preventing dimerization of the NBDs (Figure 1, Left panel). Upon ATP binding, the R-region is phosphorylated, after which it moves out from between the NBDs and allows their dimerization (Figure 1, Right panel). Following NBD dimerization, the TMDs also change their position because of the TMD-NBD attachments and then open the channel. In the cryo-EM structure of phosphorylated CFTR, TM8 and TM12 in TMD2 have shifted towards TMD1 and are engaged in new interactions with TM1 and TM2 (Figure 1, right panel)(Zhang et al., 2017). This results in obstruction of the extracellular side of the pore and blocks ion passage. Based on this observation, Zhang et al (2017) proposed that ATP binding and phosphorylation does not result in a rigid, opened channel and that phosphorylated CFTR still can control ion flow via the movement of TM8 and TM12.

Although the conformation of mature CFTR has been solved, how CFTR folds its TMDs and assembles them into a functional structure is poorly understood, caused in part by the paucity of suitable reagents. We here describe the generation and characterization of antibodies against the TMDs that allowed us to identify

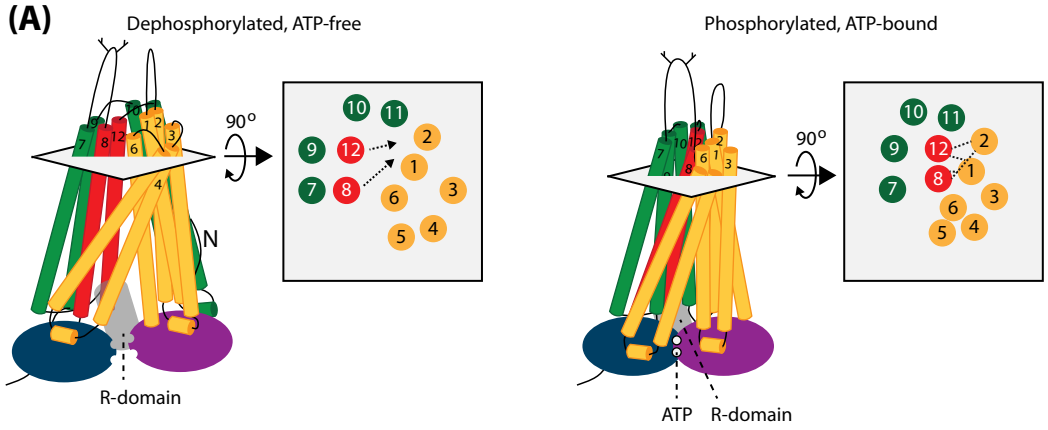


Figure 1: Model for CFTR TMDs regulating channel opening and closing.
(A) Left: Before ATP binding, TM8 and TM12 are positioned at the TMD2-NBD2 half of CFTR and are closer to TM7 and TM9. Right: After ATP binding and phosphorylation, TM8 and TM12 shift toward the other half of the protein and form an interaction with TM1 and TM2. (This model is drawn based on Zhang et al., 2017, PDB:5W81)

domain-domain interactions during CFTR folding. By using CFTR mutants and the TMD antibodies, we established the following sequence of events of CFTR domain assembly: First ICL1 tethers to NBD1 co-translationally, followed by the post-translational interaction of ICL4-NBD1 which allows TMD1 and TMD2 to assemble and ICL3 to tether onto NBD2, and in parallel, ICL2 binding to NBD2.

RESULTS

Peptide antibodies detect in-vitro synthesized CFTR domains.

We raised antibodies against peptides aa 364-381, 1135-1149 and 1172-1186 of CFTR and named them TMD1C, I4N and TMD2C, respectively (Figure 2A). Peptide sequences were selected through NIH software AbDesigner which calculates an 'immunogenicity' score based amongst others on hydropathy and secondary structure conservation, uniqueness, accessibility, and post-translational modifications. These antibodies were first tested on TMD1 and TMD2, which were generated in a combined *in-vitro* translation-translocation system. The relevant CFTR domains were synthesized from their mRNAs using rabbit reticulocyte lysate and ^{35}S -labeled methionine and cysteine. Semi-permeable cell membranes were added to the system as a source of ER membrane for the targeting, insertion, and translocation of the translating nascent chains. Total cell membranes were pelleted

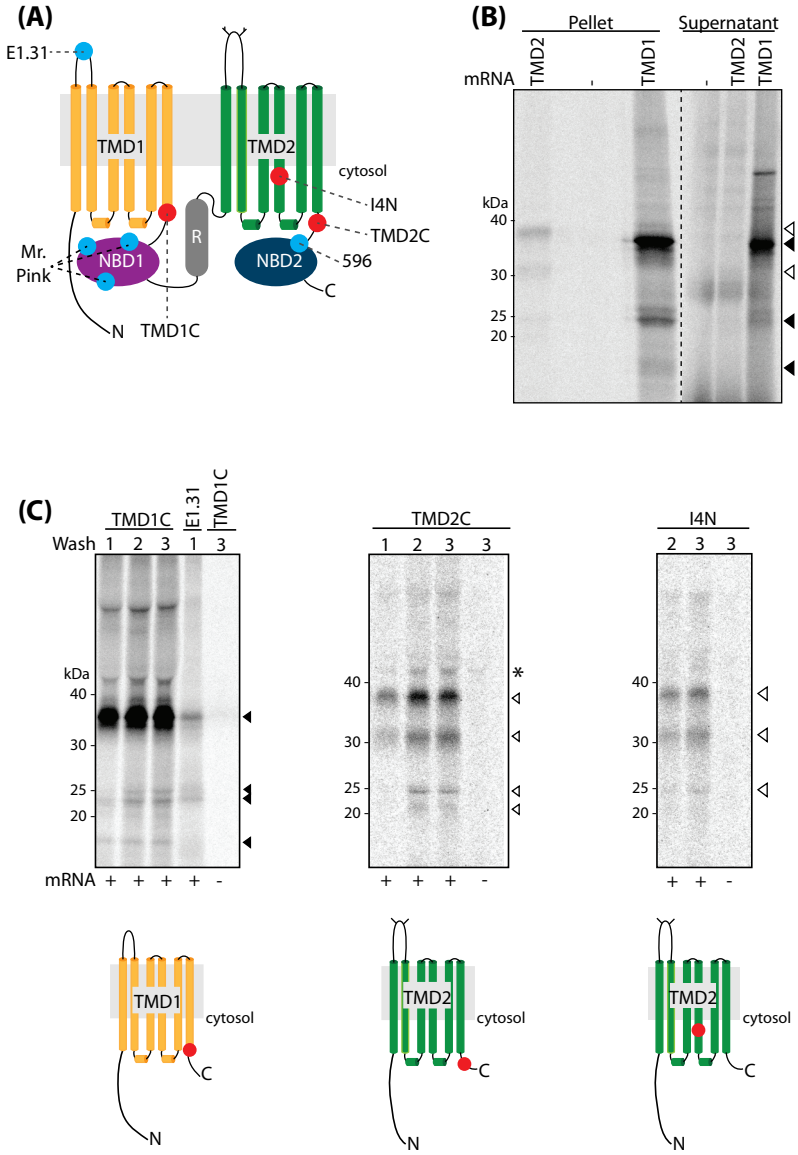


Figure 2: TMD antibodies recognize in-vitro synthesized CFTR domains.
(A) Cartoon of CFTR showing the position of the epitopes to which antibodies were developed in rabbits and mouse. Red circles indicate the epitopes of the new TMD antibodies and the blue circles represent the epitopes of already-made antibodies. (B) TMD1 and TMD2 were translated independently in vitro and translocated in the presence of semi-permeabilized cells as a source of ER membranes. Translocated (pellet fraction) and non-translocated (supernatant fraction) TMD1 and TMD2 were separated by centrifugation and analyzed by 12% SDS-PAGE. (C) Left panel: Immunoprecipitation of TMD1 in-vitro translated as in (B) with TMD1C and 3 different washes (1-3), immunoprecipitation of TMD1 with the E1.31 antibody was used as a control. Middle panel: Immunoprecipitation of TMD2 in-vitro translated as in (B) with TMD2C and 3 different washes (1-3). Right panel: Immunoprecipitation of TMD2 with I4N and washes 2 or 3. Black arrowheads: TMD1 bands; white arrowheads: TMD2 bands; *: background band.

and CFTR domains in supernatant and pellet fractions were recovered and analyzed on SDS-PAA gels.

CFTR TMDs were inserted into semi-permeable membranes during the *in-vitro* translation-translocation process, as both the expressed TMD1 and TMD2 appeared in the pellet fraction (Figure 2B). TMD1 was detected essentially as one major protein at 35 kDa while TMD2 was resolved in bands at 32 kDa and 37 kDa (Figures 2B and 2C) caused by the presence of two oligomannose-type N-glycans (2.5 kDa each) on the 37 kDa form. The electrophoretic mobilities of the expressed TMDs were lower than of the calculated translation products (45 kDa for TMD1 and 40 kDa for TMD2 (without oligosaccharide)), possibly because their mobilities in SDS-PAGE were affected by charged residues and hydrophobicity. Half of the TMD1 molecules were not inserted properly and remained in the supernatant fraction (Figure 2B), because translocation was not fully recapitulated in the reconstituted system. Despite these drawbacks, sufficient amounts of membrane-inserted TMDs were produced for antibody testing.

Immunoprecipitation of *in-vitro* translated and translocated TMD1 and TMD2 by the three antibodies showed that they recognized their epitopes in these TMD1 and TMD2 proteins (Figure 2C). To optimize analysis, we tested different buffers to wash the immunoprecipitates. The association of TMD1C to TMD1 under all 3 conditions, 0.05% SDS (Wash 1), pH 8.0 (Wash 2), and 0.5% Triton-X-100 (Wash 3), was better than for the E1.31 antibody (Figure 2C, left panel), which targets extracellular loop 1 (ECL1) of TMD1 (Figure 2A). The TMD2C antibody showed efficient binding to TMD2 with both Washes 2 and 3 (Figure 2C, middle panel), but this binding was decreased in the presence of SDS (Wash 1) (Figure 2C, middle panel). The I4N antibody showed less binding of TMD2 compared to TMD2C (Figure 2C, right panel), but did well in both Washes 2 and 3.

Our results show that the three antibodies recognized their epitopes from *in-vitro* translated domains, with TMD2C and I4N binding to TMD2 with different efficiencies. Next, we probed whether the antibodies detected the TMDs in the context of full-length CFTR expressed in cells.

TMD antibodies recognize pre- and post-assembly CFTR transmembrane domains

Since the new antibodies recognized their epitopes in *in-vitro* synthesized proteins, we next asked whether they could also recognize their epitopes in cells. We therefore expressed single TMD constructs as well as CFTR in HEK293T cells that were subsequently radiolabeled with ^{35}S-methionine and -cysteine (Figure 3A). Full-length CFTR was chased for 1 hour to obtain a pool of molecules representing various stages of maturation, thus containing both pre- and post-assembled CFTR.

With this strategy, we could investigate whether the antibodies detected the TMDs from these different molecular CFTR species. Cells expressing the single TMD1 or TMD2 domains were not subjected to a chase period, because single domains cannot undergo domain assembly nor further maturation.

TMD1C immunoprecipitated expressed TMD1 (Figure 3B, TMD1C panel). We also found that TMD1 immunoprecipitated different, additional low molecular weight species from cells than found in the *in-vitro* translation-translocation system (Figures 2C and 3B). The TMD1C epitope is located at the C-terminus of TMD1 (Figure 2A). These smaller bands therefore cannot represent TMD1 nascent chains, but rather degradation products that were generated from different cleavage sites. Alternatively, these bands report on co-immunoprecipitation of newly-synthesized chaperones that associate with TMD1 (Yates et al., 2016), despite the presence of some SDS.

While the TMD1C antibody detected singly-expressed TMD1 (Figure 3B), neither the TMD2C (Figure 3B) nor the I4N (data not shown) immunoprecipitated solely expressed TMD2. Possibly the hydrophilic D924 residue in a TM segment of TMD2 jeopardizes the insertion of TMD2 into the lipid bilayer (Kim and Skach, 2012) (Figure S1D), which makes singly expressed TMD2 vulnerable to degradation. In support of this idea, D924 needs to be stabilized by R347 for proper folding (Carveth et al., 2002; Hammerle et al., 2000). It is likely that D924 is not stabilized properly in the absence of TMD1 and may be sorted into the ER-associated degradation pathway during translation, as the antibodies did immunoprecipitate TMD2 translated in a system that does not support degradation (Figure 2B).

We next tested whether the new antibodies detected the TMDs of expressed full-length CFTR using the rabbit polyclonal MrPink as a positive control (Figure 3C, MrPink). MrPink immunoprecipitated both the ER and Golgi glycosylated forms of CFTR. TMD1C, TMD2C, and I4N antibodies all detected the ER form as efficiently as the control antibody MrPink, but they bound differently to the Golgi form (Figure 3C, TMD1C, TMD2C, and I4N). Although TMD2C recognized the Golgi form to a similar extent as MrPink, neither TMD1C nor I4N detected the Golgi form significantly, less than 4% (Figure 3C). In the SDS-containing Wash 1, TMD1C and TMD2C immunoprecipitated the CFTR ER form similarly as MrPink, whereas I4N detected only 30% of the ER form. Decreased binding of the Golgi form could be caused by shielding of the epitopes by other CFTR domains during domain assembly.

After testing the binding of the new antibodies to CFTR, we proceeded to investigate whether they could be used to detect TMD folding. The folding of individual TMDs

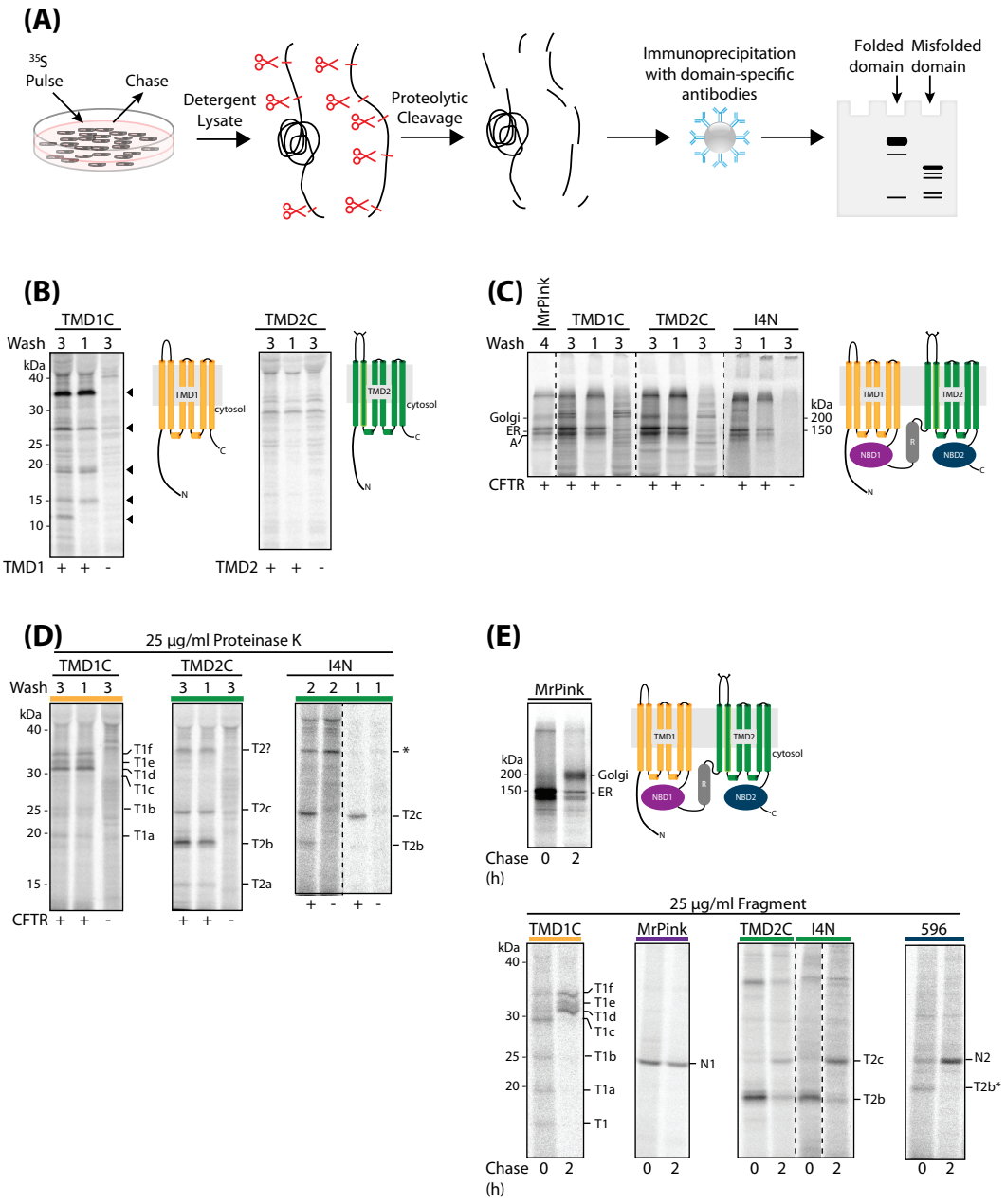

(A)
35S Pulse
Chase
Detergent Lysate
Proteolytic Cleavage
Immunoprecipitation with domain-specific antibodies
Folded domain
Misfolded domain
(B)
TMD1C
TMD2C
Wash 3 1 3
kDa
40
30
25
20
15
10
TMD1
cytosol
TMD2
TMD1 + + -
TMD2 + + -
(C)
MrPink
TMD1C
TMD2C
I4N
Wash 4 3 1 3 3 1 3 3 1 3
Golgi
ER
A
CFTR + + + - + + - + + -
kDa
200
150
NBD1
NBD2
R
(D)
25 µg/ml Proteinase K
TMD1C
TMD2C
I4N
Wash 3 1 3 3 1 3 2 2 1 1
kDa
40
30
25
20
15
T1f
T1e
T1d
T1c
T1b
T1a
T2?
T2c
T2b
T2a
*
CFTR + + - + + - + - + -
(E)
MrPink
kDa
200
150
Golgi
ER
Chase 0 2
(h)
25 µg/ml Fragment
TMD1C
MrPink
TMD2C
I4N
596
kDa
40
30
25
20
T1f
T1e
T1d
T1c
T1b
T1a
T1
N1
T2c
T2b
N2
T2b*
Chase 0 2 0 2 0 2 0 2 0 2
(h)

Figure 3: TMD antibodies recognize pre-and post-assembly CFTR transmembrane domains.
(A) Radiolabeling experiment: CFTR transiently expressed in HEK293T cells was pulse labeled with ^{35}S-methionine and -cysteine and chased for a particular length of time. Detergent lysates of transfected cells were treated with protease to cleave unstructured areas on CFTR. CFTR proteolytic fragments were immunoprecipitated by domain-specific antibodies from cell lysates and analyzed by 7.5 or 12% SDS-PAGE. (B) TMD1 or TMD2 expressed alone were pulse labeled for 30 minutes and cells were lysed. TMD1 or TMD2 were immunoprecipitated with TMD1C (left panel) or TMD2C (right panel) and immunoprecipitates were washed with washes 3 and 1. (C) Cells expressing CFTR were pulse labeled for 15 minutes, chased for 1 hour, and lysed. CFTR from the cell lysates was immunoprecipitated with the TMD antibodies and immunoprecipitates were washed with washes 1 or 3. CFTR immunoprecipitated with antibody against NBD1 (MrPink) was used as a control. (D) Detergent lysates from (C) were treated with Proteinase K and CFTR proteolytic fragments were immunoprecipitated with TMD1C (left panel), TMD2C (middle panel) or I4N (right panel) and immunoprecipitates were washed with washes 1-3. (E) Cells transiently expressing CFTR were pulse labeled for 15 minutes, with 0-h or 2-h chase and lysed and cell lysates were treated with Proteinase K. CFTR and its proteolytic fragments were immunoprecipitated from the cell lysates with antibodies against TMD1, NBD1, TMD2, and NBD2 and immune complexes were resolved by 7.5 or 12% SDS-PAGE. MrPink: antibody against NBD1; 596: antibody against NBD2; black arrowhead in (B): TMD1 band; *: background band; TMD proteolytic fragments were named according to Marjolein Mijnders Thesis, 2019.

and their interactions with other CFTR domains was tested by using a radioactive pulse and chase protocol in conjunction with a protease susceptibility assay (Figure 3A). The principle of the assay is that regions that are shielded by folding of a domain or interactions with another domain will be protected from protease cleavage, and those protease-resistant fragments may be detectable with the TMD antibodies by immunoprecipitation (Figure 3A). To test whether the antibodies recognized their epitopes in proteinase K-treated lysates from CFTR-expressing cells, we performed immunoprecipitations with TMD1C, TMD2C, and I4N. TMD1C and TMD2C bound in the presence of both 0.05% SDS (Wash 1) and 0.5% TX-100 (Wash 3), whereas I4N showed a decrease in binding upon washing with 0.05% SDS (Wash 1) when compared to high pH (Wash 2) (Figure 3D).

All new antibodies immunoprecipitated more than one fragment from proteolyzed CFTR and these proteolytic fragments showed different signal intensities, suggesting that more than one area in the TMDs was exposed to the protease. For example, T1d, e, and f from the TMD1C immunoprecipitation, T2b from the TMD2C immunoprecipitation, and T2c from I4N immunoprecipitation had higher signals than the other proteolytic fragments (Figure 3D). These differences could be due to the variation in accessibility of the epitopes at different stages of CFTR folding, or difference in ^{35}S-methionine and -cysteine content between fragments. To clarify the cause of difference in fragment signals, CFTR was pulse labeled with ^{35}S labeled methionine and cysteine for 15 minutes, chased for 0 or 2 hours, and subjected to the protease susceptibility assay (Figure 3A). The 0-h chase produced only the ER form of CFTR while the CFTR pool after 2-h of chase was mainly Golgi form. The proteolyzed fragments of CFTR were immunoprecipitated by antibodies against

TMD1, NBD1, TMD2, and NBD2 respectively.

Proteolytic fragments derived from TMD1 and TMD2 at 0-h chase were different from 2-h chase (Figures 3E and S1a). TMD1C immunoprecipitation mainly detected four fragments, namely T1, T1a, b, and c, at 0-h chase (Figure 3E, TMD1C panel). At 2-h of chase, the other three proteolytic fragments with higher molecular weight, namely T1d, e, and f, appeared and had higher signals than these four original fragments. The occurrence of larger TMD1 fragments at 2-h of chase suggested that TMD1 had increased protease resistance, indicating that TMD1 has undergone a conformational change during the 2-h of chase. A similar result was obtained for TMD2C, I4N, and 596 immunoprecipitations. A larger fragment T2c appeared on top of the original fragment T2b in TMD2 and I4N immunoprecipitations (Figure 3E, TMD2C and I4N panels), and the NBD2 proteolytic fragment N2 had higher signal intensity at 2-h of chase compared to 0-h (Figure 3E, 596 panel). NBD1 immunoprecipitation showed only one fragment (Figure 3E, MrPink panel), namely N1, and its amount did not change over time.

The original TMD1 fragments (T1a, b, and c) had much lower signals than the later-occurring T1d, e, and f fragments (Figure 3E, TMD1C panel). This was caused in part by the difference in ^{35}S incorporation, which produced the radioactive signals. Higher molecular weight species contain more methionine and cysteine residues and therefore have higher ^{35}S incorporation. Methionine and cysteine content, however, was not the major factor that caused the difference in fragment signals in this case. The size of T1c was only slightly smaller than T1d (Figure 3E, TMD1C panel), suggesting that T1c had slightly less ^{35}S incorporation than T1d. Nevertheless, its signal had almost vanished at 2-h of chase (Figure 3E, TMD1C panel), while T1d still had a strong signal. This result therefore showed that the differences in fragment signals were not caused by the methionine and cysteine content of the fragments, but most likely due to the increase in TMD1 protease resistance. A less likely explanation is a change in accessibility of antibody epitope at 2-h of chase.

Several of the bands that were immunoprecipitated with TMD1C, TMD2C, I4N, and 596 increased in molecular weight during the chase, indicating that TMD1, TMD2, and NBD2 underwent post-translational conformational changes. These could derive from the formation of a more compact structure within the domain or the increase in CFTR domain-domain interactions (Liu et al., 2017; Zhang et al., 2017). Based on the CFTR structure of Zhang et al. (2017), CFTR domains, especially its TMDs, have to maintain a certain level of flexibility for interacting with the NBDs and opening and closing the channel. The occurrence of the higher molecular weight proteolytic fragments, therefore more likely resulted from CFTR domain-domain interactions.

The higher molecular-weight proteolytic fragments appeared in parallel with the occurrence of the CFTR Golgi form (Figure S1a), indicating that the conformational changes were part of the CFTR maturation process.

The N-terminus and ICL2 are protected from protease cleavage by domain assembly

The data of Figure 3E showed that the proteolytic fragments that were recognized by the TMD1C, TMD2C, and I4N antibodies at 0-h chase represented the pre-assembly folding of TMDs, while the fragments at 2-h of chase represented post-assembly TMD conformations. Decoding these proteolytic fragments may reveal the protected areas within the domains at different protein maturation states, and the identification of the protected regions can report on the domain assembly mechanism. The strategy to identify the TMD1 proteolytic fragments employed N-terminal truncation constructs of CFTR. Because TMD1 is the first domain of CFTR, the high molecular weight proteolytic fragments at 0-h and 2-h chases may include the CFTR N-terminus. The epitope recognized by TMD1C is located at the C-terminus of TMD1, and therefore, T1a to T1f all contained the C-terminus of TMD1 or were associating with a C-terminus-containing fragment.

N-terminally truncated CFTR constructs were expressed in HEK293T cells that were subjected to the radiolabeling pulse chase - limited proteolysis protocol and proteolytic fragments were immunoprecipitated with TMD1C. Truncations at the N-terminus seriously impacted on the pattern of the TMD1 proteolytic fragments at both 0-h and 2-h chases. The molecular weight of T1f already decreased after truncation at the 4th amino acid (ΔN4) (Figure 4A, right panel, and Figure 4B) and continued until the 18th aa truncation. At this point, the T1f and T1e bands coalesced (Figure 4A, right panel) and the molecular weight of T1e started to decrease with progressive further truncations at the N-terminus. Using this method, we identified the N-termini of different TMD1 proteolytic fragments. The molecular weight of T1f reduced at ΔN4 truncation, and the closest proteolytic site before aa 4 is at aa 1-2, suggesting that the N-terminus of TMD1 proteolytic fragment T1f involved aa 1-2 (Figure 4B). The N-terminus of T1e started at aa 20 because the size of T1e decreased at ΔN20 but not before (Figure 4A right panel, and Figure 4B). T1d was still present at ΔN35, but disappeared at ΔN45, indicating that the N-terminus of T1d located in the region of aa 36-45 (Figure 4A, right panel, and Figure 4B). The only two protease cleavage sites in this region were Q39 and S42, either of which could be the possible starting point of the N-terminus of T1d. The sizes of both T1c and T1a decreased at ΔN55 but not at ΔN48 (Figure 4A left panel, and Figure 4B) indicating that the N-terminus of both T1c and T1a included aa 49-55. Immunoprecipitating C-terminal TMD1 truncation mutants with another TMD1 antibody, E1.31 (epitope aa 102-117) indicated that the C-terminus of T1a is

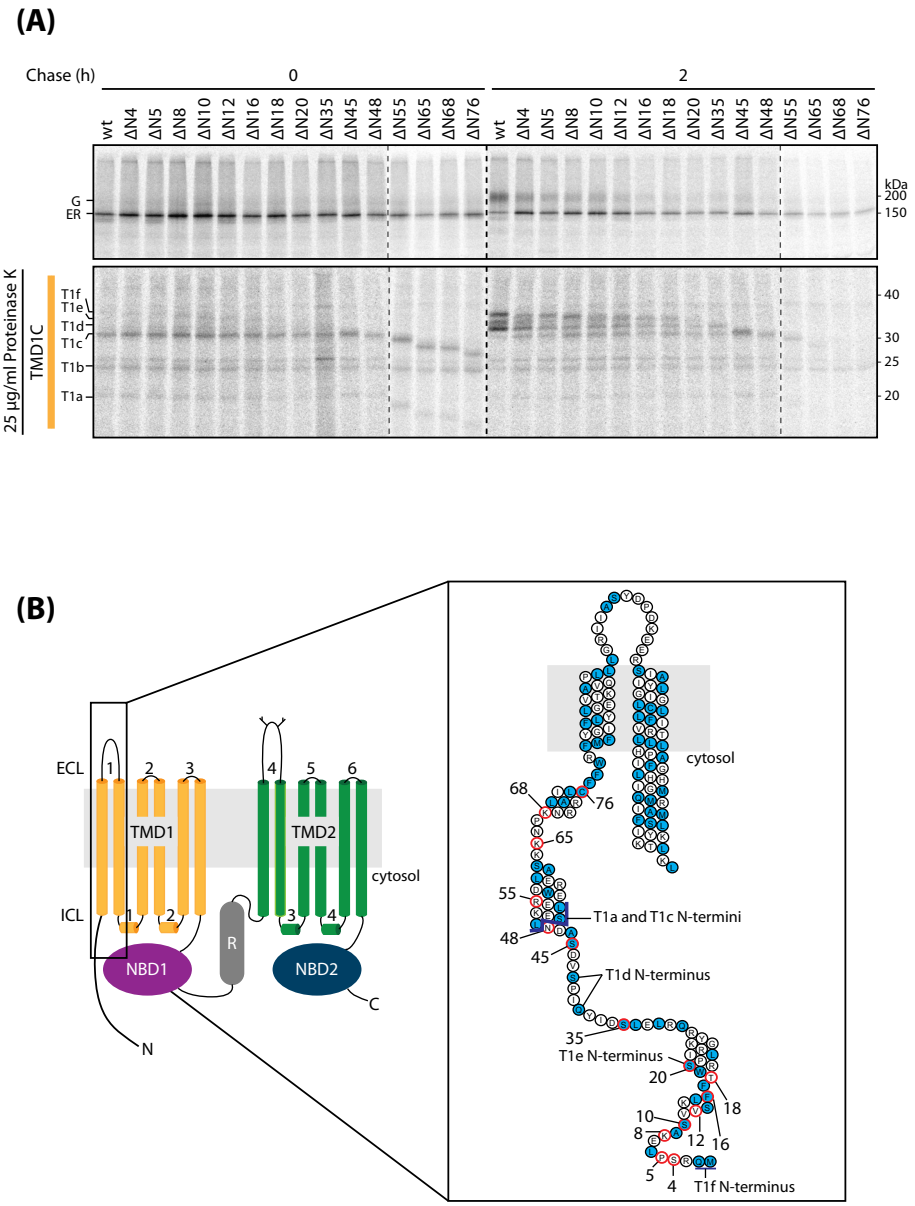


Figure 4: Identification of TMD1 proteolytic fragments.
(A) Cells transfected with a series of N-terminally truncated CFTR mutants were pulse-labeled for 15 minutes, with or without 2 hours of chase. Cell lysates were digested with Proteinase K and subjected to immunoprecipitation. CFTR mutants were immunoprecipitated by MrPink from non-protease treated lysates, while proteolytic fragments were immunoprecipitated from Proteinase K digested lysates with TMD1C. Immunoprecipitates were eluted and resolved by 7.5 or 12% SDS-PAGE. (B) Cartoon showing the N-terminal truncation sites and N-termini of TMD1 proteolytic fragments. Filled blue circles: Proteinase K cleavage sites at N-terminus of TMD1; red circles: locations of N-terminal truncations; purple line: possible Protease K cleavage sites that generate T1a and T1c.

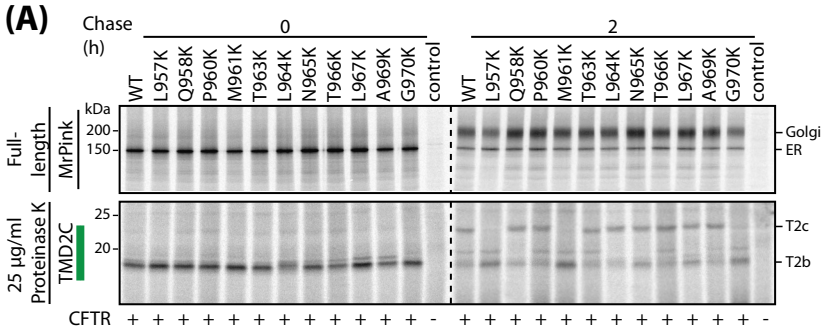
actually located in ICL2, which is the second ICL in TMD1 (Figure S1b). This finding confirmed that T1a does not contain the TMD1C epitope, implying that T1a was co-immunoprecipitated with the other TMD1 proteolytic fragments during TMD1C immunoprecipitation. The N-terminus of T1b has yet to be identified.

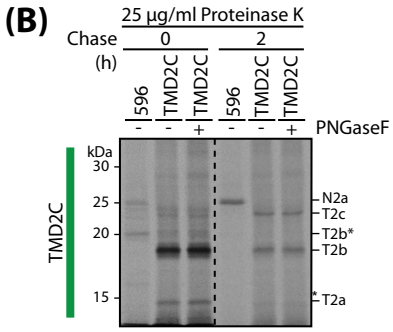
T1a includes the first four TM helixes of TMD1 (Figure S1b), which contain polar or charged residues that can bind to polar residues in other TMD helixes and maintain their stability in the lipid bilayer. As T1a is not large enough to contain both the N-terminus and the TMD1C epitope, we concluded that T1a was co-immunoprecipitated with other TMD1 fragments, possibly caused by these polar interactions. The T1a and T1c fragments were present at the end of the pulse, but less so in the 2-h chase, showing that the CFTR N-terminus and ICL2, which locates in TMD1, were exposed more to protease before domain assembly.

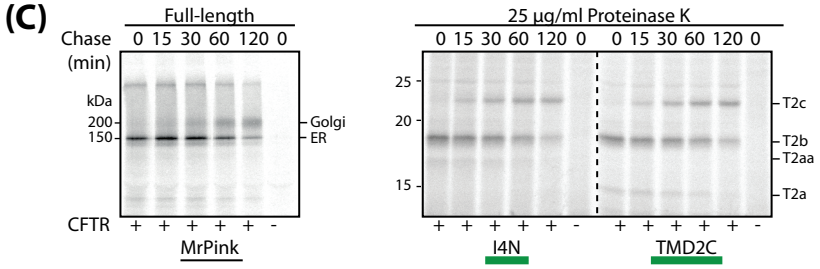
ICL4 is protected by domain assembly

TMD2 is connected via its N-terminus to the R-region and through its C-terminus to NBD2. Generating truncations at both N-terminus and C-terminus of TMD2 can therefore disturb the interaction with nearby domains (Cui et al., 2007; Du and Lukacs, 2009). Because TMD2 expressed in cells is unstable (Figure 3B) and lacked domain packing (Figure S1c), it cannot be used to investigate the fragment identities that are generated through limited proteolysis, as we did for TMD1. Fortuitously, we discovered that T2b shifted upward from its original position when one of the ICL3 residues, leucine 964, was mutated into lysine (Figure 5A). This observation provided a starting point for investigating the N-terminal boundaries of the T2b proteolytic fragment (Figure 5D). A series of CFTR mutants with lysine mutations located in their ICL3 were expressed in HEK293T cells, which were later subjected to pulse chase and limited proteolysis. The TMD2 fragments of these mutant were immunoprecipitated by TMD2C. T2b fragment from L964K was shifted upward while the same fragment of the other CFTR mutants with lysine mutations remained unaffected. This was probably because the lysine mutation at leucine L964 eliminated the Protease K cleavage site, directing the protease to the next target site, L967 or A969, and resulting in a larger T2b fragment. This finding indicated that the N-terminus of T2b was most likely starting at L964 (Figure 5D).

An additional factor that helped identification of TMD2 fragments was the presence of two consensus sites for N-linked glycosylation in extracellular loop 4 (ECL4) of TMD2, that indeed are glycosylated. Treatment of TMD2C immunoprecipitates with PNGase F therefore informs on the presence of these residues in each TMD2 proteolytic fragment. The C-terminal boundaries of all TMD2 fragments can be identified by comparing the proteolytic fragments that are immunoprecipitated by TMD2C and by the NBD2 antibody 596 to check whether they only included the


(A)
Chase (h)
0
2
WT
L957K
Q958K
P960K
M961K
T963K
L964K
N965K
T966K
L967K
A969K
G970K
control
kDa
200
150
Full-length MrPink
Golgi
ER
25 µg/ml Proteinase K TMD2C
25
20
T2c
T2b
CFTR


(B)
25 µg/ml Proteinase K
Chase (h)
0
2
596
TMD2C
PNGaseF
kDa
30
25
20
15
TMD2C
N2a
T2c
T2b*
T2b
T2a


(C)
Full-length
25 µg/ml Proteinase K
Chase (min)
0 15 30 60 120 0
kDa
200
150
Golgi
ER
25
20
15
T2c
T2b
T2aa
T2a
CFTR
MrPink
I4N
TMD2C

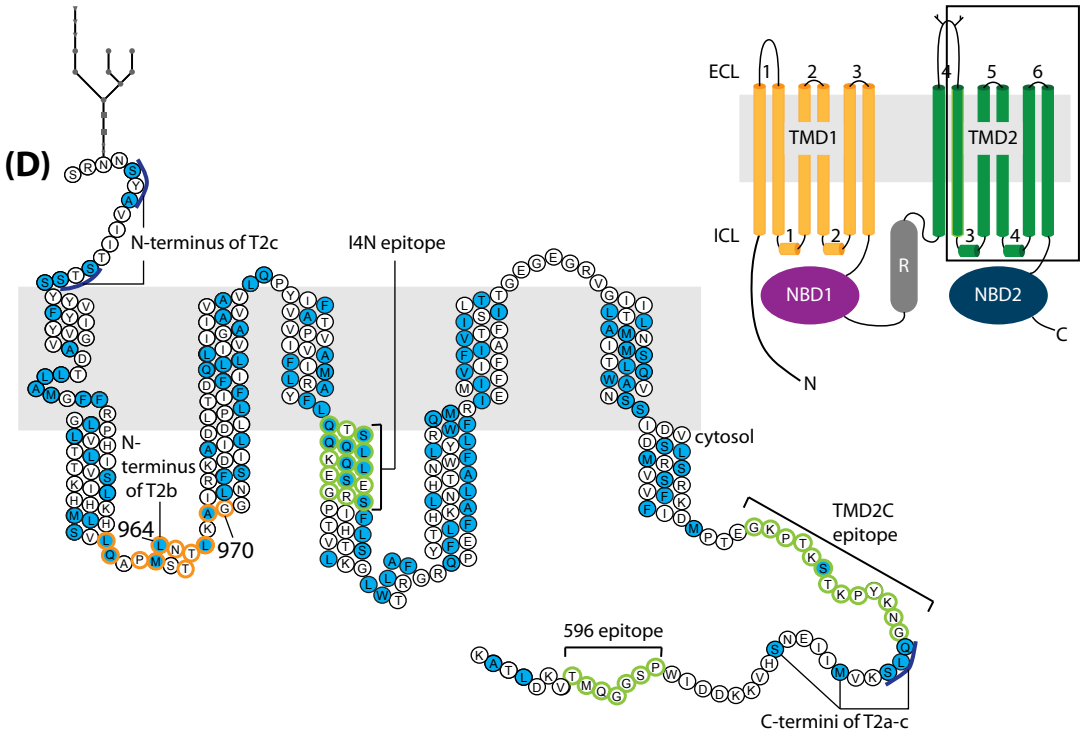


Figure 5: Identification of TMD2 proteolytic fragments.
(A) Cells transfected with CFTR ICL3 lysine mutants were pulse labeled for 15 minutes, chased for 2 hours, and lysed. Cell lysates were treated with Proteinase K and subjected to immunoprecipitation. CFTR mutants were immunoprecipitated with MrPink from the non-protease treated lysates and TMD2 proteolytic fragments were immunoprecipitated with TMD2C from Proteinase K treated lysates. (B) Cells transfected with CFTR constructs were analyzed as in (A) and the proteolytic fragments were immunoprecipitated with two antibodies, TMD2C and 596. The TMD2C immunoprecipitates were digested with PNGase F and analyzed by SDS-PAGE. (C) Cells transfected with CFTR were pulse labeled for 15 minutes and chased for different times. Lysates were treated with Proteinase K. CFTR was immunoprecipitated by MrPink from non-protease treated lysates and TMD2 proteolytic fragments were immunoprecipitated with I4N or TMD2C from protease-treated lysates. Samples were analyzed by 12% SDS-PAGE. (D) Cartoon showing the ICL3 mutation sites and the N- and C-terminal boundaries of the TMD2 proteolytic fragments. Orange circles: location of sequential lysine mutations; green circles: antibody epitopes; filled blue circles: Proteinase K cleavage sites in TMD2; purple lines: Proteinase K cleavage sites that form N- and C-termini of TMD2 proteolytic fragments.

TMD2C epitope (aa 1172-1186) or also the 596 epitope in NBD2 (aa 1204- 1211). If a particular proteolytic fragment contains both TMD2C and 596 epitopes, it will be isolated by both antibodies, and its C-terminus is located in NBD2.

None of the TMD2 proteolytic fragments shifted positions after PNGase F treatment, indicating that they did not include the glycosylation sites (aa 892-900) (Figure 5B). Calculated their apparent mass from the electrophoretic mobility, T2c, the largest TMD2 proteolytic fragment, should contain part of ECL4, while the

other two fragments, T2a and T2b, did not. As T2c did not include the glycosylation sites, its N-terminus should start from S902, A904, S909, or S911, which were the only proteolytic consensus sites in ECL4 after the glycosylation sites (Figure 5D). Figure 5B shows that T2a, b, and c were only precipitated by TMD2C and not 596, suggesting that the C-termini of these three proteolytic fragments ended between aa 1172-1186, the TMD2C epitope, and aa 1204 – 1211, the epitope of 596.

One of the TMD2 proteolytic fragments, T2b*, could only be isolated by 596 but not TMD2C and I4N (Figures 5B and 5C). This fragment was categorized as one of the TMD2 fragments because when mutations were introduced into TMD2, the electrophoretic mobility of T2b* changed (data not shown). This observation indicated that this fragment contained part of TMD2. TMD2C might be better at detecting TMD2 fragments when its epitope is close to the C-termini of the fragments and therefore failed to detect T2b*. As T2b* was not immunoprecipitated by I4N, it most likely does not contain the epitope of I4N. As the required data for describing T2b* was incomplete, the identity of this fragment remains unclear.

The calculation from its electrophoretic mobility suggested that T2a should include at least part of both I4N and TMD2C epitopes. Immunoprecipitating TMD2 proteolytic fragments with I4N showed that I4N did not detect T2a (Figure 5C), indicating that the N-terminus of T2a started after aa 1135 – 1149, the epitope of I4N (Figure 5D). A more precise N-terminus of T2a has yet to be identified.

Other than T2b and T2c, I4N also immunoprecipitated another TMD2 fragment, T2aa, which was not detected by TMD2C (Figure 5C). T2aa has not been studied in detail so far, and exact N- and C-termini of this fragment still await identification.

DISCUSSION

We raised three antibodies against TMD1 and TMD2 of CFTR. These antibodies recognized their epitopes in full-length CFTR, as well as in proteolytic fragments originating from its TMDs after limited proteolysis with Proteinase K. Application of the antibodies revealed that CFTR undergoes domain assembly after translation is terminated. Interactions between CFTR domains were demonstrated by the appearance of high molecular weight TMD1 and TMD2 proteolytic fragments. The identification of these TMD fragments showed that more packing/folding occurred at the N-terminus, ICL2, and ICL4. These observations were made with 25 μg/ml Proteinase K and it is to be expected that larger amounts of protease will cleave the protein into smaller pieces. The proteolytic fragments that are too small to be resolved in SDS-PAGE may be detected using Tris-Tricine gels in the future

for further characterization of the folding of the TMDs. Lower concentrations of Proteinase K in combination with multiple chase times or antibodies targeting different parts of the same domain may also help to fill in further our picture of the CFTR domain-assembly pathway.

Before CFTR domain assembly, the ICLs of TMD1 and TMD2 were not protected by each other and their coupling partners, NBD1 and NBD2, and were accessible to protease cleavage, generating T1a, T1b, T1c, T2a, and T2b (Figures 4A, 0-h chase, and Figure 5C). After domain assembly (at 2 h of chase), the amount of these fragments decreased and 4 larger fragments, T1d, T1e, T1f, and T2c appeared. The amounts of T1d-f were much higher than T1a-c at 2-h chase (Figure 3E, TMD1C panel), while this difference was not found between T2b and T2c (Figure 3E, TMD2C panel). This may have two reasons: first, the signal intensities of T1a-c were equally divided into three fragments, resulted in lower signals in each fragment compare to T2b. At 2-h chase, the signals of T1a-c were even below detection limit, while T2b was still detectable via phosphor screen. Second, TMD2 may also have lower protease resistance than TMD1 after domain assembly, resulting in less T2c compare to T1d-f at 2-h chase.

T2c was generated by protease cleavage in ECL4 (Figure 5D), which is the ECL connecting TM7 and TM8. According to Zhang et al. (2017), CFTR TM8 shifted towards the opposite half of the transporter and associated with TM1 and TM2 during CFTR phosphorylation. This movement could expose the protease cleavage site in ECL4 (Figure 1A), which might be the reason for production of T2c. T2c was the only proteolytic TMD2 fragment that was absent at 0-h chase and appeared after 2 h of chase (Figure 5C), suggesting that this fragment was produced after CFTR acquired its native conformation, in which the channel activity is possible. As ECL4 is one of the longest ECLs of CFTR, it is also more accessible to protease than other ECLs after CFTR domain assembly.

The CFTR domain-domain interaction that caused the changes in TMD proteolysis were confirmed using a series of intracellular loop (ICL) mutations (Kleizen and Braakman, manuscript in preparation; Marjolein Mijnders Thesis, 2019). With this knowledge, we now propose a model of how CFTR domain assembly occurs (Figure 6):

The CFTR TMDs interact with NBDs via their intracellular loops (Zhang et al., 2017). Treating TMD1 with a higher concentration of Proteinase K digested other TMD1 proteolytic fragments and only left T1a at 0-h chase, indicating that ICL1 received more protection than ICL2 before domain assembly (Kleizen and Ineke, manuscript in preparation; Marjolein Mijnders Thesis, 2019). This effect could

already be detected in CFTR nascent chain mimics that contained only TMD1 and the N-terminal half of NBD1, suggesting that the shielding of ICL1 is carried out by NBD1 (Kleizen and Braakman, manuscript in preparation; Marjolein Mijnders Thesis, 2019). The interaction between ICL1 and NBD1 may happen in parallel with NBD1 folding during CFTR translation (Figure 6A). Compared to ICL1-NBD1 binding, ICL2 interacted with NBD2 only post-translationally. This was demonstrated by the presence/absence of T1a at 0-h and 2-h chase. During 0-h chase, the ICL2-NBD2 assembly did not occur. ICL2 was accessible to protease cleavage and generated T1a. After 2 h of chase, ICL2 was protected by NBD2 or TMD2 upon domain-domain interaction and therefore T1a was no longer present in the 2-h chased samples (Figure 3E, TMD1C panel). Mutating ICL2 residues into lysines affected the folding of NBD2 at 2-h chase, indicating that ICL2-NBD2 tethering not only shielded ICL2 from protease cleavage but also assisted NBD2 folding. (Figure 6C; Marjolein Mijnders Thesis, 2019).

TMD2 interacts with other CFTR domains post-translationally. CFTR ICL3 and ICL4 are located in TMD2, ICL3 interacting with NBD2 and ICL4 with NBD1 (Figure 6C). The interaction between ICL3 and NBD2 was shown by the CFTR cryo-EM structure and all models before it (Zhang et al., 2017; Liu et al., 2017) and the Proteinase K cleavage site located in ICL3 was protected after the 2-h chase (Figure 5D). The ICL4-NBD1 association was also confirmed by the CFTR cryo-EM structure and mutations that misfolded NBD1 (Mendoza et al., 2012; Cui et al., 2007) The binding of ICL4 to NBD1 is the second event that happens in the CFTR domain assembly timeline (Figure 6B). It is because losing the ICL4-NBD1 interface during NBD1 misfolding diminishes CFTR ER export and elevates CFTR degradation (Mendoza et al., 2012; Farinha et al., 2013; He et al., 2013; Serohijos et al., 2008), while CFTR that lacks the ICL3-NBD2 interface can still leave the ER (Aleksandrov et al., 2008; Cui et al., 2007; Du and Lukacs, 2009). This finding suggests that domain-domain interactions with NBD2 are not as important as with NBD1. The change in the amount of T2a at the end of the 15-min pulse and 2-h chase demonstrated that ICL4-NBD1 binding occurred post-translationally. During the 2-h chase, this protease cleavage site in ICL4 is protected by NBD1-ICL4 interaction and therefore T2a is not present at that time (Figure 5A, 5D vii). Moreover, CFTR domain assembly also relies on the packing of its N-terminal chain around the N-terminal half of the molecule (Zhang et al., 2017)(Marjolein Mijnders Thesis, 2019). Deleting the first 55 amino acid from CFTR N-terminus diminished CFTR domain assembly (Marjolein Mijnders Thesis, 2019). This packing of the CFTR N-terminus to its TMDs is postulated to stabilize the ICL4-NBD1 interaction post-translationally, as well as the domain-domain interaction in the C-terminal half of the molecule (Figure 6D).

The factors that regulate CFTR domain assembly are largely unknown. Chaperones

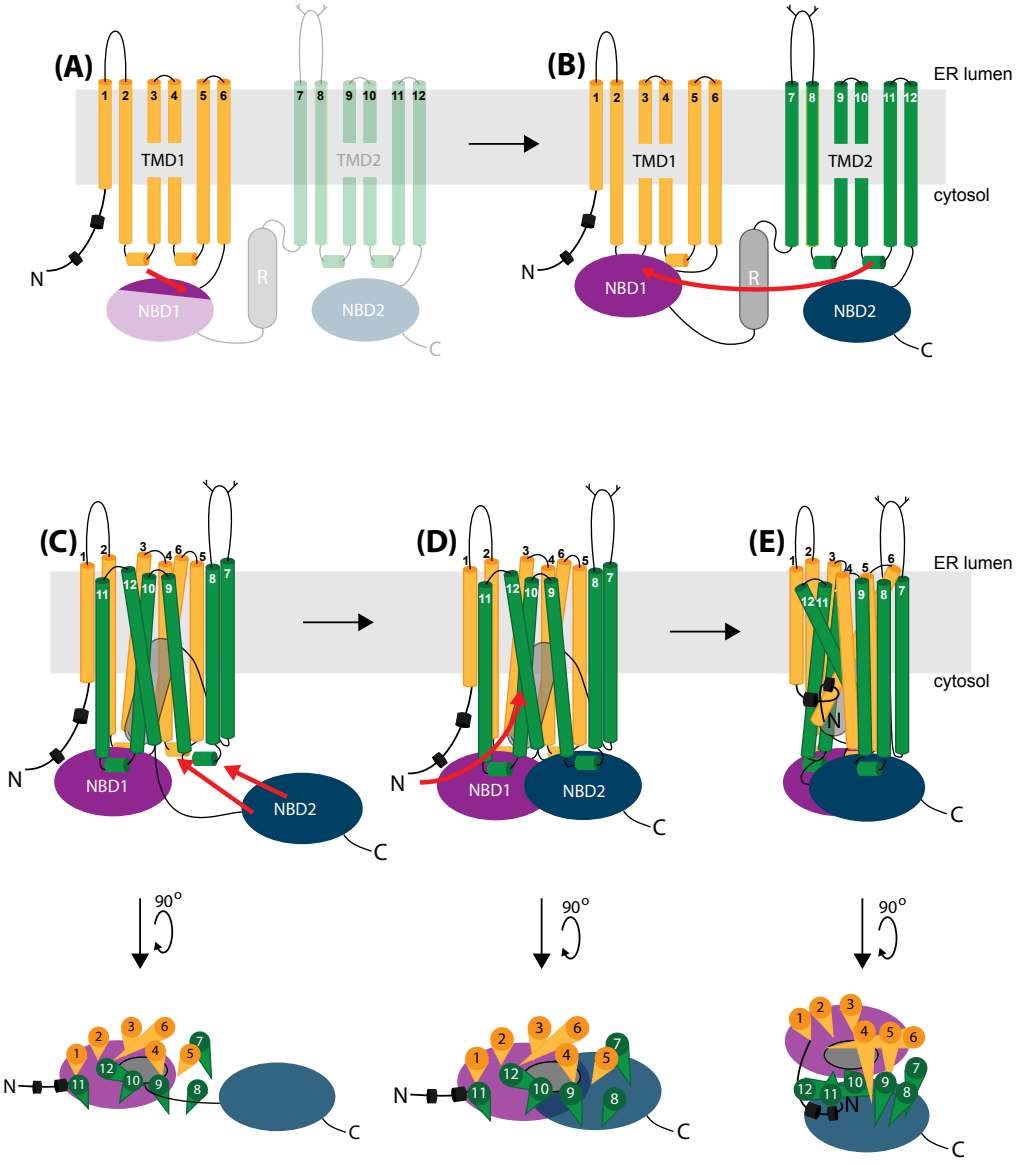


Figure 6: Order of interdomain interactions during CFTR domain assembly.
(A) The co-translational TMD1-NBD1 association is the first interdomain interaction in newly synthesized CFTR nascent chains. (B) The ICL4-NBD1 interaction occurs post-translationally and sets a critical stage in the following domain assembly cascade. (C) ICL2 and ICL3 interact with each other and NBD2 after the ICL4-NBD1 interface has been established. (D) The N-terminus moves upward and surrounds the TMD2 helixes adjacent to it. (E) CFTR after domain assembly.

such as EMC, Bap31, and Hsp90 bind to CFTR single domains TMD1, R, and TMD2 co-translationally (Loo et al., 1998; Louie et al., 2012; Wang et al., 2008; Wang et al., 2006) which may enhance domain assembly. For instance, the clamping motion that is applied on the R-region N- and C-termini during Hsp90 binding may be critical in bringing the N- and C-terminal halves of CFTR closer to each other and trigger the interaction between domains (Mayer, 2010; Schopf et al., 2017; Verba et al., 2016; Wang et al., 2006; Wayne and Bolon, 2010). However, this notion clearly requires further investigation.

Understanding domain assembly mechanisms of CFTR provides information on the folding dynamics of a multidomain membrane protein. Because CFTR has a conserved structure among Type I ABC transporters, our findings are also relevant for understanding the folding pathways of other Type I ABC transporters. Application of antibodies to unravel folding pathways of membrane proteins will help to provide a mechanistic basis for the mode of action of pharmacological interventions to treat protein misfolding diseases.

MATERIALS AND METHODS

Generation of TMD1C, TMD2C, and I4N antibodies

Peptides from the C-terminus of TMD1 (aa 364-381), ICL4 in TMD2 (aa 1135-1149), and the C-terminal part of TMD2 (aa 1172-1186) were selected with the AbDesigner algorithm of NIH (https://hpcwebapps.cit.nih.gov/AbDesigner/) and synthesized as described (Fields, 2002). The purity of synthetic peptides was analyzed by HPLC and mass spectrometry. Synthetic peptides were coupled to rabbit serum albumin (RSA) by the linker Sulfo-*m*-maleimidobenzoyl-*N*-hydroxysuccinimide ester (Sulfo-MBS, Thermo Scientific) in a RSA:MBS: peptide 1:50:50 molar ratio. RSA and Sulfo-MBS were dissolved separately in 500 µl of PBS at pH 8.4, mixed and incubated at room temperature for 45 minutes. Before mixing with the synthetic peptides, RSA-sulfo-MBS was desalted using a PD10 column (GE Healthcare) with PBS at pH 7.2, and concentrated to 1 ml (Vivaspin 20, GE Healthcare). Desalted RSA-sulfo-MBS was added to the peptides, which were dissolved in 200 µl of PBS, pH 7.2, and incubated for 2 hours at room temperature. The RSA-coupled peptides were aliquoted and shipped to Pocono rabbit farm & Laboratory, Inc. and the antibodies were produced according to Pocono's 70 days' antibody-production protocol.

Antibodies

The polyclonal rabbit antibody against NBD1 (MrPink) was generated and characterized as described (Hoelen et al., 2010). The polyclonal rabbit antibody against the HA-tag was generated using KLH-coupled HA peptide

(YPYDVPDYAYPYDVPDYA). The mouse monoclonal antibody 596 against NBD2 (Cui et al., 2007) was kindly provided by Prof. John Riordan (UNC School of Medicine, NC, USA) and the Cystic Fibrosis Foundation. The rabbit polyclonal antibody we here called E1.31 (ECL1 (31/32)) against the first extracellular loop (Peters et al., 2011) was a generous gift from Dr. Kathi Peters and Prof. Raymond Frizzell (University of Pittsburgh, PA USA).

Plasmids

CFTR variants cloned into the mammalian expression plasmid pBI-CMV2 were generously provided by Prof. Phil Thomas (UT Southwestern Medical Center, USA). The CFTR single-domain constructs were generated in pBS vectors (Kleizen et al., 2005) and shuttled into pcDNA3.1 using KpnI and XhoI restriction sites. The TMD1 construct encoded aa 1-394, NBD1 encoded aa 395-673, and TMD2 encoded aa 837-1202. The TMD1-Linker-TMD2 (TMDs-L) construct was generated by Gibson assembly from pBI-CMV2-1202x and pcDNA3.1-Pgp and included aa 1-394 and aa 845-1202 from CFTR and aa 626-683 from P-gp in between. N-terminally truncated CFTR constructs were generated from pBI-CMV2-CFTR. Sequential lysine mutations in ICL3 were generated from pBA-CMV2-CFTR by mutagenesis. The partial pcDNA3.1-based constructs CFTR (36-2480), CFTR (36-306), CFTR(36-356), CFTR(36-394) and the pCDNA3.1-TMD2-HA construct was kindly provided by Prof. Gergely Lukacs (McGill University, Montréal Québec, Canada). PCR primers are described in supplementary materials.

In-vitro translation and translocation of TMD1 and TMD2

Target mRNA was prepared by transcribing DNA using T7 RNA polymerase according to the manufacturer's instructions (Promega). *In-vitro* translations were done with rabbit reticulocyte lysate (Flexi Rabbit Reticulocyte Lysate System, Promega) and were translocated and inserted into semi-permeable cell membranes as described (Kleizen et al., 2005). In brief, target mRNA was added to the reaction mix containing rabbit reticulocyte lysate, 10 µCi/µl EasyTag Express ^{35}S Protein Labeling Mix (Perkin Elmer), and semi-permeable HEK 293T cells. The reaction proceeded at 30°C for 30 minutes. After the reaction was stopped with 1 mM cycloheximide, membranes were pelleted through centrifugation at 10,000 x g for 2 minutes at 4 °C. Newly translated proteins were retrieved from the pellet fraction by dissolving the membranes in 20 µl lysis buffer (110 mM KOAc, 20 mM HEPES, 2 mM $Mg(OAc)_2$ pH 7.2) containing 1% Triton X-100 for 10 minutes at 4 °C. Samples then were subjected to immunoprecipitation.

Cells and transfection

HEK 293T cells were maintained in DMEM supplemented with 10% FBS and 2 mM GlutaMAX (growth medium) and incubated at 37 °C with 5% CO_2. Cells were seeded

onto polylysine-coated 6 cm dishes to reach 70% confluency and transfected using linear 40 kDa polymer polyethylenimine (PEI) as described (van Willigen et al., 2019). After 4 hours, the transfection mix was replaced with growth medium and cells were cultured for 16-20 hours prior to experiments.

Radioactive pulse and chase

HEK239T cells were used in pulse-chase assays as described (Braakman et al., 1991; McCaul et al., 2019; van Willigen et al, 2019). Cells were pulse labeled for 15 minutes with 132 µCi/6 cm dish with EasyTag Express ^{35}S Protein Labeling Mix (Perkin Elmer). Radiolabeling was stopped by adding excess, unlabeled 5 µM methionine and 5 µM cysteine. At indicated chase times, cells were washed twice with ice-cold Hanks' balanced salt solution (HBSS, Life Technologies) and solubilized in ice-cold lysis buffer (20 mM MES, 100 mM NaCl, 30 mM Tris-HCl pH 7.4, 1% Triton X-100) without protease inhibitors. Nuclei were removed by centrifugation for 10 minutes at 4 °C in a microfuge at maximum speed, and the supernatant was subjected to limited proteolysis or immunoprecipitation.

Limited proteolysis

Limited proteolysis was performed as described (Hoelen et al., 2010; Kleizen et al., 2005; van Willigen et al, 2019). In brief, lysates were treated with 25 µg/ml Proteinase K (Sigma-Aldrich) for 15 minutes on ice. Proteolysis was stopped by mixing equal volumes of lysis buffer supplemented with 2 mM PMSF and 2 µg/ml CLAP (chymostatin, leupeptin, antipain and pepstatin (Sigma-Aldrich)) with the lysates. Protein aggregates were pelleted by 16,000 x g centrifugation for 5 minutes at 4 °C, and the supernatant was used for immunoprecipitation.

Immunoprecipitation

Antibodies against TMD1, NBD1, TMD2, or NBD2 were pre-incubated with protein-A Sepharose beads (GE Healthcare) for 15 minutes at 4 °C before adding protease-treated or non-treated lysates. The non-protease treated lysate was added to MrPink antibody-beads mixture and the protease-treated lysates were added to the antibody-beads mixtures containing TMD1C, E1.31, MrPink, TMD2C, I4N, or 596. The mixtures were incubated for 3 hours (TMD1C, E1.31, TMD2C, 596) or 16 hours (MrPink and I4N) at 4 °C. Beads were washed twice for 10 minutes at room temperature with either 20 mM MES, 100 mM NaCl, 30 mM Tris-HCl pH 7.4 and 0.5% Triton X-100 (Wash 1), 50 mM Tris-HCl, pH 8.0, 150 mM NaCl, 1 mM EDTA (Wash 2), 10 mM Tris-HCl pH 8.6, 300 mM NaCl, 0.05% SDS, 0.05% Triton X-100 (Wash 3), or 10 mM Tris-HCl pH 8.6, 300 mM NaCl, 0.1% SDS, 0.05% Triton X-100 (Wash 4). Beads were resuspended in 10 µl 10 mM Tris-HCl pH 6.8 containing 1 mM EDTA, and immune complexes were eluted by adding 10 µl 2x reducing Laemmli sample buffer (final concentration: 200 mM Tris-HCl pH 6.8, 3% SDS, 10% glycerol, 1

mM EDTA, 0.004% bromophenol blue, and 25 mM DTT) and heating for 5 min at 55 °C. Proteins were resolved by SDS-PAGE and visualized by phosphorimaging.

PNGase F treatment

Washed immunoprecipitates were resuspended in 10 µl PBS containing 0.2% SDS and heated to 55 °C for 5 minutes. Next, 10 µl PBS containing 2% TX-100, 1 mM PMSF, 1 µg/ml CLAP, and 500 units of PNGase F (NEB) was added to samples and the mixtures were incubated at 37 °C for 90 minutes. Reactions were stopped by addition of 5x concentrated reducing Laemmli sample buffer, heated for 5 minutes at 55 °C, and resolved by 7.5% SDS-PAGE.

SDS-PAGE and autoradiography

Samples were resolved by 7.5% and 12% SDS-PAGE, and the gels were dried and exposed to super-resolution phosphor screens (Fuji Film) for quantifications, or to Kodak MR films for shown images. Signals from screens were visualized with a Typhoon FLA-7000 scanner (GE Healthcare Life Science) and quantified with ImageQuantTL software (GE Healthcare Life Science).

ACKNOWLEDGEMENTS

We thank Dr. Kathryn Peters and Prof. Raymond Frizzell, University of Pittsburgh, PA USA, Prof. John Riordan PhD, University of North Carolina Chapel Hill, NC USA, and the Cystic Fibrosis Foundation (CFF) for kindly providing antibodies, and Prof. Gergely Lukacs, McGill University, Montréal Québec, Canada, for the pCDNA3.1-TMD2-3HA construct. We thank Laurens Kooijman for designing the peptides, and Prof. Maarten Egmond and Ruud Cox for supervising peptide synthesis. We thank Dr. Joseline Houwman for reading and commenting on this manuscript, and all members of the Braakman-Van der Sluijs lab for fruitful discussions. This project was funded by CFF (BRAAKM14XX0), the Dutch Research Council (NWO) (022.004.019), the Netherlands Organization for Health Research and Development (ZonMw TOP grant 40-00812-98-14103), and the Netherlands Cystic Fibrosis Foundation (HIT-CF grant).

REFERENCES

Aleksandrov, L., Aleksandrov, A., and Riordan, J.R. (2008). Mg2+ -dependent ATP occlusion at the first nucleotide-binding domain (NBD1) of CFTR does not require the second (NBD2). Biochem J *416*, 129-136.

Braakman, I., Hoover-Litty, H., Wagner, K.R., and Helenius, A. (1991). Folding of influenza hemagglutinin in the endoplasmic reticulum. J Cell Biol *114*, 401-411.

Carveth, K., Buck, T., Anthony, V., and Skach, W.R. (2002). Cooperativity and flexibility of cystic fibrosis transmembrane conductance regulator transmembrane segments participate in membrane localization of a charged residue. J Biol Chem *277*, 39507-39514.

Cohen, T.S., and Prince, A. (2012). Cystic fibrosis: a mucosal immunodeficiency syndrome. Nat Med *18*, 509-519.

Cui, L., Aleksandrov, L., Chang, X.B., Hou, Y.X., He, L., Hegedus, T., Gentzsch, M., Aleksandrov, A., Balch, W.E., and Riordan, J.R. (2007). Domain interdependence in the biosynthetic assembly of CFTR. J Mol Biol *365*, 981-994.

Du, K., and Lukacs, G.L. (2009). Cooperative assembly and misfolding of CFTR domains in vivo. Mol Biol Cell *20*, 1903-1915.

Du, K., Sharma, M., and Lukacs, G.L. (2005). The DeltaF508 cystic fibrosis mutation impairs domain-domain interactions and arrests post-translational folding of CFTR. Nat Struct Mol Biol *12*, 17-25.

Farinha, C.M., King-Underwood, J., Sousa, M., Correia, A.R., Henriques, B.J., Roxo-Rosa, M., Da Paula, A.C., Williams, J., Hirst, S., Gomes, C.M.*, et al.* (2013). Revertants, low temperature, and correctors reveal the mechanism of F508del-CFTR rescue by VX-809 and suggest multiple agents for full correction. Chem Biol *20*, 943-955.

Fields, G.B. (2002). Introduction to peptide synthesis. Curr Protoc Protein Sci *Chapter 18*, Unit 18 11.

Gadsby, D.C., Vergani, P., and Csanady, L. (2006). The ABC protein turned chloride channel whose failure causes cystic fibrosis. Nature *440*, 477-483.

Hammerle, M.M., Aleksandrov, A.A., Chang, X.B., and Riordan, J.R. (2000). A novel CFTR disease-associated mutation causes addition of an extra N-linked oligosaccharide. Glycoconj J *17*, 807-813.

He, L., Kota, P., Aleksandrov, A.A., Cui, L., Jensen, T., Dokholyan, N.V., and Riordan, J.R. (2013). Correctors of DeltaF508 CFTR restore global conformational maturation without thermally stabilizing the mutant protein. FASEB J *27*, 536-545.

Hoelen, H., Kleizen, B., Schmidt, A., Richardson, J., Charitou, P., Thomas, P.J., and Braakman, I. (2010). The primary folding defect and rescue of DeltaF508 CFTR emerge during translation of the mutant domain. PLoS One *5*, e15458.

Khushoo, A., Yang, Z., Johnson, A.E., and Skach, W.R. (2011). Ligand-driven vectorial folding of ribosome-bound human CFTR NBD1. Mol Cell *41*, 682-692.

Kleizen, B., van Vlijmen, T., de Jonge, H.R., and Braakman, I. (2005). Folding of CFTR is predominantly cotranslational. Mol Cell *20*, 277-287.

Liu, F., Zhang, Z., Csanady, L., Gadsby, D.C., and Chen, J. (2017). Molecular Structure of the Human CFTR Ion Channel. Cell *169*, 85-95 e88.

Loo, M.A., Jensen, T.J., Cui, L., Hou, Y., Chang, X.B., and Riordan, J.R. (1998). Perturbation of Hsp90 interaction with nascent CFTR prevents its maturation and accelerates its degradation by the proteasome. EMBO J *17*, 6879-6887.

Louie, R.J., Guo, J., Rodgers, J.W., White, R., Shah, N., Pagant, S., Kim, P., Livstone, M., Dolinski, K., McKinney, B.A.*, et al.* (2012). A yeast phenomic model for the gene interaction network modulating CFTR-DeltaF508 protein biogenesis. Genome Med *4*, 103.

Mayer, M.P. (2010). Gymnastics of molecular chaperones. Mol Cell *39*, 321-331.

McCaul, N., Yeoh, H.Y., van Zadelhoff, G., Lodder, N., Kleizen, B., and Braakman, I. (2019). Analysis of protein folding, transport, and degradation in living cells by radioactive pulse chase. J Vis Exp.

Mendoza, J.L., Schmidt, A., Li, Q., Nuvaga, E., Barrett, T., Bridges, R.J., Feranchak, A.P., Brautigam, C.A., and Thomas, P.J. (2012). Requirements for efficient correction of DeltaF508 CFTR revealed by analyses of evolved sequences. Cell *148*, 164-174.

Peters, K.W., Okiyoneda, T., Balch, W.E., Braakman, I., Brodsky, J.L., Guggino, W.B., Penland, C.M., Pollard, H.B., Sorscher, E.J., Skach, W.R*., et al.* (2011). CFTR folding consortium: methods available for studies of CFTR folding and correction. Methods Mol Biol *742*, 335-353.

Pitonzo, D., Yang, Z., Matsumura, Y., Johnson, A.E., and Skach, W.R. (2009). Sequence-specific retention and regulated integration of a nascent membrane protein by the endoplasmic reticulum Sec61 translocon. Mol Biol Cell *20*, 685-698.

Ratjen, F., and McColley, S.A. (2012). Update in cystic fibrosis 2011. Am J Respir Crit Care Med *185*, 933-936.

Riordan, J.R. (2008). CFTR function and prospects for therapy. Annu Rev Biochem *77*, 701-726.

Schopf, F.H., Biebl, M.M., and Buchner, J. (2017). The HSP90 chaperone machinery. Nat Rev Mol Cell Biol *18*, 345-360.

Serohijos, A.W., Hegedus, T., Aleksandrov, A.A., He, L., Cui, L., Dokholyan, N.V., and Riordan, J.R. (2008). Phenylalanine-508 mediates a cytoplasmic-membrane domain contact in the CFTR 3D structure crucial to assembly and channel function. Proc Natl Acad Sci U S A *105*, 3256-3261.

van Willigen, M., Vonk, A.M., Yeoh, H.Y., Kruisselbrink, E., Kleizen, B., van der Ent, C.K., Egmond, M.R., de Jonge, H.R., Braakman, I., Beekman, J.M*., et al.* (2019). Folding-function relationship of the most common cystic fibrosis-causing CFTR conductance mutants. Life Sci Alliance *2*.

Verba, K.A., Wang, R.Y., Arakawa, A., Liu, Y., Shirouzu, M., Yokoyama, S., and Agard, D.A. (2016). Atomic structure of Hsp90-Cdc37-Cdk4 reveals that Hsp90 traps and stabilizes an unfolded kinase. Science *352*, 1542-1547.

Wang, B., Heath-Engel, H., Zhang, D., Nguyen, N., Thomas, D.Y., Hanrahan, J.W., and Shore, G.C. (2008). BAP31 interacts with Sec61 translocons and promotes retrotranslocation of CFTRDeltaF508 via the derlin-1 complex. Cell *133*, 1080-1092.

Wang, X., Venable, J., LaPointe, P., Hutt, D.M., Koulov, A.V., Coppinger, J., Gurkan, C., Kellner, W., Matteson, J., Plutner, H*., et al.* (2006). Hsp90 cochaperone Aha1 downregulation rescues misfolding of CFTR in cystic fibrosis. Cell *127*, 803-815.

Wayne, N., and Bolon, D.N. (2010). Charge-rich regions modulate the anti-aggregation activity of Hsp90. J Mol Biol *401*, 931-939.

Zhang, Z., Liu, F., and Chen, J. (2017). Conformational changes of CFTR upon phosphorylation and ATP binding. Cell *170*, 483-491 e488.

SUPPLEMENTARY MATERIAL

Primers for N-terminal constructs

Wild-type	F: 5' - ATAGCTAGCACCATGCAGAGGTCGCCTCTGGAAAAG – 3' R: 5' – GGCTGAGCTATTGAAGTATCTCACATAGGCTG – 3'
ΔN4	F: 5' – ATAGCTAGCACCATGCCTCTGGAAAAGGCCAGCGTTGTC – 3' R: 5' – GGCTGAGCTATTGAAGTATCTCACATAGGCTG – 3'
ΔN5	F: 5' - ATAGCTAGCACCATGCTGGAAAAGGCCAGCGTTGTC – 3' R: 5' – GGCTGAGCTATTGAAGTATCTCACATAGGCTG – 3'
ΔN8	F: 5' – ATAGCTAGCACCATGGCCAGCGTTGTCTCCAAAC – 3' R: 5' – GGCTGAGCTATTGAAGTATCTCACATAGGCTG – 3'
ΔN10	F: 5' – ATAGCTAGCACCATGGTTGTCTCCAAACTTTTTTTCAGCTG – 3' R: 5' – GGCTGAGCTATTGAAGTATCTCACATAGGCTG – 3'
ΔN12	F: 5' – ATAGCTAGCACCATGTCCAAACTTTTTTTCAGCTGGACCAG – 3' R: 5' – GGCTGAGCTATTGAAGTATCTCACATAGGCTG – 3'
ΔN16	F: 5' – ATAGCTAGCACCATGTTCAGCTGGACCAGACCAATTTTG – 3' R: 5' – GGCTGAGCTATTGAAGTATCTCACATAGGCTG – 3'
ΔN18	F: 5' – ATAGCTAGCACCATGTGGACCAGACCAATTTTGAGG – 3' R: 5' – GGCTGAGCTATTGAAGTATCTCACATAGGCTG – 3'
ΔN20	F: 5' – ATAGCTAGCACCATGAGACCAATTTTGAGGAAAGGATAC – 3' R: 5' – GGCTGAGCTATTGAAGTATCTCACATAGGCTG – 3'
ΔN35	F: 5' – ATAGCTAGCACCATGGACATATACCAAATCCCTTCTGTT – 3' R: 5' – GGCTGAGCTATTGAAGTATCTCACATAGGCTG – 3'
ΔN45	F: 5' – ATAGCTAGCACCATGGCTGACAATCTATCTGAAAAATTGG – 3' R: 5' – GGCTGAGCTATTGAAGTATCTCACATAGGCTG – 3'
ΔN48	F: 5' – ATAGCTAGCACCATGCTATCTGAAAAATTGGAAAGAGAATG – 3' R: 5' – GGCTGAGCTATTGAAGTATCTCACATAGGCTG – 3'
ΔN55	F: 5' – ATAGCTAGCACCATGGAATGGGATAGAGAGCTGGCTTC – 3' R: 5' – GGCTGAGCTATTGAAGTATCTCACATAGGCTG – 3'
ΔN65	F: 5' – ATAGCTAGCACCATGAATCCTAAACTCATTAATGCCCTT – 3' R: 5' – GGCTGAGCTATTGAAGTATCTCACATAGGCTG – 3'
ΔN68	F: 5' – ATAGCTAGCACCATGCTCATTAATGCCCTTCGGCG – 3' R: 5' – GGCTGAGCTATTGAAGTATCTCACATAGGCTG – 3'
ΔN76	F: 5' – ATAGCTAGCACCATGTTTTTCTGGAGATTTATGTTCTATGG – 3' R: 5' – GGCTGAGCTATTGAAGTATCTCACATAGGCTG – 3'

PCR products were inserted into pBI-CMV2 plasmid at AfIII and NheI cleavage sites.

Primers for ICL3 sequential mutation

L957K	F: 5' – AAATGTTACATTCTGTTAAGCAAGCACCTATGTCAAC – 3' R: 5' – GTTGACATAGGTGCTTGCTTAACAGAATGTAACATTT – 3'
Q958K	F: 5' – GTTACATTCTGTTCTTAAAGCACCTATGTCAAC – 3' R: 5' – GTTGACATAGGTGCTTTAAGAACAGAATGTAAC – 3'
A959K	F: 5' – CATTCTGTTCTTCAAAAACCTATGTCAACCCTC – 3' R: 5' – GAGGGTTGACATAGGTTTTTGAAGAACAGAATG – 3'
P960K	F: 5' – CTGTTCTTCAAGCAAAGATGTCAACCCTCAAC – 3' R: 5' – GTTGAGGGTTGACATCTTTGCTTGAAGAACAG – 3'
M961K	F: 5' – CTTCAAGCACCTAAGTCAACCCTCAAC – 3' R: 5' – GTTGAGGGTTGACTTAGGTGCTTGAAG – 3'
S962K	F: 5' – CAAGCACCTATGAAAACCCTCAACACG – 3' R: 5' – CGTGTTGAGGGTTTTCATAGGTGCTTG – 3'
T963K	F: 5' – GCACCTATGTCAAAGCTCAACACGTTGAAAG – 3' R: 5' – CTTTCAACGTGTTGAGCTTTGACATAGGTGC – 3'
L964K	F: 5' – GCACCTATGTCAACCAAGAACACGTTGAAAGC – 3' R: 5' – GCTTTCAACGTGTTCTTGGTTGACATAGGTGC – 3'
N965K	F: 5' – GTCAACCCTCAAGACGTTGAAAGCAG – 3' R: 5' – CTGCTTTCAACGTCTTGAGGGTTGAC – 3'
T966K	F: 5' – CAACCCTCAACAAGTTGAAAGCAGG – 3' R: 5' – CCTGCTTTCAACTTGTTGAGGGTTG – 3'
L967K	F: 5' – CCCTCAACACGAAGAAAGCAGGTGGG – 3' R: 5' – CCCACCTGCTTTCTTCGTGTTGAGGG – 3'
K968R	F: 5' – CCTCAACACGTTGCGAGCAGGTGGGATTC – 3' R: 5' – GAATCCCACCTGCTCGCAACGTGTTGAGG – 3'
A969K	F: 5' – CCTCAACACGTTGAAAAAAGGTGGGATTC – 3' R: 5' – GAATCCCACCTTTTTTCAACGTGTTGAGG – 3'
G970K	F: 5' – CAACACGTTGAAAGCAAAGGGGATTCTTAATAGATTC – 3' R: 5' – GAATCTATTAAGAATCCCCTTTGCTTTCAACGTGTTG – 3'

Primers for TMD1-Linker-TMD2 construct

1st part	F: 5' – AGAATTCACACGTGAAGAAAGATTGACGGCCGCATCGATAAG – 3' R: 5' – CCTGCTGTCTGCATTGTGACCATCACTACTTCTGTAGTCGTTA-AGTT – 3'
2nd part	F: 5' – CGACTACAGAAGTAGTGATGGTCACAATGCAGACAGCAGG – 3' R: 5' – AGGTATGTGTTCCATGTAGTAAGCTTTCTGTCTTGGGCTT – 3'

3rd part	F: 5' – GCTTATCGATGCGGCCGTCAATCTTTCTTCACGTGTGAATTCT – 3' R: 5' – AAGCCCAAGACAGAAAGCTTACTACATGGAACACATACCTT – 3'

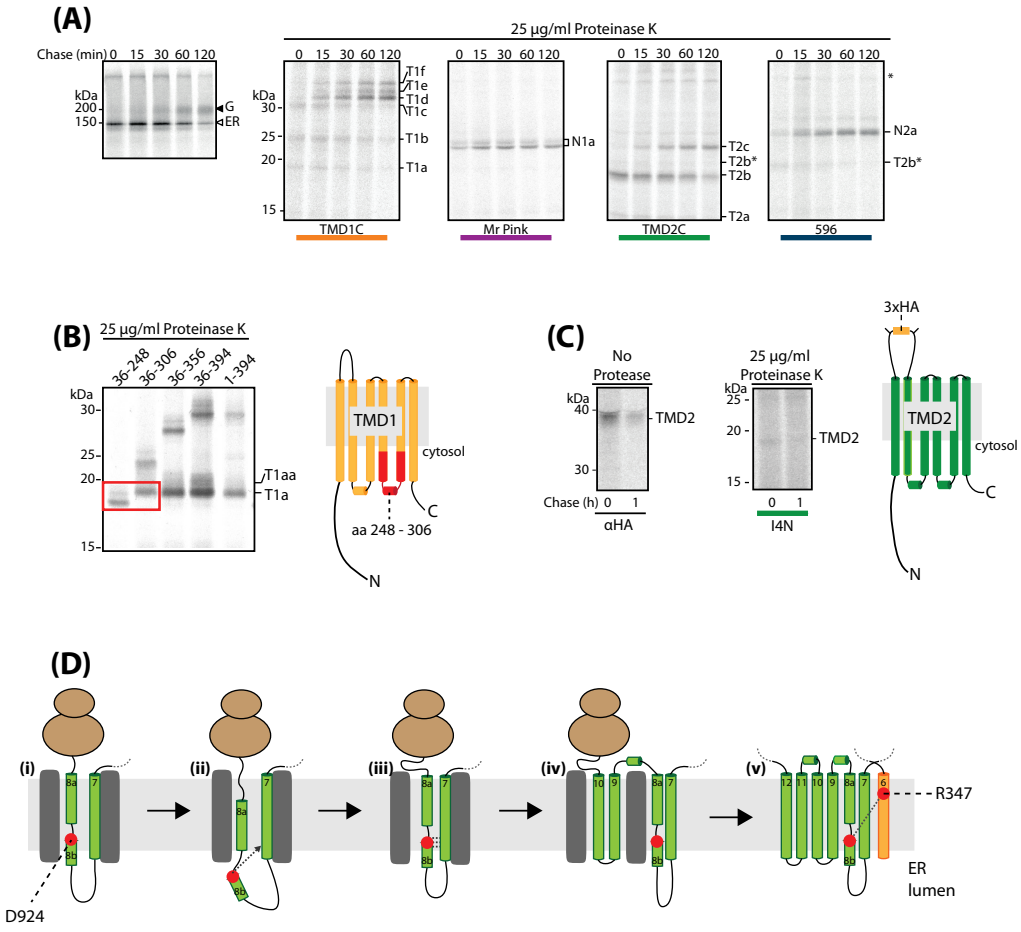


Figure S1: Identification TMD1 and TMD2 proteolytic fragments.
(A) Cells expressing CFTR were pulse labeled for 15 minutes and chased for different periods of time. Lysates were treated with Proteinase K and CFTR or its proteolytic fragments were immunoprecipitated with TMD1C, MrPink, TMD2C, and 596 and analyzed by 7.5 and 12% SDS-PAGE. (Same figure as Figure 5C.) (B) Cells expressing N- or C-terminally truncated TMD1 constructs were radiolabeled for 20 minutes and cell lysates were treated with Proteinase K. The proteolytic fragments were immunoprecipitated with TMD1C and immunoprecipitates were analyzed by 12% SDS-PAGE. The red box indicates the change in T1a mobility on SDS-PAA gel. The location of the C-terminus of the T1a fragment is indicated in the cartoon. (C) Cells transiently expressing TMD2-HA were radiolabeled for 20 minutes and lysed. An aliquot of cell lysate was subjected to immunoprecipitation with anti-HA antibody. The leftover cell lysates were treated with Proteinase K and TMD2 protease fragments were immunoprecipitated by I4N. (D) During the translation and insertion of TM8 (i), Translocon may fail to recognize and allow TM8 to extend into the ER lumen (ii). TM8 is retrieved back to the translocon channel through helix-helix packing with TM7 (iii), after which the helical pair can be inserted into the ER membrane via lateral opening of the translocon (iv). D924 is further stabilized by R347 in TMD1 during domain assembly (v). Model in (D) was drawn according to Pitonzo et al., 2009.

Chapter 4

Folding-function relationship of the most common Cystic-Fibrosis-causing CFTR conductance mutants

AUTHORS AND AFFILIATIONS:
Marcel van Willigen[1], Annelotte M Vonk[2], Hui Ying Yeoh[1], Evelien Kruisselbrink[2], Bertrand Kleizen[1], Cornelis K van der Ent[2], Maarten R Egmond[1,3], Hugo de Jonge[4], Ineke Braakman[1], Jeffrey Beekman[2], Peter van der Sluijs[1]

[1]Cellular Protein Chemistry, Department of Chemistry, Utrecht University, 3584 CH Utrecht The Netherlands; [2]Department of Pediatric Pulmonology, Wilhelmina Children's Hospital, University Medical Center, Utrecht, The Netherlands; [3]Membrane Biochemistry and Biophysics, Department of Chemistry, Utrecht University, 3584 CH Utrecht The Netherlands; [4]Department of Gastroenterology & Hepatology, Erasmus University Medical Center, Rotterdam, The Netherlands.

Running title:
Folding-function relationship of CF mutants

Article published in Life Science Alliance, 2019.

Correspondence:
Peter van der Sluijs, PhD
Cellular Protein Chemistry
Faculty of Science, Utrecht University
Padualaan 8, 3584 CH Utrecht. The Netherlands
Tel: +31(6)30729727
Email: p.vandersluijs1@uu.nl

ABBREVIATIONS

CF	Cystic Fibrosis
CFTR	Cystic Fibrosis Transmembrane Conductance Regulator
CFTR2	Website on CF-causing variants (http://cftr2.org/)
ECL	ExtraCellular Loop
FIS	Forskolin-Induced Swelling assay
IBMX	3-isobutyl-1-methylxanthine
ICL	IntraCellular Loop
ICM	Intestinal Current Measurement
M	Mucosal
NBD	Nucleotide-Binding Domain
R	Regulatory region
S	Serosal
TM	TransMembrane
TMD	TransMembrane Domain

SUMMARY BLURB

We investigated altered-conductance CFTR mutants that cause cystic fibrosis and established a tight correlation between folding and function.

ABSTRACT

Cystic fibrosis (CF) is caused by mutations in the CFTR gene, which are subdivided into six classes. Mutants of classes III and IV reach the cell surface but have limited function. Most class-III and class-IV mutants respond well to the recently approved potentiator VX-770, which opens the channel. We here revisited function and folding of some class-IV mutants and discovered that R347P is the only one that leads to major defects in folding. By this criterion as well as by its functional response to corrector drug VX-809, R347P qualifies also as a class-II mutation. Other class-IV mutants folded like wild-type CFTR and responded similarly to VX-809, demonstrating how function and folding are connected. Studies on both types of defects complement each other in understanding how compounds improve mutant CFTR function. This provides an attractive unbiased approach for characterizing mode of action of novel therapeutic compounds and helps to address which drugs are efficacious for each CF-disease variant.

Keywords:
ABC-transporter / CF / Folding / Ion channel / Organoid

INTRODUCTION

Cystic fibrosis (CF) is caused by a mutation in the Cystic Fibrosis Transmembrane conductance Regulator (CFTR), an anion channel and member of the ABC-transporter family. CFTR consists of two transmembrane-spanning domains (TMD1, TMD2), two nucleotide-binding domains (NBD1, NBD2) and an intrinsically disordered regulatory region (R). CFTR domains mostly fold co-translationally (Kleizen et al., 2005) and need extensive domain assembly to form a fully functional chloride channel.

To date over 1,800 mutations have been identified in the CFTR gene (http://genet.sickkids.on.ca). Most of these are not well characterized; therefore, the CFTR2 database on CF-causing variants was created (Sosnay et al., 2013). The initial version of CFTR2 contained 159 mutations, which account for 96% of all CF patients. Mutations in CF can be divided into six different classes I) defective synthesis of full-length protein, II) defective protein processing and trafficking, leading to retention in the endoplasmic reticulum (ER) and degradation, III) defective channel opening (gating), IV) reduced chloride permeability, V) reduced synthesis of CFTR protein or VI) reduced cell-surface stability (Castellani et al., 2008; Welsh and Smith, 1993). This classification system is outdated because mutants can belong to multiple classes (Veit et al., 2016). An example of this is CFTR-F508del, a typical class II mutant, which even when reaching the cell surface does not function properly and shows class-III and class-VI characteristics.

Clinical drugs targeting CFTR are divided into two types. The so-called correctors increase cell-surface expression by improving release from the ER (for instance by improving folding) and often also by increasing stability at the cell surface (Pedemonte et al., 2005; Van Goor et al., 2011; Van Goor et al., 2006; Yang et al., 2003). Compounds that improve channel function at the cell surface are called potentiators (Van Goor et al., 2009; Van Goor et al., 2014). Patients with class-III and class-IV mutations (R117H, R117C, G551D, G1244E, G1349D, G178R, G551S, S1251N, S1255P, S549N, and S549R, and several others) now have FDA approval to be treated with the potentiator VX-770. For a wide range of common patient mutations, VX-770 treatment improves CFTR function (Van Goor et al., 2014).

CFTR needs to obtain the proper conformation during the folding process to become a functional anion channel at the cell surface. Treatments with drugs or other small molecules aim to change the conformation in mutated proteins to a state where these can function at least partially. Understanding the functional and folding defects in CFTR mutants is crucial to better predict which drug (combination) provides the best precision medicine for CF treatment. CFTR function as measured

by sweat-chloride concentration in CF patients correlates well with CFTR function in organoids derived from those patients (Dekkers et al., 2016; Dekkers et al., 2013; Noordhoek et al., 2016). The forskolin-induced swelling assay (FIS) is used to measure CFTR function in patient-derived organoids and is also employed to interrogate individual responses to drug treatments (Dekkers et al., 2016; Dekkers et al., 2013). Most CFTR2 class-IV mutants are impaired in the formation of the pore that allows passage of anions (Linsdell, 2017; Mornon et al., 2015). R117C/H, R334W and R347P class-IV mutants all have a lower overall chloride current but for different reasons (Sheppard et al., 1993). R117H features reduced open probability (Yu et al. 2016) whereas R347P gates like wild-type but has a conductance below 30% of wild-type levels, and R334W has either a very low conductance or diminished open probability (Sheppard et al., 1993). R117 is important for maintaining the open channel (Cui et al., 2014). The presence of many positively charged residues in the pore of CFTR suggests their involvement in chloride permeation. R334 has been implicated in interacting with anions at the mouth of the pore (Smith et al., 2001), while R347 forms a salt bridge that is important for maintaining an open channel (Cotten and Welsh, 1999; Cui et al., 2013).

R117C, R117H, and R334W mutant CFTR proteins are exported from the ER with efficiencies of 49, 165, and 98% of wild-type, respectively (Van Goor et al., 2014). In sharp contrast, R347P matures very inefficiently to ~15% of wild-type (Van Goor et al., 2014). All the above mutants, however, have been re-classified as mixed class II/III/IV (Veit et al., 2016). To address the discrepancy between the 50% or higher maturation efficiency and the re-classifications, we revisited the functional properties and folding characteristics of the most common class-IV mutations in the original CFTR2 database. We investigated the folding-and-function relationship of R117C/H, R334W, and R347P, using the FIS assay in organoids, intestinal current measurements (ICM), and radiolabeling coupled to a protease-sensitivity assay of newly synthesized CFTR. We confirmed that R347P is not a 'typical' class-IV mutation. Due to its defective function and a misfolded conformation, it more closely resembled a class-II mutation. Folding of the other class-IV mutants was similar, yet not identical to that of wild-type, explaining some differences between them and documenting the strength of biochemical approaches in combination with functional studies.

RESULTS

R347P lacks residual function

To explore CFTR function of the class-IV mutants, we used ICM in Ussing chambers (Figure 1). We obtained rectal biopsies of heterozygous CF patients carrying one

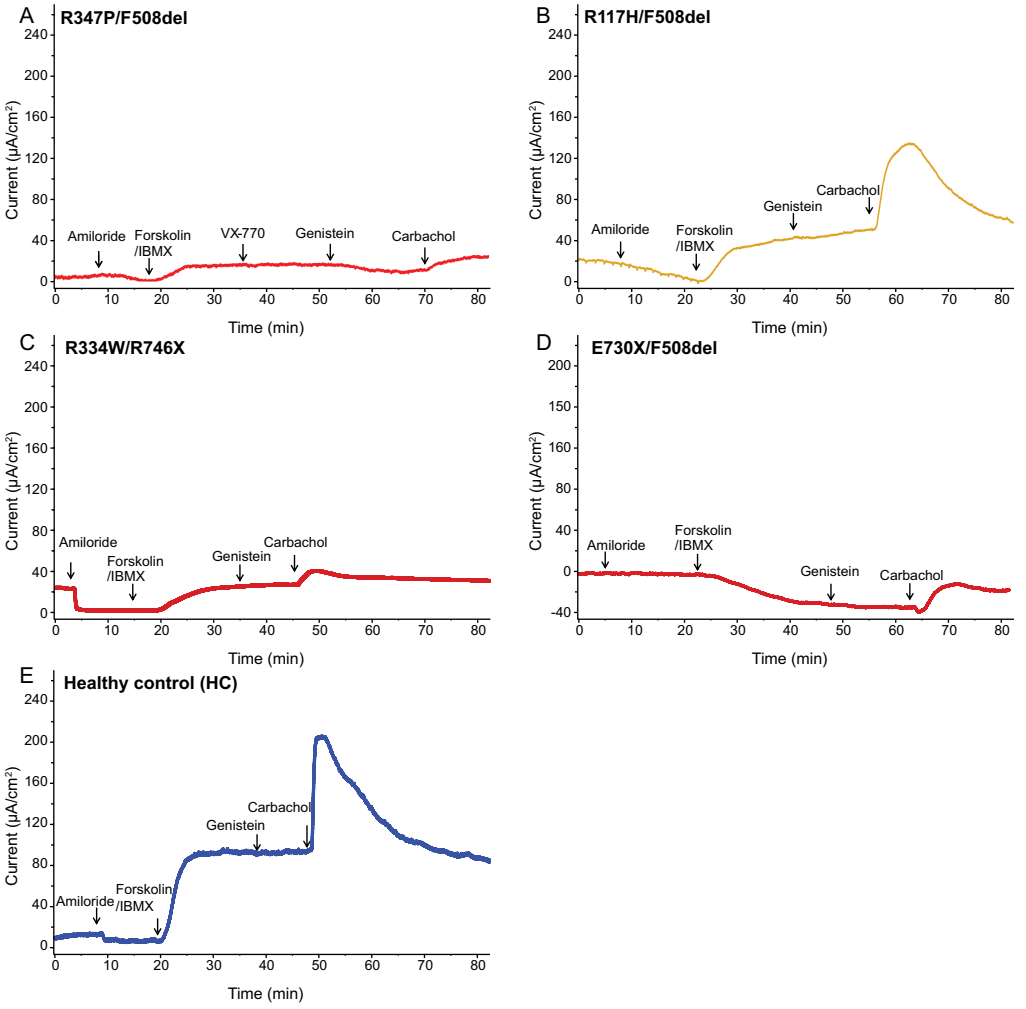


Figure 1: R347P is inactive.
ICM measurements of human rectal biopsies of tissues, which were treated with indicated compounds. (A) Tracing of an R347P/F508del patient showing no response upon forskolin/IBMX addition. Even in the presence of potentiator VX-770 there was no detectable increase in signal. (B) Tracing of R117H/F508del showing a response after addition of forskolin/IBMX. (C) Measurements of a R334W/R746X showing a slight upward deflection after forskolin/IBMX addition. (D) E730X/F508del patient showing a downward deflection upon forskolin/IBMX addition (E) Tracing of a healthy individual, showing a large anion secretory current after forskolin/IBMX addition. Arrows indicate the addition of compounds: amiloride (100 µM), forskolin (10 µM), IBMX (100 µM), VX-770 (20 µM), genistein (50 µM), carbachol (100 µM).

R117H, R347P, or E730X allele with the F508del mutation on the second allele and a R334W/R746X genotype. When CFTR is functioning properly, intestinal-current measurements yield a positive deflection in the short-circuit current (Isc), reflecting electrogenic anion (mainly chloride) secretion. In the continuous presence of the sodium-channel blocker amiloride, elevation of intracellular cAMP by forskolin

or IBMX (3-isobutyl-1-methylxanthine) triggered a large CFTR-mediated anion secretory current in rectal biopsies from healthy controls and from R117H/F508del individuals (Figure 1B and E), which was reduced in R334W/R746X (Figure 1C) and severely blunted in biopsies of R347P/F508del patients (Figure 1A). E730X/F508del biopsies even yielded a downward deflection, suggesting a net K^+ secretion with little to no CFTR activity (Figure 1D). CFTR potentiators VX-770 and/or genistein, in the presence of saturating intracellular cAMP levels did not further enhance CFTR-mediated anion secretion above the level induced by forskolin/IBMX. In contrast, the calcium-linked secretagogue carbachol further increased the short-circuit current (Isc), the magnitude of the response proportional to the cAMP response. Carbachol acts mainly through activation of basolateral K^+ channels, membrane hyperpolarization, and enhancement of the electrical driving force for chloride exit through the CFTR channel (Figure 1A-E). Again, the response was severely blunted in R347P/F508del biopsies (Figure 1A).

VX-770 does not cause swelling of R347P organoids

To confirm the effect of CFTR modulators on the functional activity of the class-IV mutants we used the FIS assay in intestinal organoids generated from rectal biopsies. Forskolin-induced activation of CFTR causes swelling of the organoids, which we then exploit as a readout for CFTR residual function. The outcomes of ICM and FIS measurements correlate well (de Winter-de Groot et al., 2018; Dekkers et al., 2013), even though each patient-derived organoid is unique and each patient may respond differently to drug treatment (Dekkers et al., 2016; Noordhoek et al., 2016). CF patients have two mutated alleles for the CFTR protein and functional activity depends on the type of mutation on each allele. Consequently, in patient-derived material both mutants likely are co-expressed, which formally complicates analysis of how individual mutations respond to drugs in the organoid system, analyzed in FIS and ICM assays. To correct for the contribution of the F508del allele, we subtracted half of the average swelling response obtained from 8 reference F508del/F508del patients (Dekkers et al., 2016). Although EC50 values would be the preferred parameters to rate drug effects by, this assay does not allow their reliable calculation, because CFTR mutants with low functionality respond so poorly to forskolin that a plateau is never reached, whereas wild-type CFTR and active mutants easily saturate the assay and plateau at ~3,200 AUC units because further swelling is not possible, leading to an underestimate of the EC50. When further swelling would be possible, the plateau would rise, moving the apparent EC50 to the right. The maximized swelling in the FIS assay therefore precludes proper readout of the EC50.

R347P/F508del was the only class-IV heterozygote that failed to give an appreciable functional response without modulators (Figure 2A'). Importantly, preincubation

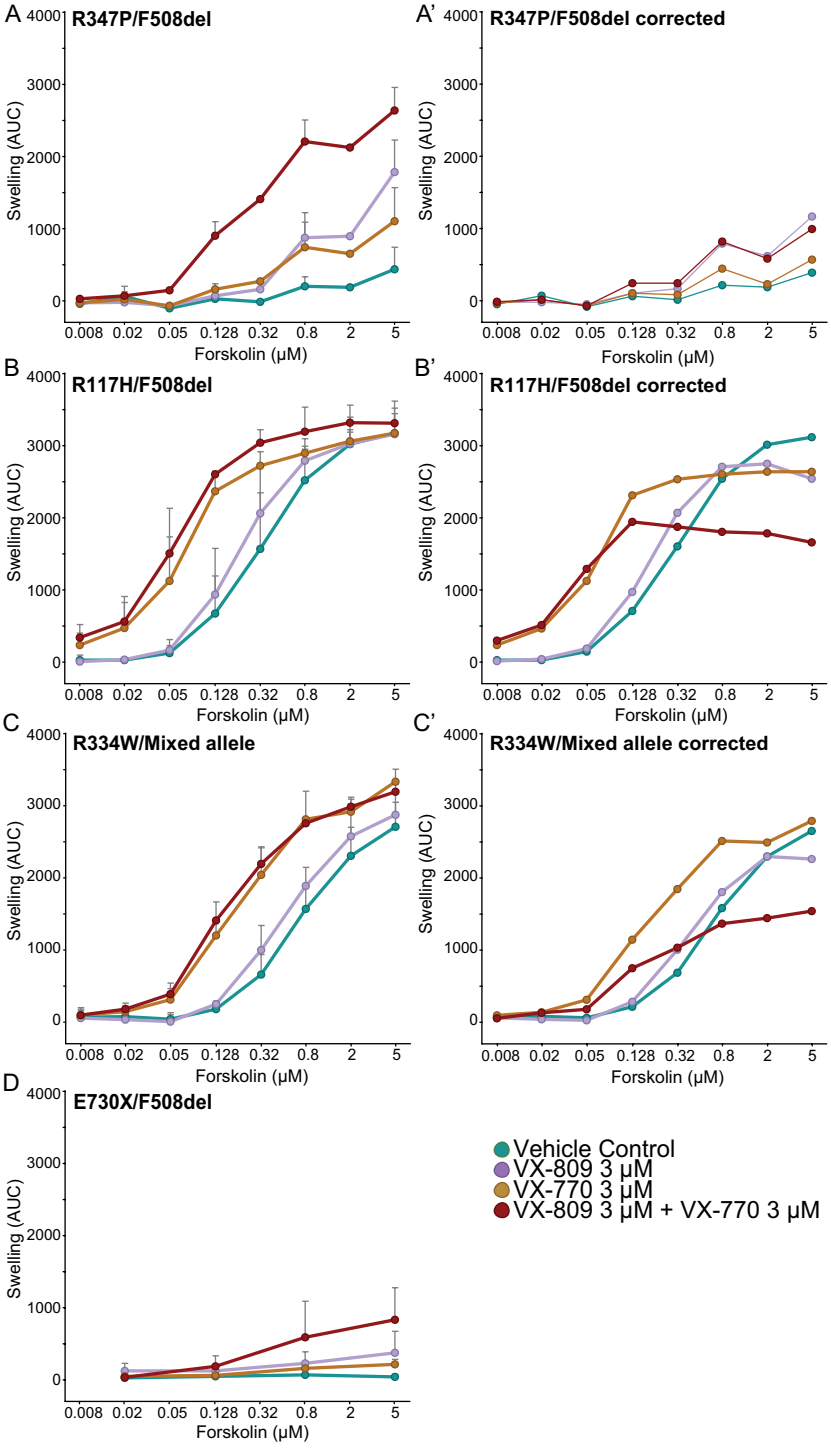

A
R347P/F508del
A'
R347P/F508del corrected
B
R117H/F508del
B'
R117H/F508del corrected
C
R334W/Mixed allele
C'
R334W/Mixed allele corrected
D
E730X/F508del
Swelling (AUC)
Forskolin (μM)
0.008 0.02 0.05 0.128 0.32 0.8 2 5
0 1000 2000 3000 4000
Vehicle Control
VX-809 3 μM
VX-770 3 μM
VX-809 3 μM + VX-770 3 μM

Figure 2: R347P is functionally unresponsive to VX-770.
Organoids of different patients were treated with an increasing concentration of forskolin and swelling was measured after 60 minutes. (A) Non-treated R347P/F508del organoids showed a low amount of swelling indicative for reduced CFTR function. VX-809 and VX-770 gave a moderate response and a combination of VX-809 and VX-770 had an additive effect. (A') Corrected response of A in which 50% of the average swelling value of F508del/F508del organoids from 8 patients from Dekkers et al. (2016) was subtracted from the values of R347P/F508del. (B) The R117H /F508del showed residual function. VX-770 alone or a combination of VX-770 and VX-809 gave a maximal effect, where a plateau was reached at lower concentrations of forskolin. (B') R117H/F508del swelling, corrected as in A' (C) R334W/Mixed allele variants with F508del, R746X, and N1303K on the second allele, had a lower but overall similar response as R117H/F508del in B. (C') Same as A' and B' but subtracted from the R334W/mixed allele. (D) The F508del/E730X had no residual response and a slight increase upon addition of either drug alone, which was additive to the combination of VX-809 and VX-770. (A-C') Data represent average ± SD of triplicate measurements of organoids from 3 distinct patients. Data in (D) represent average ± SD of triplicate measurements of an organoid from 1 patient.

of the organoids with VX-809 rescued R347P/F508del functionally, suggesting that it needs a corrector to either reach the cell surface or function at this location. Acute addition of VX-770 had similar effects as VX-809, but the strongest response of R347P/F508del was seen with both treatments (Figure 2A). Correction for the F508del allele (Figure 2A') clearly showed that the effect of VX-770 on the function of R347P is minimal and similar to that obtained with the vehicle control. This showed that the R347P allele can be rescued by VX-809 but not by VX-770 even when combined with VX-809.

Other class-IV mutants (R117H and R334W) showed CFTR function under basal conditions, which was increased by VX-770, whether corrected for the F508del allele or not (Figure 2 B,B',C,C'). The R117H/F508del curve in the presence of modulators nears that of organoids from healthy controls (Dekkers et al., 2016). The apparent negative effect of VX-809 may be due to the subtraction procedure overestimating the contribution of the F508del allele in this specific patient sample. The F508del/E730X organoid was relatively inert to VX-809 and VX-770 (Figure 2D), suggesting that the F508del allele in this patient gained little function even upon combination of modulators. Patients with the same genotype however can differ in disease phenotype and this specific patient could have low residual function (Dekkers et al., 2016; Pranke et al., 2017). We concluded that the class-IV mutations on one allele contributed significantly to the swelling of organoids derived from these patients.

Transport of R347P to the Golgi complex is impaired
Unlike the other tested class-IV mutants, R347P did not show appreciable residual function in the ICM and FIS assays. We therefore compared folding and ER-exit characteristics of R117C, R117H, R334W, and R347P in HEK293 cells. The position of the mutations is shown in a 3D representation of the human apo-CFTR structure (Liu et al., 2017) (Figure 3A). Cells were labeled with ^{35}S-methionine/cysteine during a 15-min pulse and subsequently chased in the presence of excess unlabeled amino

acids. CFTR was immunoprecipitated directly from detergent cell lysates or after subjecting the lysates to limited proteolysis as detailed before (Hoelen et al., 2010; Kleizen et al., 2005).

Synthesis of CFTR takes on average 10 min, and at least another ~30 min is needed to fold the protein into a state where it can leave the ER (Hoelen et al., 2010; Kleizen et al., 2005). Wild-type and mutant CFTR molecules were synthesized to similar levels during the 15-min pulse (Figure 3B, top left panel) and are in the ER, where wild-type folds into an ER-export-competent state. During the chase period, the folded wild-type protein (Figure 3B, top right panel) is transported to the Golgi complex where its N-linked glycans are modified into the complex-glycosylated form typical for CFTR molecules that have left the ER (Cheng et al., 1990; Hoelen et al., 2010). The fraction of class-IV mutants that reached the Golgi complex was mutation-specific, where R374P left the ER least efficiently. For comparison, we included F508del CFTR in the analysis (Figure 3B) as it fails to fold and reach the Golgi complex but instead is retained in the ER and disposed of through ER-associated degradation (Cheng et al., 1990; Jensen et al., 1995; Meacham et al., 2001; Ward et al., 1995).

R347P is severely misfolded

We next compared the folding of the class-IV mutants with wild-type and F508del CFTR, by subjecting detergent lysates prepared from radioactively labeled cells to limited proteolysis followed by immunoprecipitation with CFTR-domain-specific antibodies. Proteases will cleave a misfolded protein or a folding intermediate more efficiently than a well-folded protein, leading to different digestion patterns on an SDS-PAA gel (Hoelen et al., 2010; Kleizen et al., 2005; Sharma et al., 2001; Zhang et al., 1998). Immediately after the pulse, the TMD1 antibody immunoprecipitated three proteolytic fragments, identical for wild-type and mutant CFTR (Figure 3B, IP: TMD1, T1a-c). The wild-type CFTR TMD1 fragments disappeared over time during the chase, concomitant with the appearance of three larger (more protease-resistant, more folded) TMD1 fragments, T1d-f, which were absent from the Class-II F508del mutant. Digestion of the class-IV mutants gave the same three wild-type TMD1 fragments after the chase, except R347P, which only yielded a detectable bottom fragment T1d, because T1e and T1f were below (Figure 3B) or close to (Figures 4 and 5) detection level. The NBD1 domain was protease resistant in both pulse and chase samples of wild-type CFTR and all 4 class-IV mutants (Figure 3B, IP: NBD1), with fragment quantities relating to full-length protein as in wild-type. As expected, F508del NBD1 was protease sensitive (Hoelen et al., 2010). Immunoprecipitation with the TMD2 antibody showed a prominent fragment (T2b) immediately after the pulse, whose intensity decreased during two hours of chase. In wild-type CFTR and again 3 of the 4 class-IV mutants, TMD2 became

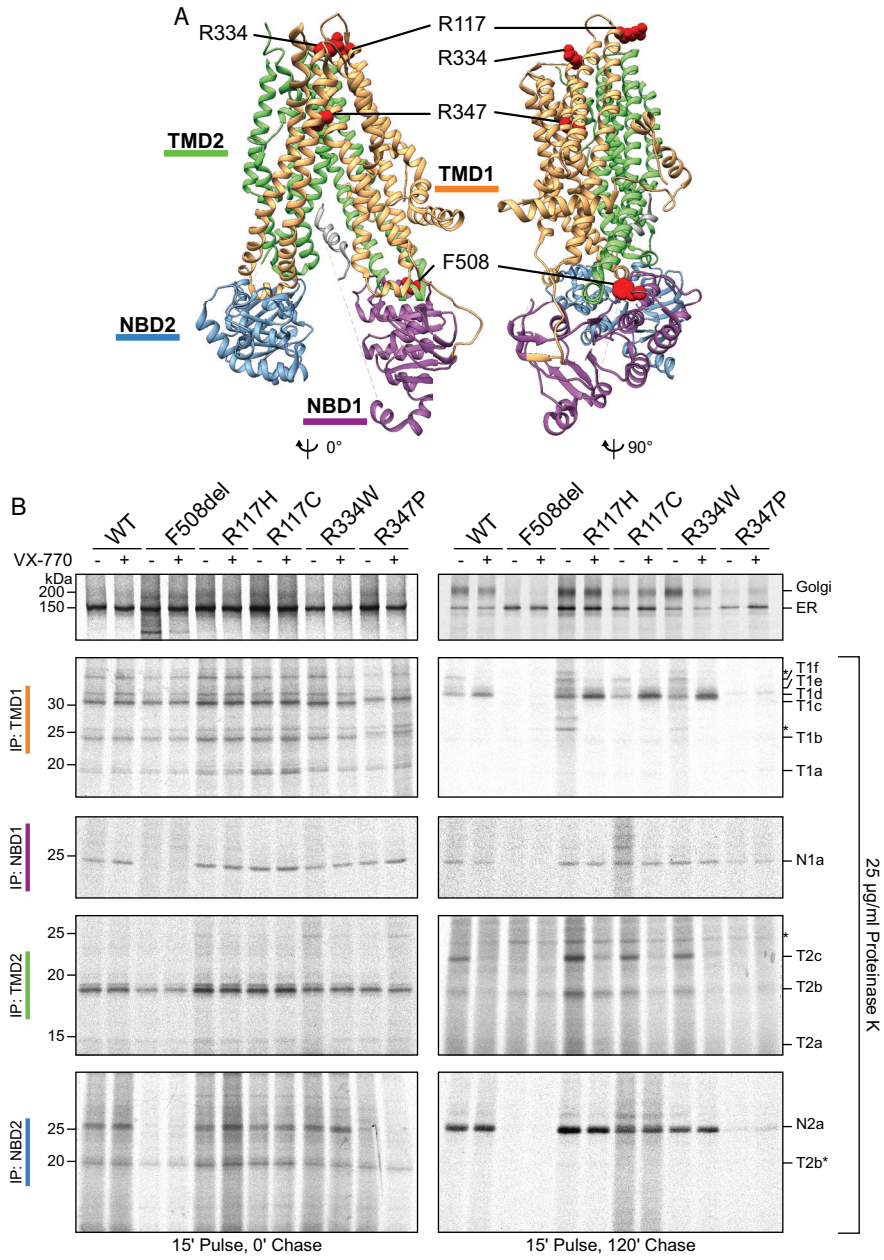


Figure 3: VX-770 does not improve R347P folding.
(A) Cryo-EM structure of human CFTR (Liu et al., 2017) (PBD: 5UAK), generated using Chimera (Pettersen et al., 2004), illustrating that R117 is in the cytoplasm in the first extracellular loop between TM1 and TM2, R334 is located in the second extracellular loop between TM3 and TM4, whereas R347 is located in TM6 inside the pore. The colors wheat, blue, gray, green, purple indicate TMD1, NBD1, R region, TMD2, NBD2, respectively. (B) CFTR was expressed in HEK293-cells, which were labeled with ^{35}S-methionine/cysteine for 15 minutes and chased for 0 and 2 hours in the presence or absence of 3 µM VX-770. Cells were lysed in 1% Triton X-100 in MNT and cell lysates were treated or not with Proteinase K at 25 µg/ml for 15 minutes. CFTR and fragments were immunoprecipitated using TMD1C (TMD1), Mr.Pink (NBD1 and full-length CFTR), TMD2C (TMD2), 596 (NBD2) antibodies. * indicates nonspecific bands.

more protease-resistant, more folded, during the chase, whereas this T2c fragment was barely detectable in the R347P and even less in the F508del CFTR digests (Figure 3B, IP: TMD2, and Figures 4 and 5). The NBD2 protease-resistant fragment, N2a, indicative of NBD2 folding, became more intense during the chase period, in wild-type CFTR as well as the class-IV mutants, but again to a much lesser extent in R347P. In the archetypical class-II F508del mutant, NBD2 remained completely protease sensitive, i.e. not folded (Figure 3B, IP: NBD2).

Whereas folding of 3 of the class-IV mutants was similar to that of wild-type CFTR, R347P formed a notable exception because all its domains except NBD1 were more Proteinase-K susceptible, documenting that its domains were less well folded than in wild-type CFTR and the other mutants (Figure 3B). Because limited proteolysis of R347P yielded some TMD1, NBD1, TMD2 and NBD2 fragments that were completely absent in F508del (Figure 3B), we concluded that R347P was slightly better folded than F508del. Protease susceptibility of R347P's TMD1 was different in 2 ways: not only less of each fragment, but also slightly larger fragments were generated than with wild-type CFTR. All fragments except T1a had a slightly lower mobility on SDS-PAA gels (Figure 3B, 4, 5, TMD1b-f), because the amino-acid change affected mobility of each R347P-containing fragment (our unpublished observations).

Most class-IV mutants respond to VX-770 conformationally

We then assessed the biochemical effects of VX-770 and VX-809 on the class-IV mutants and established whether improvement of abnormal folding could explain the outcomes of the functional experiments. Addition of VX-770 did not affect synthesis of wild-type CFTR or any of the mutants (Figure 3B left panel). Whereas it slightly decreased transport to the Golgi of some mutants (Figure 3B, right panel), steady-state CFTR levels were not affected by 3 μM VX-770 (Figure 4B). Limited proteolysis of the 2-h chase samples followed by immunoprecipitation with the TMD1 antibody showed however, that VX-770 slightly destabilized the N-terminus of TMD1 of wild-type and the R117 and R334 mutants, as the three late fragments, T1d-f, collapsed into the smallest T1d band (Figures 3B); these fragments only differ at their N-terminus (our unpublished observations). In apparent contrast, the ~2-fold increase in signal of the combined T1d-f large fragments in the presence of VX-770 (Figures 3B) confirmed that VX-770 increased overall TMD1 protease resistance (Byrnes et al., 2018). Because folding of R117H, R117C, and R334W were wild-type-like in control and VX-770-treated samples we concluded that a gross conformational defect did not account for their reduced chloride transport.

The folding defect of R347P is rescued by VX-809

Because VX-809 increased the functional response of R347P while VX-770 had little if any effect (Figure 2A), we investigated whether VX-809 rescued folding of

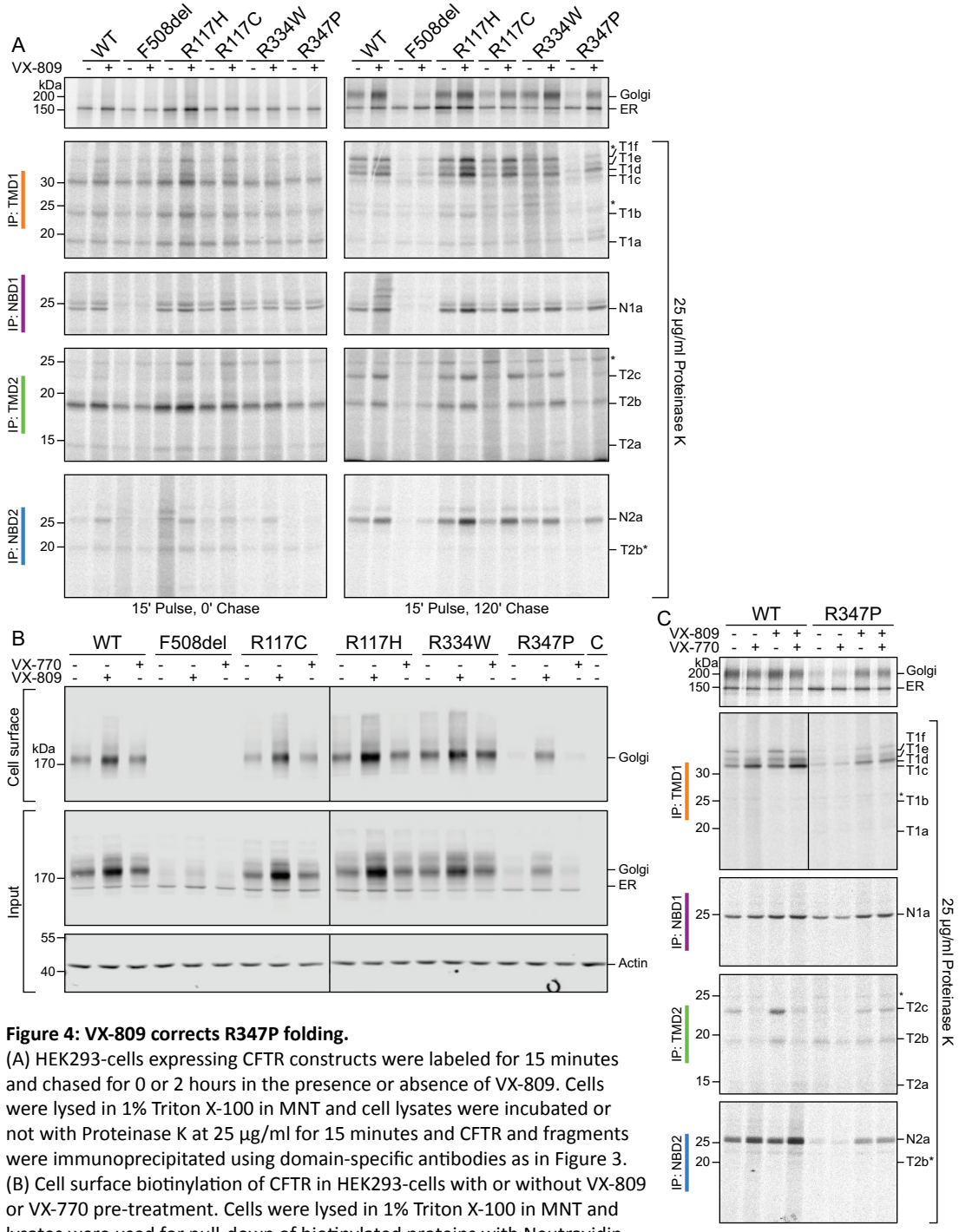


Figure 4: VX-809 corrects R347P folding.
(A) HEK293-cells expressing CFTR constructs were labeled for 15 minutes and chased for 0 or 2 hours in the presence or absence of VX-809. Cells were lysed in 1% Triton X-100 in MNT and cell lysates were incubated or not with Proteinase K at 25 µg/ml for 15 minutes and CFTR and fragments were immunoprecipitated using domain-specific antibodies as in Figure 3. (B) Cell surface biotinylation of CFTR in HEK293-cells with or without VX-809 or VX-770 pre-treatment. Cells were lysed in 1% Triton X-100 in MNT and lysates were used for pull-down of biotinylated proteins with Neutravidin-beads. 7.5% SDS-PAA gels were run and transferred to PVDF-membrane and blotted against CFTR (596) or Actin. (C) Same as in (A) but in the presence of VX-770, VX-809 or both as indicated. All lanes of IP:TMD1 were present on one gel but the solid black line indicates where lanes were removed. * indicates nonspecific bands.

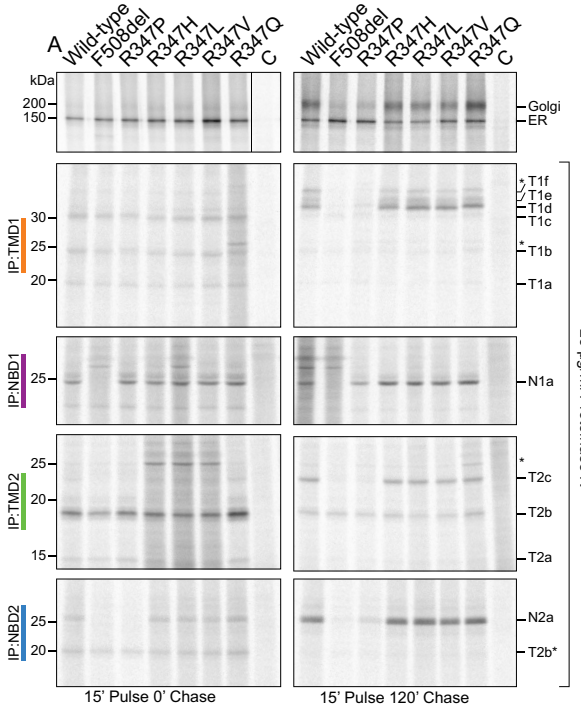
this mutant. The general effect of VX-809 was an increase in quantity of CFTR, of both full-length and protease-resistant fragments (Figure 4A, B, C; B. Kleizen, I. Braakman, unpublished observations) (Loo and Clarke, 2017; Okiyoneda et al., 2013; Ren et al., 2013; Van Goor et al., 2011). This strongly suggests that VX-809 helps CFTR fold into a more protease-resistant, stable conformation. VX-809 partially rescued F508del from the ER as seen by the appearance of a Golgi form after a chase as well as the late fragments of TMD1, TMD2 and NBD2 mentioned above (Figure 4A, right panels). VX-809 did not rescue folding of F508del NBD1 as seen in the immunoprecipitations for NBD1 (Figure 4A; Okiyoneda et al., 2013). R347P was the only mutant that responded well functionally to VX-809 in the FIS assay (Figure 2A, A'), which correlates with the increased levels of R347P after 15 min of pulse labeling, the improved transport to the Golgi complex (Figure 4A, top panels), and the increased steady- state levels (Figure 4B).

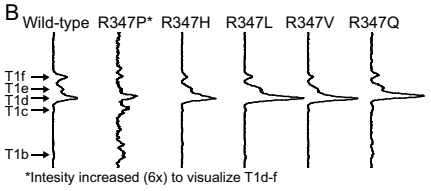
In non-treated control conditions, limited proteolysis of the R347P mutant yielded minute quantities of late TMD1 fragments. The strong improvement of R347P folding and conformation by VX-809 is demonstrated by the recovery of the late TMD1 fragments, albeit enriched for T1d (Figure 4A). The other domains also gained stability after VX-809 treatment, which hence improved the complete protein (Figure 4A) and its function (Figure 2A, A'). That VX-809 rescued the R347P mutant more efficiently than F508del was likely caused by its improving TMD1 folding, the domain that contains the R347P mutation and hence the primary defect.

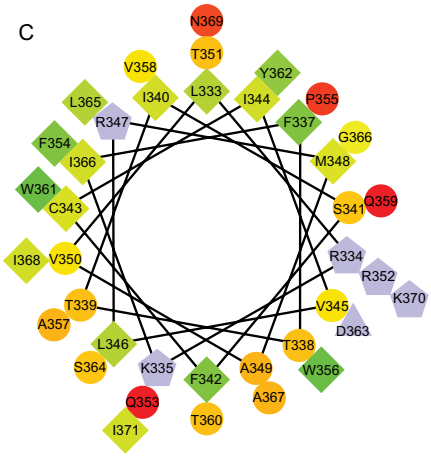
To assess whether enhanced transport of CFTR variants to the Golgi complex resulted in more molecules reaching the plasma membrane, we used cell-surface biotinylation. As shown in Figure 4B, wild-type, R117C/H, and R334W CFTR have similar cell-surface expression, whereas R347P and F508del CFTR were barely or not detectable. Plasma-membrane expression was increased to a variable extent upon VX-809 treatment (minimally for F508del), whereas VX-770 was without effect (Figure 4B). We next investigated whether R347P CFTR that had been rescued by VX-809 became responsive to VX-770 (Figure 4C). In agreement with the functional results in the FIS and ICM assays, R347P remained unresponsive to VX-770 even though VX-809 rescued the late fragments from all domains of R347P (Figure 4C).

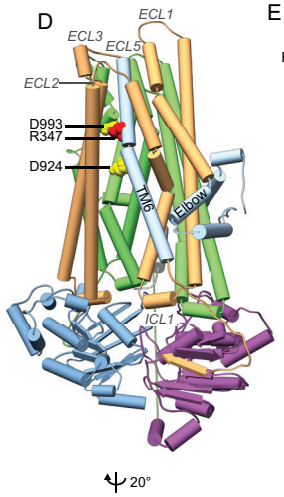
The proline residue in R347P destabilizes TM6

The reduced stability of R347P is likely due to changes in transmembrane segment 6 (TM6) of TMD1, which contains the mutated residue. The question is whether the loss of the charged amino acid or gain of the proline caused the defect. To establish the role of the proline, we used another disease-causing mutant in which R347 was changed to histidine and designed three additional mutants (Figure 5A-B). A helical-wheel representation showed that R347 is embedded in a polypeptide stretch


A
Wild-type
F508del
R347P
R347H
R347L
R347V
R347Q
C
kDa
200
150
Golgi
ER
IP:TMD1
30
25
20
T1f
T1e
T1d
T1c
T1b
T1a
IP:NBD1
25
N1a
IP:TMD2
25
20
15
T2c
T2b
T2a
IP:NBD2
25
20
N2a
T2b*
25 µg/ml Proteinase K
15' Pulse 0' Chase
15' Pulse 120' Chase


B
Wild-type
R347P*
R347H
R347L
R347V
R347Q
T1f
T1e
T1d
T1c
T1b
*Intesity increased (6x) to visualize T1d-f


C
N369
T351
V358
Y362
L365
I340
L333
I344
P355
R347
F337
G366
F354
I366
M348
W361
C343
S341
Q359
I368
V350
R334
R352
K370
T339
V345
A357
D363
L346
T338
S364
K335
A349
W356
F342
A367
Q353
T360
I371


D
ECL1
ECL3
ECL5
ECL2
D993
R347
D924
TM6
Elbow
ICL1
20°

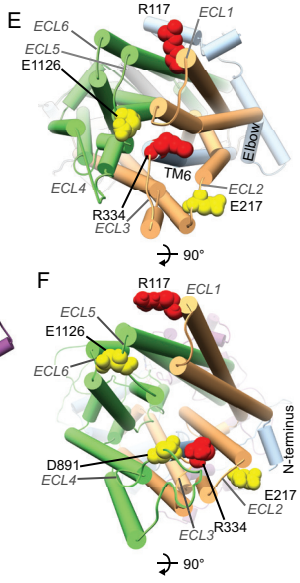

E
R117
ECL1
ECL6
ECL5
E1126
Elbow
TM6
ECL4
ECL2
E217
R334
ECL3
90°
F
R117
ECL1
ECL5
E1126
ECL6
N-terminus
D891
ECL4
E217
ECL2
R334
ECL3
90°

Figure 5: The proline in R347P destabilizes TM6.
(A) As in Figure 3B, HEK293-cells transiently expressing indicated CFTR constructs were labeled for 15 minutes and chased for 0 or 2 hours. Cells were lysed in 1% Triton X-100 in MNT and incubated with proteinase K for 15 minutes, followed by immunoprecipitation of CFTR with domain-specific antibodies. Lane labeled C is a non-transfected control. * indicates nonspecific bands. (B) Lane profiles of IP:TMD1 data shown in (A). (C) Helical wheel representation of CFTR residues 331-360, showing that R347 is largely surrounded by small hydrophobic residues. Hydrophilic (circle), hydrophobic (diamond), negatively charged (triangle), Positively charged (pentagons). Shades of green indicates the hydrophobicity with Dark green having high hydrophobicity and yellow zero hydrophobicity. Hydrophilic residues are shades of Red, more intense red means most hydrophilic residue. Potentially charged residues are light blue. (D) Cryo-EM structure of human CFTR illustrating R347 and interacting residues, helices are shown as cylinders (Liu et al., 2017) (PBD: 5UAK). R347 is highlighted in red and its interacting residues D993 and D924 are colored yellow. Transmembrane helix 6 and the N-terminus (AA 1-77) are colored in light blue. Extracellular loops (ECL) and Intracellular loop 1 (ICL1) are labeled in dark grey. The colors wheat, blue, gray, green, purple indicate TMD1, NBD1, R region, TMD2, NBD2, respectively. The arrow indicates rotation in relation to figure 3A left panel. (E) Same as in D, R117 in ECL1 and R334 in ECL2 shown as red spheres and their interacting residues E1126 in ECL5 and E217 in ECL3 are represented as yellow spheres. (F) Structural model of CFTR in the open conformation (Mornon et al., 2015), illustrating R117 and R334 in red along with their binding partners in yellow. Colors and annotations are the same as in D and E.

enriched for small hydrophobic residues (Figure 5C). We, therefore changed R347 to a valine or leucine, while the arginine-to-glutamine was made because glutamine is present at the 347 position in other ABC transporters.

The protease-digestion pattern of the four mutants was similar to that of wild-type CFTR (Figure 5A). Like in R347P, mutation to a glutamine resulted in the upward shift of the T1b-f bands (Figure 5A), due to a small change in mobility of the mutation-containing fragments. The loss of arginine caused a small alteration in late TMD1 fragments of all R347 mutants, with an enrichment of T1d over T1e and T1f compared to wild-type TMD1 (Figure 5A-B). Nevertheless, relative to this minor change, the introduction of a proline residue caused the major folding defects.

DISCUSSION

Here we investigated the structure-function relationship of the most common class-IV CF-causing CFTR mutants, defining a subgroup of CF patients also known as the altered-chloride-conductance group (Castellani et al., 2008; Welsh and Smith, 1993). CFTR mutants of this class can escape the ER and reach the plasma membrane. Patients with these mutations may benefit from treatment with a single potentiator drug to ‘activate’ the mutant CFTR protein at the cell surface. Patients carrying class-IV mutations, with the exception of R117H and R117C, do not yet have clinical approval for treatment with the VX-770 potentiator compounds. We addressed the folding characteristics of class-IV CFTR mutants to uncover the underlying mechanism for functional effects of VX-770 and corrector VX-809 treatment in this group and found that all responded and were improved conformationally by VX-809.

The corrector improved folding in all mutants but barely affected R334W and R117H function, most likely because their cell-surface levels already are at a maximum, wild-type-like level. In contrast, R347P deviated in that it benefitted well from VX-809 (in a manner distinct from F508del CFTR), yet did not have a functional VX-770 response. We have shown that all functional mutants respond to the corrector drug and that R347P responded better to corrector than to potentiator treatment, classifying R347P as bona fide class-II mutant.

An explanation of the differences between the mutants is greatly facilitated by the recent structure models of CFTR and the cryo-EM structures of CFTR and other ABC transporters, which enable structure-based experimental design and analysis. The 'hyperresponse' of R347P to correction is likely caused by VX-809 correcting precisely where the defect is, in TMD1 (Loo et al., 2013; Loo and Clarke, 2017; our unpublished results). R347P resides in transmembrane helix 6 and the cryo-EM structure of human CFTR shows that TM6 interacts with the N-terminus at the elbow-helix and packs closely to TM3 and ICL1, the first intracellular loop in TMD1, which interacts through its coupling helix with NBD1 in folded CFTR (Figure 5D) (Liu et al., 2017). Changing arginine 347 to a proline in TM6 will destabilize the helix and will likely affect the packing of TM6 with ICL1 and the N-terminus (Choi et al., 2005). VX-809 was reported to promote interactions of NBD1 with ICL1 (Loo et al., 2013; Loo and Clarke, 2017), and allosterically with ICL4 (Hudson et al., 2017; Laselva et al., 2018), both consistent with our data (Figure 4A, B, C) and our unpublished results (Kleizen and Braakman, in preparation). Corrector VX-809 improves packing of TMD1, and thereby rescues interactions with the other domains, in particular NBD1.

The destabilization of the N-terminus of TMD1 was not unique to R347P, as also VX-770 had this effect in our assays. Indeed, the N-terminus and ICL1 are affected by VX-770 to some extent (Byrnes et al., 2018). We conclude that the amino terminus in R347P is destabilized to such an extent that VX-770 failed to exert a significant effect in the two functional assays. Functional experiments suggest that (heterozygous) R347P patients can benefit from a combination treatment of the two drugs, which was shown to be beneficial to F508del homozygous patients with variable improvements between 4.7 and 6.7% (Wainwright et al., 2015).

Even though the introduction of the proline residue caused the strongest defect, the highly-conserved arginine does play a key role in maintaining the open pore architecture. R347 makes a salt bridge with aspartate residues in positions 924 and 993 of TMD2 in the open channel (Cui et al., 2013). Removal of this arginine therefore causes reduced function, as in the R347H patient mutant (Cotten and Welsh, 1999; Van Goor et al., 2014). R347V, L, and Q CFTR also folded wild-type-like

but the subtle change in TMD1 as reflected by the enrichment of the T1d-fragment (Figure 5A-B) suggests a subtle conformational defect at the N-terminus, consistent with the subtle functional defect of R347H CFTR (Cotten and Welsh, 1999; Van Goor et al., 2014).

Other class-IV mutants fold largely like wild-type CFTR albeit with some minor differences. R334 is in ECL3 with its side chain towards TM1 (Figure 5E). This must be a more tolerant part of the molecule because even introduction of a large aromatic residue such as Trp does not grossly perturb folding of the protein. In the open-channel structure model (Mornon et al., 2015) R334 is located close to ECL4 in TMD2, where R334 may have a prominent role in maintaining a stable open form by making a salt bridge with D891 (Sheppard et al., 1993) and in the closed state with E217 (Rahman et al., 2013) (Figure 5E, F).

The lack of differences between wild-type CFTR and the R117 mutants suggested that the gross conformation of the channel is not altered. R117 is in the first extracellular loop (ECL1) of TMD1 at the beginning of TM2 (Figure 5D-F) and creates or stabilizes the open-channel through a salt bridge with E1126 (Cui et al., 2014; Rahman et al., 2013; Sheppard et al., 1993; Yu et al., 2016). Lack of large structural effects in both ECL mutants suggest a minor role of ECLs in overall folding but a major role in maintaining an open pore.

An increasing number of human diseases is known to be caused by misfolding of mutant ABC transporters (Theodoulou and Kerr, 2015). Screens for small-molecule treatments have been instigated, including for Tangier disease (ABCA1), gout (ABCG2), Stargardt Eye Disease (ABCA4), progressive familial intrahepatic cholestasis type 2 (ABCB11) (Allikmets et al., 1997; Rust et al., 1999; Strautnieks et al., 1998; Woodward et al., 2009), and for congenital hyperinsulinemia (Chen et al., 2013). Unlike the last example where carbamazepine corrects the folding of the sulfonylurea receptor 1, corrector compounds and robust functional readouts are not as readily available for most ABC-transporter diseases as for CFTR. In those cases, an in-depth analysis of the folding-function relationship of the target protein provides an attractive approach for characterization of the mode of action of novel therapeutic compounds as we have shown here for CFTR.

MATERIALS AND METHODS

Reagents

VX-809 and VX-770 (Selleckchem) were dissolved in DMSO and stored at -80°C. Amiloride, forskolin, genistein, carbachol, 4,4’-diisothiocyano-2,2’-stilbenedisulfonic

acid (all from Sigma) were dissolved in water and stored at -20°C. Linear 40-kDa polymer polyethylenimine (Polysciences), was dissolved in water to 1 mg/ml, pH 7.0, this solution will be referred to as PEI from now on. The rabbit antibody Mr. Pink and mouse monoclonal 596 against CFTR have been characterized before (Gentzsch et al., 2003; Hoelen et al., 2010). The antibodies TMD1C and TMD2C were generated in rabbits against KLH-coupled peptides SLGAINKIQDFLQKQEYK and EGKPTKSTKPYKNGQ, respectively.
Mutations R347V, R347L, and R347Q were made from pBi.CMV-CFTR template with site-directed mutagenesis, using primers 5' ctgcattgttctggtcatggcggtcactc 3', 5' ctgcattgttctgctcatggcggtcactc 3' and 5' ctgcattgttctgcagatggcggtcactc 3', respectively.

Cell culture and transient expression
HEK293 cells were maintained in Dulbecco's Modified Eagle's Medium (DMEM) supplemented with 10% fetal bovine serum (qualified, E.U.-approved, South America origin) and 2 mM Glutamax at 37°C and 5% CO_2 unless specified otherwise. All reagents were purchased from Life Technologies. cDNA encoding wild-type or mutant CFTR was introduced in the NotI site of the bicistronic plasmid pBi.CMV2 (Clontech) which also drives expression of GFP. HEK293 cells were grown in 6- or 3.5-cm dishes to ~70% confluency and transfected using PEI. Five µg of DNA was added to 200 µl 150 mM NaCl and 12.5 µl PEI for 6-cm and 2.5 µg DNA was added to 100 µl 150 mM NaCl and 7.5 µl PEI for 3.5-cm dishes, these solutions were incubated for 10 minutes at room temperature. Cells then were grown in DMEM supplemented with 5% FBS, 1 mM Glutamax and DNA:PEI complexes were added. After 4 hours, media was aspirated and replaced with full growth medium.

Pulse-chase analysis
HEK293 cells were used 24 hours post-transfection for pulse-chase experiments as described (Braakman et al., 1991; Hoelen et al., 2010). Briefly, cells were labeled for 15 minutes with 143 µCi/6-cm dish of EasyTag Express ^{35}S-protein-labeling mix (Perkin Elmer). Label incorporation was stopped by adding an excess unlabeled cysteine and methionine. At indicated chase times dishes were transferred to ice and washed twice with ice-cold HBSS (Life Technologies). Cells were lysed using 1% Triton X-100 in MNT (20 mM MES, 100 mM NaCl, 30 mM Tris-HCl pH 7.5). Lysates were cleared by centrifugation at 16,000 x g and 4°C. The supernatant was used for limited proteolysis or immunoprecipitation as described (Jansens et al., 2002). Where indicated, VX-770 or VX-809 were added to 3 µM (final concentration) in media during starvation, pulse, and chase.

Limited proteolysis
Limited proteolysis was done as described (Hoelen et al., 2010; Kleizen et al., 2005). In short, detergent cell lysates were digested for 15 minutes on ice, using 25 µg/

ml proteinase K (Sigma). The reaction was stopped by adding an equal volume of MNT supplemented with 1% Triton X-100, 2 mM PMSF and 2 µg/ml of Chymostatin, Leupeptin, Antipain, Pepstatin A (CLAP, all from Sigma)

Immunoprecipitation

Following limited proteolysis, samples were transferred to 50 µl of protein-A beads (GE Healthcare) that had been pre-incubated with the antibody for 10 minutes at 4 °C. All immunoprecipitates were washed twice for 10 minutes at room temperature. Proteolytic fragments originating from TMD1 were immunoprecipitated with 8 µl of TMD1-C antibody, added to protein-A beads, incubated for 3 hours at 4°C and washed with 10 mM Tris-HCl pH 8.6, 300 mM NaCl, 0.05% SDS and 0.05% Triton X-100. NBD1 fragments were immunoprecipitated with 5 µl of Mr.Pink antibody and incubated overnight at 4°C. The immunoprecipitates were washed with 10 mM Tris-HCl pH 8.6, 300 mM NaCl, 0.1% SDS and 0.05% Triton X-100. Fragments derived from TMD2 were immunoprecipitated with 8 µl of TMD2-C antibody for 3 hours at 4°C and washed with 50 mM Tris-HCl pH 8.0, 150 mM NaCl, 1 mM EDTA. NBD2-derived fragments were immunoprecipitated with 0.25 µl 596 antibody and incubated for 3 hours at 4°C and washed using 30 mM Tris-HCl pH 7.5, 20 mM MES, 100 mM NaCl, 0.5% Triton X-100. Washed immunoprecipitates received 10 µl 10 mM Tris-HCl pH 6.8 and 10 µl 2x reducing Laemmli sample buffer and were heated for 5 minutes at 55°C.

Cell-surface biotinylation

Four hours post-transfection, cells received fresh medium containing 3 µM VX-770, 3 µM VX-809 or no drug, and were subsequently grown for 16 hours. Dishes were transferred to ice and washed twice with PBS^{++} (137 mM NaCl, 2.7 mM KCl, 8 mM Na_2HPO_4, and 2 mM KH_2PO4, 1 mM $CaCl_2$, 0.5 mM $MgCl_2$) and left to cool for 15 minutes. Buffer was aspirated and 500 µl PBS^{++} containing 0.5 mg/ml sulpho-NHS-SS-Biotin (Thermo Fisher) was added and incubated on ice After 30 minutes, buffer was removed and remaining non-reacted sulpho-NHS-SS-Biotin was quenched by washing twice with 1% BSA in PBS^{++} (Sigma). Cells were lysed in 300 µl MNT containing 1% Triton X-100, 1 mM CLAP and 1 mM PMSF. Lysates were cleared by centrifugation at 16,000 x g and 4°C. Directly after centrifugation 10 µl of lysate was transferred to an equal volume of 2x reducing Laemmli sample buffer and saved as input sample. The remaining lysate was incubated with 25 µl Neutravidin beads (Thermo Fisher) for 1 hour. Neutravidin beads were washed twice with 10 mM Tris-HCl pH 8.6, 300 mM NaCl, 0.1% SDS and 0.05% Triton X-100 before receiving 15 µl of 10 mM Tris-HCl pH 6.8 and 15 µl of 2x reducing Laemmli sample buffer. Samples were resolved by SDS-PAGE and analyzed by Western blot.

Western blot

Samples were run on 7.5% SDS-PAA gels and transferred to PVDF-membrane (Millipore) under 38 V for 18-21 hours at 4 degrees. After transfer blots were rinsed in PBS (137 mM NaCl, 2.7 mM KCl, 8 mM Na_2HPO_4, and 2 mM KH_2PO_4, 1 mm), ultrapure water and subsequently incubated in LiCoR block buffer diluted 1:1 in PBS (BB), for 1 hour at RT. CFTR was detected using 596 (1:5000) and actin with rabbit anti-actin (1:5,000, Sigma) in BB with 0.1% Tween-20 for 1 hour at RT. Blots were washed four times in PBS containing 0.1% Tween-20 before incubation with goat-anti-mouse Alexa-800 (1:10,000, LiCoR) and donkey-anti-rabbit Alexa-680 (1:10,000, LiCoR) in BB supplemented with 0.1% Tween-20 and 0.02% SDS for 1 hour at RT. Before imaging blots were washed as before with an additional wash step in PBS before imaging on LiCoR Odyssey CLx according to manufacturer specifications.

Intestinal current measurements

Trans-epithelial chloride secretion in human rectal biopsies (four per subject) were measured as described (De Jonge et al., 2004) with a prewash modification (De Boeck et al., 2011) to enhance the forskolin-induced anion secretion. Briefly, biopsies were kept in PBS on ice and mounted in micro-Ussing chambers (aperture 1.13 or 1.77 mm^2). After chambers were equilibrated, compounds were added to the mucosal (M) or serosal (S) side in the following order: 1) amiloride (0.1 mM, M) to block amiloride-sensitive electrogenic Na+ absorption, 2) forskolin (10 µM, M+S) plus 3-Isobutyl-1-methylxanthine (100 µM, M+S) to activate CFTR dependent chloride secretion, 3) VX-770 (20 µM, M+S) and/or genistein (50 µM, M+S) for potentiation of CFTR channels, 5) carbachol (100 µM, S) to activate basolateral Ca^{2+}-dependent K^+- channels and increase the electrochemical driving force for CFTR-mediated chloride secretion. Short circuit current (Isc) values (µA) were divided by the surface area of the tissue holder to obtain $\mu A.cm^{-2}$.

Crypt isolation and organoid culture from human rectal biopsies

Crypt isolation and culture of human intestinal organoids has been described (Dekkers et al., 2013; Sato et al., 2011). Biopsies obtained for intestinal current measurements (ICM) were washed with 10 mM EDTA in PBS for 30 (small intestine) or 90-120 (rectum) min. at 4°C. Supernatant was discarded and EDTA was washed away. Crypts were isolated by rapid up-and-down pipetting of the biopsies in clean PBS, upon which crypts are released from the tissue. The isolated crypts in PBS were transferred to a clean tube, centrifuged at 130 x g, and embedded in 50% Matrigel (growth-factor reduced, phenol free, BD Bioscience) and seeded (30 µl Matrigel per well, 50-200 crypts) in 24-well plates. Afterward, Matrigel was solidified by incubation for a minimum of 15 min. at 37°C and then DMEM/F12 advanced medium was added, supplemented with Primocin 100 µg/ml, 2 mM Glutamax, N2, B27 (all from Invitrogen), 1 µM N-Acetylcysteine (Sigma) and the following growth

factors: 50 ng/ml mouse Epidermal Growth Factor, 50% Wnt3a-conditioned medium and 10% Noggin-conditioned medium, 20% Rspo1-conditioned medium, 10 µM Nicotinamide (Sigma), 10 nM Gastrin (Sigma), 500 nM A83-01 (Tocris) and 10 µM SB202190 (Sigma). The medium was refreshed every 2–3 days, and organoids were passaged every 7–10 days.

Forskolin-induced swelling assay
Organoids from 7-day old cultures were plated in 4 µl of 50% Matrigel into a 96-well flat bottom plate (Nunc) immersed in 100 µl of culture medium as described earlier. One day after seeding, organoids were stained with 10 µM Calcein green for 30 minutes. Forskolin was added at indicated concentrations and the swelling was monitored for 1 hour; images were captured every 10 minutes, using a live cell confocal microscope (LSM710, Zeiss, 5x Magnification). VX-809 (3 µM) was pre-incubated 20-24 hours before measurement, whereas VX-770 (3 µM) was added directly. FIS was quantified using Volocity Imaging software (Improvision). Organoid surface area (xy plane) at t=60 min was calculated relative to that of the surface area at t=0 and averaged over three biological replicates per condition. The AUC was calculated using Prism (GraphPad). Graphs were produced in Tibco Spotfire (Perkin Elmer).

Other methods
CFTR structure from (Liu et al., 2017) PDB:5UAK and structural model from (Mornon et al., 2015). Images of protein structures were generated using Chimera software (Pettersen et al., 2004) and helical wheel representations were made using http://rzlab.ucr.edu/scripts/wheel/wheel.cgi. Western blot images were processed using Image Studio 5.2 (LiCoR).

Human material
Approval for this study was obtained by the ethics committees of the University Medical Centre Utrecht and Erasmus MC Rotterdam. Consent was obtained from all subjects participating in the current study. Rectal organoids were generated from biopsies after ICMs obtained during standard cystic-fibrosis care.

AUTHOR CONTRIBUTIONS

MvW performed radiolabeling experiments, HYY generated and characterized the antibodies against CFTR transmembrane domains, AV conducted FIS assays, EK, HdJ performed and analyzed ICS measurements. Data was analyzed by MvW, AV, HYY, EK, JB, BK, CKvdE, MRE, HdJ, IB, and PvdS. The manuscript was written by MvW, IB, and PvdS.

ACKNOWLEDGMENTS

We thank Prof. Phil Thomas and Linda Millen (Department of Physiology, UT South Western Medical Center, Dallas) for generously donating the CFTR mutants, Dr. Inez Bronsveld (Department of Pulmonary Diseases UMCU, Utrecht) for providing the ICM equipment, Dr. John Riordan, University of North Carolina – Chapel Hill, Cystic Fibrosis Foundation Therapeutics for providing antibodies. We thank Dr. Paola Vergani for critically reading the manuscript and Drs Paola Vergani and David Sheppard for sharing unpublished results. This work was funded by the Netherlands Organization for Health Research and Development (Zon-Mw TOP grant 40-00812-98-14103 to KvdE, JB, IB), by the Netherlands Cystic Fibrosis Foundation (NCFS, HIT-CF grant), by the Cystic Fibrosis Foundation (BRAAKM14XX0 to IB), by Vertex Pharmaceuticals, Gilead, and Galapagos (KvdE), including fees for serving on an advisory board paid to his institution from ProQR, and lecture fees paid to his institution from Teva Pharmaceuticals.

CONFLICT OF INTEREST

CKvdE received funding from Vertex Pharmaceuticals

REFERENCES

Allikmets, R., Singh, N., Sun, H., Shroyer, N.F., Hutchinson, A., Chidambaram, A., Gerrard, B., Baird, L., Stauffer, D., Peiffer, A*., et al.* (1997). A photoreceptor cell-specific ATP-binding transporter gene (ABCR) is mutated in recessive Stargardt macular dystrophy. Nat Genet *15*, 236-246.

Braakman, I., Hoover-Litty, H., Wagner, K.R., and Helenius, A. (1991). Folding of influenza hemagglutinin in the endoplasmic reticulum. J Cell Biol *114*, 401-411.

Byrnes, L.J., Xu, Y., Qiu, X., Hall, J.D., and West, G.M. (2018). Sites associated with Kalydeco binding on human Cystic Fibrosis Transmembrane Conductance Regulator revealed by Hydrogen/Deuterium Exchange. Sci Rep *8*, 4664.

Castellani, C., Cuppens, H., Macek, M., Jr., Cassiman, J.J., Kerem, E., Durie, P., Tullis, E., Assael, B.M., Bombieri, C., Brown, A*., et al.* (2008). Consensus on the use and interpretation of cystic fibrosis mutation analysis in clinical practice. J Cyst Fibros *7*, 179-196.

Chen, P.C., Olson, E.M., Zhou, Q., Kryukova, Y., Sampson, H.M., Thomas, D.Y., and Shyng, S.L. (2013). Carbamazepine as a novel small molecule corrector of trafficking-impaired ATP-sensitive potassium channels identified in congenital hyperinsulinism. J Biol Chem *288*, 20942-20954.

Cheng, S.H., Gregory, R.J., Marshall, J., Paul, S., Souza, D.W., White, G.A., O'Riordan, C.R., and Smith, A.E. (1990). Defective intracellular transport and processing of CFTR is the molecular basis of most cystic fibrosis. Cell *63*, 827-834.

Choi, M.Y., Partridge, A.W., Daniels, C., Du, K., Lukacs, G.L., and Deber, C.M. (2005). Destabilization of the transmembrane domain induces misfolding in a phenotypic mutant of cystic fibrosis transmembrane conductance regulator. J Biol Chem *280*, 4968-4974.

Cotten, J.F., and Welsh, M.J. (1999). Cystic fibrosis-associated mutations at arginine 347 alter the pore architecture of CFTR. Evidence for disruption of a salt bridge. J Biol Chem *274*, 5429-5435.

Cui, G., Freeman, C.S., Knotts, T., Prince, C.Z., Kuang, C., and McCarty, N.A. (2013). Two salt bridges differentially contribute to the maintenance of cystic fibrosis transmembrane conductance regulator (CFTR) channel function. J Biol Chem *288*, 20758-20767.

Cui, G., Rahman, K.S., Infield, D.T., Kuang, C., Prince, C.Z., and McCarty, N.A. (2014). Three charged amino acids in extracellular loop 1 are involved in maintaining the outer pore architecture of CFTR. J Gen Physiol *144*, 159-179.

De Boeck, K., Derichs, N., Fajac, I., de Jonge, H.R., Bronsveld, I., Sermet, I., Vermeulen, F., Sheppard, D.N., Cuppens, H., Hug, M*., et al.* (2011). New clinical diagnostic procedures for cystic fibrosis in Europe. J Cyst Fibros *10 Suppl 2*, S53-66.

De Jonge, H.R., Ballmann, M., Veeze, H., Bronsveld, I., Stanke, F., Tummler, B., and Sinaasappel, M. (2004). Ex vivo CF diagnosis by intestinal current measurements (ICM) in small aperture, circulating Ussing chambers. J Cyst Fibros *3 Suppl 2*, 159-163.

de Winter-de Groot, K.M., Janssens, H.M., van Uum, R.T., Dekkers, J.F., Berkers, G., Vonk, A., Kruisselbrink, E., Oppelaar, H., Vries, R., Clevers, H*., et al.* (2018). Stratifying infants with cystic fibrosis for disease severity using intestinal organoid swelling as a biomarker of CFTR function. Eur Respir J *52*.

Dekkers, J.F., Berkers, G., Kruisselbrink, E., Vonk, A., de Jonge, H.R., Janssens, H.M., Bronsveld, I., van de Graaf, E.A., Nieuwenhuis, E.E., Houwen, R.H*., et al.* (2016). Characterizing responses to CFTR-modulating drugs using rectal organoids derived from subjects with cystic fibrosis. Sci Transl Med *8*, 344ra384.

Dekkers, J.F., Wiegerinck, C.L., de Jonge, H.R., Bronsveld, I., Janssens, H.M., de Winter-de Groot, K.M., Brandsma, A.M., de Jong, N.W., Bijvelds, M.J., Scholte, B.J*., et al.* (2013). A functional CFTR assay using primary cystic fibrosis intestinal organoids. Nat Med *19*, 939-945.

Gentzsch, M., Cui, L., Mengos, A., Chang, X.B., Chen, J.H., and Riordan, J.R. (2003). The PDZ-binding chloride channel ClC-3B localizes to the Golgi and associates with cystic fibrosis transmembrane conductance regulator-interacting PDZ proteins. J Biol Chem *278*, 6440-6449.

Hoelen, H., Kleizen, B., Schmidt, A., Richardson, J., Charitou, P., Thomas, P.J., and Braakman, I. (2010). The primary folding defect and rescue of DeltaF508 CFTR emerge during translation of the mutant domain. PLoS One *5*, e15458.

Hudson, R.P., Dawson, J.E., Chong, P.A., Yang, Z., Millen, L., Thomas, P.J., Brouillette, C.G., and Forman-Kay, J.D. (2017). Direct Binding of the Corrector VX-809 to Human CFTR NBD1: Evidence of an Allosteric Coupling between the Binding Site and the NBD1:CL4 Interface. Mol Pharmacol *92*, 124-135.

Jansens, A., van Duijn, E., and Braakman, I. (2002). Coordinated nonvectorial folding in a newly synthesized multidomain protein. Science *298*, 2401-2403.

Jensen, T.J., Loo, M.A., Pind, S., Williams, D.B., Goldberg, A.L., and Riordan, J.R. (1995). Multiple proteolytic systems, including the proteasome, contribute to CFTR processing. Cell *83*, 129-135.

Kleizen, B., van Vlijmen, T., de Jonge, H.R., and Braakman, I. (2005). Folding of CFTR is predominantly cotranslational. Mol Cell *20*, 277-287.

Laselva, O., Molinski, S., Casavola, V., and Bear, C.E. (2018). Correctors of the Major Cystic Fibrosis Mutant Interact through Membrane-Spanning Domains. Mol Pharmacol *93*, 612-618.

Linsdell, P. (2017). Architecture and functional properties of the CFTR channel pore. Cell Mol Life Sci *74*, 67-83.

Liu, F., Zhang, Z., Csanady, L., Gadsby, D.C., and Chen, J. (2017). Molecular Structure of the Human CFTR Ion Channel. Cell *169*, 85-95 e88.

Loo, T.W., Bartlett, M.C., and Clarke, D.M. (2013). Corrector VX-809 stabilizes the first transmembrane domain of CFTR. Biochem Pharmacol *86*, 612-619.

Loo, T.W., and Clarke, D.M. (2017). Corrector VX-809 promotes interactions between cytoplasmic loop one and the first nucleotide-binding domain of CFTR. Biochem Pharmacol *136*, 24-31.

Meacham, G.C., Patterson, C., Zhang, W., Younger, J.M., and Cyr, D.M. (2001). The Hsc70 co-chaperone CHIP targets immature CFTR for proteasomal degradation. Nat Cell Biol *3*, 100-105.

Mornon, J.P., Hoffmann, B., Jonic, S., Lehn, P., and Callebaut, I. (2015). Full-open and closed CFTR channels, with lateral tunnels from the cytoplasm and an alternative position of the F508 region, as revealed by molecular dynamics. Cell Mol Life Sci *72*, 1377-1403.

Noordhoek, J., Gulmans, V., van der Ent, K., and Beekman, J.M. (2016). Intestinal organoids and personalized medicine in cystic fibrosis: a successful patient-oriented research collaboration. Curr Opin Pulm Med *22*, 610-616.

Okiyoneda, T., Veit, G., Dekkers, J.F., Bagdany, M., Soya, N., Xu, H., Roldan, A., Verkman, A.S., Kurth, M., Simon, A.*, et al.* (2013). Mechanism-based corrector combination restores DeltaF508-CFTR folding and function. Nat Chem Biol *9*, 444-454.

Pedemonte, N., Sonawane, N.D., Taddei, A., Hu, J., Zegarra-Moran, O., Suen, Y.F., Robins, L.I., Dicus, C.W., Willenbring, D., Nantz, M.H.*, et al.* (2005). Phenylglycine and sulfonamide correctors of defective delta F508 and G551D cystic fibrosis transmembrane conductance regulator chloride-channel gating. Mol Pharmacol *67*, 1797-1807.

Pettersen, E.F., Goddard, T.D., Huang, C.C., Couch, G.S., Greenblatt, D.M., Meng, E.C., and Ferrin, T.E. (2004). UCSF Chimera--a visualization system for exploratory research and analysis. J Comput Chem *25*, 1605-1612.

Pranke, I.M., Hatton, A., Simonin, J., Jais, J.P., Le Pimpec-Barthes, F., Carsin, A., Bonnette, P., Fayon, M., Stremler-Le Bel, N., Grenet, D.*, et al.* (2017). Correction of CFTR function in nasal epithelial cells from cystic fibrosis patients predicts improvement of respiratory function by CFTR modulators. Sci Rep *7*, 7375.

Rahman, K.S., Cui, G., Harvey, S.C., and McCarty, N.A. (2013). Modeling the conformational changes underlying channel opening in CFTR. PLoS One *8*, e74574.

Ren, H.Y., Grove, D.E., De La Rosa, O., Houck, S.A., Sopha, P., Van Goor, F., Hoffman, B.J., and Cyr, D.M. (2013). VX-809 corrects folding defects in cystic fibrosis transmembrane conductance regulator protein through action on membrane-spanning domain 1. Mol Biol Cell *24*, 3016-3024.

Rust, S., Rosier, M., Funke, H., Real, J., Amoura, Z., Piette, J.C., Deleuze, J.F., Brewer, H.B., Duverger, N., Denefle, P.*, et al.* (1999). Tangier disease is caused by mutations in the gene encoding ATP-binding cassette transporter 1. Nat Genet *22*, 352-355.

Sato, T., Stange, D.E., Ferrante, M., Vries, R.G., Van Es, J.H., Van den Brink, S., Van Houdt, W.J., Pronk, A., Van Gorp, J., Siersema, P.D.*, et al.* (2011). Long-term expansion of epithelial organoids from human colon, adenoma, adenocarcinoma, and Barrett's epithelium. Gastroenterology *141*, 1762-1772.

Sharma, M., Benharouga, M., Hu, W., and Lukacs, G.L. (2001). Conformational and temperature-sensitive stability defects of the delta F508 cystic fibrosis transmembrane conductance regulator in post-endoplasmic reticulum compartments. J Biol Chem *276*, 8942-8950.

Sheppard, D.N., Rich, D.P., Ostedgaard, L.S., Gregory, R.J., Smith, A.E., and Welsh, M.J. (1993). Mutations in CFTR associated with mild-disease-form Cl- channels with altered pore properties. Nature *362*, 160-164.

Smith, S.S., Liu, X., Zhang, Z.R., Sun, F., Kriewall, T.E., McCarty, N.A., and Dawson, D.C. (2001). CFTR: covalent and noncovalent modification suggests a role for fixed charges in anion conduction. J Gen Physiol *118*, 407-431.

Sosnay, P.R., Siklosi, K.R., Van Goor, F., Kaniecki, K., Yu, H., Sharma, N., Ramalho, A.S., Amaral, M.D., Dorfman, R., Zielenski, J.*, et al.* (2013). Defining the disease liability of variants in the cystic fibrosis transmembrane conductance regulator gene. Nat Genet *45*, 1160-1167.

Strautnieks, S.S., Bull, L.N., Knisely, A.S., Kocoshis, S., Dahl, N., Arnell, H., Sokal, E., Dahan, K., Childs, S., Ling, V.*, et al.* (1998). A gene encoding a liver-specific ABC transporter is mutated in progressive familial intrahepatic cholestasis. Nature Genetics *20*, 233-238.

Theodoulou, F.L., and Kerr, I.D. (2015). ABC transporter research: going strong 40 years on. Biochem Soc Trans *43*, 1033-1040.

Van Goor, F., Hadida, S., Grootenhuis, P.D., Burton, B., Cao, D., Neuberger, T., Turnbull, A., Singh, A., Joubran, J., Hazlewood, A.*, et al.* (2009). Rescue of CF airway epithelial cell function in vitro by a CFTR potentiator, VX-770. Proc Natl Acad Sci U S A *106*, 18825-18830.

Van Goor, F., Hadida, S., Grootenhuis, P.D., Burton, B., Stack, J.H., Straley, K.S., Decker, C.J., Miller, M., McCartney, J., Olson, E.R.*, et al.* (2011). Correction of the F508del-CFTR protein processing defect in vitro by the investigational drug VX-809. Proc Natl Acad Sci U S A *108*, 18843-18848.

Van Goor, F., Straley, K.S., Cao, D., Gonzalez, J., Hadida, S., Hazlewood, A., Joubran, J., Knapp, T., Makings, L.R., Miller, M.*, et al.* (2006). Rescue of DeltaF508-CFTR trafficking and gating in human cystic fibrosis airway primary cultures by small molecules. Am J Physiol Lung Cell Mol Physiol *290*, L1117-1130.

Van Goor, F., Yu, H., Burton, B., and Hoffman, B.J. (2014). Effect of ivacaftor on CFTR forms with missense mutations associated with defects in protein processing or function. J Cyst Fibros *13*, 29-36.

Veit, G., Avramescu, R.G., Chiang, A.N., Houck, S.A., Cai, Z., Peters, K.W., Hong, J.S., Pollard, H.B., Guggino, W.B., Balch, W.E.*, et al.* (2016). From CFTR biology toward combinatorial pharmacotherapy: expanded classification of cystic fibrosis mutations. Mol Biol Cell *27*, 424-433.

Wainwright, C.E., Elborn, J.S., Ramsey, B.W., Marigowda, G., Huang, X., Cipolli, M., Colombo, C., Davies, J.C., De Boeck, K., Flume, P.A.*, et al.* (2015). Lumacaftor-Ivacaftor in Patients with Cystic Fibrosis Homozygous for Phe508del CFTR.

N Engl J Med *373*, 220-231.

Ward, C.L., Omura, S., and Kopito, R.R. (1995). Degradation of CFTR by the ubiquitin-proteasome pathway. Cell *83*, 121-127.

Welsh, M.J., and Smith, A.E. (1993). Molecular mechanisms of CFTR chloride channel dysfunction in cystic fibrosis. Cell *73*, 1251-1254.

Woodward, O.M., Kottgen, A., Coresh, J., Boerwinkle, E., Guggino, W.B., and Kottgen, M. (2009). Identification of a urate transporter, ABCG2, with a common functional polymorphism causing gout. Proc Natl Acad Sci U S A *106*, 10338-10342.

Yang, H., Shelat, A.A., Guy, R.K., Gopinath, V.S., Ma, T., Du, K., Lukacs, G.L., Taddei, A., Folli, C., Pedemonte, N.*, et al.* (2003). Nanomolar affinity small molecule correctors of defective Delta F508-CFTR chloride channel gating. J Biol Chem *278*, 35079-35085.

Yu, Y.C., Sohma, Y., and Hwang, T.C. (2016). On the mechanism of gating defects caused by the R117H mutation in cystic fibrosis transmembrane conductance regulator. J Physiol *594*, 3227-3244.

Zhang, F., Kartner, N., and Lukacs, G.L. (1998). Limited proteolysis as a probe for arrested conformational maturation of ΔF508 CFTR. Nat Struct Biol *5*, 180-183.

Chapter 5

R751L-CFTR: description of clinical phenotype and molecular characterisation

AUTHORS:
Iram J Haq[1,2], Mike Althaus[3], Aaron Ions Gardner[1], Hui Ying Yeoh[4], Urjita Joshi[4], Vinciane Saint-Criq[5], Bernard Verdon[5], Jennifer Townshend[2], Christopher O'Brien[2], David Bourn[6], Mahfud Ben-Hamida[7], Matthew Thomas[2], Stephen Bourke[8], Ineke Braakman[4], Chris Ward[1], Mike Gray[5], Malcolm Brodlie[1,2].

Article submitted in 2019.

AFFILIATIONS:
[1]Institute of Cellular Medicine, Faculty of Medical Sciences, Newcastle University, Newcastle upon Tyne, UK.

[2]Paediatric Respiratory Medicine, Great North Children's Hospital, Newcastle upon Tyne Hospitals NHS Foundation Trust, Newcastle upon Tyne, UK.

[3]School of Natural and Environmental Sciences, Newcastle University, Newcastle upon Tyne, UK.

[4]Cellular Protein Chemistry, Utrecht University, Utrecht, The Netherlands.

[5]Institute for Cell and Molecular Biosciences, Faculty of Medical Sciences, Newcastle University, Newcastle upon Tyne, UK.

[6]Northern Molecular Genetics Service, Newcastle upon Tyne, UK.

[7]Department of Paediatrics, West Cumberland Hospital, Whitehaven, UK.

[8]Respiratory Medicine, Royal Victoria Infirmary, Newcastle upon Tyne, UK.

*Corresponding author: Malcolm Brodlie, MRC Clinician Scientist/ Honorary Consultant in Paediatric Respiratory Medicine, Level 3, Clinical Resource Building, Great North Children's Hospital, Queen Victoria Road, Newcastle upon Tyne, UK, NE1 4LP. E-mail: Malcolm.brodlie@newcastle.ac.uk. Tel: +44 191 2336161.

Keywords
Cystic fibrosis
R751L
Rare mutations
Primary bronchial epithelial cells
CFTR modulators

INTRODUCTION

Cystic fibrosis (CF) is a life-limiting autosomal recessive disease arising from mutations in the gene encoding the CF transmembrane conductance regulator (CFTR) protein [1]. This results in defective chloride (Cl^-) and bicarbonate ($HCO3^-$) transport, leading to subsequent airway surface dehydration [2-4]. This results in impaired mucociliary clearance, chronic endobronchial infection, neutrophilic inflammation and eventual respiratory failure [5, 6].

Approximately 2000 *CFTR* variants have been identified to date, however, a smaller proportion are disease-causing, of which F508del is the most common [7, 8]. Mutations are classified according to defects in protein production, trafficking to the plasma membrane or function at the cell surface [9]. R751L (p.Arg751Leu) is a missense mutation involving arginine to leucine substitution at codon 751 arising from a G > T change at cDNA nucleotide position c.2252 within the CFTR regulatory (R) domain [10]. Clinical information regarding R751L remains very limited, with one reported case of an infant diagnosed on newborn screening (NBS) with pancreatic insufficiency and sweat chloride of 73 mmol/L [10]. R751L has also not been characterised at a molecular level, with potential implications for: 1) mutation of the methylation site Arg^{751}, as evident with the R751P and R751C variants that cause respiratory disease [11]; 2) phosphorylation arising from proximity of R751L to key sites within the R domain and interactions with the second nucleotide binding domain (NBD2) and C-terminus [12, 13]; 3) ATP hydrolysis and channel gating given interactions of residues 748 to 778 with the first NBD (NBD1) [12]; 4) CFTR instability due to the loss of positive charge arising from arginine to leucine substitution.

In the current era of CFTR modulators, molecular understanding and characterisation of rarer mutations is required to inform appropriate treatments that improve clinical outcome. Here, we have identified a family of three individuals carrying two CFTR mutations, of which one is R751L. We describe their clinical phenotype and provide a molecular description of R751L-CFTR and the resultant impact on CFTR function using heterologous expression systems and *ex vivo* patient-derived culture models.

RESULTS

Individuals with R751L-CFTR display a mild disease phenotype

We identified three individuals with one R751L allele within the same family. One individual had F508del and two had G551D as their second allele. None of

the patients were on CFTR modulator therapies. Here we present a brief clinical summary for each individual (summarised in Table 1).

Patient 1 (F508del/R751L)
Patient 1 is a Caucasian male born in 2011. Immunoreactive trypsin (IRT) was elevated on UK NBS with identification of F508del on subsequent DNA analysis. Repeat IRT at 1 month remained elevated. In 2016, R751L was identified as the second allele following an extended screen analysis of 50 CFTR mutations.

As a young infant, initial sweat chloride was elevated (74 mmol/L), with evidence of mild pancreatic insufficiency (faecal elastase 110 μg/g). Repeat investigation at one year showed an elevated sweat chloride (88 mmol/L) and improvement of exocrine pancreatic function (487 μg/g). Growth was well maintained with height and weight parameters following the 91st centiles. *Burkholderia cepacia* was isolated on a respiratory culture in 2016 following persistent respiratory symptoms despite standard antimicrobial therapy. This was not detected on bronchoalveolar lavage both before and after targeted eradication therapy. The patient remained clinically well thereafter with regular mucolytic administration and physiotherapy for low grade sputum production. Annual chest x-ray (CXR) surveillance did not show features of respiratory disease and recent lung function assessment with forced expiratory volume in 1 second (FEV_1) was 116% predicted.

Patient 2 (G551D/F508del)
Patient 2 (aunt to patient 1) is a Caucasian female and was diagnosed with CF in 1993 at 6 months of age following elevated sweat chlorides (73 to 100 mmol/L) and persistent respiratory symptoms. Subsequent DNA analysis revealed the G551D CFTR mutation. The second mutation was identified as R751L with extended mutational analysis in 2016. IRT was negative and the patient remained pancreatic sufficient with normal faecal elastase. *Pseudomonas aeruginosa* was isolated in 2003, but eradicated with antimicrobial treatment. Patient 2 has remained well without treatment with recent predicted FEV_1 of 106% and normal CXR findings.

Patient 3 (G551D/R751L)
Patient 3 (uncle to patient 1, sister to patient 2) is a Caucasian male born in 1984 and was diagnosed with CF following the diagnosis of patient 2 in 1993. Initial DNA analysis revealed G551D as one of the CFTR mutations, and R751L was identified on extended mutational analysis in 2016. Sweat chloride values were elevated (80 to 100 mmol/L) and relevant respiratory microbiology included one *Haemophilus influenzae* isolate that was successfully treated. Semen analysis showed normal sperm function. Additional medical history included recurrent epigastric pain secondary to episodic pancreatitis. The patient remained clinically well without

Parameter	Patient 1	Patient 2	Patient 3
Age (y)	8	26	35
Sex	M	F	M
CFTR mutation	F508del/R751L	G551D/R751L	G551D/R751L
Sweat chloride (mmol/L)	71 - 88	73 - 100	80 - 100
Pancreatic status	Sufficient	Sufficient	Sufficient
Nutritional status	Height and weight: 91st centiles	BMI (kg/m^2): 39	BMI (kg/m^2): 23
CXR findings	Normal	Normal	Normal
FEV_1 (% predicted)	2.1 (116%)	4.01 L (106%)	3.94 (92%)
Respiratory microbiology	B. cepacia (eradicated)	P. aeruginosa (eradicated)	H. influenzae (treated)

Table 1: Clinical summary.
Abbreviations: BMI: body mass index; CXR: chest x-ray; F: female; FEV_1: forced expiratory volume in 1 second; M: male; y year.

treatment with normal CXR findings and recent predicted FEV_1 of 92%.

F508del/R751L HBEs have reduced but functional CFTR activity

To investigate CFTR function associated with R751L, we investigated I_{sc} responses in differentiated primary HBEs derived from patient 1 (F508del/R751L). In this system, functional CFTR is represented by a positive I_{sc} deflection arising from net anion serosal-mucosal secretion. After ENaC inhibition with amiloride, forskolin-mediated cAMP elevation resulted in CFTR activation (Figure 1A). This response was inhibited by $CFTR_{inh}$-172, confirming the presence of functional CFTR. The mean $CFTR_{inh}$-172-sensitive I_{sc} was 15% greater than the forskolin response, suggesting significant basal CFTR activity in the absence of forskolin.

Responses were compared with HBEs derived from five children without CF (Figure 1B) and three F508del homozygous children (Figure 1C), the latter as a comparator of severe disease. Despite the residual CFTR activity in F508del/R751L HBEs, there was a 69% reduction in function compared with non-CF HBEs. Although CFTR function was greater in F508del/R751L HBEs compared to F508del/F508del HBEs, this was not statistically significant. These differences were paralleled in the $CFTR_{inh}$-172 responses, where mean F508del/R751L HBE responses were lower than those in non-CF HBEs, and although greater compared with F508del/F508del HBEs, were not statistically significant. The amiloride-sensitive I_{sc} was lowest in F508del/

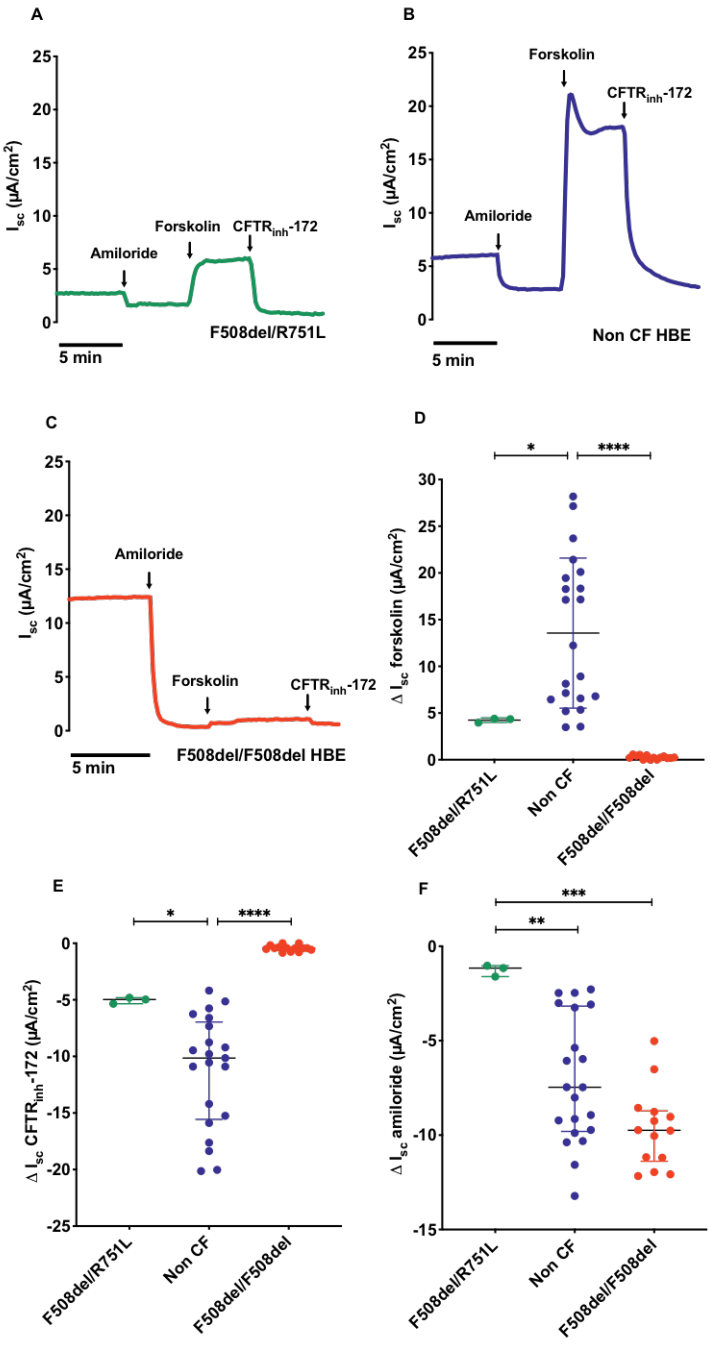


Figure 1: Short circuit current assessment in F508del/R751L patient derived HBEs demonstrate CFTR function.
A: Representative trace for F508del/R751L HBEs showing an upward I_{sc} deflection in response to forskolin, which was inhibited by CFTR$_{inh}$-172. **B:** Representative trace for a non-CF patient showing a large upward I_{sc} deflection in response to forskolin followed by a downward deflection with CFTR$_{inh}$-172. **C:** Representative trace for a F508del/F508del CF patient showing comparatively small changes in I_{sc} in response to forskolin and CFTR$_{inh}$-172. **D and E:** Comparative assessment of I_{sc} change (DI_{sc}) in response to forskolin **(D)** and CFTR$_{inh}$-172 **(E)** showed greatest responses in non-CF compared with F508del/R751L HBEs. F: Comparative DI_{sc} change in response to amiloride showed a smallest response in F508del/R751L HBEs (*p<0.05; **p<0.01; ***p<0.001; **** p<0.0001; one-way ANOVA and Tukey's post hoc comparison). All responses were measured after initial ENaC inhibition with amiloride. Depicted are values obtained from individual culture inserts with corresponding mean ± S.D. F508del/R751L HBEs: n=3 inserts; non-CF HBEs: n=21 inserts from 5 donors; F508del/F508del HBEs: n=14 inserts from 3 donors.

R751L HBEs compared with both non-CF and F508del/F508del HBEs.

These findings demonstrate residual CFTR function in F508del/R751L HBEs, which was lower in magnitude than in non-CF HBEs. ENaC function was reduced in F508del/R751L HBEs compared with non-CF and F508del/F508del HBEs.

R751L CFTR-expressing *Xenopus* oocytes demonstrate functional CFTR activity

To further investigate CFTR activity associated with R751L in isolation, I_M responses to forskolin and genistein were measured in R751L CFTR- expressing *Xenopus* oocytes, with wild-type (WT) CFTR-expressing oocytes as a positive control.

In both WT and R751L CFTR-expressing oocytes, forskolin triggered an I_M increase as indicated by the downward deflection. This was further augmented with genistein and inhibited with $CFTR_{inh}$-172 (Figure 2A-D). Comparative assessment of the total CFTR current (I_M triggered by forskolin and genistein) did not reveal significant differences between WT and R751L-CFTR (Figure 2E). Furthermore, there was no difference between WT and R751L-CFTR in relative stimulation of channel activity by forskolin with respect to total currents (Figure 2F).

These findings confirm functional CFTR activity associated with R751L, with a magnitude analogous to WT-CFTR.

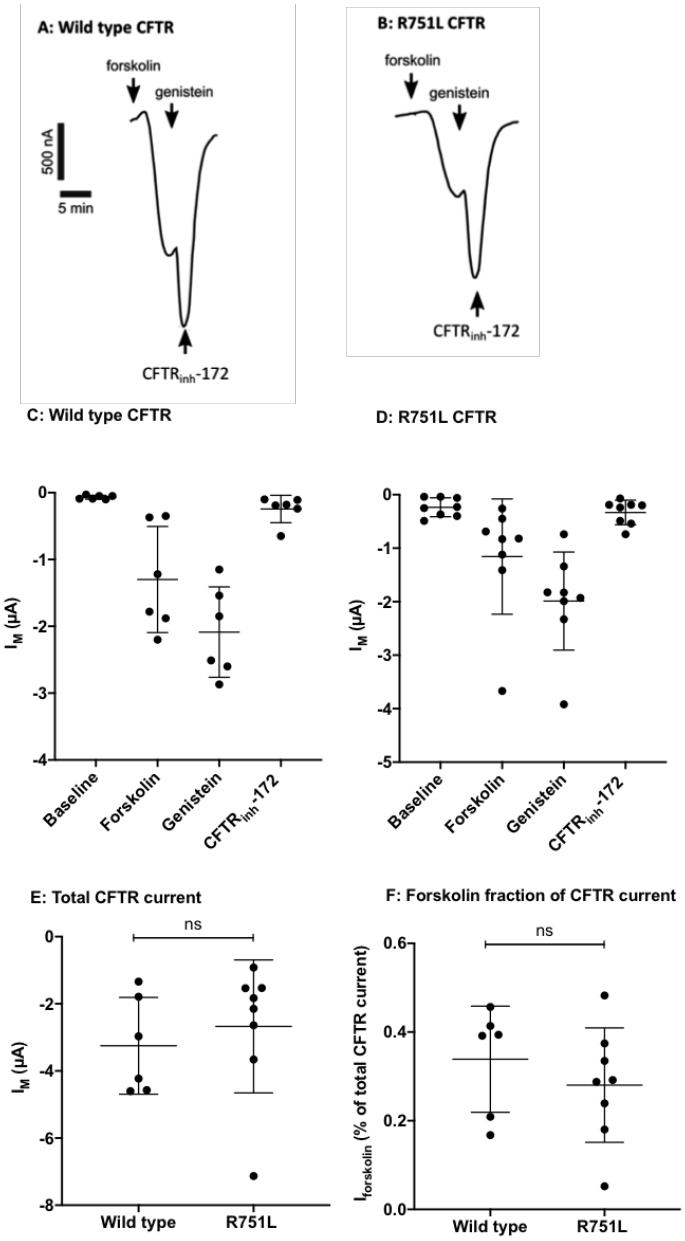


Figure 2: R751L CFTR-expressing Xenopus oocytes demonstrate similar CFTR transmembrane currents to WT-CFTR.
A and B. Representative traces for transmembrane current (I_M) measurement in response to forskolin, genistein and $CFTR_{inh}$-172 in *Xenopus* oocytes expressing wild type and R751L CFTR. Downward-deflections are indicative of anion efflux. **C and D.** I_M measurement in oocytes expressing WT (C) and R751L (D) CFTR demonstrated forskolin and genistein-induced I_M which were inhibited by $CFTR_{inh}$-172. **E.** The total CFTR I_M (the sum of forskolin and genistein-induced I_M) was the same in WT and R751L CFTR-expressing oocytes. **F.** The forskolin fraction of the CFTR current (the percentage of the total CFTR current) was also the same in WT and R751L CFTR-expressing oocytes. Data for **E** and **F** analysed with unpaired t test. Depicted are peak I_M values after drug application from individual experiments; n=6 for WT; n=8 for R751L CFTR).

Transport of CFTR to the Golgi complex is not affected by R751L
In light of residual CFTR function evident in F508del/R751L HBEs and R751L CFTR-expressing oocytes, we assessed R751L transport in the secretory pathway. HEK293 cells expressing R751L-CFTR, WT-CFTR as a positive control, and F508del-CFTR as a negative control, were labelled with ^{35}S-methionine/cysteine during a 15-minute pulse (Figure 3A, left panels) and the radiolabel was chased in the presence of excess unlabelled amino acids (Figure 3A, right panels). Detergent cell lysates were subjected in parallel to immunoprecipitation of CFTR (Figure 3A, top panels) and limited proteolysis as previously detailed (Figure 3A, other panels) [16, 18, 19].

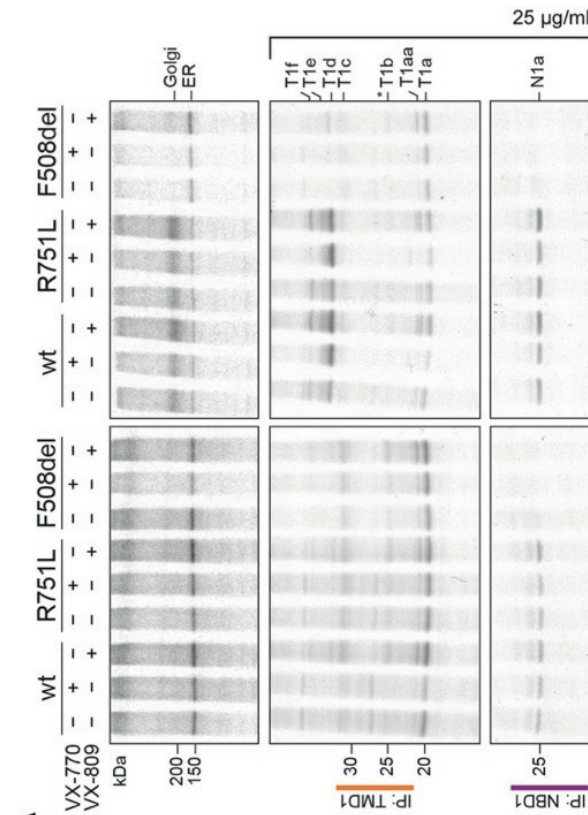
In the 15-minute pulse time, both mutants were synthesised to similar levels as WT-CFTR (Figure 3, top left panel). During the chase, WT-CFTR completed its folding and travel to the Golgi complex, where the ER form changed into the Golgi form due to glycan modifications (Figure 3, top right panel). The F508del mutation instead caused CFTR misfolding and degradation, leading to a decrease in ER form and absence of Golgi form.

These findings demonstrated that the R751L-CFTR mutant reached the Golgi as efficiently as WT-CFTR.

Folding of CFTR is not affected by R751L
To assess folding of R751L-CFTR, detergent lysates were subjected to limited Proteinase K digestion (25 μg/ml for 15 minutes on ice), followed by immunoprecipitation with CFTR-domain-specific antibodies. Using this technique, misfolded proteins demonstrate altered or increased protease resistance that can be detected by SDS-PAGE [16, 18, 19].

Immediately after synthesis (Figure 3A, left panels) TMD1 (T1 a-c) and TMD2 (T2 b) fragment patterns were the same for the R751L-CFTR, WT-CFTR and F508del-CFTR, suggesting similar folding of both TMDs. Whereas F508del NBD1 was completely protease sensitive (no resistant fragment detectable), WT and R751L NBD1 had similar protease resistances (fragment N1a). NBD2 was not resistant to digestion, and because of epitope absence, the antibody demonstrated increased immunoprecipitated background for all three constructs. Two hours after synthesis (after the 2 hour chase), R751L again was indistinguishable from WT-CFTR. TMD1, TMD2, and NBD2 became more protease resistant, yielding larger fragments, whereas NBD1 did not change its folded state over time.

The sensitivity of each construct to VX-770 or VX-809 was examined by modulator addition from 15 minutes before pulse labelling to the end of the chase. VX-809 rescued some F508del CFTR from the ER; after 2 hours of chase a Golgi band was



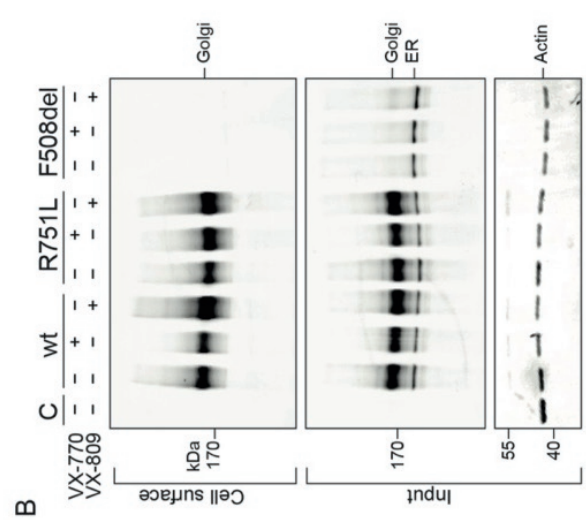


Figure 3: Impact of R751L on CFTR protein folding, transport and cell-surface biotinylation in HEK293-cells.
A. HEK293-cells expressing CFTR constructs were labelled with ^{35}S-methionine/ cysteine for 15 minutes and chased for 0 or 2 h in the presence of 3 µM VX-770 or 3 µM VX-809 or DMSO solvents. Cells were lysed in 1% Triton X-100 in MNT and lysates were treated or not with Proteinase K at 25 µg/ml for 15 minutes. CFTR and fragments were immunoprecipitated using TMD1C (TMD1), Mr Pink (NBD1 and full-length CFTR), TMD2C (TMD2), or 596 (NBD2) antibodies. Proteins were analysed on 7.5% (full-length CFTR) and 12% (proteolytic fragments) SDS-PAGE gels. * indicates nonspecific bands. **B.** Cell-surface biotinylation of HEK293 cells expressing CFTR constructs with or without VX-809 or VX-770 pre-treatment. Cells were lysed in 1% Triton X-100 in MNT and lysates were used for pull down of biotinylated proteins with Neutravidin-beads. Proteins were analysed on 7.5% SDS-PAGE gels and transferred to PVDF-membrane and blotted for CFTR (596) or actin.

visible. NBD1 was not rescued but the other domains showed a small increase in protease resistance [16]. R751L and WT-CFTR both slightly increased expression upon VX-809 treatment, yielding some more Golgi form as well. VX-770 acted the same on WT and R751L, slightly destabilising TMD1 (decrease of T1e and Tf) and TMD2 (decrease of T2b and T2c) [16]. Again, R751L was indistinguishable from WT-CFTR.

R751L and WT-CFTR show similar cell-surface localisation
To establish whether the Golgi-modified form of R751L-CFTR reached the cell surface, we compared this mutant with WT and F508del-CFTR. Cell-surface biotinylation showed that only the Golgi form of CFTR was detectable on the cell surface, and there was no difference between WT and R751L-CFTR. F508del-CFTR did not reach the cell surface detectably, neither with nor without VX-809 (Figure 3B).

In conclusion, R751L-CFTR was biochemically indistinguishable from WT-CFTR in relation to folding, domain assembly, transport out of the ER to the Golgi complex and cell surface, and responses to VX-809 and VX-770.

DISCUSSION

We have described the mild clinical phenotype of three R751L-CFTR heterozygote individuals, as confirmed by lung function stability, presence of exocrine pancreatic sufficiency and good nutritional status. Both F508del (resulting in defective protein folding) and G551D (a gating mutation) are associated with a severe phenotype, characterised by pulmonary dysfunction and pancreatic insufficiency [6]. In our study, the F508del/R751L individual experienced an increase in respiratory symptoms compared to the G551D/R751L individuals.

We have characterised the molecular effects of R751L-CFTR in two different model systems, and demonstrated that 1) the transmembrane functional properties of R751L-CFTR were similar to those evident in WT-CFTR; 2) CFTR transport to the Golgi complex and CFTR folding were not compromised by R751L presence, and 3) the biochemical responses of R751L-CFTR to VX-770 and VX-809 were indistinguishable to those seen with WT-CFTR. Our work in patient-derived F508del/R751L HBEs showed that Cl^- transport was compromised, but to a lesser degree than in F508del/F508del HBEs, which may parallel the clinical phenotype and sweat chloride of patient 1. Patient-derived G551D/R751L HBEs were not available in this study due to the absence of bronchoscopies performed in patients 1 and 2 and limitations in ethical approval, but may have provided complementary functional

information.

CFTR function is a composite of three factors: channel number, open probability and single channel conductance. Although our I_{sc} and I_M assessments measured channel function as a whole, we did not specifically investigate the impact of R751L-CFTR on single channel conductance, which would require single channel recordings using the patch clamp technique [20].

CFTR genotype is strongly correlated with sweat chloride, despite its weak correlation with clinical outcome [21, 22]. Despite their mild clinical features, presence of either F508del or G551D as the second allele in these individuals could have influenced elevated sweat chloride values (>60 mmol/L) and indeed contributed to reduced Cl- transport evident in patient-derived F508del/R751L HBEs. Elevated sweat chloride values could alternatively be explained by a reduction in ENaC function, as evident in the F508del/R751L HBEs. In the sweat duct, the combined actions of ENaC and CFTR, result in net sodium chloride absorption [23]. A reduction in ENaC-mediated sodium absorption would ultimately result in reduced chloride absorption and increased sweat chloride. Other external factors, including the presence of alternative chloride channels may have contributed to these elevated values [4]. Application of relevant CFTR modulators could ascertain the potential to improve CFTR function in F508del/R751L HBEs, but was not possible in this study. However, the R751L-CFTR construct was potentiated by VX-770, suggesting that this variant would benefit from CFTR potentiator therapy .

There is no published information to this detail regarding R751L-CFTR preceding our work. Our characterisation of R751L-CFTR has significant clinical value, and will inform the approach for patient follow-up, that will balance timely clinical surveillance with prevention of undue patient and parental anxiety. Our work will guide counselling strategies for parents with newly diagnosed infants, where previously the outlook was uncertain. CFTR potentiators currently licensed for use may have potential to benefit people with R751L-CFTR. This is an evolving field, and the molecular and clinical information provided in our study is likely to have relevance for the future management of these patients.

MATERIALS AND METHODS

Patient subjects

Patient medical records were consulted with relevant written permissions. Primary human bronchial epithelial (HBE) cells were collected from children with and

without CF undergoing a clinically indicated bronchoscopy with relevant ethical approval (UK National Research Ethics Committee 15/NE/0215).

Primary cell culture

HBEs were collected by bronchoscopic brushing of the mucosal surface of a second or third-generation bronchus. First passage HBEs were seeded on collagen-coated semipermeable inserts (Corning) and maintained in air liquid interface (ALI) culture for 3 to 4 weeks as previously described [14]. Fully differentiated HBEs were characterised through demonstration of mucus production, cilia formation and transepithelial resistance (TEER) (STX2 electrodes, EVOM2TM Epithelial Voltohmmeter, World Precision Instruments).

Short circuit current assessment

To assess CFTR function, differentiated first passage HBE ALI cultures with TEERs greater than 400 $\Omega.cm^2$ were mounted in Ussing chambers (Physiologic Instruments) to measure short-circuit currents (I_{sc}). HBEs were equilibrated in symmetrical apical and basolateral Krebs solution (containing in mM: 115 NaCl, 25 $NaHCO_3$, 5 KCl, 1 $CaCl_2$ and 1 $Mg Cl_2$; pH 7.4, 37 °C) and gassed with 5% CO_2/ 95% O_2. The following reagents (Tocris Bioscience) were sequentially added to the apical compartment and corresponding short circuit current (I_{sc}) changes recorded: amiloride (100 μM) to inhibit the epithelial sodium channel (ENaC), forskolin (10 μM) to stimulate CFTR, and $CFTR_{inh}$-172 (20 μM) to inhibit CFTR. Data were recorded and digitised using Acquire and Analysis software (version 2.3, Physiologic Instruments).

Synthesis of cRNA and heterologous expression in *Xenopus* oocytes

Plasmid DNA containing human CFTR was kindly provided by Professor Blanche Schwappach (University of Goettingen, Germany). The R751L-CFTR mutation was generated by site-directed mutagenesis using the QuikChangeLightning Kit (Agilent Technologies) according to manufacturer's instructions and using the forward (5'-ctgatcacgctgatgagaggcagtatcgcct-3') and reverse-primer (5'-aggcgatactgcctctcatcagcgtgatcag-3') sequences. Successful mutation generation was verified by DNA-sequencing and cRNA synthesized as previously described [15].

Procedures using *Xenopus* tissues were approved by the Newcastle University Animal Welfare and Ethical Review Body (project ID 630). *Xenopus* laevis ovaries (European *Xenopus* Resource Centre, Portsmouth, UK) were dissected and incubated for 90 minutes in 25 mg/ml Collagenase A (Roche) at room temperature in ORII solution (containing in mM: 82.5 NaCl, 2 KCl, 1 $MgCl_2$ x $6H_2O$ and 10 HEPES; pH 7.5). The cell suspension was washed with equal volumes of ORII and Modified Barth's solution (MBS in mM: 88 NaCl, 1 KCl, 2.4 $NaHCO_3$, 0.82 $MgSO_4$ x $7H_2O$, 0.33

$Ca(NO_3)_2$ x $4H_2O$, 0.41 $CaCl_2$ x $2H_2O$, 10 HEPES, 20 μg/ml gentamycin; pH 7.5). Stages V and VI oocytes were stored at 16 °C in MBS. Fifty-one nanolitres of cRNA were injected into oocytes with a Nanolitre-Injector (Drummond Scientific) yielding final concentrations of 12.5 ng RNA/oocyte. Injected oocytes were cultured for 3 days at 16 °C MBS.

Two-electrode voltage-clamp recordings (TEVC)
Oocytes were placed in a Lucite chamber and continuously perfused with oocyte Ringer's solution (in mM: 90 NaCl, 1 KCl, 2 $CaCl_2$ and 5 HEPES, pH 7.4). Microelectrode recordings were performed as previously described [15]. Transmembrane currents (I_M) were low-pass filtered at 1 kHz (LPF-202, Warner Instruments) and recorded by a strip-chart recorder (Kipp & Zonen). I_M responses to forskolin (5 μM), genistein (40 μM) and $CFTR_{inh}$-172 (10 μM) (Tocris Bioscience) were recorded at room temperature and digitalised using Inkscape (version 0.91).

HEK293 cell culture and transient expression
HEK293 cells were maintained in DMEM supplemented with 10% FCS and 2 mM Glutamax at 37°C and 5% CO_2. Cells were grown in 6 cm dishes to ~70% confluency and transfected using Lipofectamine 3000 (Thermo Fisher Scientific) according to manufacturer's instructions or PEI MAX40 (Polysciences) as previously described [16]. The R751L-CFTR mutant was made by Gibson assembly using the template pBi.CMV2-CFTR [16] and primers: 5'-gaggcgatactgcctctcatcagcgtgatcagc-3', 5'-tgctgatcacgctgatgagaggcagtatcgcctc-3', 5'-taaccctgataaatgcttcaataatattgaaaaaggaagagt-3', 5'-agcatttatcagggttattgtctcatgagc-3'.

Pulse-chase analysis, limited proteolysis and immunoprecipitation
HEK293 cells were used 24 h post-transfection for pulse-chase experiments as described (Supplementary methods) [16, 17]. Where indicated, VX-770 or VX-809 (Selleckchem) were added to 3 μM (final concentration) in media during starvation, pulse, and chase. Supernatants were prepared and used for limited proteolysis or direct immunoprecipitation (Supplementary methods) [16, 18].

Cell-surface biotinylation and Western blot
The pool of plasma membrane CFTR was assayed by cell-surface biotinylation followed by neutravidin pull down as described (supplementary methods). Samples were analysed by Western blot using monoclonal antibody 596 (1:5,000), rabbit anti-actin (1:5,000, Sigma), and goat-anti-mouse Alexa-800 (1:10,000, LiCoR) and donkey-anti-rabbit Alexa-680 (1:10,000, LiCoR) secondary antibodies. Detection was performed using infrared imaging (LiCoR Odyssey CLx) as previously described [16].

Statistical analysis

Results are presented as individual data points with the mean ± standard deviation (SD) for HBE inserts or *Xenopus* oocytes. Statistical analysis was performed using an unpaired t test or one-way ANOVA with Tukey's post hoc multiple comparison in GraphPad Prism software (version 8.2, GraphPad Software). *P* values of $p<0.05$ were considered statistically significant.

ACKNOWLEDGMENT

We thank Prof. Blanche Schwappach (University of Goettingen, Germany) for providing plasmid DNA containing human CFTR and Prof. John Riordan (University of North Carolina Chapel Hill, USA) and the CFF for kindly providing the 596 antibody.

SUPPORT STATEMENT

Iram J Haq was supported by a Wellcome Trust Clinical Research Training Fellowship (203520/Z/16/Z). Malcolm Brodlie was supported by a Medical Research Council Clinician Scientist Fellowship (MR/M008797/1). Mike Gray, Chris Ward and Malcolm Brodlie were supported by CF Trust Strategic Research Centre grants (SRC003 and SRC013). The PvdS-IB lab was supported by the Netherlands Organisation for Health Research and Development (ZonMw TOP 40-00812-98-14103), the Dutch Research Council (LIFT 731.017.404), and the CFF (BRAAKM14XX0). The research was supported by the National Institute for Health Research (NIHR) Newcastle Biomedical Research Centre based at Newcastle Hospitals NHS Foundation Trust and Newcastle University. The views expressed are those of the author(s) and not necessarily those of the NHS, the NIHR or the Department of Health.

REFERENCES

1. Riordan, J., et al., *Identification of the cystic fibrosis gene: cloning and characterization of complementary DNA.* Science, 1989. **245**(4922): p. 1066-1073.
2. Button, B., et al., *A periciliary brush promotes the lung health by separating the mucus layer from airway epithelia.* Science, 2012. **337**(6097): p. 937-941.
3. Haq, I.J., et al., *Airway surface liquid homeostasis in cystic fibrosis: pathophysiology and therapeutic targets.* Thorax, 2015. **71**: p. 284-287.
4. Martin, S.L., et al., *Ion channels as targets to treat cystic fibrosis lung disease.* Journal of Cystic Fibrosis, 2018. **17**(2, Supplement): p. S22-S27.
5. O'Sullivan, B.P. and Freedman, S.D., *Cystic fibrosis.* The Lancet, 2009. **373**(9678): p. 1891-1904.
6. Elborn, J.S., *Cystic fibrosis.* The Lancet, 2016. **388**(10059): p. 2519-2531.
7. Zolin, A., et al., *European cystic fibrosis society patient registry annual report 2016*. 2017: Denmark.
8. US CF Foundation, *The clinical and functional translation of CFTR (CFTR2)*.
9. Haq, I.J., et al., *Modulator therapies for cystic fibrosis.* Paediatrics and Child Health, 2019. **29**(4): p. 151-157.
10. *Cystic Fibrosis Mutation database* 01.08.2017]; Available from: http://www.genet.sickkids.on.ca/MutationDetailPage.external?sp=1987.
11. Pankow, S., C. Bamberger, and J.R. Yates, *A posttranslational modification code for CFTR maturation is altered in cystic fibrosis.* Science Signaling, 2019. **12**.
12. Bozoky, Z., et al., *Regulatory R region of the CFTR chloride channel is a dynamic integrator of phospho-dependent intra- and intermolecular interactions.* Proceedings of the National Academy of Sciences of the United States of America, 2013. **110**(47): p. E4427-E4436.
13. Stevers, L.M., et al., *Characterization and small-molecule stabilization of the multisite tandem binding between 14-3-3 and the R domain of CFTR.* Proceedings of the National Academy of Sciences of the United States of America, 2016. **113**: p. E1152-E1161.
14. Brodlie, M., et al., *Primary bronchial epithelial cell culture from explanted cystic fibrosis lungs.* Experimental Lung Research, 2010. **36**(2): p. 101-110.
15. Perniss, A., et al., *Hydrogen sulfide stimulates CFTR in Xenopus oocytes by activation of the cAMP/PKA signalling axis.* Scientific Reports, 2017. **7**(1): p. 3517.
16. van Willigen, M., et al., *Folding–function relationship of the most common cystic fibrosis–causing CFTR conductance mutants.* Life Science Alliance, 2019. **2**.
17. McCaul, N., et al., *Analysis of protein folding, transport, and degradation in living cells by radioactive pulse chase.* Journal of Visualized Experiments, 2019(144): p. e58952.
18. Hoelen, H., et al., *The primary folding defect and rescue of ΔF508 CFTR emerge during translation of the mutant domain.* PLOS ONE, 2010. **5**(11): p. e15458.
19. Kleizen, B., et al., *Folding of CFTR Is predominantly cotranslational.* Molecular Cell, 2005. **20**(2): p. 277-287.
20. Gray, M.A., et al., *Two types of chloride channel on duct cells cultured from human fetal pancreas.* American Journal of Physiology-Cell Physiology, 1989. **257**(2): p. C240-C251.
21. Durmowicz, A.G., et al., *Change in sweat chloride as a clinical end point in cystic fibrosis clinical trials: The*

Ivacaftor experience. Chest, 2013. **143**(1): p. 14-18.

22. Collaco, J.M., et al., *Sources of variation in sweat chloride measurements in cystic fibrosis.* American journal of respiratory and critical care medicine, 2016. **194**(11): p. 1375-1382.

23. Saint-Criq, V. and Gray, M.A., *Role of CFTR in epithelial physiology.* Cellular and molecular life sciences : CMLS, 2017. **74**(1): p. 93-115.

SUPPLEMENTARY METHODS

Patient subjects

Patient medical records were consulted with relevant written permissions. Primary human bronchial epithelial (HBE) cells were collected from children with and without CF undergoing a clinically indicated bronchoscopy with relevant ethical approval (UK National Research Ethics Committee 15/NE/0215).

Primary cell culture

HBEs were collected by bronchoscopic brushing the mucosal surface of a second or third-generation bronchus. First passage HBEs were seeded on collagen-coated semipermeable inserts (Corning) and maintained in air liquid interface (ALI) culture for 3 to 4 weeks as previously described [13]. Fully differentiated HBEs were characterised through demonstration of mucus production, cilia formation and transepithelial resistance (TEER) measurement (STX2 electrodes, EVOM2TM Epithelial Voltohmmeter, World Precision Instruments).

Short circuit current assessment

To assess CFTR function, differentiated first passage HBE ALI cultures with TEERs greater than 400 $\Omega.cm^2$ were mounted in Ussing chambers (Physiologic Instruments) to measure short-circuit currents (I_{sc}). HBEs were equilibrated in symmetrical apical and basolateral Krebs solution (containing in mM: 115 NaCl, 25 $NaHCO_3$, 5 KCl, 1 $CaCl_2$ and 1 $Mg\ Cl_2$, pH 7.4, 37 °C) and gassed with 5% CO_2/ 95% O_2. The following reagents (Tocris Bioscience) were sequentially added to the apical compartment and corresponding short circuit current (I_{sc}) changes recorded: amiloride (100 μM) to inhibit the epithelial sodium channel (ENaC), forskolin (10 μM) to stimulate CFTR, and $CFTR_{inh}$-172 (20 μM) to inhibit CFTR. Data were recorded and digitised using Acquire and Analysis software (version 2.3, Physiologic Instruments).

Synthesis of cRNA and heterologous expression in *Xenopus* oocytes

Plasmid DNA containing human CFTR was kindly provided by Professor Blanche Schwappach (University of Goettingen, Germany). The R751L-CFTR mutation was generated by site-directed mutagenesis using the QuikChangeLightning Kit (Agilent Technologies) according to manufacturer's instructions and using the forward (5'-ctgatcacgctgatgagaggcagtatcgcct-3') and reverse-primer (5'-aggcgatactgcctctcatcagcgtgatcag-3') sequences. Successful mutation generation was verified by DNA-sequencing and cRNA synthesized as previously described [14]. Procedures using *Xenopus* tissues were approved by the Newcastle University Animal Welfare and Ethical Review Body (project ID 630). *Xenopus* laevis ovaries (European *Xenopus* Resource Centre, Portsmouth, UK) were dissected and

incubated for 90 minutes in 25 mg/ml Collagenase A (Roche) at room temperature in ORII solution (containing in mM: 82.5 NaCl, 2 KCl, 1 $MgCl_2$ x $6H_2O$ and 10 HEPES; pH 7.5). The cell suspension was washed with equal volumes of ORII and Modified Barth's solution (MBS in mM: 88 NaCl, 1 KCl, 2.4 $NaHCO_3$, 0.82 $MgSO_4$ x $7H_2O$, 0.33 $Ca(NO_3)_2$ x $4H_2O$, 0.41 $CaCl_2$ x $2H_2O$, 10 HEPES, 20 μg/ml gentamycin, pH 7.5). Stages V and VI oocytes were stored at 16 °C in MBS. Fifty-one nanolitres of cRNA were injected into oocytes with a Nanolitre-Injector (Drummond Scientific) yielding final concentrations of 12.5 ng RNA/oocyte. Injected oocytes were cultured for 3 days at 16 °C MBS.

Two-electrode voltage-clamp recordings (TEVC)

Oocytes were placed in a Lucite chamber and continuously perfused with oocyte Ringer's solution (in mM: 90 NaCl, 1 KCl, 2 $CaCl_2$ and 5 HEPES, pH 7.4). Microelectrode recordings were performed as previously described [14]. Transmembrane currents (I_M) were low-pass filtered at 1 kHz (LPF-202, Warner Instruments) and recorded by a strip-chart recorder (Kipp & Zonen). I_M responses to forskolin (5 μM), genistein (40 μM) and $CFTR_{inh}$-172 (10 μM) (Tocris Bioscience) were recorded and digitalised using Inkscape (version 0.91). All recordings were performed at room temperature.

HEK293 cell culture and transient expression

HEK293 cells were maintained in DMEM supplemented with 10% FCS and 2 mM Glutamax at 37°C and 5% CO_2. Cells were grown in 6 cm dishes to ~70% confluency and transfected using Lipofectamine 3000 (Thermo Fisher Scientific) according to manufacturer's instructions or PEI MAX40 (Polysciences) as previously described [15]. The R751L-CFTR mutant was made by Gibson assembly using the template pBi.CMV2-CFTR [15] and primers: 5'-gaggcgatactgcctctcatcagcgtgatcagc-3', 5'-tgctgatcacgctgatgagaggcagtatcgcctc-3', 5'-taaccctgataaatgcttcaataatattgaaaaaggaagagt-3', 5'-agcatttatcagggttattgtctcatgagc-3'.

Pulse-chase analysis and limited proteolysis

HEK293 cells were used 24 h post-transfection for pulse-chase experiments as described [15, 16]. Briefly, cells were labelled for 15 minutes with 143 μCi/6-cm dish of EasyTag Express ^{35}S-protein-labeling mix (Perkin Elmer). Labelling was stopped by adding excess unlabelled cysteine and methionine and the labeled protein was chased for different periods of time. Where indicated, VX-770 or VX-809 (Selleckchem) were added to 3 μM (final concentration) in media during starvation, pulse, and chase. Dishes were transferred to ice and washed twice with ice-cold HBSS (Life Technologies). Cells were lysed using 1% Triton X-100 in MNT (in mM: 20 MES, 100 NaCl, 30 Tris-HCl, pH 7.5). Lysates were cleared by centrifugation for

10 minutes at 16,000 x g and 4°C. The supernatant was used for limited proteolysis (see below) or direct immunoprecipitation and analysis using 7.5% or 12% SDS-PAGE [15, 17]. In brief, detergent lysates were incubated with 25 µg/ml proteinase K from Tritirachium album (Sigma-Aldrich) for 15 minutes on ice. Digestions were stopped by adding an equal volume of MNT, 1% Triton X-100, 2 mM PMSF and 2 µg/ml of chymostatin, leupeptin, antipain, pepstatin A (all from Sigma-Aldrich), and fragments were immunoprecipitated using domain-specific antibodies

Immunoprecipitation

Full-length CFTR in non-treated lysates and limited-proteolysis samples were transferred to 50 µl of protein-A beads (GE Healthcare) with pre-adsorbed antibody and immunoprecipitates as described [15]. Rabbit antibodies MrPink (against NBD1), transmembrane domain (TMD) 1C (against TMD1), TMD2C (against TMD2), and mouse monoclonal 596 (against NBD2) were previously described [15]; 596 was kindly provided by Prof.. John Riordan (UNC School of Medicine, USA) [18].
All immunoprecipitates were washed twice for 10 minutes at room temperature. Proteolytic fragments originating from TMD1 were immunoprecipitated for 3 hours at 4°C with TMD1-C antibody, and washed with 10 mM Tris-HCl pH 8.6, 300 mM NaCl, 0.05% SDS, 0.05% Triton X-100. NBD1 fragments were immunoprecipitated overnight at 4°C with MrPink antibody and washed with 10 mM Tris-HCl pH 8.6, 300 mM NaCl, 0.1% SDS, 0.05% Triton X-100. Fragments derived from TMD2 were immunoprecipitated for 3 hours at 4°C with TMD2-C antibody and washed with 50 mM Tris-HCl pH 8.0, 150 mM NaCl, 1 mM EDTA. NBD2-derived fragments were immunoprecipitated for 3 hours at 4°C with 596 antibody and washed using 30 mM Tris-HCl pH 7.5, 20 mM MES, 100 mM NaCl, 0.5% Triton X-100. Washed immunoprecipitates were resuspended in 10 µl 10 mM Tris-HCl pH 6.8 and 10 µl 2x reducing Laemmli sample buffer and denatured for 5 minutes at 55°C before analysis by 12% SDS-PAGE. Gels were dried and exposed to X-ray film for display.

Cell-surface biotinylation and Western blot

The pool of plasma membrane CFTR was assayed by cell-surface biotinylation followed by neutravidin pull down and Western blot as previously described [15]. In brief, cells received fresh medium with VX-770 or VX-809 (3 µM) 4 hours after transfection and were maintained for 16 hours. Dishes were transferred to ice and washed twice with PBS^{++}. Next, dishes received 500 µl PBS^{++} containing 0.5 mg/ml sulpho-NHS-SS-Biotin (Thermo Fisher) and were incubated for 30 minutes on ice. Non-reacted sulpho-NHS-SS-Biotin was quenched and cells were lysed in 300 µl MNT, 1% Triton X-100, 1 µg/ml of Chymostatin, Leupeptin, Antipain, Pepstatin A (Sigma- Aldrich) and 1 mM PMSF. Lysates were cleared by centrifugation for 10 minutes at 16,000 x g and 4°C. An aliquot of 10 µl of lysate was transferred to an equal volume of 2x reducing Laemmli sample buffer and saved as input sample.

The remaining lysate was incubated with 25 µl Neutravidin beads (Thermo Fisher) for 1 hour and washed twice with 10 mM Tris-HCl pH 8.6, 300 mM NaCl, 0.1% SDS and 0.05% Triton X-100. Beads were resuspended in 15 µl of 10 mM Tris-HCl pH 6.8 and 15 µl of 2x reducing Laemmli sample buffer and bound proteins were eluted for 5 minutes at 55°C . Samples were resolved on 7.5% SDS-PAA gels and analysed by Western blot using monoclonal antibody 596 (1:5,000), rabbit anti-actin (1:5,000, Sigma), and goat-anti-mouse Alexa-800 (1:10,000, LiCoR) and donkey-anti-rabbit Alexa-680 (1:10,000, LiCoR) secondary antibodies. Detection was performed using infrared imaging (LiCoR Odyssey CLx).

Statistical analysis

Results are presented as individual data points with the mean ± standard deviation (SD) for individual HBE inserts or *Xenopus* oocytes. Statistical analysis was performed by an unpaired t test or one-way ANOVA and Tukey's post hoc multiple comparison in GraphPad Prism software (version 8.2, GraphPad Software). *P* values of $p<0.05$ were considered as statistically significant.

Chapter 6

The role of the ER membrane complex (EMC) in CFTR folding and stability

AUTHORS:
Hui Ying Yeoh, Peter van der Sluijs, Ineke Braakman

Abstract

Membrane proteins such as ion channels often feature charged amino acids in their transmembrane (TM) segments for structural and functional purposes. These charged residues may inhibit proper insertion into the endoplasmic reticulum (ER) membrane during protein synthesis and subsequently impair co-translational folding of transmembrane domains (TMDs). Chaperones thus likely are required for stabilizing these charged residues before successful protein folding is accomplished. The ER membrane complex (EMC) is one of the highly-conserved ER-resident complexes that was recently found to be able to chaperone TMDs with folding-challenged sequences. The mechanism of EMC chaperone activity however largely remains unknown. By using a radiolabeling, protease susceptibility assay, and immunoprecipitation, we discovered that the folding of a candidate EMC substrate, the Cystic Fibrosis Transmembrane Conductance Regulator (CFTR), was reduced upon EMC knockout. Specifically, the co-translational folding of the second transmembrane domain (TMD2) of CFTR was affected while the other domains remained unaffected. The destabilization of TMD2 also affected CFTR post-translational folding. Our experiments provide direct evidence of how EMC assists the folding of TMDs that contain destabilizing features.

INTRODUCTION

In mammalian cells, 20-30% of the open reading frames encode membrane proteins (Wallin and von Heijne, 1998) whose functions include, amongst others, small-molecule transfer, signal transduction, cell adhesion, intracellular trafficking, and membrane and organelle biogenesis (von Heijne, 2007). Eukaryotic membrane proteins are defined by the presence of one or more TM segments, which are formed by stretches of hydrophobic α-helixes that span the lipid bilayer. Correct insertion of TM segments into the ER membrane during protein synthesis is essential for subsequent protein folding. These TM segments can be inserted by two different mechanisms: the TM helixes of tail-anchored-proteins are mostly inserted post-translationally by TRC40, and multi-spanning membrane protein TM segments are inserted co-translationally by Sec61 (Favaloro et al., 2010; Hessa et al., 2007; Johnson et al., 2013; Pitonzo et al., 2009; Rapoport et al., 2004). In the case of multi-spanning membrane proteins, a nascent chain is first targeted to the Sec61 translocon after identification of its signal sequence by signal recognition particle. TM helixes are then inserted into the ER membrane by the Sec61 translocon (Ellgaard et al., 2016; Guna and Hegde, 2018; Kida, et al., 2016) (Figure 1A). Other than TRC40 and Sec61, the ER membrane complex (EMC) is also reported to act as a translocon for both post- and co-translational insertion (Chitwood and Hegde, 2019; Guna et al., 2018).

Insertion of TM helixes can be affected by the hydrophilic content of these helixes. Membrane proteins often contain charged and polar residues within their TMDs for structural and functional purposes (El Hiani et al., 2016; Zhang et al., 2017b; Johnson and Chen, 2017; Li et al., 2017; Adachi et al., 1996; Geiger et al. 2011). Such residues are usually protected by packing of helixes and domain-domain interactions during post-translational protein folding (Pitonzo et al., 2009). However, during membrane protein translation and translocation, when protein tertiary structure has not yet been established, charged residues can be exposed to the lipid bilayer and cause protein aggregation. These residues can also disrupt the binding between the nascent chain and the Sec61 translocon and lower the efficiency of insertion of TM helixes into the membrane (Onishi, et al., 2013; Feige and Hendershot, 2013). Molecular chaperones are therefore required to assist the insertion of TM helixes and protect these residues from improper contacts with the lipid bilayer.

Previous studies show that the EMC complex is required for integrating low-hydrophobicity TMDs into the lipid bilayer (Guna et al., 2018; Shurtleff et al., 2018), acting as chaperone or translocon or both. EMC contains 6 main components (EMC1-6) and 3 associated members (Figure 1B) (Jonikas, et al., 2009; Christianson

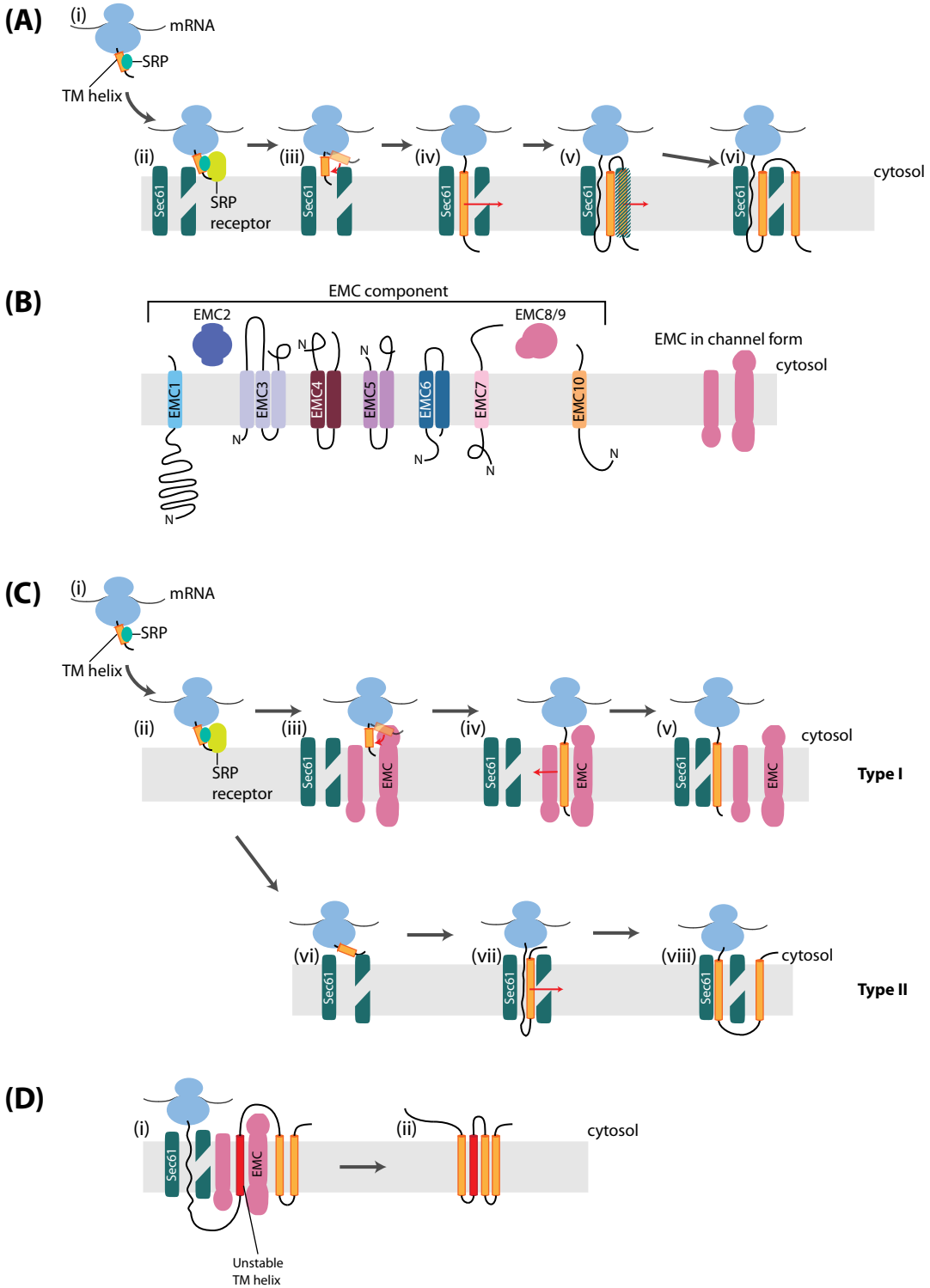

(A)
(i)
mRNA
SRP
TM helix
(ii)
SRP
receptor
Sec61
(iii)
(iv)
(v)
(vi)
cytosol
(B)
EMC component
EMC2
EMC8/9
EMC in channel form
cytosol
EMC1
EMC3
EMC4
EMC5
EMC6
EMC7
EMC10
N
(C)
(i)
mRNA
SRP
TM helix
(ii)
SRP
receptor
Sec61
(iii)
EMC
(iv)
(v)
cytosol
Type I
(vi)
(vii)
(viii)
cytosol
Type II
(D)
(i)
Sec61
EMC
Unstable
TM helix
(ii)
cytosol

Figure 1: Co-translational insertion of multi-pass membrane protein.
(A) Model with key steps of signal anchor recognition and transmembrane (TM) helix translocation and insertion into the ER membrane by the Sec61 translocon. (i) A TM helix (as an example we depicted an N_{exo} helix) emerging from the ribosome is recognized by the signal recognition particle (SRP) and guided to the ER membrane. (ii) After reaching the ER membrane, SRP binds to the SRP receptor. This binding releases SRP from the TM helix and allows the ribosome to dock on top of the Sec61 tunnel. (iii) The TM helix then extends into the Sec61 tunnel during translation without further contact with the cytosol. (iv-vi) The fully translated TM helix is inserted in the ER membrane through the lateral gate of the Sec61 translocon. (B) Cartoon of EMC members, including the 6 core components and 3 associated members, and cartoon of EMC in complex. (C) (i-v) The insertion of an N_{exo} TM helix can be mediated by EMC, after which it is positioned near the lateral gate of the Sec61 translocon. (vi-viii) In contrast to the N_{exo} TM helix, the insertion of the N_{cyt} TM helix was reported to not include the EMC. The N-terminus of the TM helix binds to the cytosolic opening of the Sec61 channel upon ribosome docking and the rest of the TM helix is extended into the Sec61 tunnel. (D) EMC may assist the insertion of TM helixes with destabilizing sequences. (i) EMC receives the folding-challenged TM helix from the Sec61 translocon and prevents it from early degradation by ERAD. (ii) After the TM helix has obtained its proper topology, it is released into the lipid bilayer by the EMC.

et al., 2011) and was first shown to function as a post-translational insertase for tail-anchored proteins with a low-hydrophobicity TM helix (Guna et al., 2018). Studies using multi-pass membrane proteins show that the EMC not only inserts low-hydrophobicity tail anchored proteins, but is also required for the co-translational membrane insertion of an N_{exo} topology (type I) membrane protein (Figure 1C top panel) (Chitwood et al., 2018; Bircham et al., 2011; Lahiri et al, 2014; Louie et al., 2012; Richard et al., 2013; Satoh et al., 2015). After being transported to the plasma membrane these membrane proteins extend their N-termini into the extracellular space. The EMC was reported to be required for incorporating the first TM helixes of N_{exo} proteins into the lipid bilayer (Figure 1C), while the following TM helixes are presumably inserted by the Sec61 translocon (Chitwood et al., 2018).

Proximity ribosome profiling shows that most EMC client proteins are transporters with TMDs containing charged residues in their TMs (Shurtleff et al., 2018). Many of these clients are N_{cyt} topology (Type II) membrane proteins, which supposedly do not rely on the EMC for ER membrane integration, suggesting that EMC functions as more than just an insertase for membrane proteins (Louie et al., 2012; Richard et al., 2013; Satoh et al., 2015; Volkmar et al., 2019). The EMC co-translationally interacts with these proteins at their TMDs and EMC depletion triggers the elevation of the translatome related to the unfolded protein response (Jonikas et al., 2009). These findings indicate that the EMC may have a chaperone function on membrane proteins that contain folding-challenged sequences. The exact mechanism of how EMC chaperones its substrates is still poorly understood. One hypothesis is that EMC binds and stabilizes the nascent chains co-translationally, preventing pre-mature degradation by the ER-associated degradation (Figure 1D), and concomitantly recruits other substrate-specific and general chaperones to assist in folding of the newly-synthesized membrane proteins (Kudze et al., 2018). The second model hypothesizes that EMC is actively involved in substrate folding (Zhang

et al., 2017a). Both models are not mutually exclusive but remain to be tested.

The CFTR paralog Yor1p is one such EMC substrate (Louie et al., 2012). Misfolded CFTR is the main cause of Cystic Fibrosis, a disease where movement of ion and water across the apical membrane is compromised, leading to accumulation of fluid in the respiratory, digestive and reproductive systems (Cohen and Prince, 2012; Ratjen and McColley, 2012). The most common misfolding mutation of CFTR is F508del, where folding of the first nucleotide binding domain (NBD1) of CFTR is defective and causes increased protein degradation (Du et al., 2005; Riordan, 2008). Understanding CFTR folding hence is important to provide insight into the development of the disease and to improve their presently available suboptimal medication. The domains of CFTR fold mostly co-translationally, assemble with each other mostly post-translationally, and CFTR is complex-glycosylated in the Golgi (Cheng et al., 1990; Kleizen et al., 2005). The folding of CFTR TMDs has received less attention than folding of its NBDs because patient mutations in TMDs are less common than F508del (van Willigen et al., 2019). CFTR TMDs contain charged residues in their TM regions. These charged residues destabilize the folding of the TMDs once exposed to the lipid bilayer. Therefore, EMC may be required for stabilizing these charged residues before CFTR TMDs interact with each other.

EMC knock-out (KO) in Saccharomyces cerevisiae decreases the expression of Yor1, but does not affect its post-translational degradation (Louie et al., 2012). Even more important, although Yor1 has high homology to CFTR, CFTR does not undergo maturation in yeast because it fails to assemble its domains properly (DS, IB, unpublished data). For that matter, we addressed whether EMC regulates CFTR expression and if so aimed to determine which of the CFTR domains depends on EMC. We used a radiolabeling pulse-chase and protease-sensitivity assays to study CFTR protein synthesis and folding in the presence and absence of the EMC (Figure 2A). Our results show that EMC KO impacted CFTR expression co-translationally but did not affect CFTR export from the ER to the Golgi or for degradation. We found that EMC is responsible for maintaining especially TMD2 stability during translation.

RESULTS

EMC KO decreased CFTR expression

A previous study (Louie et al. 2012) demonstrated that deletion of the EMC reduced the expression of CFTR F508del and its yeast homologue Yor1-F670del in baker's yeast. To check the consequences of EMC deletion in a mammalian system we transfected wild-type CFTR (named CFTR) in HEK 293T cells with and without core EMC subunits EMC5 or EMC6. We studied wild-type CFTR because unlike F508del,

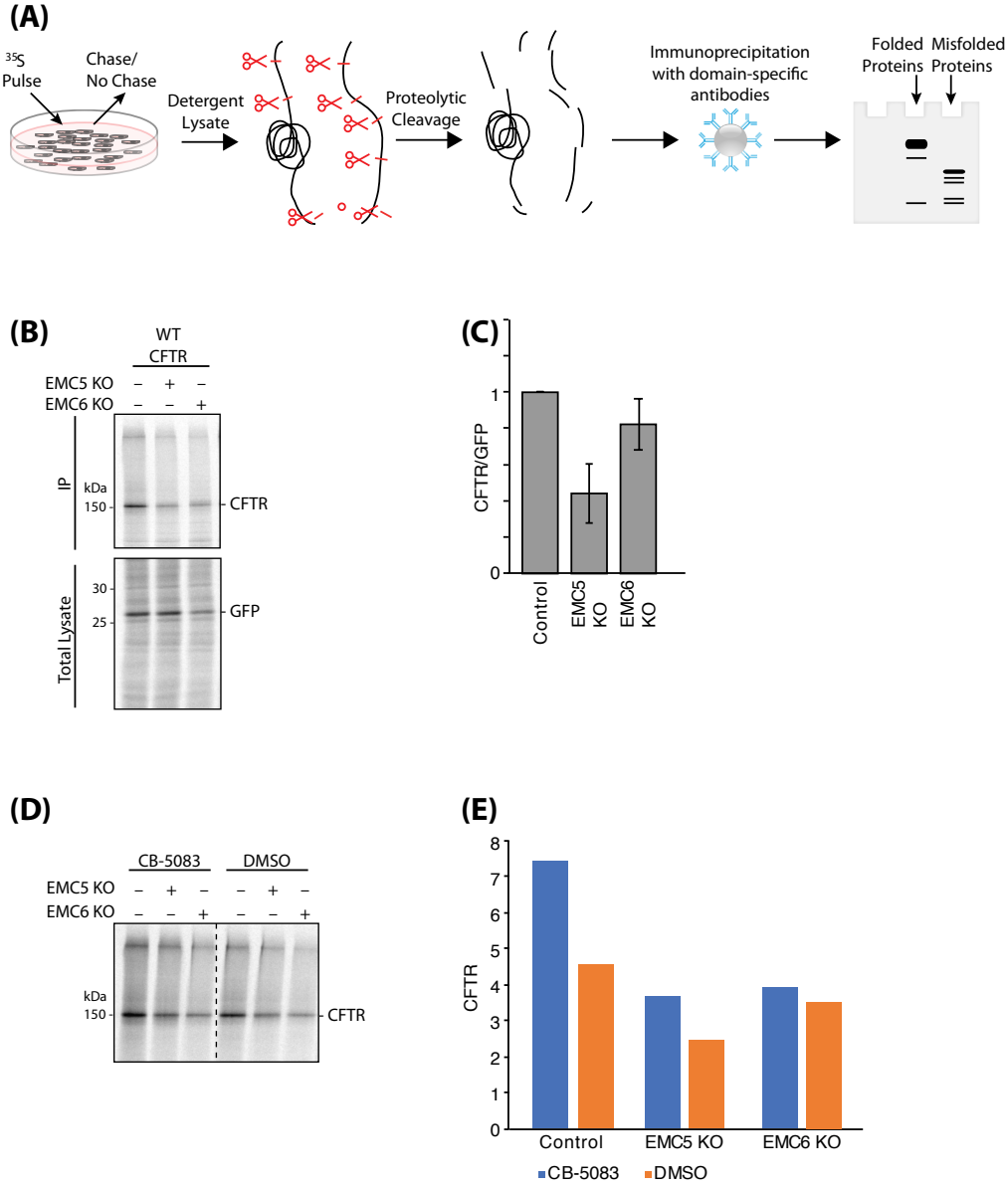


Figure 2: EMC KO decreased CFTR expression.
(A) Radiolabeling experimental scheme: HEK 293T cells transfected with CFTR constructs were pulse radiolabeled with ^{35}S-methionine and -cysteine and chased for a particular period. Cells were lysed, and detergent lysates were treated with protease to generate proteolytic fragments that were immunoprecipitated with CFTR domain-specific antibodies and analyzed by SDS-PAGE. (B) HEK 293T parent cells, and EMC5 and EMC6 KO cells transiently expressing CFTR and GFP were radiolabeled with ^{35}S-methionine and -cysteine and lysed. CFTR was immunoprecipitated from detergent cell lysates with antibody against NBD1 and analyzed by 7.5% SDS-PAGE (top panel). GFP in the total lysate was used as a transfection and translation control and analyzed by 12% SDS-PAGE (bottom panel). (C) The amounts of CFTR and GFP were quantitated and CFTR was normalized to GFP expression (n=3). (D) HEK 293T, EMC5 KO and EMC6 KO cells transiently expressing CFTR were pulse labeled with ^{35}S-methionine in the presence or absence of the p97 inhibitor CB-5083. CFTR was immunoprecipitated with antibody against NBD1 and analyzed by SDS-PAGE, and the CFTR amount was quantified and plotted in (E) (n=1).

CFTR has intact co- and post-translational folding allowing us to investigate the effect of EMC on CFTR protein folding. During translation, TMD insertion and folding of wild-type CFTR are similar to that of F508del (data not shown), therefore the effect of the EMC KO on the TMDs should be similar as well.

We co-expressed CFTR and GFP in HEK 293T cells with and without EMC5 and EMC6 and expression was checked by a pulse of ^{35}S-radiolabeling (Figure 2A). GFP was used as a control for gene transfection and protein translation. EMC5 and EMC6 are core components of the EMC and deletion of either eliminates expression of the entire complex (Guna et al., 2018). However, as compensatory networks that respond to gene deletion may be triggered differently between cell lines (Rossi et al., 2015), the phenotypes of EMC5 KO and EMC6 KO cells may differ from each other. Thus, expression and folding of CFTR in the two EMC KO cell lines may also be dissimilar and we therefore used both cell lines.

After pulse labeling, CFTR is detected as one band, the ER form, which represents the CFTR population that has completed co-translational domain folding and acquired N-glycosylation in the ER. CFTR expression in both EMC5 KO and EMC6 KO cells was lower than in the control cells (Figure 2B, top panel), while GFP expression was reduced only in the EMC6 KO cells (Figure 2B, bottom panel). Low GFP expression in EMC6 KO cells indicated less efficient gene transfection or, in general, less protein translation in EMC6 KO cells. After quantifying the amounts of both CFTR and GFP and normalizing the values of CFTR to GFP, we found that CFTR expression was reduced approximately 60% in EMC5 KO cells and 10% in EMC6 KO cells (Figure 2C). This was similar as previously reported for F508del (Louie et al., 2012). A decrease in CFTR expression can be caused by either downregulation of CFTR translation or an increase in CFTR (co-translational) degradation due to loss of EMC as chaperone. To address the latter mechanism, we blocked ER-associated degradation, which is the primary degradation pathway for proteins synthesized in the ER, using the p97 inhibitor CB-5083 (Le Moigne et al., 2017) during pulse labeling. As we hypothesized that EMC KO could destabilize CFTR TMDs and increase the CFTR degradation rate, we expected CB-5083 treatment to rescue the expression of CFTR in EMC KO cells compared to HEK 293T. Treatment of the cells with CB-5083 indeed increased expression albeit with or without knockout of EMC5, or EMC6 (Figure 2D and 2E), indicating that low CFTR expression in EMC KO cell lines is not caused primarily by the upregulation of co-translational degradation. As CB-5083 only blocks ubiquitin-modulated degradation, it is possible that CFTR was not degraded by these pathways (Zhou et al., 2015; Le Moigne et al., 2017). Because, EMC KO also induced a moderate UPR, this may have decreased protein translation in the ER (Shurtleff et al., 2018).

EMC supports TMD2 folding irrespective of NBD folding

It has not been established how EMC regulates expression of its substrates. We therefore investigated whether the TMDs played a role in this process through promoting folding and by doing so avoid premature degradation. We expected deletion of EMC to destabilize these TMDs (Shurtleff et al., 2018). CFTR has two TMDs that co-assemble to form the main body of the ion channel. Whether the TMDs interact co- or post-translationally has not been established. Although the chaperones that support folding and assembly of these TMDs have not been identified, EMC likely is one of them. To investigate the role of the EMC on the folding and interactions of the two CFTR TMDs, we expressed three constructs: CFTR, R1070W/F508del (R/F), and TMD1-Linker-TMD2 (TMDs-L) in HEK 293T cells with or without EMC5 and EMC6.

CFTR was used as control as it has intact protein folding and domain assembly and was used to examine the effect of EMC on the folding and assembly of TMDs (Figure 3A). CFTR R1070W/F508del contains misfolded NBD1 due to the F508del mutation and disrupted domain assembly, whereas the additional R1070W mutation restores a low level of domain-domain interactions (Mendoza et al., 2012). This incomplete domain-domain interaction destabilizes the TMDs of CFTR R1070W/F508del and may increase the dependence of CFTR R1070W/F508del on EMC. Lastly, CFTR TMDs-L contains no NBDs (Figure 3A) and is used to assess whether the absence of NBDs will increase the dependence of the folding and assembly of TMDs on EMC. The expression of these constructs was followed by pulse radiolabeling with ^{35}S-methionine and -cysteine and immunoprecipitation with antibodies against TMD1 and NBD1 as indicated (Figure 2B).

As expected, CFTR and its point mutants showed a reduction in their expression levels to a maximum of 60% in EMC5 KO cells and 20% in EMC6 KO cells compared to HEK 293T (Figure 3B). Next, we followed the folding of TMDs of CFTR and its mutants in EMC KO cells by a protease susceptibility assay (Kleizen et al., 2005; Hoelen et al., 2010; van Willigen et al, 2019). Lysates prepared from ^{35}S-radiolabeled cells were treated with Proteinase K, and proteolytic fragments deriving from CFTR and mutants were immunoprecipitated with domain-specific antibodies (Figure 2C). The amounts of TMD1 and TMD2 proteolytic fragments were quantitated. This quantification confirmed that the TMD proteolytic fragments in EMC KO cells showed a similar pattern of decrease (Figure 3C T1/GFP and T2/GFP) as non-proteolyzed input (Figure 3B CFTR/GFP), i.e., the amount of proteolytic fragments from both TMDs decreased in EMC5 and EMC6 KO compared to HEK 293T. As the amounts of the proteolytic fragments were affected by protein input levels, the folding of these domains needs to be estimated by normalizing to the full-length CFTR protein that the fragments derive from (Figure 3D). The calculations revealed

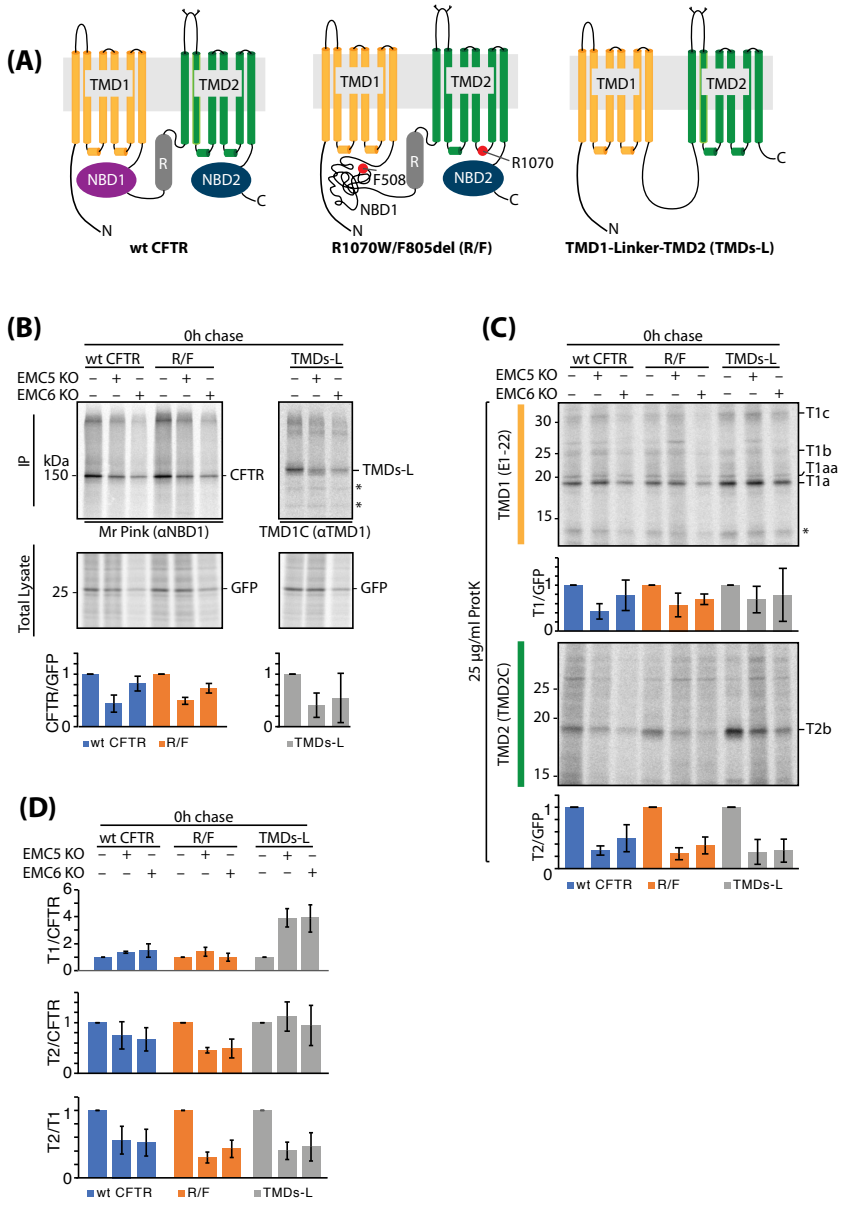


Figure 3: EMC supports TMD2 folding irrespective of NBD folding.
(A) Cartoons to show important features of CFTR and CFTR mutants. (B) HEK 293T, EMC5 KO and EMC6 KO cells transiently expressing CFTR, CFTR R1070W/F508del (R/F) and CFTR TMDs-L were radiolabeled with ^{35}S-methionine and -cysteine and lysed. CFTR was immunoprecipitated with an antibody against NBD1 and analyzed by 7.5% SDS-PAGE; TMDs-L was immunoprecipitated with the TMD1C antibody and analyzed by 12% SDS-PAGE. Co-expressed GFP was used as transfection and translation control and analyzed by 12 % SDS-PAGE (bottom panels). The amount of immunoprecipitated CFTR was quantified and compared to co-expressed GFP. These values then were normalized to HEK 293T (n=3). (C) Remaining cell lysates from (B) were treated with Proteinase K and CFTR proteolytic fragments were isolated with domain-specific antibodies and analyzed on 12% SDS-PAGE. The amounts of TMD1 and TMD2 proteolytic fragments were quantified and adjusted with GFP levels from the same condition. These values then were normalized to HEK 293T (n=3). (D) The amount of TMD1 and TMD2 proteolytic fragments were related to full-length CFTR or each other to measure the folding of the TMDs. These values were normalized to HEK 293T (n=3). (*: background bands)

that whereas folding of TMD1 of CFTR and CFTR R1070W/F508del was not affected by EMC KO (Figure 3D, T1/CFTR), folding of their TMD2 decreased approximately 25-40% in cells without EMC5 or EMC6 (Figure 3D, T2/CFTR). This finding indicates that EMC is required for stabilizing folding of TMD2 in CFTR and CFTR R1070W/F508del (Figure 3D, T1/CFTR and T2/CFTR). Stabilization of TMD2 folding was confirmed by relating the amount of proteolytic fragments of TMD2 to TMD1 (Figure 3D, T2/T1).

Remarkably, while folding of TMD1 in CFTR and CFTR R1070W/F508del remained largely unaffected during EMC KO, folding of the TMDs in TMDs-L behaved differently. TMD1 of CFTR TMDs-L folded approximately three times better after EMC KO compared to HEK 293T and folding of its TMD2 was not affected (Figure 3D, T1/CFTR and T2/CFTR). Both TMDs of CFTR TMDs-L were more protease resistant, i.e. more compact/better folded upon EMC KO compared to CFTR and CFTR R1070W/F508del. Possibly, CFTR TMDs-L may be inserted and folded through a different pathway in the absence of EMC compared to full-length CFTRs. Although TMDs-L might fold differently, its TMD1 still folded better than TMD2 in cells without EMC. This trend was consistent with CFTR and CFTR R1070W/F508del and is demonstrated even clearer when comparing the amount of the TMDs to each other (Figure 3D, T2/T1), showing that although TMD folding of CFTR TMDs-L responded differently to EMC KO, it had a similar T2/T1 ratio as CFTR and CFTR R1070W/F508del.

Our results showed that EMC KO decreased TMD2 folding but not the folding of TMD1, and this effect was independent of NBD1. As TMD1 responded differently from TMD2 to EMC KO, this suggests that TMD1 may not require EMC for its folding, whereas TMD2 does.

EMC supports TMD2 folding in TMD mutants

Figure 3 demonstrated that EMC KO destabilized folding of TMD2 but not TMD1, indicating that EMC interacts with CFTR TMD2 but not TMD1. This finding implies that although both CFTR TMDs share similar structural properties, such as charged residues within their TM area that would require chaperone binding, they may recruit a different chaperone interactome during folding of the entire protein. To determine critical residues in TMD2 with respect to the supportive role of EMC in TMD2 folding and to confirm independently that EMC does not regulate TMD1 folding, we expressed patient mutations, G85E and R347P (TMD1) and M1101K (TMD2) (van Willigen et al., 2019; Xiong et al., 1997; Zielenski et al., 1993) in the EMC KO cell lines. All examined patient mutants have alterations in their TM regions (Figure 4A), either introduced by a change from a hydrophobic to a charged residue (G85E & M1101K) or via a charged amino acid to proline (R347P). They all localize to the same area in CFTR (Figure 4A). Such mutations may disrupt the charge

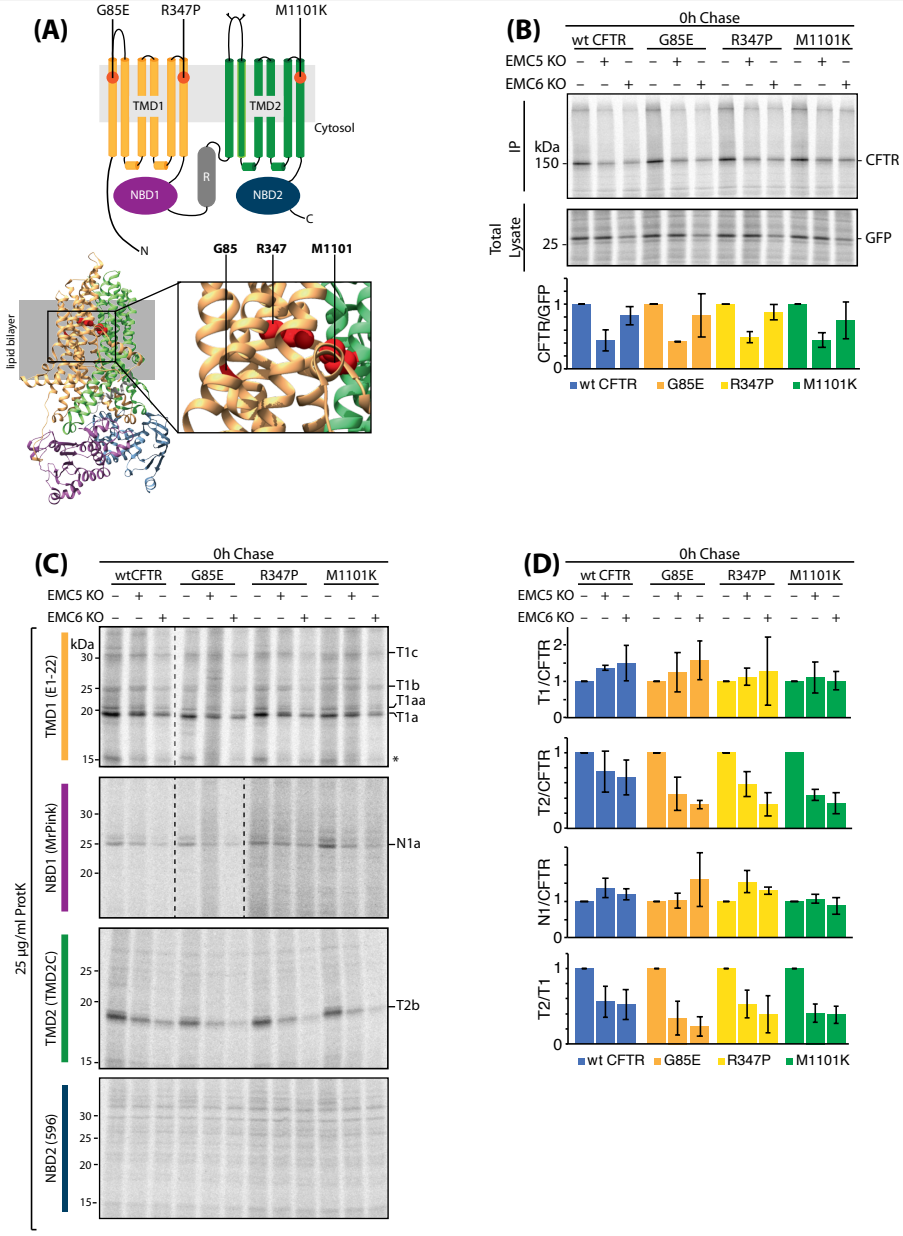


Figure 4: EMC supports TMD2 folding in TMD mutants.
(A) Top panel: Cartoon to show positions of mutations in CFTR. Bottom: The mutations in the cryo-EM structure of mature CFTR (PDB:5uak). (B) CFTR, and CFTR G85E, R347P, and M1101K mutants were transiently expressed in HEK 293T, EMC5 KO, and EMC6 KO cells. Cells were radiolabeled with ^{35}S-methionine and -cysteine and then lysed. CFTR was immunoprecipitated with an antibody against NBD1, and immune complexes were resolved by 7.5% SDS-PAGE. CFTR bands were quantified and related to GFP expression (n=3). (C) Remaining cell lysates from (B) were treated with Proteinase K and CFTR proteolytic fragments were isolated with domain-specific antibodies and analyzed on 12% SDS-PAGE. (D) The immunoprecipitated domain fragments from (C) were quantitated, compared with the amount of full-length protein that they were derived from to eliminate expression differences, and normalized to HEK 293T (*Top four panels*, n=3). Because the NBD2 fragment was below the detection limit, quantitation is not shown. To compare the folding of the TMD domains, we related the amount of TMD2 fragments to those of TMD1 (*Last panel*, n=3). (*: background bands)

balance within the protein that is required for helix packing and domain-domain interactions, thereby possibly increasing their reliance on EMC.

CFTR, G85E, R347P, and M1101K were pulse labeled for 15 min with ^{35}S-methionine and -cysteine and immunoprecipitated with antibody against NBD1. Consistent with the results of Figures 2 and 3, expression levels in the EMC5 KO cells were significantly lowered, while those in the EMC6 KO cells were less affected (Figure 4B, CFTR/GFP). Transfection must have been less efficient in the EMC KO cells. We next determined the folding of individual CFTR domains by treating the full-length proteins with Proteinase K. Proteolytic fragments were isolated with domain-specific antibodies and their amounts were quantitated as in Figure 3. These amounts then were related to their non-proteolyzed input to eliminate expression differences and calculate the folding levels of each domain. Folding of NBD2 was undetectable in CFTR and mutants (Figure 4C and 4D, N2/CFTR), because NBD2 only obtains its native, protease resistant structure during post-translational domain assembly (Figure 5D, NBD2 panel). The amount of proteolytic fragments derived from different CFTR domains followed the same pattern as the expression of their non-proteolyzed input, i.e., less fragments in EMC5 KO than EMC6 KO (Figure 4C). Folding of TMD1 and NBD1 of CFTR and its mutants improved slightly (Figure 4D, T1/CFTR and N1/CFTR), while their TMD2 folding decreased upon EMC KO (Figure 4D, T2/CFTR). By plotting T2/T1, this response was even more evident (Figure 4D, T2/T1).

All CFTR mutants showed more dramatically affected TMD2 folding than CFTR during EMC KO, indicating that G85E, R347P, and M1101K mutations disrupted TMD2 folding and increased the dependence of TMD2 to EMC. As M1101K is in TMD2, most likely this mutation interfered with TMD2 co-translational folding. However, G85E and R347P mutations are in TMD1 and should only affect TMD1 structure co-translationally. A possible explanation for low TMD2 folding in G85E and R347P mutants upon EMC KO is that TMD2 interacts with TMD1 co-translationally and this interaction is weakened by conformational changes in TMD1 due to the G85E and R347P mutations. Decreasing the TMD1-TMD2 interaction therefore increased the dependence of TMD2 on EMC to stabilize its folding. The results in Figure 4D confirmed that EMC KO decreased only TMD2 co-translational folding and that folding of TMD1 remained unaffected.

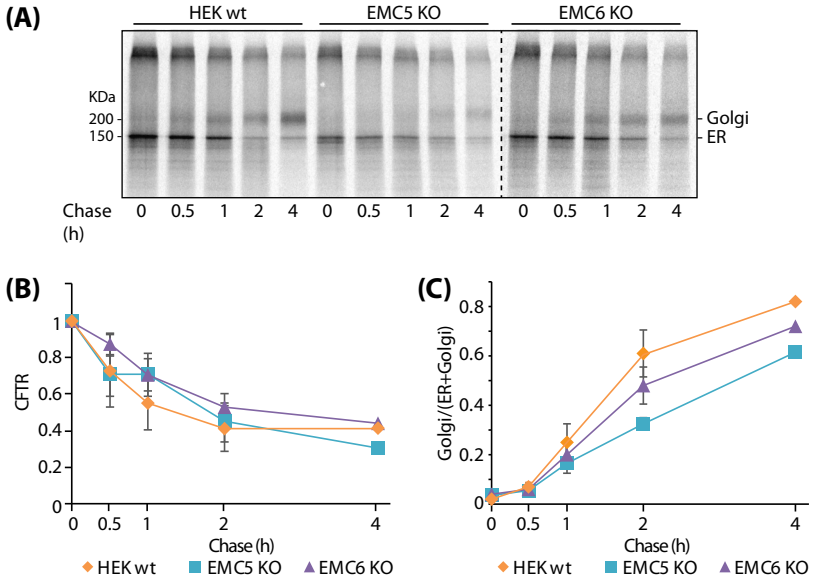
The folding of TMD1 was slightly improved upon EMC KO in comparison to the control (Figures 3D and 4D, T1/CFTR), suggesting that EMC may destabilize TMD1. This result is not surprising, as the conformation of TMD1 can be affected by TMD2, whose folding is determined by EMC (Figure 3D and 4D, T2/CFTR), during domain assembly (Du and Lukacs, 2009; Zhang et al., 2017). The intradomain

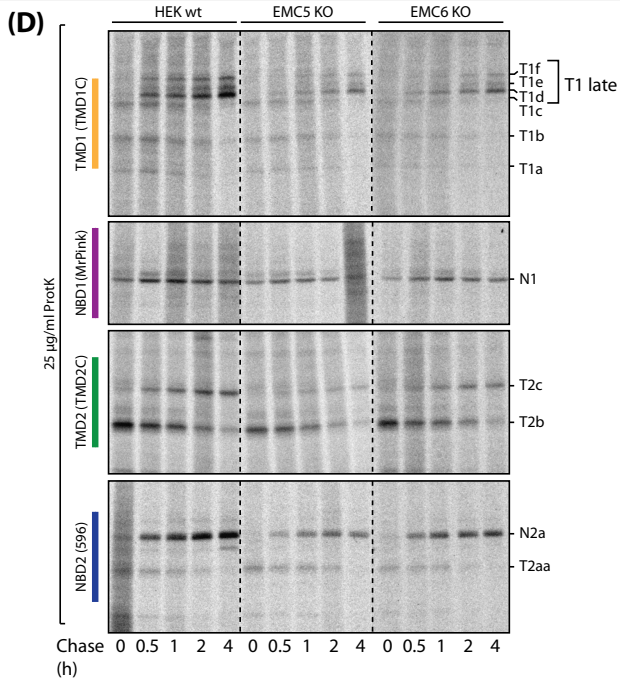
packing of TMD1 may be weakened by the TMD1-TMD2 interaction, thereby slightly destabilizing TMD1 (Du and Lukacs, 2009). In the absence of EMC, the folding of TMD2 was impaired, which decreased its coupling with TMD1 and therefore may lead to TMD1 stabilization.

Knock-out of EMC delayed export of CFTR from the ER

EMC has been found to interact co-translationally with its clients, but studies analyzing a potential role of EMC on the post-translational folding of its substrates are lacking. This is an important question since many transmembrane proteins have multiple transmembrane domains, which need to assemble (at least in part happening) post-translationally and often require chaperones to maintain the stability of the domains during this process. We therefore asked whether EMC assisted post-translational domain assembly of CFTR. CFTR was expressed in HEK 293T and EMC knock out cells and cells were pulse labeled with ^{35}S-methionine and -cysteine, chased for different periods of time, and treated with Proteinase K. CFTR proteolytic fragments were isolated with domain-specific antibodies and non-proteolyzed proteins were immunoprecipitated with antibody against NBD1.

After pulse labeling, CFTR appeared initially in its ER form, which gradually matured into a Golgi form during the chase (Figure 5A). Chasing CFTR expression post-translationally at more time points allowed us to study its total amount and its degradation rate at higher 'resolution'. The CFTR degradation rate in cells without





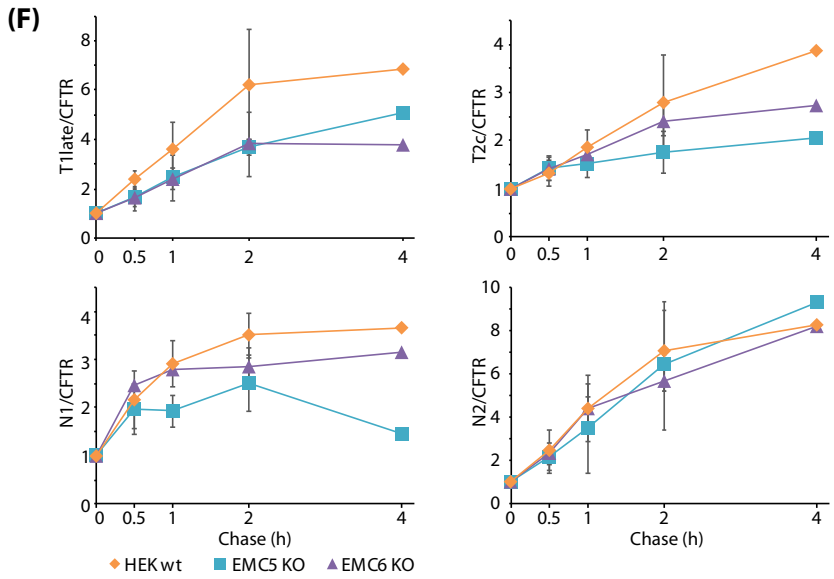


Figure 5: EMC KO delayed CFTR ER export.
(A) HEK 293T, EMC5 and EMC6 KO cells transiently expressing CFTR were radiolabeled with ^{35}S for 15 minutes, chased for different periods of time and lysed. CFTR was immunoprecipitated from a fraction of the detergent lysate with an antibody against NBD1 and analyzed by 7.5% SDS-PAGE. (B) The amount of CFTR from each time point was related to the HEK 239T at 0-h chase sample (n=3). (C) The percentages of CFTR in the Golgi form at each time point were calculated and plotted (n=3). Data from 0, 30, 60 and 120 minutes are n=3 and 240 minutes are n=2. (D) HEK 293T, EMC5 or EMC6 KO cells transiently expressing CFTR were treated as in A and cell lysates were subjected to limited proteolysis with Proteinase K. The proteolytic fragments were immunoprecipitated with domain-specific antibodies and analyzed by 12% SDS-PAGE. (F) The amounts of T1 late, N1, T2c, and N2 fragments were quantified and related to the amount of full-length CFTR that they were originating from in panel B. Data from 0, 30, 60, and 120 minutes are n=3 and 240 minutes are n=2.

EMC was similar to control HEK 293T cells, suggesting that EMC KO did not affect CFTR post-translational degradation (Figure 5B), which supports previous results obtained with Yor1 in S. cerevisiae (Louie et al., 2012). Assaying CFTR post-translationally also allowed us to measure its ER export rate, which is represented by the percentage of the Golgi form. At 2h and 4h chase, the percentage of the Golgi form in EMC5 KO cells was lower than in the control and EMC6 KO cells (Figure 5C), suggesting that CFTR ER export was delayed in the absence of EMC5. CFTR ER export was also delayed in EMC6 KO cells but not as much as in EMC5 KO cells.

The delay in CFTR ER export could be caused by impaired folding of CFTR, including its domain folding and subsequent domain assembly. Figures 3 and 4 showed that TMD2 folding was negatively impacted upon EMC KO. Disruption in folding could prevent proper interaction between TMD2 and the other domains, which decreases the extent of CFTR folding and assembly, and block the export of CFTR from the ER. In our experiment, post translational domain assembly of CFTR was demonstrated by the occurrence of high-molecular-weight proteolytic fragments, such as T1 late in TMD1 and T2c in the TMD2 immunoprecipitation (Figure 5D). Domain assembly shields a larger area within a domain, decreasing protease accessibility, and resulting in larger proteolytic fragments. Quantifying the amount of these fragments provide us with information on CFTR domain assembly status with respect to EMC. Because NBD2 obtains its structure and folding during domain assembly it can be used to investigate CFTR domain assembly.

Immunoprecipitated T1 late, T2c, and N2 fragments that were generated from CFTR after different chase times were quantitated and normalized to the non-proteolyzed input. Analysis showed that the amounts of these proteolytic fragments increased throughout the chase, although this appeared to be somewhat less in cells with EMC KO (Figure 5F, T1 late/CFTR, T2c/CFTR, N2/CFTR). The amount of T1 late, NBD1, and T2c was reduced 25-50% in EMC5 KO and EMC6 KO cells compared to control cells after 120 min of chase (Figure 5F, T1 late/CFTR, N1/CFTR, and T2c/CFTR). For NBD2, the amount of N2 was similar among control, EMC5, and EMC6 KO cells after 120 min chase (Figure 5F, N2/CFTR). This result suggested that the folding of NBD2 was impacted less upon EMC KO. Our initial findings indicated that EMC KO tended to suppress the level of post-translational domain assembly of TMD1, TMD2, and NBD1 because of the decrease in TMD2 folding.

DISCUSSION

Our study demonstrated that EMC stabilized the folding of CFTR TMD2. Eliminating EMC from cells decreased expression of CFTR and folding of TMD2, but not of the

other CFTR domains. Introducing single charged or hydrophobic mutations into TMD1 or TMD2 enhanced the dependence of TMD2, but not of TMD1 on EMC. Deletion of EMC also lowered post-translational domain assembly and ER export of CFTR.

EMC5 and EMC6 are the core components of the EMC and deleting either should eliminate the expression of the whole complex (Guna et al., 2018). One would therefore expect that EMC5 KO and EMC6 KO cells present the same phenotypes. Nevertheless, Figure 2B demonstrated a difference in CFTR expression in EMC5 KO and EMC6 KO cells. CFTR expression in EMC5 KO cells was lower than after EMC6 knockout. This suggested that either EMC5 is more important than EMC6 in CFTR biogenesis, or that the two cell lines recruited different recovery and compensation mechanisms after knockout of the respective EMC subunit. Regardless of this difference however, both cell lines displayed impaired CFTR TMD2 folding (Figure 3D, T2/T1). Based on this result, we established that TMD2 requires EMC for proper folding. This phenotype was also consistent with that of a truncated version of CFTR (TMDs-L), which included only TMD1 and TMD2 in its structure (Figure 3D, T2/T1). In contrast to CFTR and CFTR- R1070W/F508del, the TMDs of TMDs-L, in particular TMD1, folded especially well in cells without EMC, suggesting that the TMDs of TMDs-L may be inserted and folded using an alternative (perhaps backup) machinery that filled the void of the deleted EMC.

Because EMC was required for TMD2 folding (Figure 3D and 4D, T2/T1), while TMD1 folding may not need it or even be destabilized by EMC (Figure 3D and 4D, T1/CFTR), the two CFTR TMDs may be assisted by different chaperone interactomes. Although TMD1 and TMD2 have similar structures (Zhang et al., 2017b), TMD2 has a lower stability than TMD1 (Enquist et al., 2009; Pitonzo et al., 2009), because TMD2 contains a hydrophilic, unwound region in its second TM helix, TM8. This region contains residue D924, which is thermodynamically unfavorable for insertion into the ER membrane (Figure S1, i) (Carveth et al., 2002; Pitonzo et al., 2009). Due to its hydrophilicity, the Sec61 translocon may fail to recognize TM8 during translation, resulting in extension of the TM helix into the ER lumen. TM8 may be retrieved back to the lipid bilayer through helix-helix packing with TM7 (Figure S1, ii, iii, iv), which is also located in TMD2, but TM7 cannot fully stabilize TM8. D924 is eventually stabilized by interacting with R347 from TMD1 during post-translational domain assembly (Figure S1, v). Before domain assembly is complete, TMD2 thus may have a higher chance for aggregation due to its partially stabilized TM8 and may rely on EMC binding for protection of the charged residues in TM8.

The interactions between EMC and TMD2 may not be restricted to TM8 only. We found that co-translational folding of TMD2 in the M1101K mutant decreased

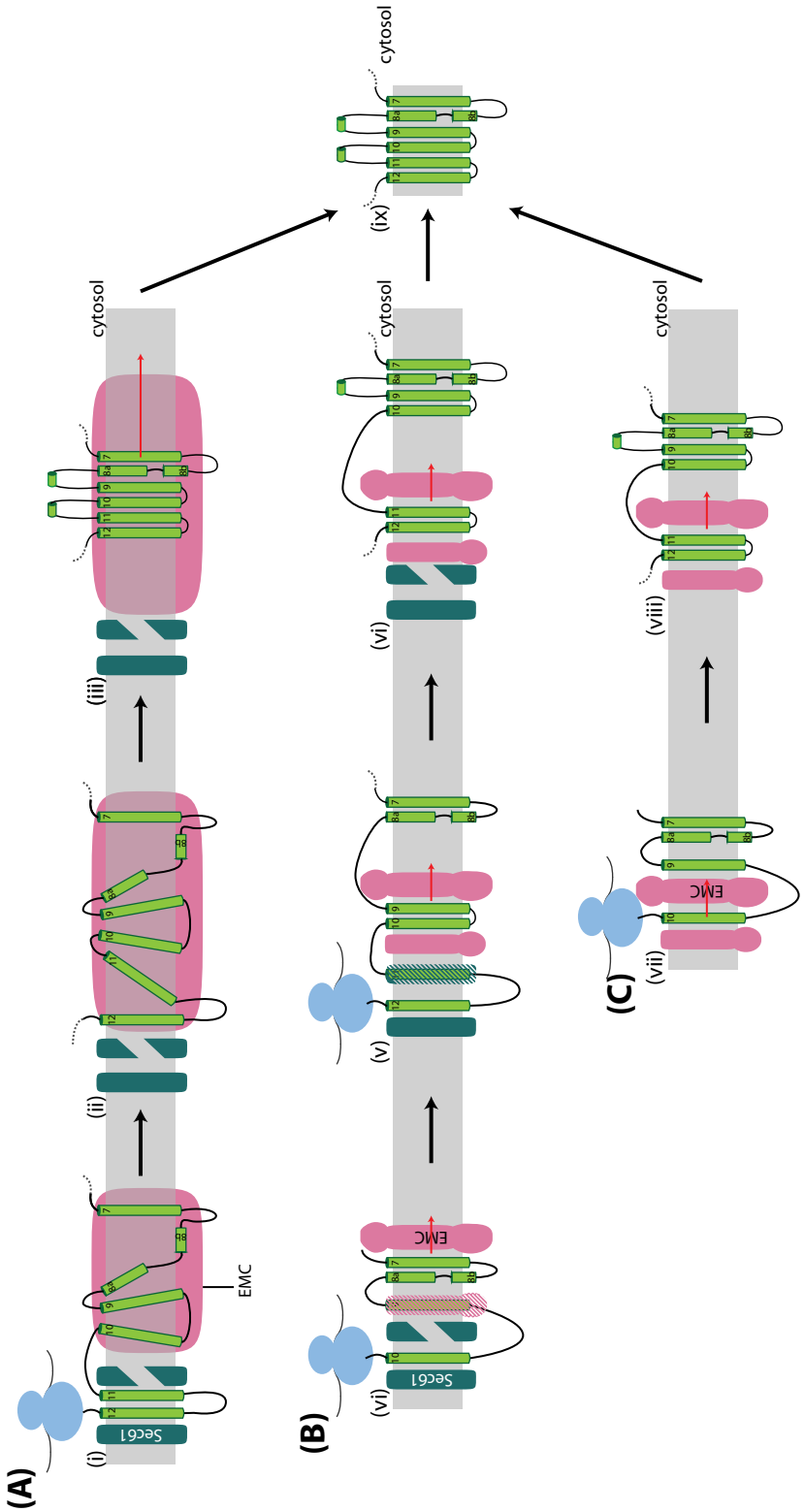


Figure 6: EMC assists CFTR TMD2 folding.
EMC can insert TMD2 in three ways: (A) (i) After translocation and insertion into the ER membrane by the Sec61 translocon, unfolded TMD2 is detected by EMC co-translationally. (ii) EMC binds to the unpaired or uninserted helixes and assists TMD2 helix-helix packing and repositions the uninserted helix back into the ER membrane. (iii) After TMD2 acquires its correct folding, (ix) it is released from the EMC for subsequent CFTR folding. (B) (iv) EMC is closely associated with the Sec61 translocon and receives unpaired or unfolded TM helixes from the Sec61 translocon during translation. (v), (vi) Upon binding to TMD2 helixes, EMC assists their folding and pairing after which (ix) EMC releases TMD2 for post-translational CFTR folding and domain assembly. (C) (vii), (viii) EMC acts as a translocon and is responsible for translocating and inserting TMD2 helixes. (ix) After translation is completed, TMD2 is released into the lipid bilayer by EMC for subsequent folding.

during EMC KO (Figure 4D, T2/CFTR and T2/T1), suggesting that EMC can also detect the folding deficiency in TM12 resulting from the introduction of the M1101K mutation. TM12 in CFTR does not contain charged residues and is therefore unlikely to interact with EMC, which presumably binds co-translationally to charged amino acids in the TM. Such residues are distributed throughout the 6 TM helixes of TMD2 and need to be paired and stabilized by each other (Carveth et al., 2002; Pitonzo et al., 2009) or chaperones to prevent random interactions and protein aggregation within the ER membrane. Based on our results, we propose three models for the roles of EMC in CFTR folding: EMC binds and stabilizes the folding-challenged sequences in the TMD2 helixes. This interaction either chaperones TMD2 until it completes its proper folding (Figure 6A), or assists the integration of TMD2 helixes into the ER membrane during translation (Figure 6B). Alternatively, EMC itself acts as a translocon for TMD2 (Figure 6C). The third model is less likely because according to Chitwood et al., EMC is required for the translocation and insertion of membrane proteins with N_{exo} topology (Type I), while N_{cyt} (Type II) membrane proteins, like TMD2, are translocated and inserted by Sec61 translocon (Chitwood et al., 2018). Surprisingly, introduction of G85E and R347P mutations into TMD1 also increased the co-translational dependence of TMD2 on EMC compared to wild-type CFTR. This suggested that CFTR TMDs may already start assembling together co-translationally to stabilize the folding of one another. Disrupting TMD1 structure decreases this association and may diminish TMD1 stabilization through TMD2 folding, which could serve to enhance interaction of TMD2 with EMC. After TMD2 acquires its correct conformation, it is released from EMC and proceeds with CFTR domain assembly. Without EMC, TMD2 folding decreases and this subsequently lowers domain assembly of CFTR.

In conclusion, we found impaired folding of TMD2 upon deletion of EMC5 and EMC6, which affected subsequent folding of the newly synthesized full-length CFTR molecule since CFTR domain assembly (Figure 5F) and ER export rate (Figure 5C) were reduced in EMC KO cells and were not restored to control levels. This may be because impaired folding of TMD2 disrupted its interaction with the other CFTR domains and thereby interfered with the outcome of the CFTR folding pathway to the final functional structured domains (Liu et al., 2017; Zhang et al., 2017b). Future experiments will pinpoint the precise interaction between CFTR and the EMC, and the binding mechanism and selection criteria of EMC on CFTR and related ABC transporters.

MATERIALS AND METHODS

Reagents

HEK 293T, EMC5 KO and EMC6 KO cells were generously provided by Dr. John Christianson (University of Oxford, Ludwig Institute, UK). CFTR plasmids in pBI-CMV2 and pEZT plasmid were generous gifts from Prof. Phil Thomas (UT Southwestern Medical Center, USA). The TMD1-Linker-TMD2 (TMDs-L) construct was generated by Gibson assembly and included aa 1-394 from CFTR, aa 626-683 from P-gp, and aa 845-1202 from CFTR. The pCDNA3.1-TMD2-HA construct was kindly provided by Prof. Gergely Lukacs (McGill University, Montréal Québec, Canada). The PCR primers for Gibson assembly are described in supplementary materials. The rabbit antibody MrPink against NBD1 was characterized in our lab before (Hoelen et al., 2010). The rabbit antibodies TMD1C (aa 364-381), E1-22(aa 102- 117) and TMD2C (aa 1172-1186) against TMD1 and the TMD2 C-terminus have been described in Chapter 2 of this thesis. Mouse monoclonal antibody 596 against NBD2 (Cui et al, 2011) was kindly provided by Prof. John Riordan (UNC School of Medicine, USA). The p97 inhibitor CB-5083 was purchased from MedChemExpress, dissolved in DMSO, and stored at -20 ^{o}C. Protease K from *Engyodontium album* was purchased from Sigma, and Lipofectamine 3000 was purchased from ThermoFisher Scientific.

Cell culture and transfection

HEK 293T cells were seeded on polylysine-coated 6 cm dishes and maintained in full culture medium (DMEM supplemented with 10% FBS, and 2 mM GlutaMAX) at 37 ^{o}C with 5% CO_2. After reaching 70% confluency, cells were transfected using Lipofectamine 3000 according to protocols from ThermoFisher Scientific. Subsequently, cells were grown in full culture medium at 37 ^{o}C with 5% CO_2 for 16-20 hours prior to experiments.

Radioactive pulse and chase

HEK239T cells were used in pulse chase assays as described (Braakman et al., 1991; McCaul et al., 2019; van Willigen et al., 2019). Briefly, cells were labeled for 15 minutes with 132 µCi/6cm dish with EasyTag Express ^{35}S Protein Labelling Mix (Perkin Elmer). Radiolabeling was stopped by adding excess, unlabeled methionine and cysteine (both 5 mM final concentration). At indicated chase times, cells were washed twice with ice-cold Hank's balanced salt solution (HBSS, Life Technologies) and lysed in ice-cold lysis buffer (20 mM MES, 100 mM NaCl, 30 mM Tris-HCl pH 7.4, and 1% Triton X-100) without protease inhibitors. Nuclei were removed by centrifugation for 10 minutes at 4°C and 16,000 x g and the supernatants were subjected to limited proteolysis or immunoprecipitation.

Limited proteolysis

Limited proteolysis was performed as described (Kleizen et al., 2005; Hoelen et al., 2010; van Willigen et al., 2019). In brief, cell lysates were treated with 25 µg/ml Proteinase K (Sigma-Aldrich) for 15 minutes on ice. Proteolysis was stopped by adding an equal volume of lysis buffer supplemented with 2 mM PMSF and chymostatin, leupeptin, antipain and pepstatin (all 2 µg/ml) (Sigma-Aldrich) to the lysates. Protein aggregates were pelleted by 16,000 x g centrifugation for 5 minutes at 4 °C, and supernatant was used for immunoprecipitation.

Immunoprecipitation

Antibodies against TMD1, NBD1, TMD2, or NBD2 were pre-incubated with protein-A beads (GE Healthcare) for 15 minutes at 4°C before adding protease-treated or non-treated lysates. The non-protease treated lysate was added to MrPink antibody-beads mixture and protease-treated lysates were added to the antibody-beads mixtures containing TMD1C, E1-22, MrPink, TMD2C, or 596. The mixtures were incubated for 3 hours (TMD1C, E1-22, TMD2C, 596) or 16 hours (MrPink) at 4°C. Beads were washed twice for 10 minutes at room temperature with either: 10 mM Tris-HCl pH 8.6, 300 mM NaCl, 0.1% SDS, 0.05% Triton X-100 (for MrPink); 10 mM Tris-HCl pH 8.6, 300 mM NaCl, 0.05% SDS, 0.05% Triton X-100 (for TMD1C and E1-22); 20 mM MES, 100 mM NaCl, 30 mM Tris-HCl pH 7.4 and 0.5% Triton X-100 (for 596); or 50 mM Tris-HCl, pH 8.0, 150 mM NaCl, 1 mM EDTA (for TMD2C). The beads were resuspended in 10 µl 10 mM Tris-HCl pH 6.8 containing 1 mM EDTA, and immunoprecipitated proteins were eluted by adding 10 µl 2x reducing Laemmli sample buffer (final concentration: 200 mM Tris-HCl pH 6.8, 3% SDS, 10% glycerol, 1 mM EDTA, 0.004% bromophenol blue, and 25 mM DTT), vortexed, and heated at 55 ^{o}C for 5 minutes. Samples were resolved by SDS-PAGE.

SDS-PAGE and autoradiography

Samples were resolved by 7.5% and 12% SDS-PAGE, and gels were dried and exposed to super-resolution phosphor screens (Fuji Film). Signals were visualized with a Typhoon FLA-7000 scanner (GE Healthcare Life Science) and quantified with ImageQuantTL software (GE Healthcare Life Science).

ACKNOWLEDGMENTS

We thank Prof. John Riordan, University of North Carolina Chapel Hill, NC USA, and the Cystic Fibrosis Foundation for kindly providing 596 antibody, and Dr. John Christianson and Dr. Norbert Volkmar, Oxford University UK, for EMC-deleted cells and sharing their unpublished information, and Prof. Gergely Lukacs, McGill University, Montréal Québec, Canada, for the pCDNA3.1-TMD2-3HA construct. We thank Dr. Joseline Houwman for reading and commenting on this manuscript, and all members of the Braakman-Van der Sluijs lab for fruitful discussions. This project was funded by CFF (BRAAKM14XX0), the Netherlands Organization for Health Research and Development (ZonMw TOP grant 40-00812-98-14103), and the Netherlands Cystic Fibrosis Foundation (HIT-CF grant).

REFERENCES

Adachi, T., Schamel, W.W., Kim, K.M., Watanabe, T., Becker, B., Nielsen, P.J., and Reth, M. (1996). The specificity of association of the IgD molecule with the accessory proteins BAP31/BAP29 lies in the IgD transmembrane sequence. EMBO J *15*, 1534-1541.

Bircham, P.W., Maass, D.R., Roberts, C.A., Kiew, P.Y., Low, Y.S., Yegambaram, M., Matthews, J., Jack, C.A., and Atkinson, P.H. (2011). Secretory pathway genes assessed by high-throughput microscopy and synthetic genetic array analysis. Mol Biosyst *7*, 2589-2598.

Carveth, K., Buck, T., Anthony, V., and Skach, W.R. (2002). Cooperativity and flexibility of cystic fibrosis transmembrane conductance regulator transmembrane segments participate in membrane localization of a charged residue. J Biol Chem *277*, 39507-39514.

Cheng, S.H., Gregory, R.J., Marshall, J., Paul, S., Souza, D.W., White, G.A., O'Riordan, C.R., and Smith, A.E. (1990). Defective intracellular transport and processing of CFTR is the molecular basis of most cystic fibrosis. Cell *63*, 827-834.

Chitwood, P.J., Juszkiewicz, S., Guna, A., Shao, S., and Hegde, R.S. (2018). EMC is required to initiate accurate membrane protein topogenesis. Cell *175*, 1507-1519 e1516.

Christianson, J.C., Olzmann, J.A., Shaler, T.A., Sowa, M.E., Bennett, E.J., Richter, C.M., Tyler, R.E., Greenblatt, E.J., Harper, J.W., and Kopito, R.R. (2011). Defining human ERAD networks through an integrative mapping strategy. Nat Cell Biol *14*, 93-105.

Cohen, T.S., and Prince, A. (2012). Cystic fibrosis: a mucosal immunodeficiency syndrome. Nat Med *18*, 509-519.

Du, K., and Lukacs, G.L. (2009). Cooperative assembly and misfolding of CFTR domains in vivo. Mol Biol Cell *20*, 1903-1915.

Du, K., Sharma, M., and Lukacs, G.L. (2005). The DeltaF508 cystic fibrosis mutation impairs domain-domain interactions and arrests post-translational folding of CFTR. Nat Struct Mol Biol *12*, 17-25.

El Hiani, Y., Negoda, A., and Linsdell, P. (2016). Cytoplasmic pathway followed by chloride ions to enter the CFTR channel pore. Cell Mol Life Sci *73*, 1917-1925.

Ellgaard, L., McCaul, N., Chatsisvili, A., and Braakman, I. (2016). Co- and post-translational protein folding in the ER. Traffic *17*, 615-638.

Enquist, K., Fransson, M., Boekel, C., Bengtsson, I., Geiger, K., Lang, L., Pettersson, A., Johansson, S., von Heijne, G., and Nilsson, I. (2009). Membrane-integration characteristics of two ABC transporters, CFTR and P-glycoprotein. J Mol Biol *387*, 1153-1164.

Favaloro, V., Vilardi, F., Schlecht, R., Mayer, M.P., and Dobberstein, B. (2010). Asna1/TRC40-mediated membrane insertion of tail-anchored proteins. J Cell Sci *123*, 1522-1530.

Feige, M.J., and Hendershot, L.M. (2013). Quality control of integral membrane proteins by assembly-dependent membrane integration. Mol Cell *51*, 297-309.

Geiger, R., Andritschke, D., Friebe, S., Herzog, F., Luisoni, S., Heger, T., and Helenius, A. (2011). BAP31 and BiP are essential for dislocation of SV40 from the endoplasmic reticulum to the cytosol. Nat Cell Biol *13*, 1305-1314.

Guna, A., and Hegde, R.S. (2018). Transmembrane domain recognition during membrane protein biogenesis and quality control. Curr Biol *28*, R498-R511.

Guna, A., Volkmar, N., Christianson, J.C., and Hegde, R.S. (2018). The ER membrane protein complex is a transmembrane domain insertase. Science *359*, 470-473.

Hessa, T., Meindl-Beinker, N.M., Bernsel, A., Kim, H., Sato, Y., Lerch-Bader, M., Nilsson, I., White, S.H., and von Heijne, G. (2007). Molecular code for transmembrane-helix recognition by the Sec61 translocon. Nature *450*, 1026-1030.

Johnson, N., Powis, K., and High, S. (2013). Post-translational translocation into the endoplasmic reticulum. Biochim Biophys Acta *1833*, 2403-2409.

Johnson, Z.L., and Chen, J. (2017). Structural basis of substrate recognition by the multidrug resistance protein MRP1. Cell *168*, 1075-1085 e1079.

Jonikas, M.C., Collins, S.R., Denic, V., Oh, E., Quan, E.M., Schmid, V., Weibezahn, J., Schwappach, B., Walter, P., Weissman, J.S.*, et al.* (2009). Comprehensive characterization of genes required for protein folding in the endoplasmic reticulum. Science *323*, 1693-1697.

Kida, Y., Ishihara, Y., Fujita, H., Onishi, Y., and Sakaguchi, M. (2016). Stability and flexibility of marginally hydrophobic-segment stalling at the endoplasmic reticulum translocon. Mol Biol Cell *27*, 930-940.

Kleizen, B., van Vlijmen, T., de Jonge, H.R., and Braakman, I. (2005). Folding of CFTR is predominantly cotranslational. Mol Cell *20*, 277-287.

Kudze, T., Mendez-Dorantes, C., Jalloh, C.S., and McClellan, A.J. (2018). Evidence for interaction between Hsp90 and the ER membrane complex. Cell Stress Chaperones *23*, 1101-1115.

Lahiri, S., Chao, J.T., Tavassoli, S., Wong, A.K., Choudhary, V., Young, B.P., Loewen, C.J., and Prinz, W.A. (2014). A conserved endoplasmic reticulum membrane protein complex (EMC) facilitates phospholipid transfer from the ER to mitochondria. PLoS Biol *12*, e1001969.

Le Moigne, R., Aftab, B.T., Djakovic, S., Dhimolea, E., Valle, E., Murnane, M., King, E.M., Soriano, F., Menon, M.K., Wu, Z.Y.*, et al.* (2017). The p97 Inhibitor CB-5083 is a unique disrupter of protein homeostasis in models of multiple myeloma. Mol Cancer Ther *16*, 2375-2386.

Li, N., Wu, J.X., Ding, D., Cheng, J., Gao, N., and Chen, L. (2017). Structure of a pancreatic ATP-sensitive potassium channel. Cell *168*, 101-110 e110.

Liu, F., Zhang, Z., Csanady, L., Gadsby, D.C., and Chen, J. (2017). Molecular structure of the human CFTR ion channel. Cell *169*, 85-95 e88.

Louie, R.J., Guo, J., Rodgers, J.W., White, R., Shah, N., Pagant, S., Kim, P., Livstone, M., Dolinski, K., McKinney, B.A.*, et al.* (2012). A yeast phenomic model for the gene interaction network modulating CFTR-DeltaF508 protein biogenesis. Genome Med *4*, 103.

Mendoza, J.L., Schmidt, A., Li, Q., Nuvaga, E., Barrett, T., Bridges, R.J., Feranchak, A.P., Brautigam, C.A., and Thomas, P.J. (2012). Requirements for efficient correction of DeltaF508 CFTR revealed by analyses of evolved sequences. Cell *148*, 164-174.

Onishi, Y., Yamagishi, M., Imai, K., Fujita, H., Kida, Y., and Sakaguchi, M. (2013). Stop-and-move of a marginally hydrophobic segment translocating across the endoplasmic reticulum membrane. J Mol Biol *425*, 3205-3216.

Pitonzo, D., Yang, Z., Matsumura, Y., Johnson, A.E., and Skach, W.R. (2009). Sequence-specific retention and regulated integration of a nascent membrane protein by the endoplasmic reticulum Sec61 translocon. Mol Biol Cell *20*, 685-698.

Rapoport, T.A., Goder, V., Heinrich, S.U., and Matlack, K.E. (2004). Membrane-protein integration and the role of the translocation channel. Trends Cell Biol *14*, 568-575.

Ratjen, F., and McColley, S.A. (2012). Update in cystic fibrosis 2011. Am J Respir Crit Care Med *185*, 933-936.

Richard, M., Boulin, T., Robert, V.J., Richmond, J.E., and Bessereau, J.L. (2013). Biosynthesis of ionotropic acetylcholine receptors requires the evolutionarily conserved ER membrane complex. Proc Natl Acad Sci U S A *110*, E1055-1063.

Riordan, J.R. (2008). CFTR function and prospects for therapy. Annu Rev Biochem *77*, 701-726.

Rossi, A., Kontarakis, Z., Gerri, C., Nolte, H., Holper, S., Kruger, M., and Stainier, D.Y. (2015). Genetic compensation induced by deleterious mutations but not gene knockdowns. Nature *524*, 230-233.

Satoh, T., Ohba, A., Liu, Z., Inagaki, T., and Satoh, A.K. (2015). dPob/EMC is essential for biosynthesis of rhodopsin and other multi-pass membrane proteins in Drosophila photoreceptors. Elife *4*.

Shurtleff, M.J., Itzhak, D.N., Hussmann, J.A., Schirle Oakdale, N.T., Costa, E.A., Jonikas, M., Weibezahn, J., Popova, K.D., Jan, C.H., Sinitcyn, P.*, et al.* (2018). The ER membrane protein complex interacts cotranslationally to enable biogenesis of multipass membrane proteins. Elife *7*.

van Willigen, M., Vonk, A.M., Yeoh, H.Y., Kruisselbrink, E., Kleizen, B., van der Ent, C.K., Egmond, M.R., de Jonge, H.R., Braakman, I., Beekman, J.M.*, et al.* (2019). Folding-function relationship of the most common cystic fibrosis-causing CFTR conductance mutants. Life Sci Alliance *2*.

Volkmar, N., Thezenas, M.L., Louie, S.M., Juszkiewicz, S., Nomura, D.K., Hegde, R.S., Kessler, B.M., and Christianson, J.C. (2019). The ER membrane protein complex promotes biogenesis of sterol-related enzymes maintaining cholesterol homeostasis. J Cell Sci *132*.

von Heijne, G. (2007). The membrane protein universe: what's out there and why bother? J Intern Med *261*, 543-557.

Wallin, E., and von Heijne, G. (1998). Genome-wide analysis of integral membrane proteins from eubacterial, archaean, and eukaryotic organisms. Protein Sci *7*, 1029-1038.

Xiong, X., Bragin, A., Widdicombe, J.H., Cohn, J., and Skach, W.R. (1997). Structural cues involved in endoplasmic reticulum degradation of G85E and G91R mutant cystic fibrosis transmembrane conductance regulator. J Clin Invest *100*, 1079-1088.

Zhang, S., Xu, C., Larrimore, K.E., and Ng, D.T.W. (2017a). Slp1-Emp65: A guardian factor that protects folding polypeptides from promiscuous degradation. Cell *171*, 346-357 e312.

Zhang, Z., Liu, F., and Chen, J. (2017b). Conformational changes of CFTR upon phosphorylation and ATP binding. Cell *170*, 483-491 e488.

Zhou, H.J., Wang, J., Yao, B., Wong, S., Djakovic, S., Kumar, B., Rice, J., Valle, E., Soriano, F., Menon, M.K.*, et al.* (2015). Discovery of a first-in-class, potent, selective, and orally bioavailable inhibitor of the p97 AAA ATPase (CB-5083). J Med Chem *58*, 9480-9497.

Zielenski, J., Fujiwara, T.M., Markiewicz, D., Paradis, A.J., Anacleto, A.I., Richards, B., Schwartz, R.H., Klinger, K.W., Tsui, L.C., and Morgan, K. (1993). Identification of the M1101K mutation in the cystic fibrosis transmembrane conductance regulator (CFTR) gene and complete detection of cystic fibrosis mutations in the Hutterite population. Am J Hum Genet *52*, 609-615.

SUPPLEMENTARY MATERIAL

Primers for TMD1-Linkter-TMD2 construct

Vector (pBI-CMV2) and TMD1	F: 5' – AGAATTCACACGTGAAGAAAGATTGACGGCCGCATCGATAAG – 3' R: 5' – CCTGCTGTCTGCATTGTGACCATCACTACTTCTGTAGTCGTTAAGTT – 3'
Pg-P linker	F: 5' – CGACTACAGAAGTAGTGATGGTCACAATGCAGACAGCAGG – 3' R: 5' – AGGTATGTGTTCCATGTAGTAAGCTTTCTGTCTTGGGCTT – 3'
TMD2 and vector	F: 5' – GCTTATCGATGCGGCCGTCAATCTTTCTTCACGTGTGAATTCT – 3' R: 5' – AAGCCCAAGACAGAAAGCTTACTACATGGAACACATACCTT – 3'

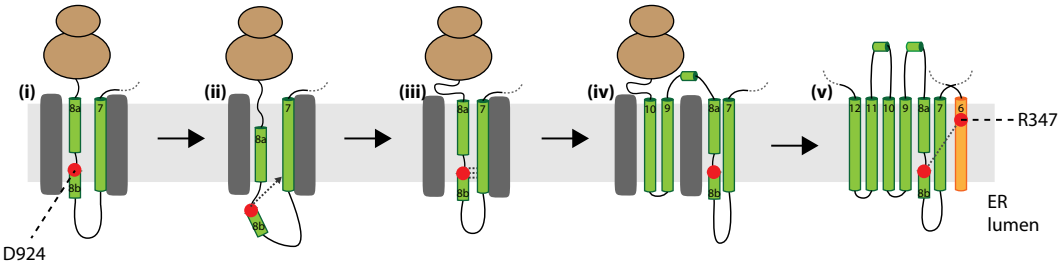


Figure S1: Model for CFTR domain assembly in the absence of EMC
During translation and insertion of TM8 (i), Sec61 may fail to recognize TM8 and allow it to extend into the ER lumen (ii). TM8 is retrieved back to the translocon channel through helix-helix packing with TM7 (iii), after which the helical pair can be inserted into the ER membrane via lateral opening of the translocon (iv). D924 is further stabilized by R347 in TMD1 during domain assembly (v).

Chapter 7

The role of Bap31 in CFTR folding and quality control

AUTHORS:
Hui Ying Yeoh, Jisu Im, Robert Jan Lebbink, Joseline Houwman, Peter van der Sluijs, Ineke Braakman

ABSTRACT

Cystic Fibrosis Transmembrane Conductance Regulator (CFTR) is an ion channel with charged residues in its transmembrane (TM) regions that are required for the interaction between the two transmembrane domains (TMDs), TMD1 and TMD2 during the formation of the channel. Before TMD1 and TMD2 interact with each other, these charged residues are exposed to the lipid bilayer and may require chaperone binding to prevent CFTR aggregation. Bap31 is thought to be a chaperone for CFTR because of its charged TM residues, which may bind pre-domain assembly CFTR and sort it to ER-associated degradation (ERAD) via TMD1. To study the connection between Bap31 and charged residues in the TMs of CFTR, we examined CFTR domain stability and assembly using mutational analysis or knockout of BAP31 using a combined pulse-chase and limited-proteolysis approach. Our results showed that the charged residues in the TM of Bap31 are required to stabilize CFTR TMDs post-translationally and that the association with Bap31 supports efficient CFTR domain assembly. We therefore propose that Bap31 chaperones CFTR folding by preventing charged residues within the CFTR TM from interacting with the lipid bilayer and acts as quality control for CFTR domain assembly.

INTRODUCTION

Cystic Fibrosis Transmembrane Conductance Regulator is a multi-pass membrane protein that contains two TMDs, two NBDs and an unstructured R-region (Liu et al., 2017; Riordan et al., 1989; Zhang et al., 2017). CFTR functions as an anion channel and opens upon dimerization of the NBDs and phosphorylation of the R-region (Cheng et al., 1991; Gunderson and Kopito, 1995). Disrupting the conformation of CFTR causes Cystic Fibrosis, a disease in which the movement of ions and water across the apical membrane is compromised, leading to accumulation of thick mucus, which leads to infections in the respiratory, digestive and reproductive systems (Cheung and Deber, 2008; Cohen and Prince, 2012; Ratjen and Grasemann, 2012). The most common mutation in the *CFTR* gene that causes cystic fibrosis is F508del. Loss of the phenylalanine at this position impairs NBD1 folding and promotes CFTR degradation in the ER (Du et al., 2005; Riordan, 2008).

The CFTR channel is formed through association of the TMDs. Charged or polar residues are situated at the surface of the channel to stabilize the contact site between the hydrophobic TMDs and the aqueous environment inside the channel (El Hiani et al., 2016; Li et al., 2018; Zhang et al., 2017). The charged residues also form salt bridges to enhance interactions between the TMDs (Cotten and Welsh, 1999; Pitonzo et al., 2009; Skach, 2009). Each CFTR TMD contains at least 2 charged residues (El Hiani et al., 2016), which poses the challenge of how to maintain stability of such a TMD and to minimize thermodynamic instability caused by the charged residues in the lipid bilayer before the protein is properly folded. Charged residues within a lipid bilayer can only interact with molecules that have similar chemical properties such as membrane proteins that also have charged residues within their TM areas. This requirement suggests the existence of membrane-bound molecular chaperones for CFTR TMDs during folding. Several chaperones for folding of CFTR TMDs have already been studied, including Sec61 (Carveth et al., 2002; Pitonzo et al., 2009), the EMC complex (Louie et al., 2012), and Bap31 (Lambert et al., 2001; Wang et al., 2008). However, details of their binding and mechanism of action remain to be established.

Bap31 is an ER resident protein with 3 transmembrane helixes in its N-terminus and an extracellular C-terminus with a coiled-coil region and a double lysine (KKEE) motif for ER retention (Kim et al., 2015). The topology of Bap31 however is not without controverse since a domain organization with a cytoplasmic C terminus has also been described (Geiger et al., 2011). Bap31 is ubiquitously expressed and mainly functions in the quality control of membrane proteins and in modulating apoptosis in conjunction with caspase-8 (Breckenridge et al., 2003). Clients of Bap31 include MHC class I (Abe et al., 2009; Ladasky et al., 2006), membrane-bound

immunoglobulin D (Adachi et al., 1996; Schamel et al., 2003), tetraspanin (Bartee et al., 2010), cellubrevin (Annaert et al., 1997), CD11b/CD18 (Zen et al., 2004), and CFTR (Lambert et al., 2001; Wang et al., 2008). The interaction of Bap31 with these clients occurs via different principles, for instance, Bap31 binds to MHC class I in the presence of its homolog Bap29 for entering COPII vesicles (Paquet et al., 2004). Bap31 together with Bap29 also coregulates the dislocation of SV40 from the ER to the cytoplasm (Geiger et al., 2011). Alternatively, Bap31 interacts with CD11b/CD18 through its cytosolic tail, which is also important in transport of cellubrevin (Annaert et al., 1997; Zen et al., 2004). The interactions between membrane-bound immunoglobulin D and Bap31 occur via the transmembrane regions of both proteins (Adachi et al., 1996). Lastly, Bap31 is involved in CFTR quality control and promotes CFTR degradation through Derlin-1 (Wang et al., 2008).

The molecular mechanisms underlying the selection of clients for quality control by Bap31 are not well understood. The interaction between Bap31 and CFTR occurs during translation (Figure 1A and 1B). Immunoprecipitation using CFTR non-ribosome attached nascent-chain mimics isolated a cluster of proteins including Bap31 and translocon components (Wang et al., 2008). Bap31 can already be detected in the protein cluster that co-immunoprecipitated with a detached nascent chain mimic of only the first 370 amino acids of CFTR (Figure 1B). Co-immunoprecipitation with full-length F508del uncovered another cluster of proteins that includes Derlin-1, but not the Sec61 translocon. Silencing of Derlin-1 inhibits CFTR retro-translocation, suggesting that CFTR is degraded via the Derlin-1 complex in the ERAD pathway (Sun et al., 2006; Wang et al., 2008). Knockdown of Bap31 in mammalian cells reduces CFTR retro-translocation and degradation. This phenotype could not be rescued by overexpression of Derlin-1, indicating that the Derlin-1-ERAD pathway degrades CFTR via Bap31 (Figure 1C and 1D).

To address the selection criteria of Bap31 for CFTR and its chaperone function on the charged residues in the TM segments, we investigated CFTR folding in the absence of Bap31 or after introduction of BAP31 variants, using radioactive labeling and a protease-sensitivity assay followed by immunoprecipitation with domain-specific antibodies (Figure 1E). Our results suggest that Bap31 stabilized CFTR TMDs post-translationally and promoted CFTR degradation via binding to unassembled TMDs.

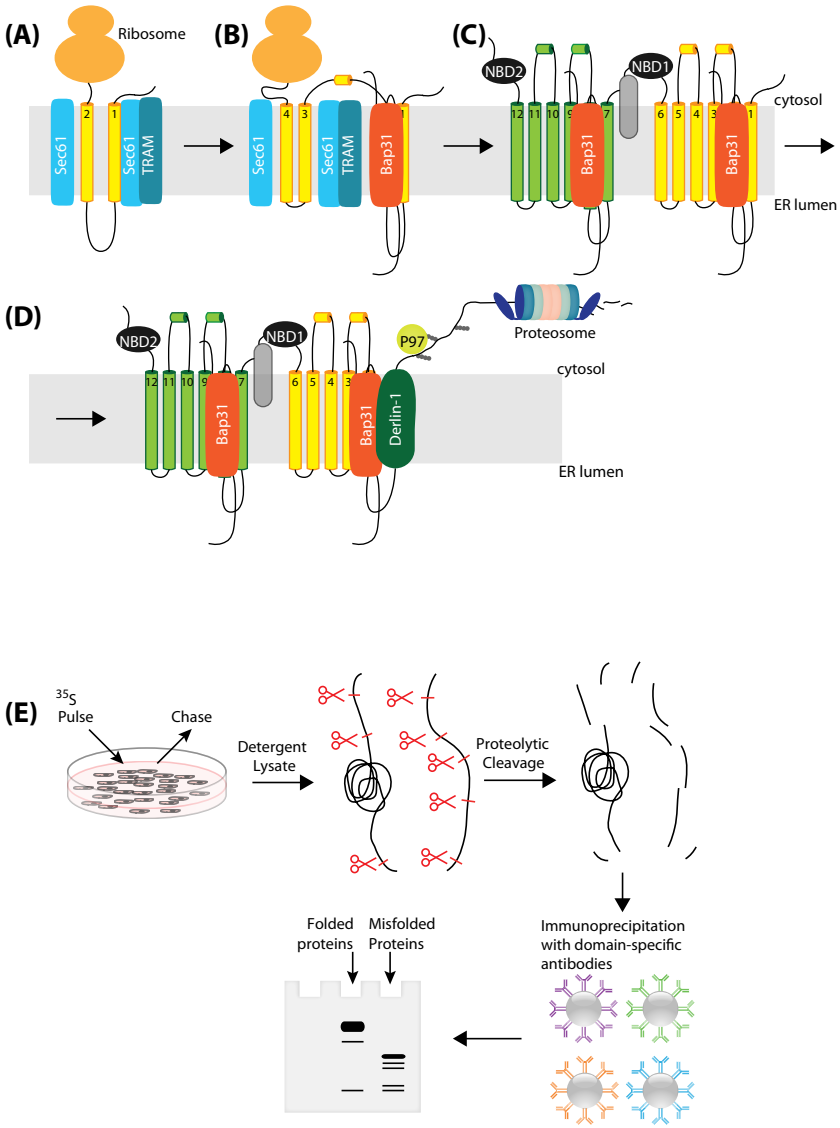


Figure 1: Bap31 interacts with CFTR co-translationally and degrades CFTR through the Derlin-1 complex. (A) CFTR TMD1 is translated and inserted into the lipid bilayer by the Sec61 translocon. (B) Bap31 binds to inserted CFTR TMD1 during translation. (C) Bap31 continues to bind to CFTR after translation. (D) Bap31 transfers CFTR molecules to the Derlin-1 dependent ERAD pathway. (E) Scheme of ^{35}S radiolabeling, protease susceptibility assay, and immunoprecipitation.

RESULTS

Bap31 knockdown in Cystic Fibrosis Bronchial Epithelial cells does not affect CFTR expression

Previously, Bap31 knockdown (KD) was shown to increase the steady-state level of CFTR (Lambert et al., 2001; Wang et al., 2008). A possible role of Bap31 in CFTR domain folding and assembly however has not been investigated. To address this question, we silenced Bap31 to 20% of wild-type levels in Cystic Fibrosis Bronchial Epithelial cells stably expressing wild-type CFTR (CFTR-CFBE) cells and analyzed its effect on wild-type CFTR (named CFTR) expression. Both the ER and Golgi forms of CFTR were detected on Western blot after Bap31 depletion using siRNA (Figure 2A). The ER form of CFTR represents the pool that has achieved folding of single domains but has not yet assembled its domains. The Golgi form, on the other hand, represents CFTR molecules that have traveled to the Golgi complex, acquired complex glycans, have already established domain assembly, and may be exported to the plasma membrane.

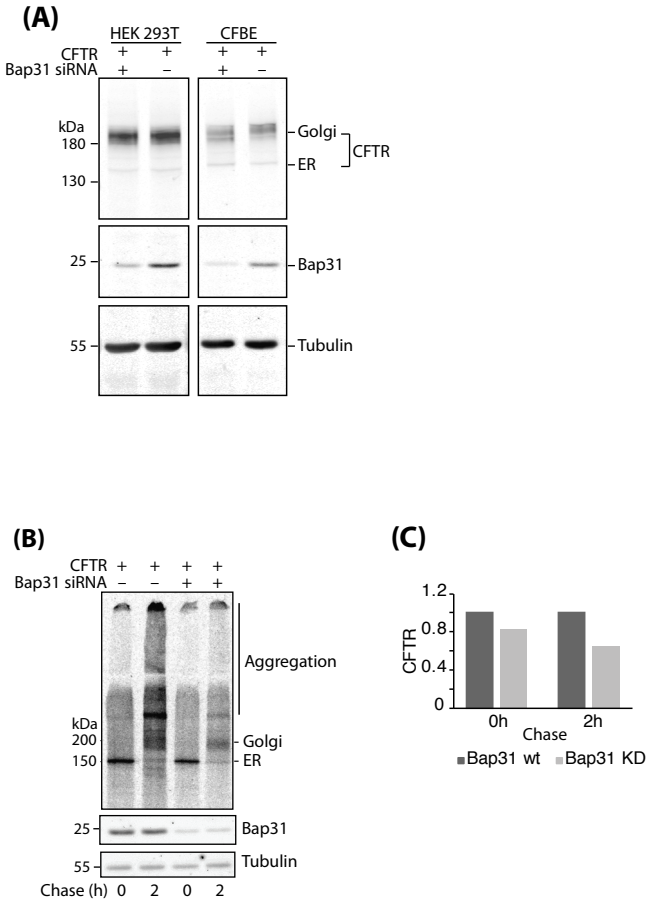


Figure 2: Bap31 knockdown in CFBE cells does not affect CFTR expression. (A) CFTR and Bap31 expression in HEK 293T and CFBE cells, with or without Bap31 siRNA, was probed by Western blot. Tubulin was used as loading control. (B) CFBE cells stably expressing CFTR were transfected with Bap31 siRNA 48 hours before the pulse-chase experiment. Cells were radiolabeled with ^{35}S-methionine and -cysteine for 15 minutes and were chased for 2 hours. CFTR was immunoprecipitated from detergent cell lysates and analyzed by 7.5% SDS-PAGE by MrPink. Bap31 and tubulin were detected by Western blot. (C) The total amount of CFTR from (B) was quantified (n=2) and normalized to the Bap31 control (wt: wild-type; KD: knockdown).

We checked synthesis and turnover by pulse-chase analysis. Cells were labeled for 15 min with ^{35}S-methionine and -cysteine and the label was chased in the absence of radioactive amino acids, after which CFTR was immunoprecipitated from the detergent cell lysates (Figure 2B, C). CFTR only occurred in the ER form after the pulse while both ER and Golgi forms of CFTR were found after the chase (Figure 2B). The amount of newly synthesized CFTR at the end of the pulse period was similar in the knockdown and control cells (Figure 2C), suggesting that Bap31 has no role in CFTR translation or that residual Bap31 might still maintain a role in regulation of CFTR expression. Previous studies demonstrated that a higher level of knockdown (90% reduction of Bap31 expression) is necessary for eliminating Bap31 function. We therefore generated a Bap31 knockout (KO) cell line using the CRISPR/cas9 technique.

Establishment of a Bap31 KO cell line

Knockout of Bap31 was performed in HEK293T cells and was first validated at the protein level by Western blot (Figure 3A), which showed that Bap31 expression was

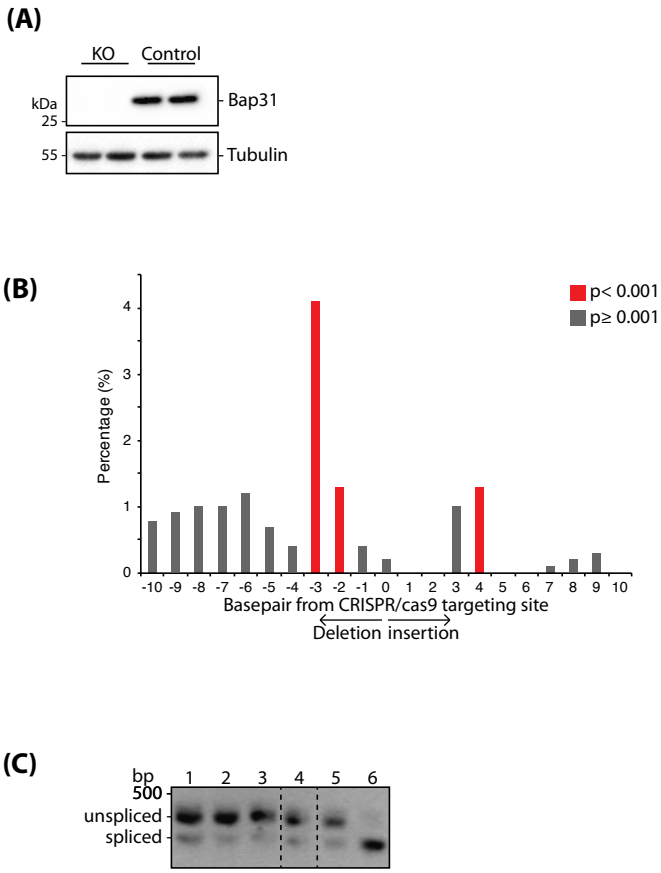


Figure 3: Establishment of a Bap31 KO cell line.
(A) Cell lysates of wt HEK 293T cells and HEK 293T cells after Bap31 knockout (KO) were analyzed by Western Blot with antibodies against Bap31 and tubulin. (B) Genomic DNA from Bap31 KO cells was harvested and amplified with Bap31-specific primers. The population of Bap31 genes with no deletion/insertion or with deletion or insertion up to 10 nucleotides from the CRISPR/cas9 targeting site were calculated with TIDE software (Brinkman et al., 2014). (C) XBP1 splicing in the Bap31 KO cell line was assayed by RT-PCR of XBP1 mRNA and analysis by agarose gel electrophoresis (1: wt HEK 293T control; 2: Bap31 KO clone 1; 3: Bap31 KO clone 2; 4: Transfection of Bap31 plasmid into Bap31 KO clone 1 cells; 5: Transfection of CFTR plasmid into Bap31 KO clone 1 cells; 6: 6 h of 10 µM Tunicamycin treatment).

below detection level. We subsequently determined the CRISPR/cas9 target site in the knockout cells at the genomic level. Classifying the PCR products amplified from DNA of the Bap31 KO cells by TIDE analysis showed that at least three alleles of the Bap31 gene could be detected. Two of these have 2- and 4-base pair (bp) frameshift mutations, which may result in a non-functional protein, and a 3-bp frameshift mutation (Figure 3B). The fact that Bap31 was not detected by Western blot suggested that the 3bp-deletion failed to produce a functional protein. Although TIDE analysis revealed the genotype of our Bap31 KO cells, it cannot discriminate however between scenarios where the three distinct alleles belong to a monoclonal cell population or originate from three different cell populations that were mixed during the beginning of selection. A future analysis is therefore needed to establish the precise genotype in the knockout cell line.

Since elimination of Bap31 may result in accumulation of its client proteins in the ER and could stress the cell via the Unfolded Protein Response (UPR) (Friedlander et al., 2000), we analyzed XBP1 splicing, the hallmark of UPR stress. The amount of spliced XBP1 in the Bap31 KO cells (Figure 3C, lane 2 and 3) was similar to that of control cells (Figure 3C, lane 1), arguing that reduced levels of Bap31 did not elicit a UPR stress response. Re-introduction of wild-type Bap31 (named Bap31) nor ectopic expression of CFTR impacted XBP1 splicing (Figure 3C, lane 4 and 5), while treatment of cells with the ER stress-inducer tunicamycin greatly increased splicing of XBP1 (Figure 3C, lane 6).

Knockout of Bap31 increased the level of ectopically expressed CFTR TMDs

Earlier studies showed that Bap31 regulates CFTR degradation via binding to TMD1 (Wang et al., 2008). TMD1 and TMD2 have a similar structure and distribution of charged residues in the TMs (Zhang et al., 2017), but TMD2 has a lower stability than TMD1, because it contains an unstructured hydrophilic region in its second TM segment that may interfere with efficient insertion (Pitonzo et al., 2009). In this context, TMD2 may require more chaperoning in the ER membrane than TMD1 and may also bind to Bap31. To examine whether Bap31 affected TMD2, we examined biosynthesis of the TMD2 domain in Bap31 knockout cells, which were labeled for 15 minutes with ^{35}S-methionine and -cysteine followed by detergent lysis and immunoprecipitation with a domain-specific antibody. We first confirmed the effects of Bap31 KO on TMD1 synthesis and found higher expression in the knockout cells than in cells in which Bap31 had been re-introduced (Figure 4A). In contrast, synthesis of transfected NBD1 was not affected by manipulation of Bap31 levels (Figure 4B). Importantly, this result showed that knockout of Bap31 did not pleiotropically affect protein translation. We then proceeded with a CFTR construct consisting of TMD1 and TMD2 in which the destabilizing R region was replaced by the corresponding 60-aa linker of Pgp, another ABC transporter (Figure 4C).

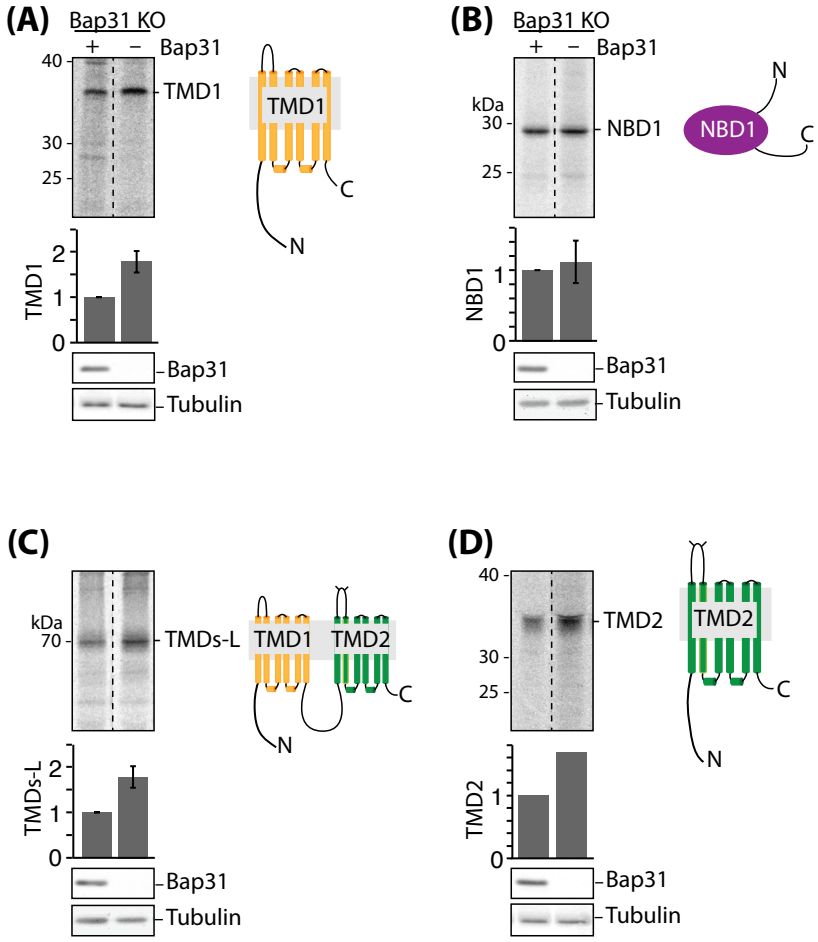


Figure 4: Bap31 KO increased expression of CFTR TMDs.
CFTR TMD1 (A), NBD1 (B), TMD1-Linker-TMD2 (TMDs-L) (C), or NBD1 (D) were expressed in Bap31 KO cells with or without Bap31 rescue. Cells were radiolabe`led with ^{35}S-methionine and -cysteine for 15 minutes and CFTR domains were immunoprecipitated from the detergent lysate with domain-specific antibodies TMD1C (TMD1, TMDs-L), anti-HA (TMD2), and MrPink (NBD1). Immunoprecipitated proteins were analyzed by 7.5% or 12% SDS-PAGE and quantitations were normalized to their Bap31 wt control (TMD1, TMDs-L and NBD1 were n=3, TMD2 was n=2).

In accordance with the TMD1 construct we found ~60% higher expression in the absence of Bap31 for the TMD1-Linker-TMD2 construct. Lastly, a fourth construct consisting of TMD2 only (Figure 4D) also yielded higher expression in cells without Bap31, showing that Bap31 is involved in control of CFTR degradation via both transmembrane domains.

Charged residues in the transmembrane domains of Bap31 regulate binding to CFTR

Interactions between Bap31 and substrates such as membrane-bound IgD, membrane associated RING-CH (MARCH) and CFTR occur via the TMD segments (Adachi et al., 1996; Bartee et al., 2010; Wang et al., 2008). The binding mechanism of Bap31 to the TMDs of these clients, however, is not clear. Bap31 contains 3 charged residues, E15, R117, and R118, in its TMD (Figure 5A) (Geiger et al., 2011). These charged residues are involved in binding to the structural protein VP2 of SV40 and regulate the retro-translocation of VP2 across the ER membrane into the cytosol (Geiger et al., 2011). Whether they have a more general role in Bap31 association with other cellular membrane proteins has not been established. We therefore examined their role in binding to CFTR TMD1 by using Bap31 knockout cells as a recipient cell line for a rescue approach. A Bap31 mutant in which the three charged residues were changed into alanines (Bap31-3A) was co-expressed with CFTR TMD1 in Bap31 KO cells. CFTR TMD1 was immunoprecipitated and co-immunoprecipitating Bap31 was detected via Western blot (Figure 5B, first panel from top). As can be seen in Figure 5B, a robust signal was seen for Bap31 binding to TMD1, whereas a weak association occurred with Bap31-3A (Figure 5B, first panel

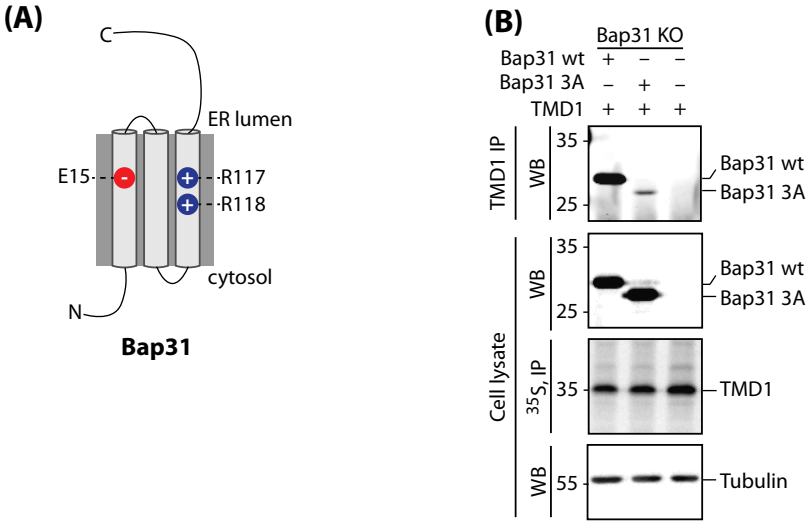


Figure 5: Charged residues in the transmembrane domains of Bap31 regulate binding to CFTR.
(A) Bap31 cartoon with the location of transmembrane charged residues. (B) CFTR TMD1 was expressed in Bap31 KO cells transfected with Bap31 and Bap31-3A. Cells were labeled with ^{35}S-methionine and -cysteine. Cells were lysed and TMD1 was immunoprecipitated, Bap31 and Bap31-3A were detected on Western blot with an antibody against Bap31. TMD1 was immunoprecipitated and quantitated by phosphorimaging (WB: Western Blot; IP: Immunoprecipitation; 3A: Bap31 E15A R117118A mutant).

from top). Future experiments need to be carried out with CFTR TMD2 to determine whether Bap31 has a preference for one of the CFTR TMDs.

Mutations destabilize CFTR TMDs post-translationally and block domain assembly
Figure 5B showed that charged residues in Bap31 are required for binding to TMD1 and that mutation of these residues lowers binding. This indicates that Bap31 binds to TMD1 via ionic interactions in the TM segments and may thus be responsible for chaperoning charged residues in the TM segments. Because an earlier report suggests that Bap31 selectively interacts with the core-glycosylated form of CFTR (Wang et al., 2008), we next investigated whether Bap31 could act as a chaperone to stabilize CFTR TMDs before the two TMDs assemble during post-translational domain interaction. We therefore selected CFTR-R1070W/F508del (R/F) and CFTR-R347P. These two CFTR patient mutants failed to achieve domain assembly, leaving the charged residues in their TMDs uncoupled in the lipid bilayer, which would destabilize the TMDs (Mendoza et al., 2012; van Willigen et al., 2019). The stability of these two CFTR mutants therefore might be more sensitive to perturbation of the interaction with Bap31 (Figure 6A). The features of the two mutants and CFTR were investigated by a radiolabeling pulse-chase and Proteinase K susceptibility assay. HEK293T cells expressing the CFTR variants were pulsed for 15 minutes, chased for 2 hours, and the lysates were treated with 25 μg/ml Proteinase K. The proteolytic fragments were immunoprecipitated with antibodies against the different CFTR domains. As expected, we only detected the ER form of CFTR after the pulse and both ER and Golgi forms after the chase (Figure 6B). The ER form was core-glycosylated and had not undergone domain assembly, while the Golgi form had already established domain assembly and was complex-glycosylated. The domain assembly of CFTR is represented by a typical pattern of proteolytic fragments originating from TMD1, TMD2, and NBD2, namely T1 late (T1d-f), T2c, and N2, and which can only be detected at 2-h chase (Figure 6C).

The CFTR-R/F mutant showed similar expression as CFTR after pulse labeling but a relatively high amount of the ER form at the expense of the Golgi form after the 2-h chase (Figure 6B top panel). This mutant has a misfolded NBD1 due to deletion of the F508 residue (Figure 6A), which disrupts the ICL4-NBD1 interface and prevents CFTR domain assembly (Du et al., 2005). Misfolded NBD1 also promotes degradation of this mutant. The additional R1070W mutation does not rescue NBD1 but stabilizes the ICL4-NBD1 interface and allows some domain assembly (Mendoza et al., 2012). This minimal restoration of domain assembly decreases F508del CFTR degradation and therefore provides a window of opportunity to investigate the post-translational protein folding of CFTR-R/F. Compared to CFTR, CFTR-R/F still has a higher degradation rate and reduced ER export (Figure 6B). The degradation rate was obtained by calculating the difference between the amount of protein at

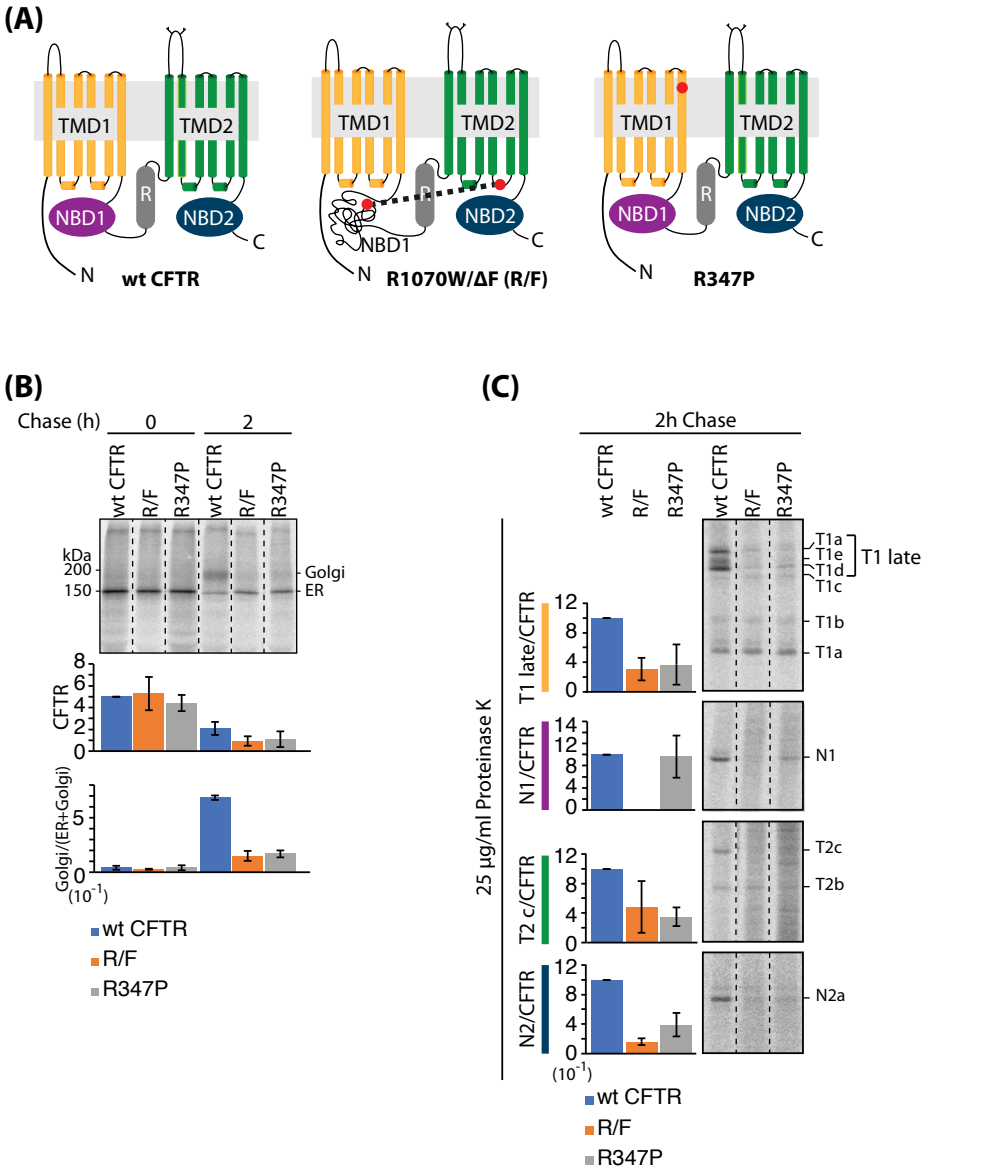


Figure 6: R1070W/F508del and R347P mutations inhibit CFTR domain assembly and destabilize CFTR TMDs post-translationally.

(A) Cartoon to show features of CFTR and its mutants. (B) HEK239T cells transiently expressing CFTR, CFTR-R/F, or CFTR-R347P were radiolabeled with ^{35}S-methionine and -cysteine for 15 minutes, chased for 2-hours, and lysed. CFTR and mutants were immunoprecipitated from the detergent lysate and analyzed by 7.5% SDS-PAGE. The amount of immunoprecipitated proteins was quantified and normalized to the wild-type CFTR sample at 0-h chase (n=3). (C) Samples of cell lysates from cells with 2-h chase were treated with Proteinase K and the proteolytic fragments were immunoprecipitated with TMD1C (TMD1), MrPink (NBD1), TMD2C (TMD2) and 596 (NBD2) antibodies. Samples then were analyzed by 12% SDS-PAGE. The proteolytic fragments that represented CFTR domain assembly, T1 late (T1d-T1f), T2c, and N2 were quantified and related to the amount of full-length CFTR. These measurements were then normalized to wild-type CFTR (n=3). The percentage of the Golgi form was calculated from band intensities of the high mannose (ER) and complex-glycosylated (Golgi) forms according to (Golgi/(ER+Golgi)) and plotted (n=3). (R/F: CFTR-R1070W/F508del, T1: TMD1, N1: NBD1, T2: TMD2, N2: NBD2)

0-h and 2-h chases, and export from the ER was represented by the percentage of its Golgi form. The total amount of CFTR-R/F and the percentage of the Golgi form after 2 hours of chase were lower than for CFTR (Figure 6B). CFTR-R/F also had less efficient domain assembly compared to CFTR (Figure 6C). The amount of T1 late, T2c, and N2 proteolytic fragments of CFTR-R/F were reduced compared to CFTR, after correcting for expression differences between CFTR-R/F and CFTR (Figure 6C). Impaired domain assembly indicated less interaction between the TMDs of CFTR-R/F and a higher chance of exposure of its TM charged residues to the lipid bilayer. The exposed charged TM residues may ultimately rely more on Bap31 assistance for stabilization, which may be reduced in Bap31-3A.

Similar amounts of CFTR-R347P and CFTR-R/F were synthesized during the pulse periods (Figure 6B). CFTR-R347P has an intact NBD1, but a disturbed domain assembly caused by the R347 mutation in TM6 (Figure 6A). The mutation twists TM6 into a kinked structure, which prevents the binding of the N-terminus to the TMD2 helixes and disrupts the interaction between the TMDs (van Willigen et al., 2019). This leads to a decrease in domain assembly, lowers the amounts of T1 late, T2c, and N2 proteolytic fragments compared to CFTR (Figure 6C; van Willigen et al., 2019), and increases ER retention and degradation of the mutant, as reflected by the decrease of the Golgi form and protein amount at 2-h chase (Figure 6B). Low domain assembly levels in CFTR-R347P results in a similar situation as with the CFTR-R/F mutant, where the charged residues within the TM area are exposed to the lipid bilayer due to inefficient domain-domain interactions. As with CFTR-R/F, chaperones may also be required during CFTR-R347P domain assembly to stabilize these partially exposed charged residues.

Bap31 stabilizes mutant CFTR TMDs post-translationally

To examine the role of Bap31 on TMD stability, we expressed CFTR-R347P and CFTR-R/F in Bap31 KO cells reconstituted with Bap31 or Bap31-3A. Protein synthesis was analyzed by a 15 min pulse labeling with ^{35}S-methionine and-cysteine, followed by a 0- or 2-h chase. Domain stability was checked by treating the lysates with 25 µg/ml Proteinase K and proteolytic fragments of each domain were immunoprecipitated with domain-specific antibodies (Figure S1a).

Expression of CFTR and the two mutants was higher in the absence of Bap31 as previously reported (Figure 7A) (Lambert et al., 2001; Wang et al., 2008), probably because Bap31 KO interfered with degradation of CFTR (Wang et al., 2008). Re-introduction of Bap31 or Bap31-3A reduced expression of CFTR both at 0-h and at 2-h chase (Figure 7A), showing that Bap31-3A affected CFTR expression to the same extent as Bap31. Bap31 KO and Bap31-3A expression also did not affect domain folding of CFTR and mutants at 0-h chase (Figure 7B). TMD1, NBD1, and

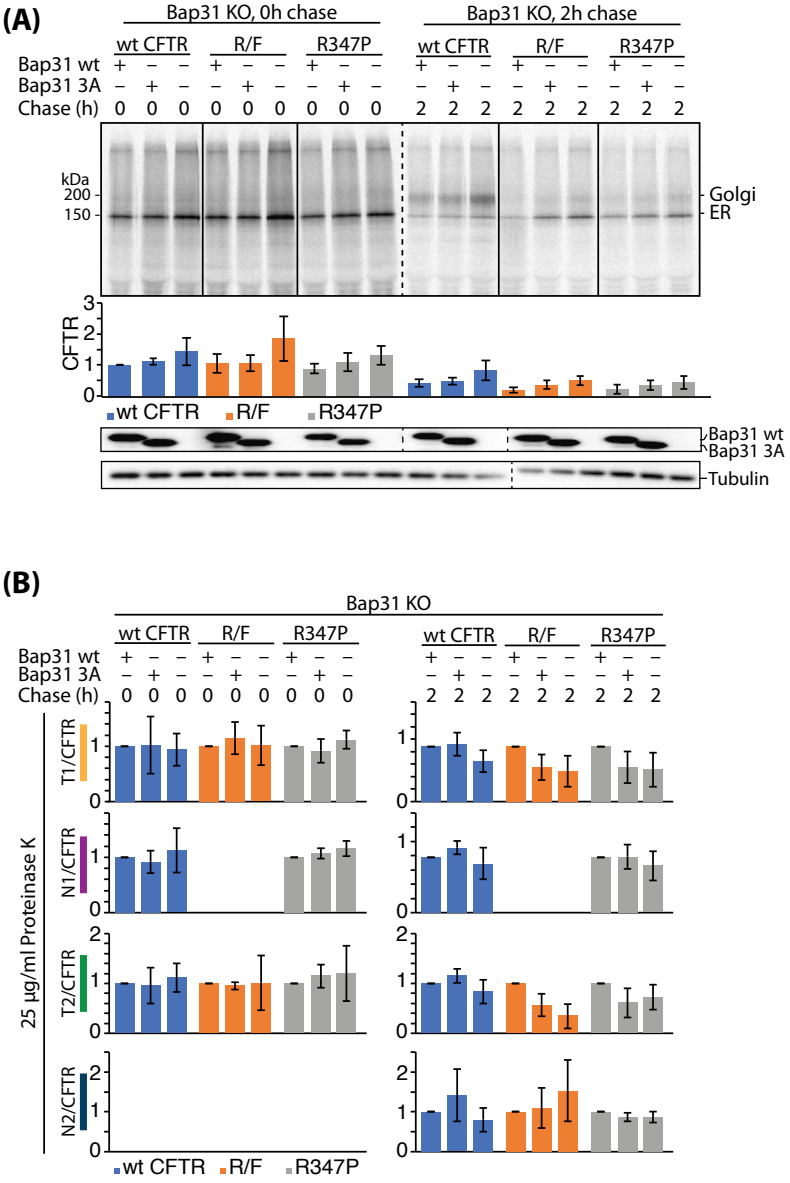


Figure 7: Bap31 stabilizes mutant TMDs.
(A) CFTR and mutants were expressed in Bap31 KO cells or KO cells rescued with wt Bap31 or Bap31-3A. Cells were pulsed for 15 minutes, chased for 2 hours and lysed. CFTRs were immunoprecipitated by MrPink and analyzed by 7.5% SDS-PAGE. CFTR protein amount from immunoprecipitation was quantified and normalized to wt CFTR sample at wt Bap31, 0-h chase condition (n=3). The expression of Bap31 and Tubulin was checked with Western blot. (B) Samples of non-digested cell lysates were treated with Proteinase K and the proteolytic fragments were immunoprecipitated with domain-specific antibodies and analyzed by 12% SDS-PAGE. The amount of proteolytic fragments per domain was quantified and related to their original full-length protein for measuring the folding and stability. The stability of TMD1 (T1a-T1f), NBD1 (N1) and TMD2 (T2b-T2c) at 0-h and 2-h chase time points were normalized to the Bap31 control (n=3). R/F: CFTR R1070W/F508del mutant; T1: TMD1, N1: NBD1, T2: TMD2, N2: NBD2.

TMD2 originating from CFTR or mutants thereof had folded similarly at the end of the pulse in Bap31 and Bap31-3A reconstituted cells as well as in Bap31 KO cells (Figure 7B, T1/CFTR, N1/CFTR, and T2/CFTR). NBD1 in CFTR-R/F was misfolded, explaining why no bands were immunoprecipitated by the NBD1-specific antibody (Figure S1A and Figure 7B, N1/CFTR at 0-h chase). Since NBD2 obtains its structure during domain assembly it is the only domain in the expressed CFTR constructs that could not be detected at the start of the chase (Figure 7B, N2/CFTR). The effects of Bap31-3A and KO on CFTR domain folding were appreciably more profound after a 2-h chase period (Figure 7B). At this time, proteolytic fragments that reflect CFTR domain assembly, such as T1 late, T2c, and N2a, were detected in CFTR but not in the CFTR-R/F and CFTR-R347P mutants.

Quantitation of the proteolytic fragments and domain assembly fragments showed that TMD1 folding of CFTR was impaired in Bap31 KO cells compared to the same cells transfected with Bap31 and Bap31-3A (Figure 7B, T1/CFTR). CFTR TMD2 and NBD fragments were also less prevalent in Bap31 KO cells, although not as significant (Figure 7B, N1/CFTR, T2/CFTR, and N2/CFTR). Thus domain folding of TMD1 and TMD2 in the CFTR-R/F and CFTR-R347P mutants was less efficient in the Bap31 KO and Bap31-3A transfectants, while their NBDs were not so much affected (Figure 7B). In Bap31 knockout cells or cells transfected with Bap31-3A, the folding of CFTR-R/F TMD1 was reduced to 60% (Figure 7B, T1/CFTR), and the folding of TMD2 decreased nearly 50%, compared to Bap31 expressing cells (Figure 7B, T2/CFTR). NBD1 folding was still not restored in the Bap31 knockouts cells or cells with transfected with Bap31, or Bap31-3A (Figure 7B, N1/CFTR) and CFTR-R/F NBD2 folding was largely the same (Figure 7B, N2/CFTR). Domain folding of CFTR-R347P responded similarly as CFTR-R/F to Bap31-3A expression and Bap31 KO, with the exception of NBD1. The folding of CFTR-R347P TMD1 was reduced 30% and that of TMD2 decreased 50% after Bap31 KO and Bap31-3A transfection (Figure 7B, T1/CFTR and T2/CFTR). CFTR-R347P had a folded NBD1 and the folding levels of both its NBDs were not affected by Bap31-3A expression or Bap31 KO in either 0-h or 2-h chase (Figure 7B, N1/CFTR and N2/CFTR).

CFTR-R/F and CFTR-R347P mutants had low levels of domain assembly (Figure 6C). Their proteolytic fragments at 2-h chase mainly represented single domain folding during the post-translational period (Figure S1A). Impaired TMD folding of CFTR-R/F and CFTR-R347P in cells without Bap31 or with ectopically expressed Bap31-3A (Figure 7B) suggested that Bap31 charged residues were required for maintaining post-translational domain folding of CFTR TMDs. Compared to CFTR mutants, the absence of Bap31 charged residues did not exert significant effect on the TMDs of wild-type CFTR. This probably is because wild-type CFTR had intact domain assembly, where the TMDs supported and stabilized each other's folding. In this

case, the charged residues of Bap31 were not required. CFTR expressed in Bap31 KO cells had less proteolytic fragments derived from TMD1 at 2-h chase compared to cells expressing Bap31 or Bap31-3A (Figure 7B, T1/CFTR). This result suggested that Bap31 KO may decrease the interaction of TMD1 with other CFTR domains. Small decreases in proteolytic fragments of the other CFTR domain imply that domain assembly in the rest of the three domains could also be slightly impacted (Figure 7B, N1/CFTR, T2/CFTR, and N2/CFTR).

Bap31 KO impaired CFTR domain assembly and degradation

We showed in Figure 7B that charged residues in Bap31 TM stabilized the folding of the CFTR TMDs post-translationally, but had limited consequences for CFTR domain assembly. In the absence of Bap31 we only observed diminished post-translational folding of TMD1 (Figure 7B), and the Bap31-3A mutant did not affect the folding of any tested CFTR domain after a 2-h chase period (Figure 7B). Because TMD1 interfaces with NBD1, TMD2, and NBD2 during domain assembly and since these interactions are important for stabilizing the CFTR domain-domain interaction in general (Loo et al., 2008; Xiong et al., 1997), post-translational folding of TMD1 could therefore impact CFTR domain assembly. To analyze more precisely the role of Bap31 on CFTR domain assembly, we focused on the changes of domain-specific proteolytic fragments at different maturation states in cells without Bap31, and cells transfected with Bap31 or Bap31-3A. Cells were pulsed with ^{35}S-methionine and -cysteine and chased for different periods of time, treated with 25 µg/ml of Proteinase K, and proteolytic fragments were immunoprecipitated with domain-specific antibodies.

CFTR expression levels in Bap31 KO cells were higher than in the Bap31 or Bap31-3A transfectants (Figure 8A). CFTR levels gradually decreased during the chase in all of the three cell lines (Figure 8A). The disappearance of CFTR was slightly more pronounced in the cells that were transfected with Bap31 constructs, compared to Bap31 KO cells (Figure 8B), suggesting that post-translational CFTR degradation may be less in the absence of Bap31. As Bap31 has been reported to be part of the escort machinery for ER export of some of its clients, it may also function as a membrane protein adapter for CFTR to enter ER exit sites, where it could continue to act as quality control mediator and hand over CFTR to the ERAD pathway. Degradation rates of CFTR were the same in cells expressing Bap31-3A and Bap31 (Figure 8C), suggesting that charged residues in the TM segments of Bap31 were not involved in connecting CFTR to the degradation pathway. A previous study reported that an antibody against the Bap31 C-terminus blocked CFTR degradation, suggesting that Bap31 interacts with the Derlin-1-regulated ERAD through its C-terminus (Wang et al., 2008).

Bap31 KO affected not only CFTR degradation rate, but also its domain assembly. Through the pulse-chase approach, we ascertained that the CFTR population gradually traversed the maturation pathway from the high mannose ER form to the complex-glycosylated Golgi form (Figure 8A). Concomitant with this change, the population of domain-assembled CFTR also increased. As mentioned before, CFTR domains will interact with each other and assemble into a functional protein during post-translational domain assembly, and this event is represented by the group of TMD1, TMD2 and NBD2 domain proteolytic fragments; namely T1 late, T2c, and N2 (Figure S1b). After quantifying proteolytic fragments and normalizing to expression level (Figure 8D), we found that domain assembly of TMD1, NBD1 and TMD2 was 50-75% reduced at all chase times (Figure 8D). Although CFTR expression was almost doubled upon Bap31 KO compared to cells that express Bap31 constructs, domain assembly was not affected in the Bap31-rescued cells. In spite of the fact that NBD1 has no proteolytic fragments representing its domain assembly level after 2 hours of chase (Figure S1b, NBD1 panel), NBD1 folding was also 70% lower in the Bap31 KO cells compared to Bap31 and Bap31-3A transfectants (Figure 8D, N1/CFTR). The decrease in domain assembly in the absence of Bap31 was independent of the folding status of the individual domains, because co-translational domain folding, represented by proteolytic fragments at 0-h chase (Figure S1a, and Figure S1b), was invariant in the three cell lines (Figure 7B, 0-h chase). CFTR domain assembly rates in cells expressing Bap31 and Bap31-3A were similar (Figure 8D all domains), suggesting that charged TM residues in Bap31 are not involved in regulating CFTR domain assembly.

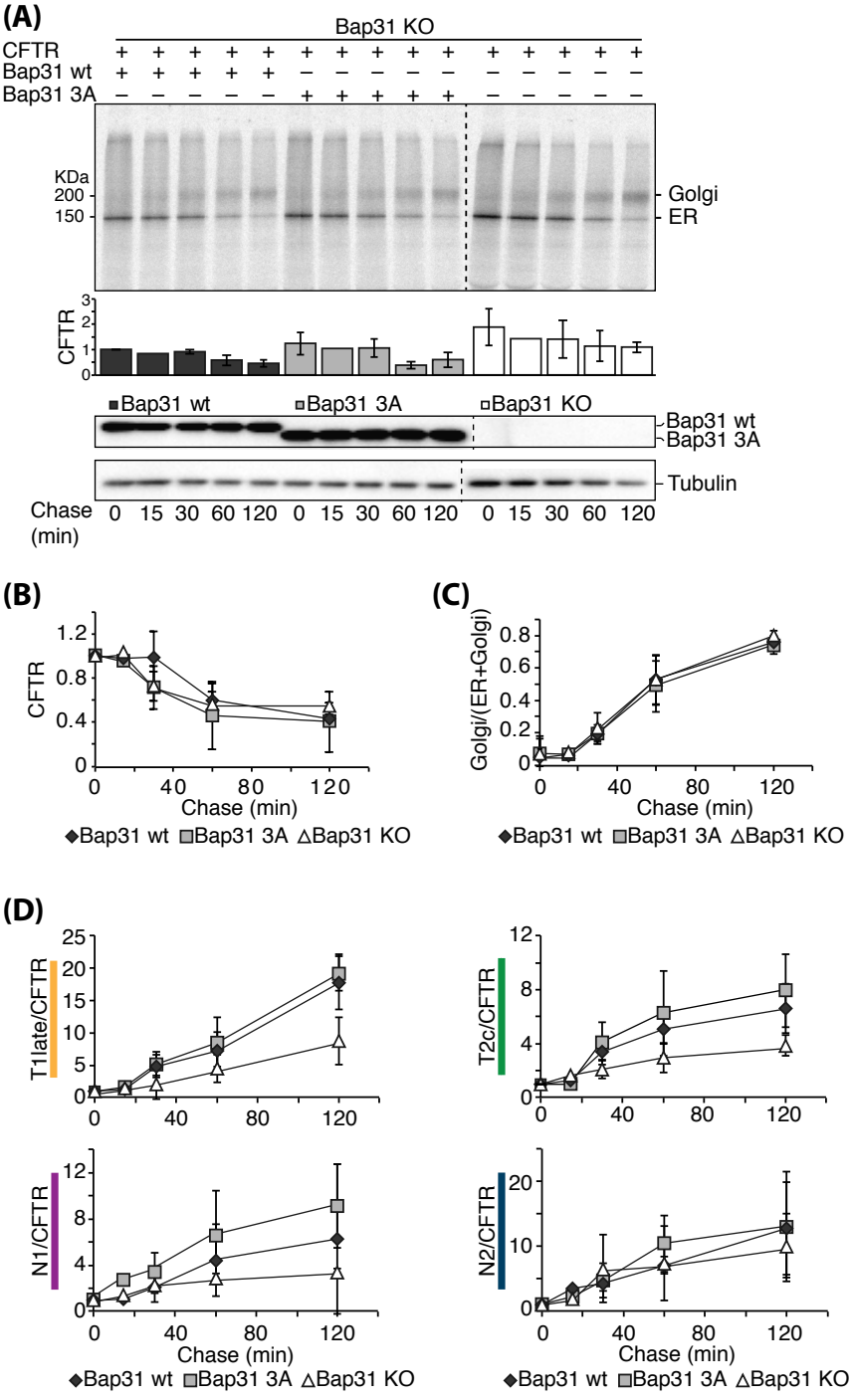

(A)
Bap31 KO
CFTR
Bap31 wt
Bap31 3A
KDa
200
150
Golgi
ER
CFTR
Bap31 wt
Bap31 3A
Bap31 KO
Bap31 wt
Bap31 3A
Tubulin
Chase (min)
0 15 30 60 120 0 15 30 60 120 0 15 30 60 120
(B)
CFTR
Chase (min)
Bap31 wt Bap31 3A Bap31 KO
(C)
Golgi/(ER+Golgi)
Chase (min)
Bap31 wt Bap31 3A Bap31 KO
(D)
T1late/CFTR
T2c/CFTR
N1/CFTR
N2/CFTR
Chase (min)
Bap31 wt Bap31 3A Bap31 KO

Figure 8: Bap31 KO impairs CFTR domain assembly and degradation.
(A) CFTR was co-transfected with or without Bap31 or Bap31-3A in Bap31 KO cells. Cells were labeled for 15 minutes, chased for 15, 30, 60, or 120 minutes, and lysed. CFTR was immunoprecipitated with MrPink and analyzed by 7.5% SDS-PAGE. The amount of CFTR was quantified and normalized to wild-type Bap31 control at 0-h chase. Bap31 and tubulin expression were checked on Western blot. (B) The amount of total CFTR at 0-h chase was quantitated and normalized to 0-h chase in each transfectant. (C) The amount of CFTR Golgi form of Bap31 cells and cells expressing Bap31 or Bap31-3A was quantitated and related to the total amount of CFTR and normalized to the 0-h chase values. (D) The cell lysates from (A) were treated with Proteinase K and proteolytic fragments were immunoprecipitated with domain-specific antibodies and analyzed by 12% SDS-PAGE. The domain fragments that represented CFTR domain assembly (Figure S1b), such as T1 late (T1d-T1f), T2c, and N2 were quantitated separately and related to full-length CFTR. These related values were normalized to 0-h chase sample of each Bap31 variant and plotted as domain assembly graph. (T1 late: TMD1, N1: NBD1, T2: TMD2, N2: NBD2) (n=3 for 0 and 2-h chase; n=1 for 15-, 30- and 60-min chase).

DISCUSSION

Bap31 was previously found to bind CFTR co-translationally at TMD1 and promote CFTR degradation through the Derlin-1 pathway. The connection between these two events, however, has not been elucidated. It is also unclear whether Bap31 has a chaperone function on the TMDs of CFTR. We showed here that Bap31 stabilized CFTR TMD folding post-translationally and promoted CFTR domain assembly as well as degradation. The charged residues in the Bap31 TMs were important for Bap31-assisted post-translational folding and degradation of two CFTR mutants but did not play a significant role in regulating wild-type CFTR domain assembly and degradation. The effect of the charges we tested by mutating all three charged TM residues, E15, R117, and R118, into alanines. We found residual binding of Bap31-3A to TMD1, suggesting that other parts of Bap31 contribute to the Bap31-CFTR interaction.

The charged residues of Bap31 are thought to engage the charged residues of TMD1 within the ER membrane, an interaction that is most likely driven by ionic forces within the lipid bilayer (Call et al., 2002; Johansson and Lindahl, 2009). This suggested that Bap31 could act as a chaperone for protecting the charged TM residues in the unassembled TMDs. The Bap31 chaperone effect was confirmed in Figure 7B, where the post-translational domain folding of the TMDs of both CFTR-R/F and CFTR-R347P decreased in the absence of Bap31 or in cells expressing Bap31-3A (Figure 7B, 2-h chase). CFTR-R/F and CFTR-R347P had compromised domain assembly, suggesting that the charged TM residues in their TMDs could not interact and stabilize each other post-translationally and therefore may require chaperone assistance. In the absence of this chaperone, the charged TM residues of CFTR-R/F and CFTR-R347P will disturb the stability of their TMDs and result in a decrease of folding as shown in Figure 7B. In the absence of Bap31 or in Bap31-3A transfected cells, co-translational folding of TMDs was not affected, although

both wild-type and mutant Bap31 lowered newly-synthesized CFTR levels (Figure 7B, 0-h chase). This is rather surprising, as the chaperone for unassembled TMDs will be required mostly during translation when domain assembly has not yet been established. The delayed Bap31 chaperone effect in full-length CFTR (but not the individual TMDs (Figure 4)) suggests that other chaperones may bind to CFTR prior to Bap31. Candidate chaperones for this are TRAP, TRAM, EMC (see Chapter 6), or the Sec62/63 complex, which interact with substrates with folding-challenging TMD sequences (Fons et al., 2003; Jung et al., 2014; Muller et al., 2010; Shurtleff et al., 2018; Sommer et al., 2013; Tamborero et al., 2011).

The charged TM residues of Bap31 were critical for post-translationally chaperoning the TMDs of CFTR mutants (Figure 7B, T1/CFTR and T2/CFTR at 2-h chase). Nevertheless, this effect was not seen in wild-type CFTR, probably because the charged TM residues of wild-type CFTR were stabilized by post-translational domain assembly, which was absent in CFTR mutants. Bap31 binding, independent of its charged TM residues, was more needed for establishing efficient domain assembly of wild-type CFTR. Domain assembly of CFTR increased by the expression of Bap31 with or without its charged TMDs (Figures 7B and 8D). Bap31 may assist CFTR domain assembly by enhancing the contacts between TMD1 and TMD2 and thereby may retain CFTR in the ER. Bap31 mostly binds to CFTR via the charged TM residues (Figure 5B), which are the sites where the two TMDs assemble (Pitonzo et al, 2009). A single molecule of Bap31 may not be large enough to bind to both TMDs and shield all charges in CFTR. As TMD1 alone already bound Bap31, we propose a stoichiometry of 1 molecule of Bap31 per TMD (Figure 9). CFTR molecules that fail to assemble will have single TMDs available for binding. Bap31 will bind to these TMDs and shuttle the protein that cannot assemble at all into the degradation pathway. Only CFTR molecules with their domains assembled properly can avoid this sorting and enter ER exit sites for transport along the secretory pathway. Eliminating Bap31 expression may thus decrease CFTR domain assembly as well as degradation, as shown in Figures 8B and 8D. In conclusion, Bap31 stabilizes the TMDs while CFTR has not yet achieves its domain assembly, as seen in CFTR mutants. The Bap31 binding also sorted the molecule into degradation pathway when the TMDs failed to assemble.

In this study, we illustrated the binding of Bap31 to CFTR and the resulting quality control. Our finding provides a starting point for investigating the intramembrane CFTR folding network and its related chaperone interactome. Based on our data, we propose a model for the role of Bap31 in CFTR folding: Bap31 binds to unassembled CFTR TMDs post-translationally (where this may start co-translationally) (Figures 9A and 9B). This binding most likely happens at TM6 in TMD1 and TM8 in TMD2, respectively, as these TMs contain charged residues that are responsible for TMD1-

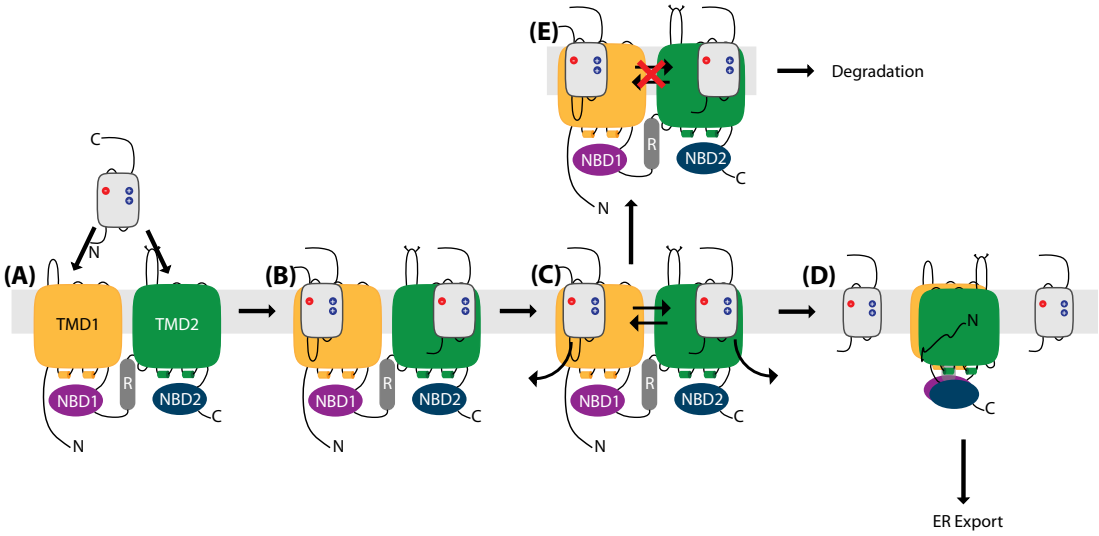


Figure 9: Model of Bap31 as quality control machinery for CFTR domain assembly.
(A) Bap31 binds to each CFTR TMD individually. (B) Bap31 remains bound when TMD1 and TMD2 do not interact with each other. (C) The binding of Bap31 to each TMD is substituted by the TMD1-TMD2 interaction during domain assembly. (D) CFTR released from Bap31 is then sorted into ER export pathway. (E) When CFTR domain assembly is blocked, the binding of Bap31 to TMDs is not replaced by the TMD1-TMD2 interaction. Prolonged Bap31 binding sorts CFTR in the ERAD pathway.

TMD2 assembly (Pitonzo et al., 2009). During CFTR domain assembly, the interaction between TMD1 and TMD2 will reduce their Bap31 binding (Figure 9C) and will eventually release Bap31 from CFTR (Figure 9D). CFTR then progresses through the secretory pathway to the plasma membrane. Once CFTR domain assembly has failed to occur, the binding between Bap31 and CFTR TMDs will sustain (Figure 9E). This prolonged binding can stabilize the TMDs post translationally, but will ultimately sort CFTR to ERAD via the Derlin-1 pathway.

MATERIALS AND METHODS

Plasmids, siRNA, and antibodies

CFTR plasmids in pBI-CMV2 were a generous gift from Prof. Phil Thomas (UT Southwestern Medical Center, Dallas TX, USA). The CFTR single-domain constructs were generated in pBS vectors (Kleizen et al., 2005) and subcloned to pcDNA3.1 using KpnI and XhoI restriction sites. The TMD1-Linker-TMD2 (TMDs-L) construct was generated by Gibson assembly and encoded aa 1-394 from CFTR, aa 626-

683 from P-gp, and aa 845-1202 from CFTR. The pCDNA3.1-TMD2-HA construct was kindly provided by Prof. Gergely Lukacs (McGill University, Montréal Québec, Canada). The PCR primers for Gibson assembly are described in supplementary materials. BAP31 cDNAs in pcDNA3 were provided by Prof. Ari Helenius (ETH Zurich Switzerland). siRNA targeting Bap31 were purchased from ThermoFisher Scientific. The rabbit antibody MrPink against NBD1 was characterized before (Hoelen et al., 2010). Rabbit antibodies TMD1C and TMD2C against TMD1 and TMD2 C-terminus (aa 364-381 and aa 1172-1186), respectively, and E1-22 against the fourth extracellular loop (aa 102-aa 117) of CFTR will be characterized elsewhere. A polyclonal rabbit antibody against HA-tag was generated using KLH-coupled HA peptide (YPYDVPDYAYPYDVPDYA). The mouse monoclonal antibody 596 against NBD2 (Cui et al., 2012) was kindly provided by Prof. John Riordan (UNC School of Medicine, USA). The rat monoclonal antibody against Bap31 was from Thermo Fisher Scientific and mouse monoclonal antibody against alpha tubulin was from Synaptic Systems (Göttingen).

Cell culture, transfection and generation of a Bap31-knockout

HEK 293T cells were seeded onto polylysine-coated 6 cm dishes and maintained in DMEM supplemented with 10% FBS, and 2 mM GlutaMAX) at 37°C with 5% CO_2. After reaching 70% confluency, cells were transfected using linear 40 kDa polymer polyethylenimine as described (van Willigen et al., 2019). After 4 hours, the transfection mix was replaced with culture medium and cells were grown for 16-20 hours prior to experiments. Bap31 KO HEK 293T cells were created using the CRISPR-cas9 system as described (Ran et al., 2013b). CRISPR-cas9 plasmids RP448 with target gDNA sequence (Clone 1: 5' – gAACAAAGACCTCCGCATAG – 3' or Clone 2: 5' – GCCACCTTCCTCTATGCGG – 3') inserted in the BsmBI site were generated as described (Cong et al., 2013; Ran et al., 2013a; Ran et al., 2013b). The CRISPR-cas9 plasmid was transfected in HEK 293T cells. After 24 hours, transfected cells were selected by the addition of 5 µg/ml puromycin (Thermo Fisher Scientific) for 48 hours. Next, the cells were recovered for 2 days and clones were selected by limited dilution. Clones then were analyzed by Western blot to confirm the knockout. For genomic analysis, genomic DNA was isolated from target cell lines (~1×10^6 cells) using the TRIzol reagents from ThermoFisher Scientific. PCR reactions were carried out with 50 ng genomic DNA using Q5® High-Fidelity 2x Master Mix (New England Biolab) and primers 5'-GCACTGCTCTTCCCGAAGAACGCCTTTCAG -3' (F) and 5'-ACATAGATCTTCCTGCCTCTCGGGGGCATT-3' (R). PCR products were sequenced and sequence data were analyzed with TIDE (https://tide.deskgen.com/) (Brinkman et al., 2014) for categorizing Bap31 alleles from Bap31 KO cells.

RNA extraction and RT-PCR

To detect XBP1 splicing, mRNA was extracted from target cell lines (~1×10^6

cells) using the TRIzol reagents from ThermoFisher Scientific. cDNA from XBP1 mRNA was synthesized using the first strand cDNA synthesis kit (ThermoFisher Scientific) and amplified by PCR. Human XBP1 primer sequences were as follows: 5'- GAAGAGAACCAAAAACTTTTGC -3' and 5'-GGATATCAGACTCTGAATCTG - 3'. PCR products were analyzed on a 3.5% agarose gel.

Radioactive pulse and chase

HEK239T cells were used 24 hours post-transfection in a pulse-chase assay as described previously (Braakman et al., 1991; McCaul et al., 2019; van Willigen et al., 2019). In brief, cells were labeled for 15 minutes with 132 μCi/6 cm dish of EasyTag Express ^{35}S Protein Labeling Mix (Perkin Elmer). Radiolabeling was stopped by adding excess, unlabeled, 5 mM methionine and 5 mM cysteine. At indicated chase times, cells were washed twice with ice-cold HBSS (Life Technologies) and lysed in ice-cold lysis buffer (20 mM MES, 100 mM NaCl, 30 mM Tris-Cl pH 7.4, and 1% Triton X-100) without protease inhibitors. The cell nuclei were pelleted by 16,000 x g centrifugation for 10 minutes at 4°C, and the supernatant was subjected to limited proteolysis or immunoprecipitation.

Limited proteolysis

Limited proteolysis was performed as described (Hoelen et al., 2010; Kleizen et al., 2005; van Willigen et al., 2019). Cell lysates were treated with 25 μg/ml Proteinase K (Sigma-Aldrich) for 15 minutes on ice. Proteolysis was stopped by adding 2 mM PMSF and 20 μg/ml chymostatin, leupeptin, antipain and pepstatin (final concentrations, all from Sigma-Aldrich) to the lysate. Protein aggregates were pelleted by 16,000 x g centrifugation for 5 minutes at 4°C, and the supernatant was used for immunoprecipitation.

Immunoprecipitation

The antibodies against TMD1, NBD1, TMD2, or NBD2 were pre-incubated with protein-A Sepharose beads (GE Healthcare) for 15 minutes at 4 °C before adding protease-treated or non-treated samples. Lysates were subsequently incubated with beads for 16 hours (MrPink) or 3 hours (TMD1C, TMD2C, 596) at 4°C. Beads were washed twice with indicated wash buffers for 10 minutes at room temperature with either 10 mM Tris-HCl pH 8.6, 300 mM NaCl, 0.1% SDS, 0.05% Triton X-100 (for MrPink); 10 mM Tris-Cl pH 8.6, 300 mM NaCl, 0.05% SDS, 0.05% Triton X-100 (for TMD1C); 20 mM MES, 100 mM NaCl, 30 mM Tris-HCl pH 7.4 and 0.5% Triton X-100 (for 596); or 50 mM Tris-HCL, pH 8.0, 150 mM NaCl, 1 mM EDTA (for TMD2C). Beads were resuspended in 10 mM Tris-HCl pH 6.8 containing 1 mM EDTA, and the proteins were eluted by adding sample buffer (200 mM Tris-Cl pH 6.8, 3% SDS, 10% glycerol, 1 mM EDTA, 0.004% bromophenol blue, and 25 mM DTT, all final concentration) and heating for 5 min at 55°C.

SDS-PAGE and autoradiography
Samples were analyzed by 7.5% and 12% SDS-PAGE, and the gels were dried and exposed to super-resolution phosphor screens (Fuji Film). Signals from screens were visualized with a Typhoon FLA-7000 scanner (GE Healthcare Life Science), and quantified with ImageQuantTL software (GE Healthcare Life Science).

Western blotting
Proteins were transferred onto PVDF membrane (Immobilon-FL, Sigma-Aldrich) at 70V for 90 minutes. The membrane was blocked with LiCor Block Buffer (Odyssey® Blocking Buffer, LI-COR Bioscience) for 1 hour, and were incubated with primary antibodies against CFTR R-domain (570, mouse, 1:3,000), tubulin (mouse, 1:5,000), or Bap31 (rat 1:3,000) in PBS (137 mM NaCl, 2.7 mM KCl, 8 mM Na_2HPO_4, and 2 mM KH_2PO_4, pH 7.4) containing 0.1% Tween 20 (PBST) and 2.5% BSA for 1 hour at room temperature. The membrane was rinsed three times with PBST, followed by incubation with Alexa 680 secondary antibody (1:10,000) for another 30 minutes at room temperature. The membrane was subsequently rinsed twice with PBST, once with PBS, and signals were visualized with the Odyssey® Imaging System (LI-COR Bioscience).

ACKNOWLEDGMENTS

We thank Prof. John Riordan, University of North Carolina Chapel Hill, NC USA, and the Cystic Fibrosis Foundation for kindly providing 596 antibody, Prof. Ari Helenius and Dr. Roger Geiger, ETH Zürich Switzerland, for wild-type Bap31 and Bap31-3A constructs, and Prof. Gergely Lukacs, McGill University, Montréal Québec, Canada, for the pCDNA3.1-TMD2-3HA construct. We thank Dr. Joseline Houwman for reading and commenting on this manuscript, and all members of the Braakman-Van der Sluijs lab for fruitful discussions. This project was funded by CFF (BRAAKM14XX0), the Netherlands Organization for Health Research and Development (ZonMw TOP grant 40-00812-98-14103), and the Netherlands Cystic Fibrosis Foundation (HIT-CF grant).

REFERENCES

Abe, F., Van Prooyen, N., Ladasky, J.J., and Edidin, M. (2009). Interaction of Bap31 and MHC class I molecules and their traffic out of the endoplasmic reticulum. J Immunol *182*, 4776-4783.

Adachi, T., Schamel, W.W., Kim, K.M., Watanabe, T., Becker, B., Nielsen, P.J., and Reth, M. (1996). The specificity of association of the IgD molecule with the accessory proteins BAP31/BAP29 lies in the IgD transmembrane sequence. EMBO J *15*, 1534-1541.

Annaert, W.G., Becker, B., Kistner, U., Reth, M., and Jahn, R. (1997). Export of cellubrevin from the endoplasmic reticulum is controlled by BAP31. J Cell Biol *139*, 1397-1410.

Bartee, E., Eyster, C.A., Viswanathan, K., Mansouri, M., Donaldson, J.G., and Fruh, K. (2010). Membrane-associated RING-CH proteins associate with Bap31 and target CD81 and CD44 to lysosomes. PLoS One *5*, e15132.

Braakman, I., Hoover-Litty, H., Wagner, K.R., and Helenius, A. (1991). Folding of influenza hemagglutinin in the endoplasmic reticulum. J Cell Biol *114*, 401-411.

Breckenridge, D.G., Stojanovic, M., Marcellus, R.C., and Shore, G.C. (2003). Caspase cleavage product of BAP31 induces mitochondrial fission through endoplasmic reticulum calcium signals, enhancing cytochrome c release to the cytosol. J Cell Biol *160*, 1115-1127.

Brinkman, E.K., Chen, T., Amendola, M., and van Steensel, B. (2014). Easy quantitative assessment of genome editing by sequence trace decomposition. Nucleic Acids Res *42*, e168.

Call, M.E., Pyrdol, J., Wiedmann, M., and Wucherpfennig, K.W. (2002). The organizing principle in the formation of the T cell receptor-CD3 complex. Cell *111*, 967-979.

Carveth, K., Buck, T., Anthony, V., and Skach, W.R. (2002). Cooperativity and flexibility of cystic fibrosis transmembrane conductance regulator transmembrane segments participate in membrane localization of a charged residue. J Biol Chem *277*, 39507-39514.

Cheng, S.H., Rich, D.P., Marshall, J., Gregory, R.J., Welsh, M.J., and Smith, A.E. (1991). Phosphorylation of the R domain by cAMP-dependent protein kinase regulates the CFTR chloride channel. Cell *66*, 1027-1036.

Cheung, J.C., and Deber, C.M. (2008). Misfolding of the cystic fibrosis transmembrane conductance regulator and disease. Biochemistry *47*, 1465-1473.

Cohen, T.S., and Prince, A. (2012). Cystic fibrosis: a mucosal immunodeficiency syndrome. Nat Med *18*, 509-519.

Cong, L., Ran, F.A., Cox, D., Lin, S., Barretto, R., Habib, N., Hsu, P.D., Wu, X., Jiang, W., Marraffini, L.A.*, et al.* (2013). Multiplex genome engineering using CRISPR/Cas systems. Science *339*, 819-823.

Cotten, J.F., and Welsh, M.J. (1999). Cystic fibrosis-associated mutations at arginine 347 alter the pore architecture of CFTR. Evidence for disruption of a salt bridge. J Biol Chem *274*, 5429-5435.

Cui, G., Song, B., Turki, H.W., and McCarty, N.A. (2012). Differential contribution of TM6 and TM12 to the pore of CFTR identified by three sulfonylurea-based blockers. Pflugers Arch *463*, 405-418.

Du, K., Sharma, M., and Lukacs, G.L. (2005). The DeltaF508 cystic fibrosis mutation impairs domain-domain interactions and arrests post-translational folding of CFTR. Nat Struct Mol Biol *12*, 17-25.

El Hiani, Y., Negoda, A., and Linsdell, P. (2016). Cytoplasmic pathway followed by chloride ions to enter the CFTR channel pore. Cell Mol Life Sci *73*, 1917-1925.

Fons, R.D., Bogert, B.A., and Hegde, R.S. (2003). Substrate-specific function of the translocon-associated protein complex during translocation across the ER membrane. J Cell Biol *160*, 529-539.

Friedlander, R., Jarosch, E., Urban, J., Volkwein, C., and Sommer, T. (2000). A regulatory link between ER-associated protein degradation and the unfolded-protein response. Nat Cell Biol *2*, 379-384.

Geiger, R., Andritschke, D., Friebe, S., Herzog, F., Luisoni, S., Heger, T., and Helenius, A. (2011). BAP31 and BiP are essential for dislocation of SV40 from the endoplasmic reticulum to the cytosol. Nat Cell Biol *13*, 1305-1314.

Gunderson, K.L., and Kopito, R.R. (1995). Conformational states of CFTR associated with channel gating: the role ATP binding and hydrolysis. Cell *82*, 231-239.

Hoelen, H., Kleizen, B., Schmidt, A., Richardson, J., Charitou, P., Thomas, P.J., and Braakman, I. (2010). The primary folding defect and rescue of DeltaF508 CFTR emerge during translation of the mutant domain. PLoS One *5*, e15458.

Johansson, A.C., and Lindahl, E. (2009). Protein contents in biological membranes can explain abnormal solvation of charged and polar residues. Proc Natl Acad Sci U S A *106*, 15684-15689.

Jung, S.J., Kim, J.E., Reithinger, J.H., and Kim, H. (2014). The Sec62-Sec63 translocon facilitates translocation of the C-terminus of membrane proteins. J Cell Sci *127*, 4270-4278.

Kim, W.T., Choi, H.S., Hwang, H.J., Jung, H.S., and Ryu, C.J. (2015). Epitope mapping of antibodies suggests the novel membrane topology of B-cell receptor associated protein 31 on the cell surface of embryonic stem cells: The novel membrane topology of BAP31. PLoS One *10*, e0130670.

Kleizen, B., van Vlijmen, T., de Jonge, H.R., and Braakman, I. (2005). Folding of CFTR is predominantly cotranslational. Mol Cell *20*, 277-287.

Ladasky, J.J., Boyle, S., Seth, M., Li, H., Pentcheva, T., Abe, F., Steinberg, S.J., and Edidin, M. (2006). Bap31 enhances the endoplasmic reticulum export and quality control of human class I MHC molecules. J Immunol *177*, 6172-6181.

Lambert, G., Becker, B., Schreiber, R., Boucherot, A., Reth, M., and Kunzelmann, K. (2001). Control of cystic fibrosis transmembrane conductance regulator expression by BAP31. J Biol Chem *276*, 20340-20345.

Li, M.S., Cowley, E.A., El Hiani, Y., and Linsdell, P. (2018). Functional organization of cytoplasmic portals controlling access to the cystic fibrosis transmembrane conductance regulator (CFTR) chloride channel pore. J Biol Chem *293*, 5649-5658.

Liu, F., Zhang, Z., Csanady, L., Gadsby, D.C., and Chen, J. (2017). Molecular structure of the human CFTR ion channel. Cell *169*, 85-95 e88.

Loo, T.W., Bartlett, M.C., and Clarke, D.M. (2008). Processing mutations disrupt interactions between the nucleotide binding and transmembrane domains of P-glycoprotein and the cystic fibrosis transmembrane conductance regulator (CFTR). J Biol Chem *283*, 28190-28197.

Louie, R.J., Guo, J., Rodgers, J.W., White, R., Shah, N., Pagant, S., Kim, P., Livstone, M., Dolinski, K., McKinney, B.A.*, et al.* (2012). A yeast phenomic model for the gene interaction network modulating CFTR-DeltaF508 protein biogenesis. Genome Med *4*, 103.

McCaul, N., Yeoh, H.Y., van Zadelhoff, G., Lodder, N., Kleizen, B., and Braakman, I. (2019). Analysis of protein folding, transport, and degradation in living cells by radioactive pulse chase. J Vis Exp.

Mendoza, J.L., Schmidt, A., Li, Q., Nuvaga, E., Barrett, T., Bridges, R.J., Feranchak, A.P., Brautigam, C.A., and Thomas, P.J. (2012). Requirements for efficient correction of DeltaF508 CFTR revealed by analyses of evolved sequences. Cell *148*, 164-174.

Muller, L., de Escauriaza, M.D., Lajoie, P., Theis, M., Jung, M., Muller, A., Burgard, C., Greiner, M., Snapp, E.L., Dudek, J.*, et al.* (2010). Evolutionary gain of function for the ER membrane protein Sec62 from yeast to humans. Mol Biol Cell *21*, 691-703.

Paquet, M.E., Cohen-Doyle, M., Shore, G.C., and Williams, D.B. (2004). Bap29/31 influences the intracellular traffic of MHC class I molecules. J Immunol *172*, 7548-7555.

Pitonzo, D., Yang, Z., Matsumura, Y., Johnson, A.E., and Skach, W.R. (2009). Sequence-specific retention and regulated integration of a nascent membrane protein by the endoplasmic reticulum Sec61 translocon. Mol Biol Cell *20*, 685-698.

Ran, F.A., Hsu, P.D., Lin, C.Y., Gootenberg, J.S., Konermann, S., Trevino, A.E., Scott, D.A., Inoue, A., Matoba, S., Zhang, Y*., et al.* (2013a). Double nicking by RNA-guided CRISPR Cas9 for enhanced genome editing specificity. Cell *154*, 1380-1389.

Ran, F.A., Hsu, P.D., Wright, J., Agarwala, V., Scott, D.A., and Zhang, F. (2013b). Genome engineering using the CRISPR-Cas9 system. Nat Protoc *8*, 2281-2308.

Ratjen, F., and Grasemann, H. (2012). New therapies in cystic fibrosis. Curr Pharm Des *18*, 614-627.

Riordan, J.R. (2008). CFTR function and prospects for therapy. Annu Rev Biochem *77*, 701-726.

Riordan, J.R., Rommens, J.M., Kerem, B., Alon, N., Rozmahel, R., Grzelczak, Z., Zielenski, J., Lok, S., Plavsic, N., Chou, J.L*., et al.* (1989). Identification of the cystic fibrosis gene: cloning and characterization of complementary DNA. Science *245*, 1066-1073.

Schamel, W.W., Kuppig, S., Becker, B., Gimborn, K., Hauri, H.P., and Reth, M. (2003). A high-molecular-weight complex of membrane proteins BAP29/BAP31 is involved in the retention of membrane-bound IgD in the endoplasmic reticulum. Proc Natl Acad Sci U S A *100*, 9861-9866.

Shurtleff, M.J., Itzhak, D.N., Hussmann, J.A., Schirle Oakdale, N.T., Costa, E.A., Jonikas, M., Weibezahn, J., Popova, K.D., Jan, C.H., Sinitcyn, P*., et al.* (2018). The ER membrane protein complex interacts cotranslationally to enable biogenesis of multipass membrane proteins. Elife *7*.

Skach, W.R. (2009). Cellular mechanisms of membrane protein folding. Nat Struct Mol Biol *16*, 606-612.

Sommer, N., Junne, T., Kalies, K.U., Spiess, M., and Hartmann, E. (2013). TRAP assists membrane protein topogenesis at the mammalian ER membrane. Biochim Biophys Acta *1833*, 3104-3111.

Sun, F., Zhang, R., Gong, X., Geng, X., Drain, P.F., and Frizzell, R.A. (2006). Derlin-1 promotes the efficient degradation of the cystic fibrosis transmembrane conductance regulator (CFTR) and CFTR folding mutants. J Biol Chem *281*, 36856-36863.

Tamborero, S., Vilar, M., Martinez-Gil, L., Johnson, A.E., and Mingarro, I. (2011). Membrane insertion and topology of the translocating chain-associating membrane protein (TRAM). J Mol Biol *406*, 571-582.

van Willigen, M., Vonk, A.M., Yeoh, H.Y., Kruisselbrink, E., Kleizen, B., van der Ent, C.K., Egmond, M.R., de Jonge, H.R., Braakman, I., Beekman, J.M*., et al.* (2019). Folding-function relationship of the most common cystic fibrosis-causing CFTR conductance mutants. Life Sci Alliance *2*.

Wang, B., Heath-Engel, H., Zhang, D., Nguyen, N., Thomas, D.Y., Hanrahan, J.W., and Shore, G.C. (2008). BAP31 interacts with Sec61 translocons and promotes retrotranslocation of CFTRDeltaF508 via the derlin-1 complex. Cell *133*, 1080-1092.

Xiong, X., Bragin, A., Widdicombe, J.H., Cohn, J., and Skach, W.R. (1997). Structural cues involved in endoplasmic reticulum degradation of G85E and G91R mutant cystic fibrosis transmembrane conductance regulator. J Clin Invest *100*, 1079-1088.

Zen, K., Utech, M., Liu, Y., Soto, I., Nusrat, A., and Parkos, C.A. (2004). Association of BAP31 with CD11b/CD18. Potential role in intracellular trafficking of CD11b/CD18 in neutrophils. J Biol Chem *279*, 44924-44930.

Zhang, Z., Liu, F., and Chen, J. (2017). Conformational Changes of CFTR upon Phosphorylation and ATP Binding. Cell *170*, 483-491 e488.

SUPPLEMENTARY MATERIAL

Table 1: Primers for TMD1-Linker-TMD2 construct

pBI-CMV2 + CFTR	F: AGAATTCACACGTGAAGAAAGATTGACGGCCGCATCGATAAG R: CCTGCTGTCTGCATTGTGACCATCACTACTTCTGTAGTCGTTAAGTT
CFTR + Pg-P	F: CGACTACAGAAGTAGTGATGGTCACAATGCAGACAGCAGG R: AGGTATGTGTTCCATGTAGTAAGCTTTCTGTCTTGGGCTT
Pg-P + CFTR + pBI-CMV2	F: GCTTATCGATGCGGCCGTCAATCTTTCTTCACGTGTGAATTCT R: AAGCCCAAGACAGAAAGCTTACTACATGGAACACATACCTT

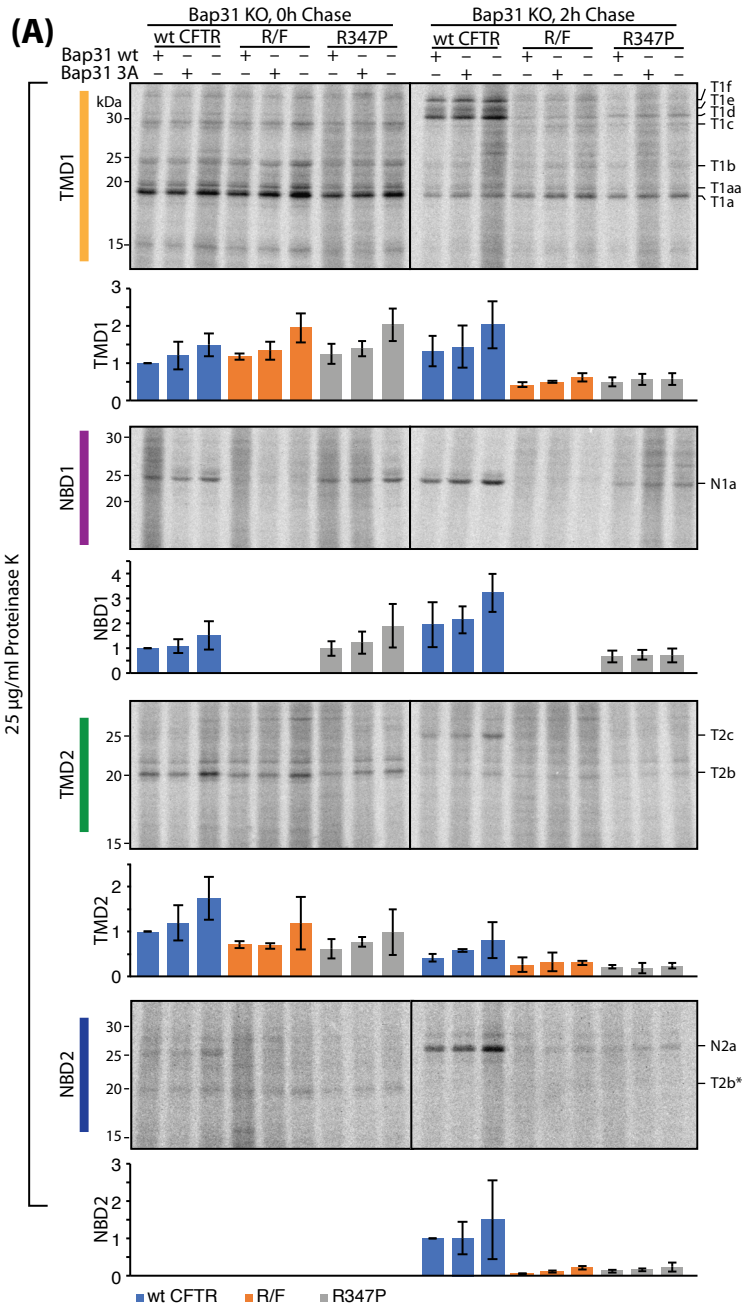
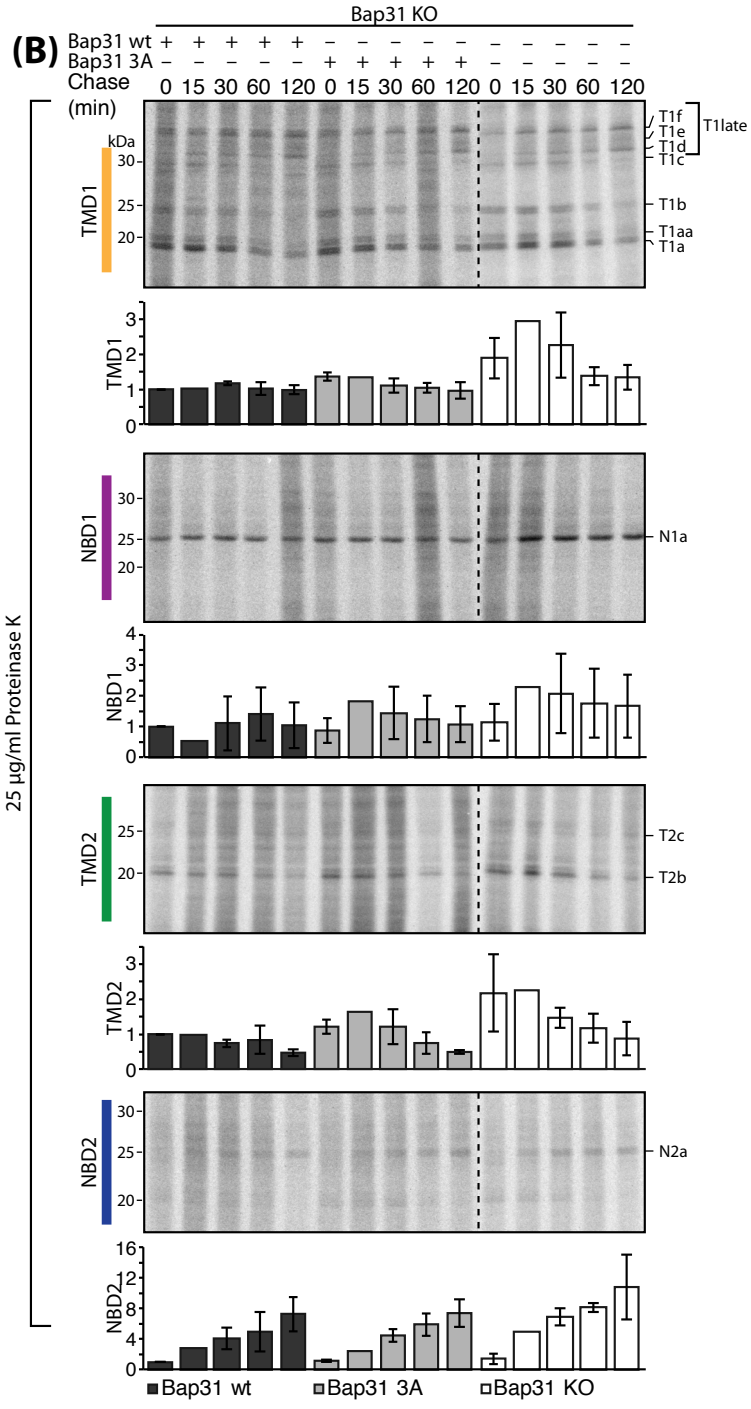


Figure S1: CFTR domain folding and assembly under Bap31 KO and Bap31-3A expression. (A) CFTR, CFTR-R/F, and CFTR-R347P were expressed in Bap31 KO cells with or without cotransfected Bap31 or Bap31-3A. Cells were radiolabeled with ^{35}S for 15 minutes, chased for 2 h, and lysed. Cell lysates were treated with Proteinase K and proteolytic fragments were immunoprecipitated with domain-specific antibodies and analyzed by 12% SDS-PAGE. The domain fragments of TMD1 (T1a-T1f), NBD1 (N1a), TMD2 (T2b-T2c) and NBD2 (N2a) were quantitated separately and normalized to wild-type CFTR at 0-h chase (n=3). (B) CFTR was expressed in Bap31 KO cells with or without co-transfected Bap31 or Bap31-3A. Cells were radiolabeled with ^{35}S for 15 minutes, chased for different periods of time, and lysed. The cell lysates were treated with Proteinase K and the proteolytic fragments were immunoprecipitated by domain-specific antibodies and analyzed by 12% SDS-PAGE. The fragments that represent CFTR domain assembly, T1late (T1d-T1f), T2c, and N2a, were quantitated separately and normalized to the wild-type Bap31 sample at 0-h chase (n=3).


(B)
Bap31 KO
Bap31 wt + + + + + – – – – – – – – – –
Bap31 3A – – – – – + + + + + – – – – –
Chase (min) 0 15 30 60 120 0 15 30 60 120 0 15 30 60 120
kDa
TMD1
30
25
20
T1f
T1e
T1d
T1c
T1late
T1b
T1aa
T1a
TMD1
3
2
1
0
NBD1
30
25
20
N1a
NBD1
4
3
2
1
0
25 µg/ml Proteinase K
TMD2
25
20
T2c
T2b
TMD2
3
2
1
0
NBD2
30
25
20
N2a
NBD2
16
12
8
4
0
Bap31 wt
Bap31 3A
Bap31 KO

Chapter 8

General Discussion

AUTHORS:
Hui Ying Yeoh, Peter van der Sluijs, Ineke Braakman

GENERAL DISCUSSION

Stabilization of TMDs during membrane protein folding in the endoplasmic reticulum (ER)

There are three principal challenges in membrane protein folding: firstly, transmembrane (TM) helixes initially can be translocated or inserted into a wrong position and need to be re-located back to their native orientation during the subsequent folding process (Feige and Hendershot, 2013; Lu et al., 2000). Secondly, the hydrophobic stretches of TMDs in proteins that are destined for the Golgi complex and plasma membrane are longer than the thickness of the ER membrane. As a consequence, the ER membrane cannot fully cover the hydrophobic stretches at the N- and C-terminal end of the helixes. This situation is called 'hydrophobic mismatch' which can cause protein aggregation at the border of the membrane (Basu et al., 2014; Killian and Nyholm, 2006). Finally, membrane proteins such as ion channels contain charged residues in their TM areas for functional and structural purposes (El Hiani et al., 2016). During folding, these residues are usually coupled with their interaction partners, which are other charged residues in either the same or different TMDs (Cui et al., 2013; Rahman et al., 2013; Sheppard et al., 1993). Uncoupled charged residues can generate free charges and can lead to random interactions within the ER membrane and cause protein aggregation (Kida et al., 2016; Onishi et al., 2013). The abovementioned challenges can be overcome by deployment of chaperones binding onto destabilizing sequences and preventing them from exposure to their surrounding environment.

Unfortunately the requisite chaperones have not yet been identified. In this thesis, we used the Cystic Fibrosis Transmembrane Conductance Regulator (CFTR) as a model protein to study how TMDs acquire and maintain their stability with the assistance of membrane-bound chaperones. The choice for CFTR as model protein was largely based on the fact that it has a domain architecture typical for type-I ABC-transporters and faces all three challenges for proper folding (Lee et al., 2016; Liu et al., 2017; Vasiliou et al., 2009). To study the folding of the CFTR transmembrane domains (TMDs), we first raised antibodies against the TMDs and characterized them in **Chapter 3**. The antibodies were then used to analyze the folding of two CFTR patient mutants, R347P and R751L, which revealed a connection between folding and function of CFTR (**Chapter 4 and Chapter 5**). Next, we employed the antibodies to investigate the role of candidate membrane-bound chaperones Bap31 (**Chapter 7**) and the ER membrane complex (EMC) (**Chapter 6**) in CFTR folding. These studies were carried out using a radioactive pulse and chase (**Chapter 2**) coupled to limited proteolysis assay (Hoelen et al., 2010; Kleizen et al., 2005). We discovered that the TMDs fold during translation and post-translationally assemble with other CFTR domains into a functional molecule where structure

is clearly intertwined with function. For instance R751P, a mutant that folds like wild-type CFTR responds to corrector VX-809 and potentiator VX-770 like the wild-type protein while R347L, with a defect in domain assembly responds to the drugs differently. We also demonstrated that the EMC is involved in proper folding and possibly insertion of TMD2. On the other hand we uncovered a role for BAP31 in chaperoning charged residues in the CFTR TM area for the interaction of the N-terminal and C-terminal halves of CFTR.

Detecting TMD-folding and assembly in an ABC transporter

The information regarding the structure of TMDs of CFTR mainly comes from cryo-EM images (Liu et al., 2017; Zhang et al., 2017b). The folding pathway of CFTR to its native form *in vivo* however has not been elucidated, mainly because the requisite reagents and assays were not available. With the new TMD antibodies, we found that the TMDs already folded co-translationally because they were relatively resistant to protease digestion, producing the proteolytic fragments T1a, T1b, T1c, and T2b, originating from TMD1 and TMD2, respectively **(Chapter 3 Figure 3 and 4)**. Protease susceptibility of the TMDs continued to increase post-translationally, resulting in the appearance of four other fragments, namely T1d, T1e, T1f, and T2c **(Chapter 3, Figure 3 and 4)**. This observation suggested that the TMDs underwent conformational changes post-translationally, likely resulting from domain assembly, as CFTR mutations that disrupt domain assembly, such as F508del and R1070W, impair the generation of TMDs post-translational proteolytic fragments, but not of the co-translational fragments (data not shown).

We also identified the proteolytic fragments derived from the TMDs, which showed that the post-translational fragments T1d, T1e, T1f, and T2c, not only contained sequences that overlapped with their co-translational fragments T1a, T1b, T1c, and T2b, but also included some other sequences. For instance, the post-translational fragments of TMD1 include the N-terminus and the second intracellular loop (ICL2), while those of TMD2 contains ICL3. These regions actually represent the coupling sites between the TMDs and the nucleotide binding domains (NBDs) during post-translational domain assembly (Zhang et al., 2017b), in which the N-terminus attaches to the adjacent TMDs, ICL2 couples with NBD2, while ICL4 assembles with NBD1. The attachment of the N-terminus to the TMDs strengthens the coupling between CFTR domains at the N-terminal side of the protein and likely also prevents encounters with the protease and thus protects it against proteolytic cleavage. Compared to the CFTR N-terminus, ICL2 in TMD2, will most likely be coupled and protected by NBD2, as mutating the residues in ICL2 disrupt the folding of NBD2. The assembly between ICL4 and NBD1 is in accord with predictions from the cryoEM structure and awaits to be confirmed by independent methods (Zhang et al., 2017b). As CFTR structurally resembles type-I ABC transporters, these may also

fold via the same hierarchical pathway.

In contrast, type-II ABC transporters may establish their folding differently. The ICLs from one TMD only bind to one NBD instead of via a cross-interaction with the other NBD from the opposite side of the molecule (Lee et al., 2016). For instance, in the absence of cross-interaction, all of the TMD-NBD coupling in a type-II ABC transporter may be completed co-translationally and before the TMDs assemble with each other post-translationally.

The new TMD antibodies also revealed that the TMDs in CFTR may stabilize each other. The chaperone effect of one TMD to another is usually hard to detect. Firstly, because mutations such as G85E and R347P in TMDs will usually disrupt all CFTR domain-domain interactions and impact the folding of all domains. Secondly, uncoupled TMDs will probably remain bound and stabilized by chaperones leaving no folding defect to be detected. With the new TMD antibodies (**Chapter 6)** we demonstrated that under certain circumstances, the chaperoning effect of one TMD to another could be documented. Both a hydrophobic to charged mutation in G85E and the reverse scenario in R347P (both in TMD1) decreased TMD2 folding co-translationally during deletion of the EMC chaperone, suggesting that TMD2 may already be stabilized by TMD1 during translation. These findings demonstrate that the novel TMDs antibodies are very useful for analysis of inter-domain interactions of the CFTR folding pathway.

The epitopes of the TMD antibodies are mostly localized in the C-termini of TMD1 and TMD2, indicating that the proteolytic fragments derived from the N-termini of these domains may not be detected after limited proteolysis. In **Chapter 3**, we discovered that TMD1 has a more compacted structure and therefore its N-terminus likely was protected during protease digestion and remained in the proteolytic fragments (T1c, T1d, T1e, T1f), while the N-the terminus of TMD2 had been cleaved off. This finding suggested that an antibody targeting the N-terminus of TMD2 may be required in the future for more precise mapping of the folding of this domain.

Application of novel TMD antibodies for analysis of CFTR mutant folding
After the characterization of the TMD antibodies, we used TMD1C and TMD2C, to investigate the folding dynamics of CFTR patient mutants R347P and R751L in **Chapter 4** and **Chapter 5**. Both antibodies detected the co- and post-translational folding of TMDs in the mutants successfully. The TMDs and NBDs of R347P acquired their folding co-translationally but failed to achieve post-translational domain assembly, while the TMDs and NBDs of R751L folded like wild-type CFTR. The latter folding phenotype is probably due to the location of R751 in the unstructured R-domain, which controls opening and closing of the channel during ATP binding

and phosphorylation (Zhang et al., 2017b). To remain its flexibility for shifting back and forward, the R-domain will probably establish minimal interactions with other CFTR domains during domain assembly and likely therefore will not affect the folding of other domains. Consequentially, we predict that the R751L mutation will only affect the function of the R-domain which leads to CF, but not the folding of CFTR.

In contrast to R751L, R347 locates in TM6, the last TM helix of TMD1, which is also the contact site of TMD1 and TMD2 for domain assembly. R347 is reported to form a salt bridge with D924, which is located in the second helix of TMD2, and tether the two TMDs during domain assembly (Du et al., 2005; Liu et al., 2017; Pitonzo et al., 2009; Zhang et al., 2017b). A proline mutation at this position may prevent the interaction of these two residues and inhibit TMD1-TMD2 coupling. R347P may also alter the structure of TM6 and disrupt its assembly with the N-terminus, causing a conformational defect in the N-terminal half of the channel (Cotten and Welsh, 1999; Van Goor et al., 2014; van Willigen et al., 2019).

The formation of salt bridge between R347 and D924 can be the main trigger for initiating TMD1-TMD2 binding, as shown by the model in **Chapter 3**, where these two residues are already in close proximity at the beginning of domain assembly. Similar events may be found among other ABC transporters. Most ABC transporters have two TMDs and some of them, such as SUR1, Pgp, MRP1, and ABCG2, contain at least several polar residues in their TM areas (Johnson and Chen, 2017; Kim and Chen, 2018; Li et al., 2017; Taylor et al., 2017). Nonetheless, the coupling between these charged residues and their role in domain assembly of the transporters require further exploration. Besides ABC transporters, many other membrane proteins, such as membrane-bound immunoglobulin D (IgD), yeast proteins Fsk1, Fsk2, Mrh1, and Pma1 and their associated membrane protein chaperones Bap31 and EMC (Schamel et al., 2003; Shurtleff et al., 2018), have polar and charged residues localized in their TM areas. These hydrophilic residues have been proven to mediate the chaperone-substrate interactions, indicating that hydrophilic residues with a TM can drive binding between two TMDs.

Detecting co-translational folding of TMDs by EMC

EMC detects folding-challenged sequences in a TMD and stabilizes them. **Chapter 6** demonstrated that EMC co-translationally stabilizes TMD2 in CFTR but not TMD1, probably because TMD2 is less stable than TMD1. TMD2 contains a hydrophilic stretch in TM8, its second TM helix. The characteristic residue in this stretch is D924, which prevents Sec61 from recognizing the TM helix and therefore inhibits correct insertion of TM8, thereby extending the helix into the ER lumen (Pitonzo et al., 2009). TM8 is retrieved back to the ER membrane after being coupled with

charged residues in TM7 at a later timepoint of TMD2 folding and D924 is further stabilized by R347 in TMD1 during domain assembly (Pitonzo et al., 2009). EMC may be required for retrieving TM8 back to the ER membrane and stabilizing D924 before the two TMDs assemble. Interestingly, TMD2 has two aspartate residues in its TM area but TMD1 does not contain any. This might be a possible selection criterium of EMC for TMD2 over TMD1. Most reported EMC substrates, including Fks1, Fks2, Mrh1, and Pma1, have aspartates localized in their TM area (Shurtleff et al., 2018). EMC may be the common chaperone for some other types of type-I ABC transporters, such as SUR1, Pgp, and MRP1, as they also contain aspartates in their TM helixes. A putative more general role for EMC and assembly of these ABC transporters still awaits to be tested. Nevertheless, due to its pleiotropic function and wide specificity spectrum, EMC may also have additional selection criteria for substrate binding other than the presence of a aspartate residue in a TM.

Most investigations on EMC function, focus on the activity of the entire complex while the understanding of the function of its individual subunits is very limited. One study demonstrated that EMC1 binds specifically to the positive charged residues in membrane-embedded capsid protein VP1, VP2 or VP3 of SV40 via the D961 in its TMD, to help transferring the virion across the ER membrane and enter the cytosol (Bagchi et al., 2016). Other than that, there is no further data on the clients of EMC1 in mammalian cells. Another EMC subunit, EMC3, is reported to be co-immunoprecipitated with Fks1, Fks2, Mrh1, Pma1, and ABCA3 (Shurtleff et al., 2018; Tang et al., 2017). Nevertheless, other EMC components are also found in these co-immunoprecipitations, suggesting that these can also bind the other EMC members rather than only EMC3 which complicates the assignment of substrates to EMC3. The EMC members that contain charged residues in their TM area, such as EMC1, 3, 4, and 5 are probably the core components responsible for detecting folding-challenged sequences like aspartate residues in the TM area. So far, except for EMC1, there is no direct evidence to show that the charged residues in EMC3, 4, and 5 are involved in substrate binding.

Although we identified a possible selection criterium of EMC, how EMC actually chaperones its substrates remains unclear. Two models, which are not mutually exclusive, have been proposed for EMC chaperone function: in the first, EMC may receive TM helixes that did not insert properly one by one from the lateral gate of Sec61 translocon, stabilizing them, and then releasing them into the lipid bilayer (Shurtleff et al., 2018). In the second model, EMC acts as a chaperone to assist the folding of an entire TMD until it acquires its native conformation (Zhang et al., 2017a). In **Chapter 6** we demonstrated that EMC may function as a mix of these two models: EMC stabilizes the entire TMD2 in CFTR, however it may not chaperone TMD2 folding nor attach to the TM helixes sequentially. In this Chapter, TMD2 relies

more on EMC for structural support when the TMD1-TMD2 assembly is disrupted by mutations in the TM area. TMD2 stabilization by EMC will most likely include all of its TM helixes, as most of them contain charged residues and sequential binding would expose the non-engaged charged residues in the TM to the lipid bilayer and trigger protein aggregation. In wild-type CFTR, EMC may bind to TMD2 and stabilizes it until it coupled with TMD1 during CFTR domain assembly (Du and Lukacs, 2009). This binding mechanism may not be unique to CFTR but can possibly be found in all EMC substrates, as they also contain charged residues in more than one TM helix (Shurtleff et al., 2018).

Post-translational stabilization of TMDs by Bap31

Most ABC transporters contain two TMDs that have to be assembled together to form a channel. The folding hierarchy of CFTR (**Chapter 3**) indicates that this process occurs post-translationally. Yet the precise pathway and the associated chaperones and quality control machineries are incompletely understood. In **Chapter 7** we show that the membrane-embedded chaperone Bap31 detected the uncoupled TMD1 of CFTR and the free charged residues in its TM areas. This feature allowed Bap31 to stabilize the uncoupled TMDs until domain-domain interaction are completed or the quality control machinery takes over. The charged residues within the TMDs of CFTR that are involved in TMD1-TMD2 assembly, such as R347 and D924 (**Chapter 4**) (Pitonzo et al., 2009), may be the main target of Bap31, as they will most likely be uncoupled and exposed to the lipid bilayer before domain assembly occurs. These charges will be critical for binding of quality control machinery involved in sensing the TMD1-TMD2 interaction.

Detection of uncoupled charged residues in the TM area can be a common mechanism for Bap31 to bind its substrates, as several other Bap31 substrates, such as membrane IgD, also contains charged residues in TM areas (Geiger et al., 2011; Schamel et al., 2003). Nevertheless other Bap31 clients such as MHC class I and tetraspanins do not contain charged residues in their TMDs (Abe et al., 2009; Bartee et al., 2010). This suggested that Bap31 can bind to clients through hydrophobic residues in its TMDs or other domains, a hypothesis that is supported by the results of **Chapter 7**, where mutating charged residues in the TMD of Bap31 diminished binding to CFTR but did not eliminate the interaction.

In fact, how Bap31 binds to its substrates may define the subsequent sequel of events. Substrate binding that includes polar residues in TM areas of both Bap31 and its clients, like CFTR and membrane IgD, will sort the clients into quality control pathways (Geiger et al., 2011; Kim et al., 2015; Schamel et al., 2003; Wang et al., 2008). On the other hand, substrate binding through the Bap31 C-terminus, as has been found for MHC class I and cellubrevin, will sort the membrane proteins into an

ER export pathway with Bap31 acting as a possible cargo receptor (Abe et al., 2009; Annaert et al., 1997). These two functions are not necessarily mutually exclusive, since CFTR may also interact with the Bap31 C-terminus, as both TMD1 and TMD2 possess extracellular loops that are accessible to the C-terminus of Bap31 while it binds to the TMDs. Nevertheless, a mechanism where Bap31 acts as CFTR cargo receptor does not seem likely, because Bap31 mostly binds to TMD1 of CFTR with its charged residues in the TM area **(Chapter 7)** and because CFTR is thought to employ a cargo receptor of the Cornichon family (CNIHs) for ER export (Louie et al., 2012).

EMC and Bap31 coordinate with other chaperones during TMD folding

EMC recruits either substrate-specific or general chaperones to assist the folding of TMDs (Shurtleff et al., 2018). Chaperones, such as Hsp40, Hsp70, Hsc70, Hsp90, and Calnexin, may be gathered to support the folding of the CFTR domains (Amaral, 2004; Lopes-Pacheco et al., 2015; Matsumura et al., 2011; Okiyoneda et al., 2008; Pankow et al., 2015; Wang et al., 2006). CFTR TMD2 protrudes a long loop (ECL4) that contains the only two CFTR glycosylation sites into the ER lumen (Liu et al., 2017). The folding of this part of TMD2 may thus also be detected by Calnexin and Calreticulin that can be recruited by the EMC (Chang et al., 2008). As CFTR is a plasma membrane-resident protein, its TM helixes likely are longer than the thickness of ER membrane and cause hydrophobic mismatch. Along with the EMC, these chaperones may also shield the exposed hydrophobic stretches of TMD2 at the ER luminal side. Hsp70 and Hsp90 have been reported to interact with the cytosolic domains of CFTR, which means that they are less likely to be recruited by EMC (Schmidt et al., 2009; Wang et al., 2006). Even though TMD2 has cytosolic protrusions, interactions between Hsp70/Hsp90 with TMD2 have not been reported. The EMC may attract the post-translational chaperone Bap31 to TMD2, as this chaperone stabilizes TM charged residues and is also involved in TMD1 folding.

Bap31 binds co-translationally to TMD1 of CFTR but only intervenes with its folding post-translationally **(Chapter 7)**. The absence of an effect of Bap31 on co-translational CFTR folding suggests that Bap31 may bind to its substrate in later stages of translation, for example, after insertion and folding of a TMD. This means that TMD stabilization during translation will be mainly supported by other chaperones that assist in early TMD folding, such as TRAP, TRAM, Sec62, Sec63, or EMC (Heinrich and Rapoport, 2003; Meyer et al., 2000; Pfeffer et al., 2017; Shurtleff et al., 2018), and that early stabilization will not be affected by Bap31. In the case of CFTR, Bap31 can also be recruited by EMC to TMD2 because EMC is able to gather other chaperones to folding membrane proteins (Shurtleff et al., 2018). Bap31 may be the last chaperone that supports the folding of membrane proteins before they enter the ER export pathway **(Chapter 7, Figure 9)**. However, coordination between Bap31 and other cargo receptors in general has not been explored.

Studying the interaction of EMC and Bap31 with CFTR reveals the coordination between the two chaperones and how they are involved in membrane protein folding (Figure 1). We also demonstrated that they feature different functions and specificities towards CFTR domains. This coordination may resemble the chaperone interactome in or at the plasma membrane. Misfolded or uncoupled membrane proteins can be detected and stabilized in a similar mechanism by different quality control components, although such chaperoning events may be found much less often than in the ER due to the difference in function between the two cellular compartments (Apaja et al., 2010; Okiyoneda et al., 2010; Rocks et al., 2010).

Understanding the binding site of the chaperones on CFTR can help with the discovery of target sites for pharmaceutical chaperones to correct the folding of CFTR mutations that cause structural changes. Because CFTR has the same structure as the other type I ABC transporters and encompasses the common problems of general membrane protein folding, A model of chaperone-assist folding of CFTR possibly may also be applied to the folding of type I ABC transporters and other membrane proteins. Combining the results of **Chapter 2-7,** we propose the following model for the role of chaperones in folding and assembly of CFTR: After Sec61 inserts the TM helixes of CFTR into the ER membrane, EMC will bind to TMD2 to stabilize its hydrophilic sequences in the TM area and improve its insertion while TMD1 insertion and folding will be assisted by other translocon-associated chaperones such as TRAP or TRAM. After the TMDs acquire their native fold, they are released from these chaperones and with their TM charged residues bind to Bap31. Bap31 stabilizes these charged residues until TMD1-TMD2 interaction. This contact discharges Bap31 from the TMDs to allow domain assembly, after which CFTR is sorted in ER export pathways and delivered to the Golgi and plasma membrane.

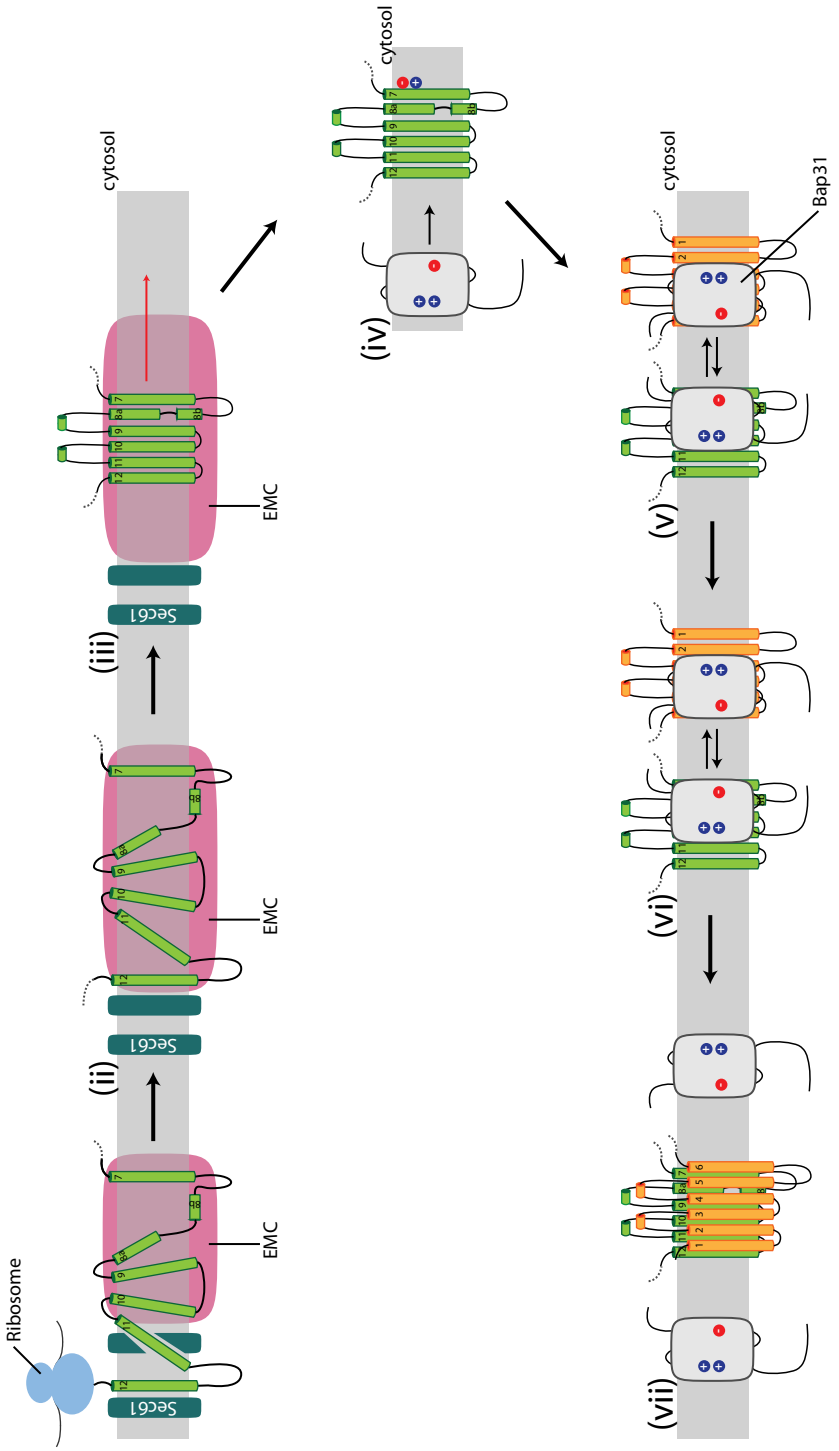


Figure 1: The roles of EMC and Bap31 in CFTR folding.
(i) The newly synthesized TMD2 of CFTR translocated into the Sec61 translocon, and passed from the translocon to the EMC. (ii) The EMC stabilizes improperly inserted TM helixes and charged TM residues to assist TMD2 in acquiring its correct folding. (iii) After TMD2 is inserted and folded properly, it is released into the ER membrane by the EMC. (iv) The free charges in uncoupled TMD2 attract Bap31 to bind to TM7 and TM8. (v) In the meantime, another Bap31 molecule binds to TMD1 at the charged TM residues in TM6. (iv) The charged TM residues in TMD1 and TMD2 interact with each other during CFTR domain assembly. (v) The subsequent interaction between TMD1 and TMD2 discharges Bap31 making it available for a new cycle of detecting free TM charges in membrane protein and CFTR is released to the ER export machinery.

REFERENCES

Abe, F., Van Prooyen, N., Ladasky, J.J., and Edidin, M. (2009). Interaction of Bap31 and MHC class I molecules and their traffic out of the endoplasmic reticulum. J Immunol *182*, 4776-4783.

Amaral, M.D. (2004). CFTR and chaperones: processing and degradation. J Mol Neurosci *23*, 41-48.

Annaert, W.G., Becker, B., Kistner, U., Reth, M., and Jahn, R. (1997). Export of cellubrevin from the endoplasmic reticulum is controlled by BAP31. J Cell Biol *139*, 1397-1410.

Apaja, P.M., Xu, H., and Lukacs, G.L. (2010). Quality control for unfolded proteins at the plasma membrane. J Cell Biol *191*, 553-570.

Bagchi, P., Inoue, T., and Tsai, B. (2016). EMC1-dependent stabilization drives membrane penetration of a partially destabilized non-enveloped virus. Elife *5*.

Bartee, E., Eyster, C.A., Viswanathan, K., Mansouri, M., Donaldson, J.G., and Fruh, K. (2010). Membrane-associated RING-CH proteins associate with Bap31 and target CD81 and CD44 to lysosomes. PLoS One *5*, e15132.

Basu, I., Chattopadhyay, A., and Mukhopadhyay, C. (2014). Ion channel stability of Gramicidin A in lipid bilayers: effect of hydrophobic mismatch. Biochim Biophys Acta *1838*, 328-338.

Chang, X.B., Mengos, A., Hou, Y.X., Cui, L., Jensen, T.J., Aleksandrov, A., Riordan, J.R., and Gentzsch, M. (2008). Role of N-linked oligosaccharides in the biosynthetic processing of the cystic fibrosis membrane conductance regulator. J Cell Sci *121*, 2814-2823.

Cotten, J.F., and Welsh, M.J. (1999). Cystic fibrosis-associated mutations at arginine 347 alter the pore architecture of CFTR. Evidence for disruption of a salt bridge. J Biol Chem *274*, 5429-5435.

Cui, G., Freeman, C.S., Knotts, T., Prince, C.Z., Kuang, C., and McCarty, N.A. (2013). Two salt bridges differentially contribute to the maintenance of cystic fibrosis transmembrane conductance regulator (CFTR) channel function. J Biol Chem *288*, 20758-20767.

Du, K., and Lukacs, G.L. (2009). Cooperative assembly and misfolding of CFTR domains in vivo. Mol Biol Cell *20*, 1903-1915.

Du, K., Sharma, M., and Lukacs, G.L. (2005). The DeltaF508 cystic fibrosis mutation impairs domain-domain interactions and arrests post-translational folding of CFTR. Nat Struct Mol Biol *12*, 17-25.

El Hiani, Y., Negoda, A., and Linsdell, P. (2016). Cytoplasmic pathway followed by chloride ions to enter the CFTR channel pore. Cell Mol Life Sci *73*, 1917-1925.

Feige, M.J., and Hendershot, L.M. (2013). Quality control of integral membrane proteins by assembly-dependent membrane integration. Mol Cell *51*, 297-309.

Geiger, R., Andritschke, D., Friebe, S., Herzog, F., Luisoni, S., Heger, T., and Helenius, A. (2011). BAP31 and BiP are essential for dislocation of SV40 from the endoplasmic reticulum to the cytosol. Nat Cell Biol *13*, 1305-1314.

Heinrich, S.U., and Rapoport, T.A. (2003). Cooperation of transmembrane segments during the integration of a double-spanning protein into the ER membrane. EMBO J *22*, 3654-3663.

Hoelen, H., Kleizen, B., Schmidt, A., Richardson, J., Charitou, P., Thomas, P.J., and Braakman, I. (2010). The primary folding defect and rescue of DeltaF508 CFTR emerge during translation of the mutant domain. PLoS One *5*, e15458.

Johnson, Z.L., and Chen, J. (2017). Structural basis of substrate recognition by the multidrug resistance protein MRP1. Cell *168*, 1075-1085 e1079.

Kida, Y., Ishihara, Y., Fujita, H., Onishi, Y., and Sakaguchi, M. (2016). Stability and flexibility of marginally hydrophobic-segment stalling at the endoplasmic reticulum translocon. Mol Biol Cell *27*, 930-940.

Killian, J.A., and Nyholm, T.K. (2006). Peptides in lipid bilayers: the power of simple models. Curr Opin Struct Biol *16*, 473-479.

Kim, W.T., Choi, H.S., Hwang, H.J., Jung, H.S., and Ryu, C.J. (2015). Epitope mapping of antibodies suggests the novel membrane topology of B-cell receptor associated protein 31 on the cell surface of embryonic stem cells: The novel membrane topology of BAP31. PLoS One *10*, e0130670.

Kim, Y., and Chen, J. (2018). Molecular structure of human P-glycoprotein in the ATP-bound, outward-facing conformation. Science *359*, 915-919.

Kleizen, B., van Vlijmen, T., de Jonge, H.R., and Braakman, I. (2005). Folding of CFTR is predominantly cotranslational. Mol Cell *20*, 277-287.

Lee, J.Y., Kinch, L.N., Borek, D.M., Wang, J., Wang, J., Urbatsch, I.L., Xie, X.S., Grishin, N.V., Cohen, J.C., Otwinowski, Z.*, et al.* (2016). Crystal structure of the human sterol transporter ABCG5/ABCG8. Nature *533*, 561-564.

Li, N., Wu, J.X., Ding, D., Cheng, J., Gao, N., and Chen, L. (2017). Structure of a pancreatic ATP-sensitive potassium channel. Cell *168*, 101-110 e110.

Liu, F., Zhang, Z., Csanady, L., Gadsby, D.C., and Chen, J. (2017). Molecular structure of the human CFTR ion channel. Cell *169*, 85-95 e88.

Lopes-Pacheco, M., Boinot, C., Sabirzhanova, I., Morales, M.M., Guggino, W.B., and Cebotaru, L. (2015). Combination of correctors rescue DeltaF508-CFTR by reducing its association with Hsp40 and Hsp27. J Biol Chem *290*, 25636-25645.

Louie, R.J., Guo, J., Rodgers, J.W., White, R., Shah, N., Pagant, S., Kim, P., Livstone, M., Dolinski, K., McKinney, B.A.*, et al.* (2012). A yeast phenomic model for the gene interaction network modulating CFTR-DeltaF508 protein biogenesis. Genome Med *4*, 103.

Lu, Y., Turnbull, I.R., Bragin, A., Carveth, K., Verkman, A.S., and Skach, W.R. (2000). Reorientation of aquaporin-1 topology during maturation in the endoplasmic reticulum. Mol Biol Cell *11*, 2973-2985.

Matsumura, Y., David, L.L., and Skach, W.R. (2011). Role of Hsc70 binding cycle in CFTR folding and endoplasmic reticulum-associated degradation. Mol Biol Cell *22*, 2797-2809.

Meyer, H.A., Grau, H., Kraft, R., Kostka, S., Prehn, S., Kalies, K.U., and Hartmann, E. (2000). Mammalian Sec61 is associated with Sec62 and Sec63. J Biol Chem *275*, 14550-14557.

Okiyoneda, T., Barriere, H., Bagdany, M., Rabeh, W.M., Du, K., Hohfeld, J., Young, J.C., and Lukacs, G.L. (2010). Peripheral protein quality control removes unfolded CFTR from the plasma membrane. Science *329*, 805-810.

Okiyoneda, T., Niibori, A., Harada, K., Kohno, T., Michalak, M., Duszyk, M., Wada, I., Ikawa, M., Shuto, T., Suico, M.A.*, et al.* (2008). Role of calnexin in the ER quality control and productive folding of CFTR; differential effect of calnexin knockout on wild-type and DeltaF508 CFTR. Biochim Biophys Acta *1783*, 1585-1594.

Onishi, Y., Yamagishi, M., Imai, K., Fujita, H., Kida, Y., and Sakaguchi, M. (2013). Stop-and-move of a marginally hydrophobic segment translocating across the endoplasmic reticulum membrane. J Mol Biol *425*, 3205-3216.

Pankow, S., Bamberger, C., Calzolari, D., Martinez-Bartolome, S., Lavallee-Adam, M., Balch, W.E., and Yates, J.R., 3rd (2015). F508 CFTR interactome remodelling promotes rescue of cystic fibrosis. Nature *528*, 510-516.

Pfeffer, S., Dudek, J., Schaffer, M., Ng, B.G., Albert, S., Plitzko, J.M., Baumeister, W., Zimmermann, R., Freeze, H.H., Engel, B.D.*, et al.* (2017). Dissecting the molecular organization of the translocon-associated protein complex. Nat Commun *8*, 14516.

Pitonzo, D., Yang, Z., Matsumura, Y., Johnson, A.E., and Skach, W.R. (2009). Sequence-specific retention and regulated integration of a nascent membrane protein by the endoplasmic reticulum Sec61 translocon. Mol Biol Cell *20*, 685-698.

Rahman, K.S., Cui, G., Harvey, S.C., and McCarty, N.A. (2013). Modeling the conformational changes underlying channel opening in CFTR. PLoS One *8*, e74574.

Rocks, O., Gerauer, M., Vartak, N., Koch, S., Huang, Z.P., Pechlivanis, M., Kuhlmann, J., Brunsveld, L., Chandra, A., Ellinger, B.*, et al.* (2010). The palmitoylation machinery is a spatially organizing system for peripheral membrane proteins. Cell *141*, 458-471.

Schamel, W.W., Kuppig, S., Becker, B., Gimborn, K., Hauri, H.P., and Reth, M. (2003). A high-molecular-weight complex of membrane proteins BAP29/BAP31 is involved in the retention of membrane-bound IgD in the endoplasmic reticulum. Proc Natl Acad Sci U S A *100*, 9861-9866.

Schmidt, B.Z., Watts, R.J., Aridor, M., and Frizzell, R.A. (2009). Cysteine string protein promotes proteasomal degradation of the cystic fibrosis transmembrane conductance regulator (CFTR) by increasing its interaction with the C terminus of Hsp70-interacting protein and promoting CFTR ubiquitylation. J Biol Chem *284*, 4168-4178.

Sheppard, D.N., Rich, D.P., Ostedgaard, L.S., Gregory, R.J., Smith, A.E., and Welsh, M.J. (1993). Mutations in CFTR associated with mild-disease-form Cl- channels with altered pore properties. Nature *362*, 160-164.

Shurtleff, M.J., Itzhak, D.N., Hussmann, J.A., Schirle Oakdale, N.T., Costa, E.A., Jonikas, M., Weibezahn, J., Popova, K.D., Jan, C.H., Sinitcyn, P.*, et al.* (2018). The ER membrane protein complex interacts cotranslationally to enable biogenesis of multipass membrane proteins. Elife *7*.

Tang, X., Snowball, J.M., Xu, Y., Na, C.L., Weaver, T.E., Clair, G., Kyle, J.E., Zink, E.M., Ansong, C., Wei, W.*, et al.* (2017). EMC3 coordinates surfactant protein and lipid homeostasis required for respiration. J Clin Invest *127*, 4314-4325.

Taylor, N.M.I., Manolaridis, I., Jackson, S.M., Kowal, J., Stahlberg, H., and Locher, K.P. (2017). Structure of the human multidrug transporter ABCG2. Nature *546*, 504-509.

Van Goor, F., Yu, H., Burton, B., and Hoffman, B.J. (2014). Effect of ivacaftor on CFTR forms with missense mutations associated with defects in protein processing or function. J Cyst Fibros *13*, 29-36.

van Willigen, M., Vonk, A.M., Yeoh, H.Y., Kruisselbrink, E., Kleizen, B., van der Ent, C.K., Egmond, M.R., de Jonge, H.R., Braakman, I., Beekman, J.M.*, et al.* (2019). Folding-function relationship of the most common cystic fibrosis-causing CFTR conductance mutants. Life Sci Alliance *2*.

Vasiliou, V., Vasiliou, K., and Nebert, D.W. (2009). Human ATP-binding cassette (ABC) transporter family. Hum Genomics *3*, 281-290.

Wang, B., Heath-Engel, H., Zhang, D., Nguyen, N., Thomas, D.Y., Hanrahan, J.W., and Shore, G.C. (2008). BAP31 interacts with Sec61 translocons and promotes retrotranslocation of CFTRDeltaF508 via the derlin-1 complex. Cell *133*, 1080-1092.

Wang, X., Venable, J., LaPointe, P., Hutt, D.M., Koulov, A.V., Coppinger, J., Gurkan, C., Kellner, W., Matteson, J., Plutner, H.*, et al.* (2006). Hsp90 cochaperone Aha1 downregulation rescues misfolding of CFTR in cystic fibrosis. Cell *127*, 803-815.

Zhang, S., Xu, C., Larrimore, K.E., and Ng, D.T.W. (2017a). Slp1-Emp65: A guardian factor that protects folding polypeptides from promiscuous degradation. Cell *171*, 346-357 e312.

Zhang, Z., Liu, F., and Chen, J. (2017b). Conformational changes of CFTR upon phosphorylation and ATP binding. Cell *170*, 483-491 e488.

SUMMARY

Thirty percent of eukaryotic proteins are membrane proteins, which contain at least one transmembrane domain (TMD) formed by one or more transmembrane (TM) helixes. These proteins carry out a large variety of functions, including transporting small molecules and ions, transducing signals, cell adhesion, protein trafficking, and membrane formation. Membrane proteins are synthesized in the Endoplasmic Reticulum (ER), an organelle specifically endowed with machinery for executing general protein folding and post-translational modifications. The TMDs of membrane proteins may encounter several folding challenges during biogenesis, many of which can be resolved by binding to chaperones. In **Chapter 1**, we discuss these problems and the putative membrane-bound chaperones that may be involved in solving them. Although the role of cytoplasmic chaperones in protein folding has been extensively studied, interactions between membrane proteins and membrane-bound chaperones are only recently being explored.

In **Chapter 1** we also describe the Cystic Fibrosis Transmembrane Conductance Regulator (CFTR), our model protein for studying membrane protein folding and chaperones in the ER. CFTR is a member of the ABC transporter family. It has two TMDs and two cytoplasmic nucleotide binding domains (NBDs) and an unstructured R-region. The domain hierarchy of CFTR comprises TMD1 followed by NBD1, (R), TMD2, and NBD2, and is highly conserved among ABC transporters. CFTR poses many typical folding problems that are common in membrane proteins, which makes it an ideal example for uncovering the folding pathway of these proteins. Disrupting CFTR conformation can cause Cystic Fibrosis, a disease that causes mucus accumulation and promotes infections in the respiratory, digestive, and reproductive systems. Understanding CFTR folding will therefore also provide medically relevant information about this disease.

In this thesis, we analyzed CFTR biogenesis and maturation using a radioactive pulse-chase assay. This is a powerful tool for studying the conformational maturation, trafficking between organelles, and degradation of target proteins in live cells (**Chapter 2**). In this approach, a small fraction of the total protein pool is 'tagged' during short radiolabeling times (<30 min; i.e pulse) and maturation and protein trafficking is then followed during tightly controlled chase times. When combined with limited proteolysis, immunoprecipitation with domain-specific antibodies, and nonreducing/reducing SDS-polyacrylamide gel electrophoresis (SDS-PAGE), folding processes of a target protein can be examined in great detail.

CFTR folds in two steps: the domains of CFTR fold during biosynthesis and when biosynthesis is completed they assemble to form a functional protein. It is therefore

important to understand the folding of each domain as this is profoundly connected to the overall conformation of CFTR. Due to a paucity of suitable reagents, the folding of CFTR transmembrane domains (TMDs) and their assembly is poorly understood. We thus generated three antibodies against TMD1 and TMD2 to study the folding of these TMDs in **Chapter 3**. These antibodies revealed that the TMDs undergo post-translational conformational changes that are the result of CFTR domain assembly.

The antibodies generated **in Chapter 3** were then used to detect the folding of a series of CFTR patient mutants. While investigating the folding of CFTR class III and IV mutants, whose grouping is based on the ability to reach the cell surface albeit in a form with limited function, we discovered that mutation R347P is mis-classified (**Chapter 4**). R347P is the only mutation in the class III and IV mutations that leads to major defects in domain assembly. As R347 is located in TMD1, a mutation into proline may disrupt the interaction between the TMDs of CFTR and interfere with domain assembly. R347P does not respond to the recently approved potentiator VX-770, which opens the channel, whereas most other class-III and class-IV mutants do respond to it. By this criterion and by its functional response to corrector drug VX-809, R347P qualifies also as a class-II mutation. Our study demonstrated that the new antibodies can detect CFTR conformation defects and provide an unbiased approach for characterizing the mode of action of novel therapeutic compounds. These antibodies can therefore be used for investigating which drugs are effective for which cystic fibrosis disease variant.

R347 is one of the charged residues located in the TM area of CFTR. Such amino acids at these specific locations in a membrane protein serve both structural and functional purposes. Nevertheless, the uncoupled TM charged residues can disturb the thermodynamics of the ER membrane, and how to stabilize them is one of the main problems of membrane protein folding.

We also used the antibodies described in Chapter 3 to characterize the effect of the R751L mutation on CFTR folding (**Chapter 5**). In comparison to R347P, R751L exerted less effect on CFTR domain folding and assembly but impaired CFTR function. This likely is because R751 is located in the R-region, a part of the protein that does not play a main role in CFTR domain assembly but is responsible for channel opening and closing. In **Chapter 5**, we showed that R751L folds and responds to VX-770 and VX-809 like wild-type protein instead of another CFTR mutant, delF508, whose domain folding and assembly are heavily disrupted. Like Chapter 4, Chapter 5 also demonstrated a correlation between CFTR folding and its function in vivo in man.

The ER membrane complex (EMC) is a highly conserved ER-resident complex

that can chaperone TMDs with charged amino acid sequences, though the precise mechanism how it does this remains largely unknown. The EMC was reported to interact with CFTR, and this finding was confirmed and extended in **Chapter 6**. By using a radiolabeling coupled protease susceptibility assay, and immunoprecipitation with the TMD antibodies, we discovered that EMC assists the folding of TMD2, but not of the other domains, and that EMC prevents early degradation of CFTR in the ER. CFTR post-translational assembly was also decreased due to a destabilized TMD2 in cells without EMC. These experiments provide direct evidence of how EMC assists the folding of polytopic TMDs that contain destabilizing features.

In **Chapter 6** we also showed that CFTR TMD2 engaged the chaperone EMC during translation. This binding is most likely driven by ionic forces at the TM areas of the two proteins, as they both contain charged residues. Another CFTR chaperone, Bap31, also contains charged TM residues and binds to pre-domain assembly CFTR. Bap31 interacts with TMD1 and sorts CFTR to ER-associated degradation (ERAD), but its function in chaperoning CFTR charged residues has not been studied. In **Chapter 7**, using the TMD antibodies, our results revealed that the charged residues in the Bap31 TMs are required to stabilize TMDs of CFTR post-translationally and Bap31 binding maintains efficient CFTR domain assembly. We therefore propose that Bap31 chaperones CFTR folding by preventing CFTR TM charged residues from interacting with the lipid bilayer and thus acts as quality control for CFTR domain assembly.

Finally, in the discussion (**Chapter 8)**, we reviewed the results in a broader context, considering what the possible selection criteria and binding mechanisms of EMC and Bap31 could be. In this chapter we also relate the folding mechanism of CFTR to other type-I ABC transporters and membrane proteins. Finally, we propose a model of how these two chaperones act in the folding of CFTR. This model may also provide a useful description for understanding the folding pathways of other membrane proteins that require both the EMC and Bap31.

SAMENVATTING

Eiwitten zijn verantwoordelijk voor de uitvoerende functies van de cel en ze komen voor als oplosbare en membraan-gebonden versies, waarvan de laatsten in de plasmamembraan van de cel zitten en daarom aangeduid worden als transmembraan (TM)-eiwitten. Hiervan zijn er ongeveer half zo veel als van het aantal oplosbare eiwitten. Een TM-eiwit kan een of meerdere keren met een hydrofoob TM-domein (TMD) door het membraan rijgen. TM-eiwitten vervullen een grote verscheidenheid aan functies, zoals o.a. het transporteren van kleine moleculen en ionen, doorgeven van signalen van buiten de cel naar binnen en vice versa, en het hechten van cellen aan elkaar. Membraaneiwitten worden gemaakt in het endoplasmatisch reticulum (ER), een compartiment dat specifiek is uitgerust met een zogenaamde chaperonne-machinerie om eiwitten te laten vouwen tot een vorm die nodig is voor hun functie. Het deel van een TM-eiwit dat zich in het cytosol bevindt, wordt door een andere groep chaperonnes gevouwen. In tegenstelling tot de grote kennis die we hebben over de vouwing van dit deel van een TM-eiwit, weten we weinig over de mechanismen hoe TM chaperonnes bijdragen aan de vouwing van een TMD, o.a. omdat het pas sinds kort mogelijk is deze vraag experimenteel te benaderen.

In Hoofdstuk 1 zetten we op een rij hoe membraangebonden chaperonnes een rol zouden kunnen spelen bij het vouwen van TM-eiwitten aan de hand van CFTR (Cystic Fibrosis Transmembrane Conductance Regulator), ons modeleiwit. CFTR is lid van de ABC-transporterfamilie en heeft twee TMDs, twee cytoplasmatische nucleotide-bindende domeinen (NBDs) en een ongestructureerd R-domein. In de architectuur van CFTR zijn TMD1, NBD1, R, TMD2 en NBD2 in deze volgorde aan elkaar geschakeld, een arrangement dat karakteristiek is voor de ABC-transporterfamilie. De structuur van CFTR, met afwisselende gedeeltes in het cytosol, in de membraan en buiten de cel, komt ook voor bij andere membraaneiwitten en vormt een grote uitdaging voor de eiwitvouwingsmachinerie. Hierdoor is CFTR een ideaal model voor het ophelderen van de vouwing van complexe membraaneiwitten. Verstoring van de CFTR-functie door erfelijke afwijkingen in de DNA volgorde kan Cystic Fibrosis (taaislijmziekte) veroorzaken. Bij deze ziekte vormen zich slijmophopingen in de luchtwegen, het spijsverteringskanaal en de voortplantingsorganen. In longen worden hierdoor de ingeademde bacteriën niet voldoende efficiënt afgevoerd waardoor infecties ontstaan, die uiteindelijk de meest voorkomende doodsorzaak voor patiënten zijn. Inzicht in CFTR-vouwing zal daarom ook medisch relevante informatie over de ziekte opleveren.

In Hoofdstuk 2 hebben we methoden beschreven voor het meten en analyseren van CFTR-vouwing met behulp van radioactieve ‘pulse chase’. Pulse-chase labeling met

radioactieve aminozuren voor nieuw te vormen eiwitten is een krachtig hulpmiddel voor het bestuderen van eiwitvouwing, het vervoer van eiwitten tussen organellen en de afbraak van eiwitten in cellen. In deze benadering wordt een kleine fractie van de totale hoeveelheid eiwit tijdens haar aanmaak radioactief gelabeld gedurende korte radiolabelingstijden ('pulse'). Vouwing kan worden gevolgd gedurende de 'chase' waar geen radioactieve bouwstenen meer aanwezig zijn. In combinatie met 'limited proteolysis', immunoprecipitatie met domeinspecifieke antilichamen en reducerende SDS-polyacrylamidegelelektroforese (SDS-PAGE), kunnen vouwingsprocessen van het te bestuderen eiwit tot in detail worden onderzocht.

CFTR vouwt bij benadering in twee stappen, waarbij de domeinen eerst individueel vouwen tijdens de synthese. Wanneer deze stap is voltooid, assembleren de domeinen tot een functioneel eiwit. Het is daarom belangrijk om de vouwing van elk domein te begrijpen, aangezien dit direct verband houdt met de vorm en functtie van het gehele CFTR. Vanwege het gebrek aan geschikte reagentia is het vouwen van CFTR transmembraandomeinen (TMDs) en hun assemblage nog slechts ten dele begrepen. We hebben daarom antilichamen tegen TMD1 en TMD2 gemaakt om het vouwen van de TMDs te bestuderen in Hoofdstuk 3. Met deze antistoffen konden we laten zien dat de TMDs post-translationele vormveranderingen ondergaan die het resultaat zijn van domeinassemblage van CFTR.

Vervolgens werden de nieuwe antilichamen ingezet om het vouwen van een reeks CFTR patiënten-mutanten te bestuderen (Hoofdstukken 4 en 5). In Hoofdstuk 5 hebben we aangetoond dat de milde R751L-mutant vergelijkbaar vouwt en reageert op geneesmiddelen als wild-type CFTR. In Hoofdstuk 4 hebben we CFTR klasse-IV-mutanten onderzocht, waarvan we ondermeer hebben vastgesteld dat mutatie R347P verkeerd is geclassificeerd. R347P is de enige mutatie in klasse IV die leidt tot grotere defecten in domeinassemblage. Aangezien R347 zich bevindt in TMD1, kan een mutatie van arginine naar proline de interactie tussen de TMDs van CFTR verstoren en daarmee ook de domeinassemblage. R347P reageert niet op het onlangs goedgekeurde geneesmiddel VX-770, dat het CFTR kanaal opent, terwijl de meeste andere klasse-IV-mutanten er wel op reageren. Door dit criterium en door de functionele verbetering door corrector-geneesmiddel VX-809, kwalificeren we R347P dan ook als een klasse II-mutatie. Onze studie toonde aan dat de nieuwe antilichamen conformatie-defecten in CFTR kunnen detecteren en een nieuwe benadering bieden voor het karakteriseren van de werkingswijze van nieuwe therapeutische middelen. Deze antilichamen kunnen daarom worden gebruikt om te onderzoeken welke geneesmiddelen effectief zijn voor welke variant van taaislijmziekte.

R347 is een van de geladen aminozuren in het eerste TMD van CFTR. Dergelijke aminozuren op zulke specifieke locaties in membraaneiwitten dienen zowel structurele als functionele doeleinden. De lading van R347 is niet gekoppeld aan die van een ander residue in TMD1. Het ER-membraancomplex (EMC) is een geconserveerd eiwitcomplex, dat TMDs met geladen aminozuursequenties kan begeleiden als chaperonne in een nog niet precies begrepen mechanisme. Van het EMC werd eerder gerapporteerd dat het bindt aan CFTR hetgeen we konden bevestigen en uitdiepen in Hoofdstuk 6. Met de pulse-chase-methode gevolgd door limited proteolysis en immunoprecipitatie met de TMD-antilichamen, ontdekten we dat het EMC tijdens de synthese helpt bij het vouwen van TMD2, in een interactie die hoogstwaarschijnlijk gedreven wordt door ladings-krachten in de TM-gebieden van de twee eiwitten. Deze chaperonne functie is specifiek voor TMD2 en werd niet gezien voor de andere domeinen. Daarnaast voorkomt het EMC vroege afbraak van CFTR in het ER. In cellen zonder EMC werd post-translationele assemblage van CFTR verlaagd als gevolg van een gedestabiliseerd TMD2. Deze experimenten bieden direct inzicht in de rol van EMC bij het vouwen van TMDs die destabiliserende eigenschappen bevatten.

Een ander CFTR-chaperonne, Bap31 bevat net als EMC geladen TM-residuen en bindt aan CFTR vóór domein-assemblage. Bap31 werkt samen met TMD1 en sorteert CFTR naar de ER-geassocieerde afbraak route, maar de functie van Bap31 als chaperonne van CFTR-geladen residuen is niet onderzocht. In Hoofdstuk 7 laten we met behulp van de TMD-antistoffen zien dat de geladen residuen in de TMDs van Bap31 nodig zijn om de TMDs van CFTR post-translationeel te stabiliseren en dat Bap31-binding een efficiënte CFTR-domeinassemblage mogelijk maakt. We vermoeden daarom dat Bap31 CFTR helpt met vouwen door te voorkomen dat geladen residuen in de TMDs interacties aangaan met andere membraaneiwitten en daarmee fungeert als facilitator en kwaliteitscontrole voor CFTR-domeinassemblage.

Ten slotte worden in Hoofdstuk 8 de resultaten van de experimentele hoofdstukken in een bredere context besproken, met nadruk op de mogelijke selectiecriteria en bindings-mechanismen van EMC en Bap31. Verder correleren we het vouwings-mechanisme van CFTR met andere type I ABC-transporters en stellen we een model voor hoe de twee chaperonnes werken bij het vouwen van CFTR. Dit model kan ook een nuttige beschrijving bieden voor het begrijpen van de vouwingsroutes van andere membraaneiwitten die zowel EMC als Bap31 gebruiken.

ACKNOWLEDGMENT

I am truly grateful that I could join CPC for this five-year journey. I have learned a lot from my projects and the people around me. I would like to thank my family, friends, and colleagues for their help and support during these five years. This thesis could not be written without them.

CURRICULUM VITAE

Hui Ying Yeoh was born on 7th July 1988 in Melaka, Malaysia. After finishing her high school, she studied Biomedical Science in Victoria University of Wellington, New Zealand, from 2006 and 2010. After that, she started her MSc in University of Glasgow, United Kingdom, in 2011 and completed it in 2013 by doing research in biochemistry in the research groups of Dr. Brian Smith and Prof. Neil Bulleid. In 2014, she started working at Utrecht University in Cellular Protein Chemistry group, under the supervision of Prof. Ineke Braakman and Dr. Peter van der Sluijs. The results of this research are presented in this thesis.

